DOT/FAA/TC-20/13

Federal Aviation Administration
William J. Hughes Technical Center
Aviation Research Division
Atlantic City International Airport
New Jersey 08405

Flight Loads and Airframe Usage Analysis of Next-Generation Airtankers – BAe-146 and RJ-85

January 2026

Final Report

This document is available to the U.S. public through the National Technical Information Services (NTIS), Springfield, Virginia 22161.

This document is also available from the Federal Aviation Administration William J. Hughes Technical Center at actlibrary.tc.faa.gov.

U.S. Department of Transportation
Federal Aviation Administration

NOTICE

Technical Report Documentation Page

1. Report No.	2. Government Accession No.	3. Recipient's Catalog No.
DOT/FAA/TC-20/13		

4. Title and Subtitle	5. Report Date
FLIGHT LOADS AND AIRFRAME USAGE ANALYSIS OF NEXT-GENERATION AIRTANKERS – BAe-146 and RJ-85	January 2026
	6. Performing Organization Code

7. Author(s)	8. Performing Organization Report No.
Kamran Rokhsaz, Linda K. Kliment, and Elizabeth Rollins	

9. Performing Organization Name and Address	10. Work Unit No. (TRAIS)
Wichita State University 1845 Fairmount Wichita, KS 67260-0044	11. Contract or Grant No. Cooperative Agreement 17-G-004

12. Sponsoring Agency Name and Address	13. Type of Report and Period Covered
U.S. Department of Transportation Federal Aviation Administration Air Traffic Organization NextGen & Operations Planning Office of Research and Technology Development Washington, DC 20591	Phase I Final Report
	14. Sponsoring Agency Code ANM-210L

15. Supplementary Notes

The Federal Aviation Administration William J. Hughes Technical Center Aviation Research Division COR was Dr. Sohrob Mottaghi.

16. Abstract

This report addresses in-flight recorded data from eight BAe-146s and eight RJ-85s flown in support of the United State Forest Service aerial firefighting operations. All flight data was recorded at 32 Hz by IONode100 units supported by Latitude Technologies, Corp. All data was examined for integrity, and anomalies and inaccuracies were identified and outlined. Similarities between BAe-146 and RJ-85 were used to rationalize combining their results.

Flights were divided into firefighting, ferry, and maintenance/training missions. Firefighting flights were divided into five separate phases. Statistical results of the airframe usage were presented and compared with aircraft limitations. This information includes altitude, airspeed, duration and distance, number of retardant drops per flight, maximum and minimum vertical load factors, flap cycling frequency, and takeoff and landing weights. Unreliable pitch-and-roll angle and cabin pressure recordings prevented examination of these parameters. In several cases, the vertical accelerations were shown to exceed the limit load factors with flaps extended. Detailed examination of the data revealed that these occurred mostly during the drop phase. Also, in a number of cases, the maximum indicated airspeed was shown to be slightly above the prescribed limits.

The recorded normal accelerations were shown to contain frequencies due to structural vibration. Results of the effect of different filters on flight loads spectra are presented in an appendix. Based on these results, a low-pass, eighth-order Butterworth filter with an 8-Hz cutoff frequency was used to attenuate the structural frequencies. After filtering, vertical load factors were divided into gust and maneuver loads using the two-second rule.

Using the method of peaks-between-means, exceedance spectra for gust and maneuver loads were developed for ground-air-ground cycles, as well as for specific flight phases. These results were compared to those of the legacy airtankers and other aircraft flown in support of firefighting missions and as civil transport. The gust load factor spectra are shown to be similar to other United States Forest Service aircraft being flown in the same environment. The maneuver load factor spectra are shown to indicate smaller loads than those of legacy airtankers, but considerably exceeding in frequency those of civil transport.

Derived gust velocities were extracted for BAe-146 aircraft and their cumulative occurrences were presented. Erroneous recording of the aircraft weight prevented inclusion of data from RJ-85 airframes.

The report concludes with some recommendations for improved data acquisition for future efforts.

17. Key Words	18. Distribution Statement
flight profiles, flight loads spectrum, statistical loads data	This document is available to the U.S. public through the National Technical Information Service (NTIS), Springfield, Virginia 22161. This document is also available from the Federal Aviation Administration William J. Hughes Technical Center at actlibrary.tc.faa.gov.

19. Security Classif. (of this report)	20. Security Classif. (of this page)	21. No. of Pages	22. Price
Unclassified	Unclassified	196	

ACKNOWLEDGEMENTS

The work reported in this document was performed by the Flight Loads Group within the Department of Aerospace Engineering of the College of Engineering at Wichita State University (WSU). This effort was funded by the Federal Aviation Administration (FAA) under the cooperative agreement 17-G-004. At WSU, the principal investigators were Dr. Kamran Rokhsaz, Dr. Linda K. Kliment, and Dr. Elizabeth Rollins of the Department of Aerospace Engineering. The format used for presentation of the statistical data was adopted from the work previously performed by the principal investigators and the University of Dayton Research Institute. The Program Manager for the FAA was Dr. Sohrob Mottaghi of the FAA William J. Hughes Technical Center. Technical guidance was provided by Mr. David Rathfelder of the FAA Policy & Standards Division.

TABLE OF CONTENTS

	Page
EXECUTIVE SUMMARY	XVIII
1. INTRODUCTION	1
2. AIRCRAFT DESCRIPTION	2
3. DATA COLLECTION	3
3.1 FLIGHT DATA RECORDER	3
3.2 AVAILABLE DATA	4
4. WICHITA STATE UNIVERSITY DATA PROCESSING	4
4.1 PREPROCESSING	4
4.1.1 Unified Data Format	4
4.1.2 Missing Data	6
4.1.3 Missing Airspeeds	6
4.1.4 Obtaining Terrain Elevation	7
4.2 DATA CONDITIONING	8
4.2.1 Normalizing Vertical Load Factor	8
4.2.2 Removing Data Spikes	8
4.2.3 Filtering Vertical Load Factor	10
4.2.4 Smoothing of Noisy Signals	12
4.2.5 Takeoff and Landing	12
4.2.6 Weight Estimation	12
4.2.7 Other Data Integrity Issues	14
4.3 DERIVED AND EXTRACTED PARAMETERS	17
4.3.1 Flight Duration and Distance	17
4.3.2 Sign Convention	17

4.3.3 Peak and Valley Selection 18
4.3.4 Separation of Maneuver and Gust Load Factors 18
4.3.5 Phases of Flight 19
4.3.6 Derived Gust Velocities 21
5. DATA PRESENTATION 24
5.1 AIRFRAME USAGE 24
5.1.1 Ground-Air-Ground Usage – All Missions 24
5.1.2 Phase-Specific Usage – Firefighting Missions 29
5.1.3 Summary of Usage 32
5.2 FLIGHT LOADS 33
5.2.1 Correlation with AGL Altitude 33
5.2.2 Correlation with MSL Altitude 35
5.2.3 Summary of Flight Loads 37
5.3 DERIVED GUST VELOCITIES 38
5.3.1 Firefighting Phases 38
5.3.2 Overall Flights 39
5.3.3 Summary of Derived Gust Velocities 40
5.4 COMPARISONS WITH OTHER SOURCES 40
6. SUMMARY AND CONCLUSION 42
6.1 SUMMARY 42
6.2 CONCLUSIONS 44
7. REFERENCES 45
APPENDIX A—FILTERING VERTICAL ACCELERATIONS
APPENDIX B—USAGE DATA PRESENTATION
APPENDIX C—FLIGHT LOADS BY ABOVE GROUND LEVEL ALTITUDE

APPENDIX D—FLIGHT LOADS BY MSL ALTITUDE

APPENDIX E—DERIVED GUST VELOCITIES

APPENDIX F—COMPARISONS WTH OTHER SOURCES

LIST OF FIGURES

Figure	Page
Figure 1. Example of noise in squat switch signal	8
Figure 2. Example of spikes in recorded data	9
Figure 3. Normal acceleration showing contribution of structural modes (a) frequency content (b) close-up view of time history	11
Figure 4. An example of filtered normal acceleration	12
Figure 5. Probability distribution of takeoff and landing weights (a) takeoff weight (b) landing weight	13
Figure 6. Example of drifting airspeed	14
Figure 7. Example of erroneous pressure altitude	15
Figure 8. Example of erroneous airspeed	15
Figure 9. Example of drifting attitude indications	16
Figure 10. Sign convention for airplane accelerations	18
Figure 11. Peak-between-means classification of loads	19
Figure 12. Schematic of various flight phases	20
Figure 13. A typical flight time history with two drops	20
Figure 14. Estimate of maximum lift coefficient for RJ-85	26
Figure 15. Typical peak load factors associated with the drop phase	27
Figure 16. Typical peak load factors associated with the drop phase (continued)	28
Figure A-1. Typical frequency content of normal acceleration	A-2
Figure A-2. Close-up view of time history of vertical acceleration	A-3
Figure A-3. Effect of filter order on gain and time history - ω_c = 8 Hz (a) gain (b) sample time history	A-5
Figure A-4. Effect of cutoff frequency on gain and time history – eighth-order filter (a) gain (b) sample time history	A-6
Figure A-5. Effect of FIR filters on gain and time history	A-8

Figure A-6. Effect of FIR filters on gain and time history (continued) A-9

Figure A-7. Effect of data skipping on signal time history A-10

Figure A-8. Close-up view of a segment of data from Figure A-7 A-10

Figure A-9. Cumulative occurrence of incremental vertical load factor as recorded A-12

Figure A-10. Cumulative occurrence of incremental gust and maneuver vertical load factor – effect of Butterworth filter order A-14

Figure A-11. Cumulative occurrence of incremental gust and maneuver vertical load factor – effect of Butterworth filter cutoff frequency A-15

Figure A-12. Cumulative occurrence of incremental gust and maneuver vertical load factor – effect of fir filters A-17

Figure A-13. Cumulative occurrence of incremental gust and maneuver vertical load factor – effect of data skipping A-18

Figure A-14. Cumulative occurrence of incremental gust and maneuver vertical load factor – comparison of various filters A-19

Figure A-15. Total number of loads per 1000 hours over 27.4 hours of operation A-22

Figure B-1. Number of flights based on duration B-5

Figure B-2. Distances and durations B-6

Figure B-3. Maximum MSL altitudes and corresponding flight distance B-6

Figure B-4. Maximum MSL altitude and coincident indicated airspeed B-7

Figure B-5. Maximum indicated airspeed and coincident MSL altitude B-7

Figure B-6. *V-n* diagram compared with sea-level limits B-8

Figure B-7. *V-n* diagram compared with sea-level limits (continued) B-9

Figure B-8. *V-n* diagram with speed brake deployed B-10

Figure B-9. Frequency of flap and speed brake deployment B-11

Figure B-10. Number of drops per flight B-12

Figure B-11. Distribution of total drop duration per flight B-12

Figure B-12. Probability distribution of takeoff and landing weights B-13

Figure B-13. Probability distribution of takeoff and landing weights (continued) B-14

Figure B-14. Probability distribution of takeoff and landing airspeeds B-16

Figure B-15. Probability distribution of takeoff and landing airspeeds (continued) B-17

Figure B-16. Maximum and minimum lateral load factor and coincident vertical load factor at landing B-17

Figure B-17. Number of occurrences by duration – cruise 1 B-18

Figure B-18. Correlation of distance and duration – cruise 1 B-18

Figure B-19. Maximum MSL altitude and corresponding distance – cruise 1 B-19

Figure B-20. Maximum MSL altitude and coincident indicated airspeed – cruise 1 B-19

Figure B-21. Maximum indicated airspeed and coincident MSL altitude – cruise 1 B-20

Figure B-22. Number of occurrences by duration – cruise 2 B-20

Figure B-23. Correlation of distance and duration – cruise 2 B-21

Figure B-24. Maximum MSL altitude and corresponding distance – cruise 2 B-21

Figure B-25. Maximum MSL altitude and coincident indicated airspeed – cruise 2 B-22

Figure B-26. Maximum indicated airspeed and coincident MSL altitude – cruise 2 B-22

Figure B-27. Number of occurrences by duration – entry B-23

Figure B-28. Correlation of distance and duration – entry B-23

Figure B-29. Maximum MSL altitude and corresponding distance – entry B-24

Figure B-30. Maximum MSL altitude and coincident indicated airspeed – entry B-24

Figure B-31. Maximum indicated airspeed and coincident MSL altitude – entry B-25

Figure B-32. *V-n* diagram – entry B-26

Figure B-33. Number of occurrences by duration – drop B-27

Figure B-34. Correlation of distance and duration – drop B-27

Figure B-35. Maximum MSL altitude and corresponding distance – drop B-28

Figure B-36. Maximum MSL altitude and coincident indicated airspeed – drop B-28

Figure B-37. Maximum indicated airspeed and coincident MSL altitude – drop B-29

Figure B-38. *V-n* diagram – drop B-29

Figure B-39. Number of occurrences by duration – exit B-30

Figure B-40. Correlation of distance and duration – exit B-30

Figure B-41. Maximum MSL altitude and corresponding distance – exit B-31

Figure B-42. Maximum MSL altitude and coincident indicated airspeed – exit B-31

Figure B-43. Maximum indicated airspeed and coincident MSL altitude – exit B-32

Figure B-44. *V-n* diagram – exit B-33

Figure B-45. *V-n* diagram – exit (continued) B-34

Figure C-1. Cumulative occurrences of incremental vertical gust load factor – cruise 1 C-5

Figure C-2. Cumulative occurrences of incremental vertical maneuver load factor – cruise 1 C-6

Figure C-3. Cumulative occurrences of incremental vertical gust load factor – cruise 2 C-8

Figure C-4. Cumulative occurrences of incremental vertical maneuver load factor – cruise 2 C-9

Figure C-5. Cumulative occurrences of incremental vertical gust load factor – entry C-11

Figure C-6. Cumulative occurrences of incremental vertical maneuver load factor – entry C-12

Figure C-7. Cumulative occurrences of incremental vertical gust load factor – drop C-14

Figure C-8. Cumulative occurrences of incremental vertical maneuver load factor – drop C-15

Figure C-9. Cumulative occurrences of incremental vertical gust load factor – exit C-17

Figure C-10. Cumulative occurrences of incremental vertical maneuver load factor – exit C-18

Figure C-11. Cumulative occurrences of incremental vertical gust load factor, firefighting flights C-20

Figure C-12. Cumulative occurrences of incremental vertical maneuver load factor, firefighting flights C-21

Figure C-13. Cumulative occurrences of incremental vertical gust load factor, ferry flights C-23

Figure C-14. Cumulative occurrences of incremental vertical maneuver load factor, ferry flights C-24

Figure C-15. Cumulative occurrences of incremental vertical gust load factor, maintenance/training flights C-26

Figure C-16. Cumulative occurrences of incremental vertical maneuver load factor, maintenance/training flights C-27

Figure D-1. Cumulative occurrences of incremental vertical gust load factor – cruise 1 D-5

Figure D-2. Cumulative occurrences of incremental vertical maneuver load factor – cruise 1 D-6

Figure D-3. Cumulative occurrences of incremental vertical gust load factor – cruise 2 D-8

Figure D-4. Cumulative occurrences of incremental vertical maneuver load factor – cruise 2 D-9

Figure D-5. Cumulative occurrences of incremental vertical gust load factor – entry D-11

Figure D-6. Cumulative occurrences of incremental vertical maneuver load factor – entry D-12

Figure D-7. Cumulative occurrences of incremental vertical gust load factor – drop D-14

Figure D-8. Cumulative occurrences of incremental vertical maneuver load factor – drop D-15

Figure D-9. Cumulative occurrences of incremental vertical gust load factor – exit D-17

Figure D-10. Cumulative occurrences of incremental vertical maneuver load factor – exit D-18

Figure D-11. Cumulative occurrences of incremental vertical gust load factor – firefighting flights D-20

Figure D-12. Cumulative occurrences of incremental vertical maneuver load factor – firefighting flights D-21

Figure D-13. Cumulative occurrences of incremental vertical gust load factor – ferry flights D-23

Figure D-14. Cumulative occurrences of incremental vertical maneuver load factor – ferry flights D-24

Figure D-15. Cumulative occurrences of incremental vertical gust load factor – maintenance/training flights D-26

Figure D-16. Cumulative occurrences of incremental vertical maneuver load factor – maintenance/training flights D-27

Figure E-1. Cumulative occurrences of derived gust velocity – cruise 1 E-5

Figure E-2. Cumulative occurrences of derived gust velocity – cruise 2 E-7

Figure E-3. Cumulative Occurrences of Derived Gust Velocity – entry E-9

Figure E-4. Cumulative occurrences of derived gust velocity – drop E-11

Figure E-5. Cumulative occurrences of derived gust velocity – exit E-13

Figure E-6. Cumulative occurrences of derived gust velocity, overall firefighting flight with all phases E-15

Figure E-7. Cumulative occurrences of derived gust velocity, ferry flights E-17

Figure E-8. Cumulative occurrences of derived gust velocity, maintenance flights E-19

Figure F-1. Cumulative occurrences of incremental vertical gust load factor, comparison of all firefighting phases F-2

Figure F-2. Cumulative occurrences of incremental vertical maneuver load factor, comparison of all firefighting phases F-2

Figure F-3. Cumulative occurrences of incremental vertical load factor for different missions compared with Boeing 737-400, Airbus A-320, and CAADRP 2 F-3

Figure F-4. Cumulative occurrences of incremental vertical gust load factor for different missions compared with Boeing 737-400 and Airbus A-320 F-3

Figure F-5. Cumulative occurrences of incremental vertical gust load factor for different missions compared with USFS lead airplane F-4

Figure F-6. Cumulative occurrences of incremental vertical maneuver load factor for different missions compared with Boeing 737-400, Airbus A-320, and CAADRP 1 F-4

Figure F-7. Cumulative occurrences of incremental vertical maneuver load factor for different missions compared with USFS P2V and P3A F-5

Figure F-8. Cumulative occurrences of derived gust velocity for different missions compared with commercial operations F-6

LIST OF TABLES

Table	Page
Table 1. Next-generation airtankers	2
Table 2. Airtankers and limitations	3
Table 3. Aircraft limitations	3
Table 4. Available data from 2014–2017	4
Table 5. Channels generated for final analysis	5
Table 6. Flap and speed brake detents	6
Table 7. Files rejected during preprocessing	7
Table 8. Parameter maximum rate of change	9
Table 9. Averages and standard deviations of takeoff and landing weights	14
Table 10. Codes used to flag various anomalies	17
Table 11. MSL and AGL altitude bands	19
Table 12. Flight phase separation criteria	21
Table 13. Estimates of the maximum lift coefficient	25
Table A-1. Effect of data skipping on RMS values of deviation from average acceleration over 128 seconds of sample data	A-11
Table A-2. Cumulative occurrences of incremental vertical gust load factor per 1000 hours	A-20
Table A-3. Cumulative occurrences of incremental vertical maneuver load factor per 1000 hours	A-21
Table B-1. Statistical formats – usage data	B-1
Table B-2. Statistical formats – usage data	B-1
Table B-3. Statistical formats – usage data (continued)	B-3
Table B-4. Summary of flights, durations, and distances	B-5
Table B-5. Frequency of flap and speed brake deflections	B-10

Table B-6. Flight time with flap or speed brake deflection B-11

Table B-7. Takeoff and landing weights B-13

Table B-8.Takeoff and landing indicated airspeeds B-15

Table C-1. Statistical formats – flight loads data by above ground level (AGL) altitude C-1

Table C-2. Statistical formats – flight loads data by AGL altitude C-2

Table C-3. Summary of durations and distances for all firefighting flight phases C-4

Table C-4. Summary of durations and distances – cruise 1 C-4

Table C-5. Summary of durations and distances – cruise 2 C-7

Table C-6. Summary of durations and distances – entry C-10

Table C-7. Summary of durations and distances – drop C-13

Table C-8. Summary of durations and distances – exit C-16

Table C-9. Summary of durations and distances for firefighting flights C-19

Table C-10. Summary of durations and distances for ferry flights C-22

Table C-11. Summary of durations and distances for maintenance/training flights C-25

Table D-1. Statistical formats – flight loads data by mean sea level (MSL) altitude D-1

Table D-2. Statistical formats – flight loads data by MSL altitude D-2

Table D-3. Summary of durations and distances for all firefighting flight phases D-4

Table D-4. Summary of durations and distances – cruise 1 D-4

Table D-5. Summary of durations and distances – cruise 2 D-7

Table D-6. Summary of durations and distances – entry D-10

Table D-7. Summary of durations and distances – drop D-13

Table D-8. Summary of durations and distances – exit D-16

Table D-9. Summary of durations and distances – firefighting flights D-19

Table D-10. Summary of durations and distances – ferry flights D-22

Table D-11. Summary of durations and distances – maintenance/training flights D-25

Table E-1. Statistical formats – derived gust velocities by above ground level (AGL) and mean sea level (MSL) altitude E-1

Table E-2. Statistical formats – derived gust velocities by AGL and MSL altitude E-1

Table E-3. Durations and distances for all firefighting flight phases E-3

Table E-4. Summary of durations and distances – cruise 1 E-4

Table E-5. Summary of durations and distances – cruise 2 E-6

Table E-6. Summary of durations and distances – entry E-8

Table E-7. Summary of durations and distances – drop E-10

Table E-8. Summary of durations and distances – exit E-12

Table E-9. Summary of durations and distances for overall firefighting flights E-14

Table E-10. Summary of durations and distances for overall ferry flights E-16

Table E-11. Summary of durations and distances for overall maintenance/training flights E-18

Table F-1. Statistical formats – comparisons with other sources F-1

LIST OF ACRONYMS

AGL	Above ground level
ASM	Aerial Supervision Modules
CAADRP	Civil Aircraft Airworthiness Data Recording Program
DFDR	Digital flight data recorder
EAS	Equivalent airspeed
FFT	Fast Fourier Transform
FIR	Finite impulse response
GAG	Ground-Air-Ground
GPS	Global Positioning System
IAS	Indicated Airspeed
KIAS	Knots Indicated Airspeed
MSL	Mean sea level
NED	National Elevation Dataset
NTSB	National Transportation Safety Board
OLM	Operational Loads Monitoring
RMS	Root mean squared
TAS	True Airspeed
USFS	United States Forest Service
V_{MO}	Maximum Operating Speed
WSU	Wichita State University

EXECUTIVE SUMMARY

This report covers the first phase of a three-year effort by Wichita State University (WSU) to examine airframe usage and to analyze flight loads from a fleet of next-generation airtankers used for aerial firefighting. United States Forest Service (USFS) funded this effort through Federal Aviation Administration (FAA) as an element of its Operational Loads Monitoring (OLM) program.

Phase I involves using the data collected by a new generation of digital flight data recorders (DFDRs) installed on a fleet of BAe-146-200 and Avro RJ-85A airframes modified as heavy airtankers. The recorded data was collected by the USFS and stored in a central repository managed by HBM-nCode Federal, LLC. This data was made available to WSU for further analysis.

The fleet consists of eight BAe-146-200 and eight Avro RJ-85A airframes, operated by two different companies. These aircraft were all equipped with IONode™ DFDRs supported by Latitude Technologies Corporation. These recorders had a larger number of channels than those previously used, and, therefore, provided more detailed information concerning airframe usage.

The recorded data consists of basic flight parameters, such as airspeed, altitude, and flight and drop durations. In addition, some systems' usage, such as flap and airbrake deployment, were quantified. Analysis of the recorded material resulted in usage information, presented in statistical format. The formats used for presentation of the results were kept consistent with past practices. These results were developed for individual phases of flight, as well as for the entire Ground-Air-Ground (GAG) cycles.

Since data was acquired at 32 Hz, the presence of structural modes in normal acceleration was detected. The effectiveness of several filters at eliminating the extraneous load factors was investigated. An eighth-order Butterworth filter with an 8-Hz cutoff frequency was deemed to be the most robust choice.

Vertical load factors were separated into gust and maneuver loads using the two-second rule. For each load type, exceedance spectra were developed for each phase of flight, including each GAG cycle for various altitude bands. As seen in previous low-altitude operations, the frequency of occurrence of the loads correlated better with altitude above ground level than it did when divided by altitude relative to mean sea level.

The statistical formats used in this report were developed previously for other investigations associated with the OLM projects. As such, they offer a convenient means of comparing the results with the operational limitations of the aircraft and those from other aircraft. Operators can use these results to better understand factors that affect the structural integrity of these airframes. Likewise, the results enable aircraft manufacturers to better understand the actual airframe usage and loads. Finally, this information can be used to refine regulations concerning the design of these aircraft.

1. INTRODUCTION

As a result of the investigation of two in-flight airframe failures of heavy airtankers, the National Transportation Safety Board (NTSB) issued Recommendation A-04-29 [1]. In this document, the NTSB recommended for the United States Forest Service (USFS) to:

"... develop maintenance and inspection programs for aircraft that are used in firefighting operations that take into account and are based on: 1) the airplane's original design requirements and its intended mission and operational life; 2) the amount of operational life that has been used before entering firefighting service; 3) the magnitude of maneuver loading and the level of turbulence in the firefighting environment and the effect of these factors on remaining operational life ..."

In response, the USFS started requiring operators to install digital flight data recorders (DFDRs) on aircraft in firefighting service and make the data available to the USFS for further processing and analysis [2]. Presently, this data is collected methodically and is stored in a central repository, accessible to the USFS and the operators. The latter group can use the stored data for refining their procedures and for training the pilots and the crew. At the same time, the USFS uses the data to determine the statistical usage of the airframes, and to develop flight loads spectra for comparison with the airframes' design standards and operating limitations. If needed, regulating agencies also can use the results of such analysis to refine the standards governing such operations.

The USFS prioritized the analysis of flight data according to criticality, starting with legacy heavy airtankers, which were under immediate scrutiny. At the time, these aircraft consisted of P2V and P3A airframes that were retired from their military roles. The statistical usage and flight loads spectra of these airtankers were presented in references [3] through [5], culminating in a formal FAA report. While additional data was being collected from heavy airtankers, the focus was shifted to smaller aircraft used as lead planes, as Aerial Supervision Modules (ASM), and for Air Tactical Group Supervision. Some of the results of this phase were presented in references [6] through [8]. Currently, the final report for this effort is under review and awaiting publication [9].

In 2012, the USFS and the Department of the Interior concluded that the large airtanker fleet must be replaced with newer, faster, and more cost-effective aircraft [10]. At this writing, most of the legacy heavy airtanker fleet was decommissioned and then replaced with more modern airframes. Table 1 summarizes the current state of the large airtanker fleet.

Large next-generation airtanker missions are defined as those that deliver 3,000-5,000 gallons of retardant to the fire [11]. The Bombardier CL-415 is a water scooper and is the only airplane included in Table 1 that was built specifically for firefighting. Having a retardant capacity of 1500 gallons places it outside the large airtanker category. Nonetheless, it is included among the next-generation airtankers because additional airframes were acquired and placed into service by the operator. The DC-10, due to its very large retardant capacity, is categorized as a Very Large Air Tanker.

Table 1. Next-generation airtankers

Operator	Type	Retardant Capacity (gal)	Number of Airtankers
Neptune	BAe-146-200	3,000	8
Aero-Flite	Avro RJ-85A	3,100	8
Aero-Flite	Bombardier CL-415	1,500	4
Erickson	Boeing MD-87	4,000	5
10-Tanker	Boeing DC-10-10/30	11,600	4
Coulson	Lockheed EC130Q	4,000	1
Coulson	Lockheed 382G	4,000	2

In 2015, the USFS, through the FAA, supported an exploratory study of the next-generation airtankers conducted by the Flight Loads Group at WSU. The main goal of this project was to perform a preliminary analysis of their usage and flight loads, and to assess the feasibility of a logical grouping of these aircraft for future analysis. The secondary goal was to examine the quality of the data recorded by the DFDRs.

The preliminary investigation revealed that the next-generation airtankers could be divided into three groups for further analysis. This division was based on timing and availability of sufficient data for meaningful statistical analysis, as well on the specific airframes' characteristics. The first group, consisting of BAe-146-200 and Avro RJ-85A (hereinafter referred to as BAe-146 and RJ-85) airframes, are the subject of the present report. These two airframes are based on the same design and have a large amount of flight data already collected. The original intent also was to include data from the MD-87 fleet. However, data collection on these aircraft was halted between late 2015 and mid-2017. There also was some concern that the configuration layout could affect the flight loads spectra, as implied in reference [12]. Therefore, the first phase of this project was limited to the analysis of airframe usage and flight loads spectra of BAe-146 and RJ-85 airframes. The data used for this analysis was collected from mid-2014 on RJ-85 and mid-2015 on BAe-146 to the end of 2017. Because of the similarity between the two airframes, results from the two are combined in this report.

2. AIRCRAFT DESCRIPTION

Table 2 lists the aircraft characteristics for both the BAe-146 and the RJ-85. Table 3 shows the aircraft limitations, per reference [13]. The two airframes were essentially identical except for their gross takeoff weights and the installation of the retardant tank. On BAe-146, the retardant tank was internal, while an external conformal tank was used on RJ-85.

Table 2. Airtankers and limitations

Parameter	BAe-146	RJ-85
Gross Takeoff Weight (lb)	91,700	97,000
Full Fuel Weight* (lb)	15,000	18,000
Maximum Retardant* Weight (lb)	27,000	28,000
Maximum Retardant* (gallons)	3,000	3,100
Wing Span (ft)	86.4	
Wing Area (square ft)	832	
Overall Length (ft)	93.7	

*These may be slightly different from actual values

Table 3. Aircraft limitations

Parameter	BAe-146	RJ-85
Indicated Airspeed with Flaps (KIAS)		
Up (V_{MO})	295	300
18 deg. (Takeoff, Approach)	210	215
18 deg. (Low-Speed Hold)	175	175
24 deg. (Takeoff, Approach, Climb)	180	180
30 deg. (Takeoff)	170	170
33 deg. (Landing)	145	150
Load Factors (g)		
Flaps Retracted	-1.0/+2.5	-1.0/+2.5
Flaps Extended	0.0/+2.0	0.0/+2.0
Maximum Operating Altitude (ft)		
Flaps Retracted	30,000	31,000[1]/35,000[2]
Flaps Extended	14,000	14,000
Max. Cabin Pressure Differential (psi)	6.55	6.55

1. 12/5/1996 Revision
2. 4/21/1997 Revision
KAIS = Knots Indicated Airspeed

3. DATA COLLECTION

3.1 FLIGHT DATA RECORDER

All aircraft were equipped with IONode™ DFDRs supported by Latitude Technologies Corporation. These recorders had a larger number of channels than those previously used, and, therefore, provided more detailed information concerning airframe usage. The recorded data was processed by Latitude software. Several channels were added in this step, such as calculation of true and equivalent airspeeds and aircraft weight. The data was then stored in a uniform 32-Hz format on the HBM-nCode library. This information was downloaded in .CSV format by the WSU team for further analysis.

3.2 AVAILABLE DATA

Table 4 shows the amount of data from each airframe that was available for analysis at the end of 2017. While the airframes are identified individually in this table, for the final presentation, the results were combined. Not all files contain flight information, as shown in this table. Also, not all files were useful for analysis due to data integrity issues discussed later.

Table 4. Available data from 2014–2017

	Number of Files				Files Containing Flights			
Tanker	2014	2015	2016	2017	2014	2015	2016	2017
1	---	163	951	377	---	158	533	325
2	---	133	167	347	---	133	120	268
3	---	---	312	545	---	---	209	463
4	---	3	322	350	---	3	185	304
5	---	233	809	305	---	225	382	239
6	---	---	---	378	---	---	---	313
7	---	202	500	393	---	185	288	322
8	---	313	633	473	---	258	319	415
Total BAe-146	---	1,047	3,694	3,168	---	962	2,036	2,649
9	101	6	172	534	100	6	165	526
10	99	---	264	64	93	---	242	60
11	9	---	498	431	9	---	498	418
12	---	20	302	503	---	20	299	501
13	---	3	234	429	---	2	179	428
14	---	---	144	266	---	---	105	262
15	---	---	99	109	---	---	88	100
16	---	---	---	434	---	---	---	430
Total RJ-85	209	29	1713	2770	202	28	1576	2725

4. WICHITA STATE UNIVERSITY DATA PROCESSING

4.1 PREPROCESSING

Preprocessing of the data was performed in two phases, resulting in information needed for final analysis.

4.1.1 Unified Data Format

Depending on the aircraft and the fire season, the recorded data varied in format. Therefore, a common set of channels was identified first. Then a preprocessor was developed for each aircraft

and each unique data format. These codes would use the recorded data as input and produce output data in a uniform format for all aircraft under consideration. These output data were written in 32-Hz format throughout and resembled that used in previous analyses. Where necessary, the original data was examined to verify apparent anomalies. Table 5 shows the channels that were output by the preprocessors.

Other tasks performed while generating a uniform data format were ensuring uniformity of the binary format for the squat switch and the bay doors. Furthermore, flap and speed brake/spoiler deflections, which were recorded in percentages or degree, were placed into detents according to the values shown in Table 6.

Table 5. Channels generated for final analysis

Channel	Parameter	Channel	Parameter
1	Line Number	17	Yaw Rate (degrees per second)
2	Elapsed Time (seconds)	18	Dynamic Pressure (psf)
3	Latitude (degrees)	19	Static Pressure (psf)
4	Longitude (degrees)	20	Outside Air Temperature (F)
5	Heading (degrees)	21	Cabin Pressure Diff (psi)
6	GPS Elevation (feet)	22	Indicated Airspeed (KIAS)
7	Pressure Altitude (feet)	23	Equivalent Airspeed (KEAS)
8	GPS Ground Speed (knots)	24	True Airspeed (KTAS)
9	Vertical Speed (feet per minute)	25	Weight on Wheels (binary)
10	Longitudinal Acceleration (g)	26	Flap Deflection (detent)
11	Lateral Acceleration (g)	27	Speed Brake (detent)
12	Normal Acceleration (g)	28	Bay Door (binary)
13	Pitch (degrees)	29	Fuel Quantity[1] (pound)
14	Pitch Rate (degrees per second)	30	Retardant Quantity (pound)
15	Roll (degrees)	31	Instantaneous Weight[1] (pound)
16	Roll Rate (degrees per second)	32	Terrain Elevation[2] (feet)

1. Not available in all data files
2. Obtained during preprocessing
GPS = Global Positioning System

Table 6. Flap and speed brake detents

Detent	Flap/Speed Brake Deployment
0	Flaps < 10 degrees
1	10 < Flaps < 20 degrees
2	20 < Flaps < 26 degrees
3	Flaps > 26 degrees
4	20% < Speed Brake/Spoiler < 50%
5	50% < Speed Brake/Spoiler < 75%
6	75% < Speed Brake/Spoiler

4.1.2 Missing Data

Many files contained missing data appearing as "-1.#IND". When the preprocessor encountered this during airborne phases, that line of data was replaced with the values of the immediately preceding line. If more than 100 consecutive lines had to be replaced, the entire flight was rejected as having too many missing lines. No limit was used on the number of replaced lines for ground phases, or if they occurred non-consecutively during airborne phases. Table 7 shows the number of files that were rejected due to this issue. Files marked as containing flight in Table 4 are those that were eventually used for analysis.

4.1.3 Missing Airspeeds

In a number of cases, none of the airspeeds were present in the recorded data. In such cases, the GPS speed was used in place of indicated airspeed and the substitution was flagged in the output. The associated results were omitted in postprocessing in cases where indicated airspeed was of interest, such as in *V-n* diagrams.

Table 7. Files rejected during preprocessing

Tanker	Number of Files			
	2014	2015	2016	2017
1	0	0	0	0
2	0	0	3	3
3	0	0	0	0
4	0	0	0	0
5	0	7	5	0
6	0	0	0	1
7	0	2	8	3
8	0	3	1	1
Total BAe-146	0	12	17	8
9	1	0	31	0
10	1	0	16	0
11	0	0	17	6
12	0	0	24	3
13	0	0	10	0
14	0	0	0	1
15	0	0	0	2
16	0	0	0	1
Total RJ-85	2	0	98	13

4.1.4 Obtaining Terrain Elevation

Previous research [9] demonstrated clear correlation of the flight loads spectra with altitude above ground level (AGL). However, this information was not part of the recorded data. Therefore, the aircraft GPS coordinates were used to obtain the terrain elevation using the National Elevation Dataset (NED) that is maintained by US Geological Survey. From reference [14],

> *NED data are available nationally (except for Alaska) at resolutions of 1 arc-second (about 30 meters) and 1/3 arc-second (about 10 meters), and in limited areas at 1/9 arc-second (about 3 meters). In most of Alaska, only lower resolution source data are available. As a result, most NED data for Alaska are at 2-arc-second (about 60 meters) grid spacing. Part of Alaska is available at the 1- and 1/3-arc-second resolution, and plans are in development for a significant improvement in elevation data coverage of the state.*

Querying NED for terrain elevations proved to be the most time-consuming part of the data preprocessing. Due to the enormous number of lines in each data file, it proved to be impractical

to obtain the terrain elevation for every time step. Instead, ground elevation was retrieved for every second of flight (i.e., every 32 lines) and interpolated between. It was reasoned that for the purpose of the present analysis, and in light of the inherent resolution of NED, this would result in AGL altitudes with sufficient fidelity. Nonetheless, processing of each flight file required approximately eight minutes of uninterrupted online communication with the NED website.

Some flights took place outside of the United States where terrain elevation could not be obtained. In these cases, the terrain elevation was set to -1000000 ft and the output was flagged as not having correct ground elevation. Once ground elevation was obtained and interpolated, it was added to the flight file as the 32nd column, as shown in Table 5. Files that did not contain airborne segments were skipped.

4.2 DATA CONDITIONING

4.2.1 Normalizing Vertical Load Factor

Values of vertical acceleration were averaged for all instances when the aircraft was on the ground. The average was used to remove any bias in all recorded values in that file.

4.2.2 Removing Data Spikes

In some cases, rapid changes in the squat switch signal flagged false takeoffs or landings. These spikes were removed if they did not match the signal with those from one second before *and* after. One example is shown in Figure 1, where the signal changes seven times in less than five seconds. However, this strategy did not work in those cases, where the signal prevented clear identification of the airborne segments. Such files were excluded from analysis.

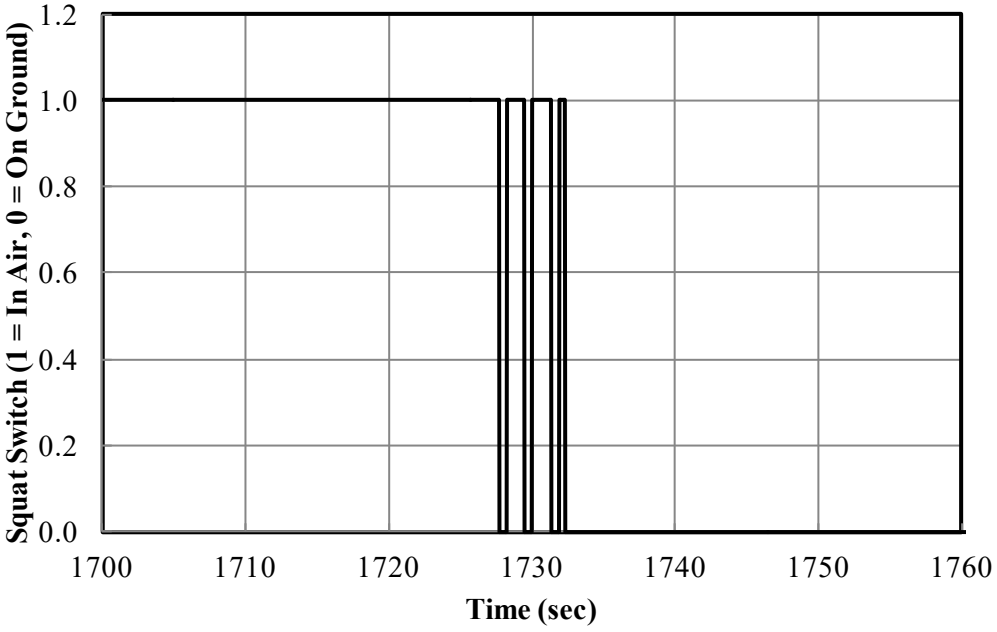

Figure 1. Example of noise in squat switch signal

Additionally, if the rate of change of an analog parameter over one time step exceeded a prescribed level, the second value was treated as a spike. This was observed routinely in some pressure-related information, as shown in Figure 2. Spikes were removed by replacing their values with that of the preceding line. Removal of a spike from any parameter was flagged in the output. Table 8 shows the prescribed maximum rate of change for various parameters. Spike removal was applied only to these parameters.

Table 8. Parameter maximum rate of change

Parameter	Maximum Rate of Change
GPS Altitude (ft)	10,000 ft/s
Pressure Altitude (ft)	10,000 ft/s
Average Altitude (ft)	10,000 ft/s
Dynamic Pressure (psf)	100 psf/s
Static Pressure (psf)	1,000 psf/s
Outside Air Temperature (F)	100 F/s
Cabin Pressure Differential (psi)	10 psi/s
Airspeeds (IAS, TAS, EAS) (knots)	500 knots/s

EAS = Equivalent airspeed, IAS = Indicated Airspeed, TAS = True Airspeed

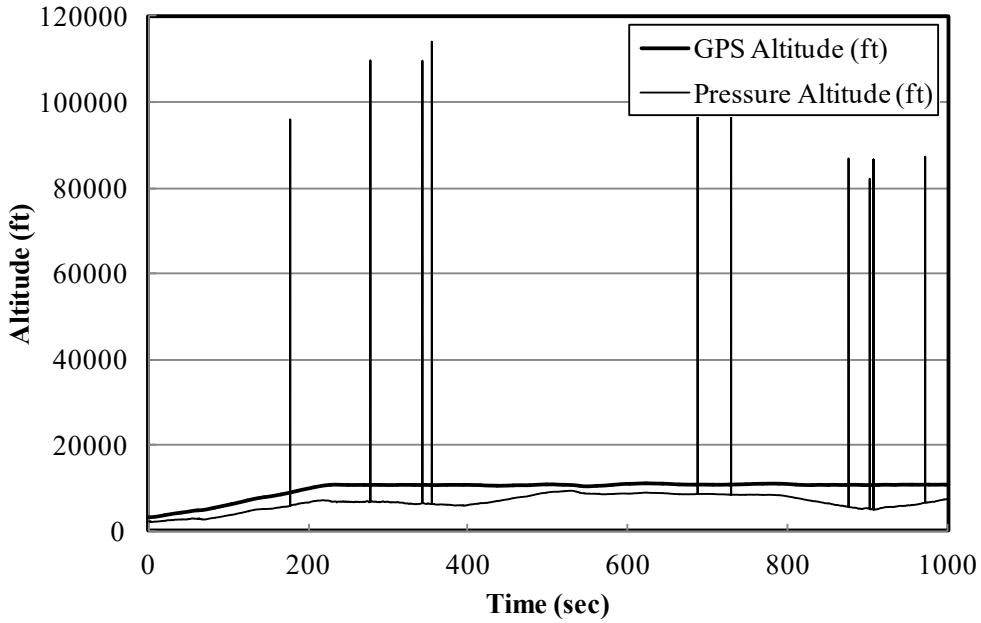

Figure 2. Example of spikes in recorded data

4.2.3 Filtering Vertical Load Factor

Frequency analysis of the data collected at 32 Hz shows the presence of what appeared to be structural modes in the recorded vertical acceleration. Figure 3 shows an example of a short climb segment. Two recorders onboard the same airframe collected the data—one recorded at 8 Hz; the second, at 32 Hz. The frequency of 0.5 Hz corresponds to the limit separating gust and maneuver load factors, which also is delineated in this figure.

Figure 3 shows the presence of higher frequencies in the 32-Hz data. However, on a transport aircraft, the lowest wing-bending mode has a frequency in the range of 3-10 Hz. Therefore, it is doubtful that frequencies above 12 Hz can be attributed to gust loads. For the purpose of developing maneuver and gust loads spectra, these higher frequencies had to be filtered, otherwise, they would result in an excessive number of counts in the latter. However, some results could still be reasonably questioned, even after filtering the higher frequencies (see example in Figure 4).

After examining the effects of various filtering schemes on the flight loads spectra, it was decided to use an eighth-order Butterworth filter with a cutoff frequency of 8 Hz. Appendix A provides the details leading to this choice. Employing this filter required transferring the data into the frequency domain using a Fast Fourier Transform, which, in turn, required the number of lines to be a power of 2. Therefore, data was processed in groups of 4096 lines, truncating the remainder. At a sample rate of 32 Hz, the results ignored at most the last 128 seconds of a flight file. Also, for this reason, files shorter than 8192 lines were not processed.

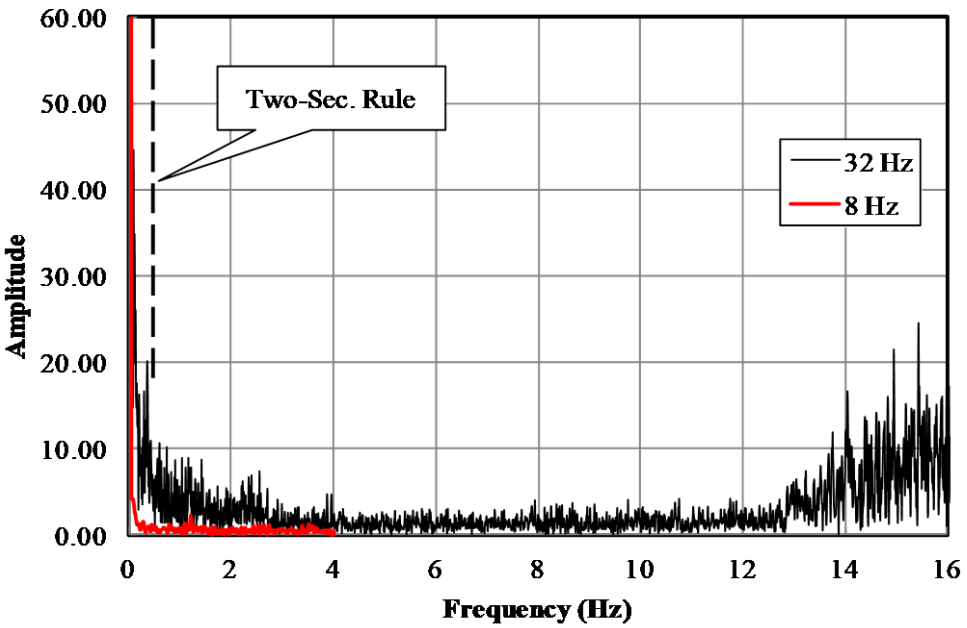

(a)

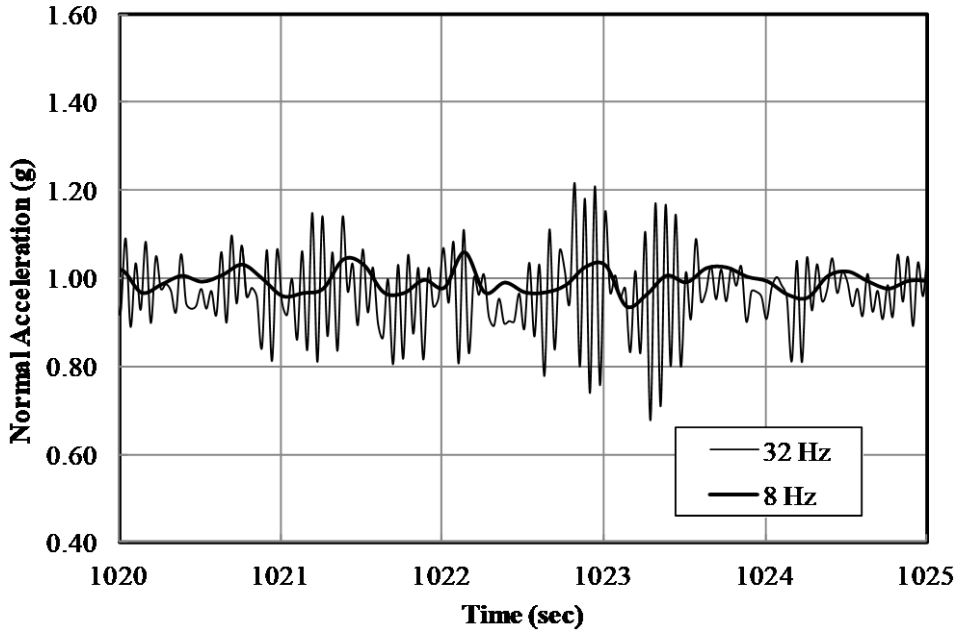

(b)

Figure 3. Normal acceleration showing contribution of structural modes (a) frequency content (b) close-up view of time history

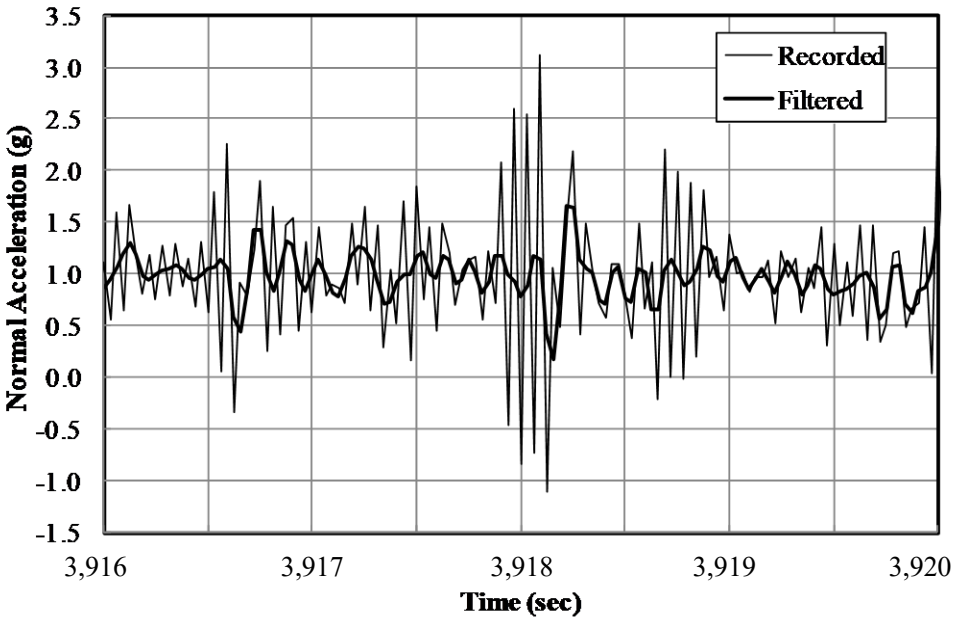

Figure 4. An example of filtered normal acceleration

4.2.4 Smoothing of Noisy Signals

Pressure altitude, cabin pressure, outside air temperature, and dynamic pressure were extremely noisy. These values were replaced by their two-second central averages.

4.2.5 Takeoff and Landing

Takeoffs and landings were marked by a change in squat switch signal if it remained in the new state for three seconds. If the flight was missing the takeoff portion, the first minute of the file was replaced by a simulated ground phase. If the file ended while the airplane was still in the air, the last minute was replaced by a simulated ground phase.

4.2.6 Weight Estimation

The aircraft weight entered into the calculations only in determining the derived gust velocities. Much of the data collected in 2014-2016 did not include instantaneous aircraft and fuel weights. In these cases, attempts at estimating the weight were unsuccessful due to large uncertainties in takeoff and landing weights, especially for flights other than firefighting missions. This can be seen in the form of very large standard deviations shown in Figure 5, with associated values given in Table 9. Therefore, derived gust velocities were estimated only in those cases where the weight was a recorded parameter. Due to an error while storing the weights in the nCode library, all RJ-85 flights were eliminated from these calculations.

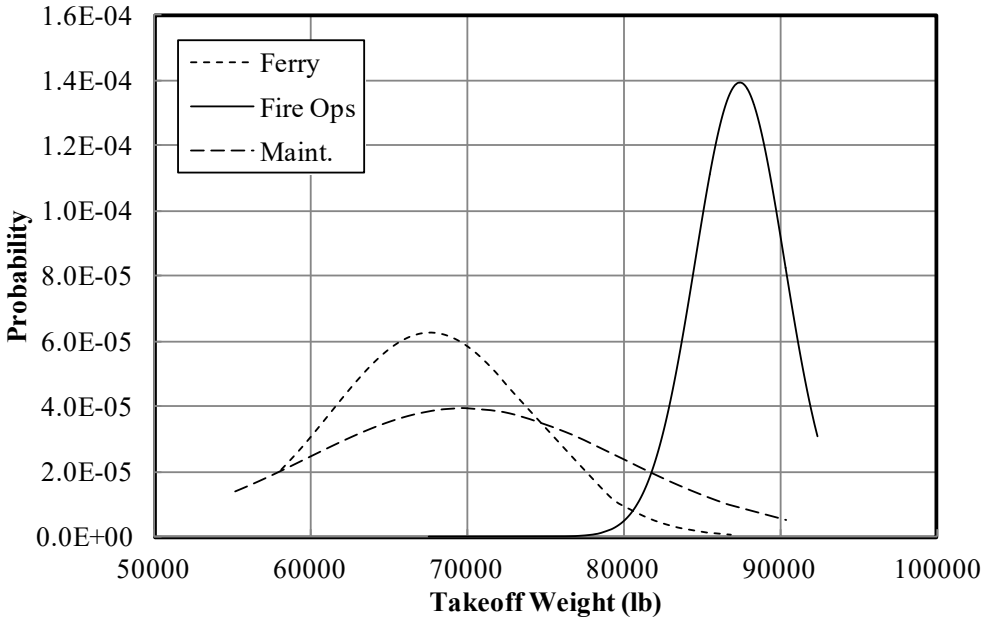

(a)

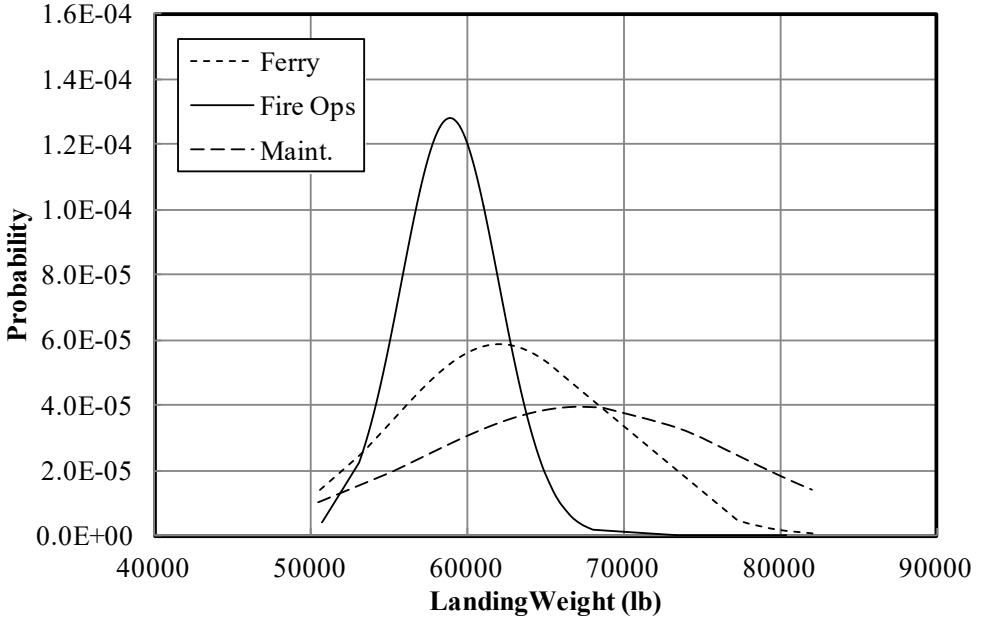

(b)

Figure 5. Probability distribution of takeoff and landing weights (a) takeoff weight (b) landing weight

Table 9. Averages and standard deviations of takeoff and landing weights

Mission	Takeoff Weight (lb)		Landing Weight (lb)	
	Average	St. Dev.	Average	St. Dev.
Ferry	67,638	6,389	62,095	6,778
Firefighting	87,447	2,867	58,883	3,110
Maint.	69,767	10,056	67,314	10,152

4.2.7 Other Data Integrity Issues

There were other errors and anomalies in the data that rendered the information suspect and not useful in many cases.

In a few cases, extremely high values of indicated, true, and equivalent airspeeds were detected. A closer examination of the flight files showed what appeared to be drifting airspeed values. Figure 6 shows an example where indicated airspeed stabilized at 450 KIAS. From this figure it is evident that even before reaching unreasonable values, the recorded indicated airspeed was erroneous. Flight files with this detected behavior were separated manually and eliminated from the results pertaining to airspeed. While flight files with extreme values, as shown in this figure, could be eliminated from the results in postprocessing, automatic detection of such erroneous recordings was not possible.

Also, there were many cases where unreasonably high differences between GPS speed and true airspeed were present. Differences greater than 50 knots were flagged in the output. Slightly over 27% of the flights did not have reliable indicated airspeeds. These flights were removed from analysis in those cases where this parameter was of interest. At this writing, representatives from Latitude have not offered a reason for erroneous airspeeds.

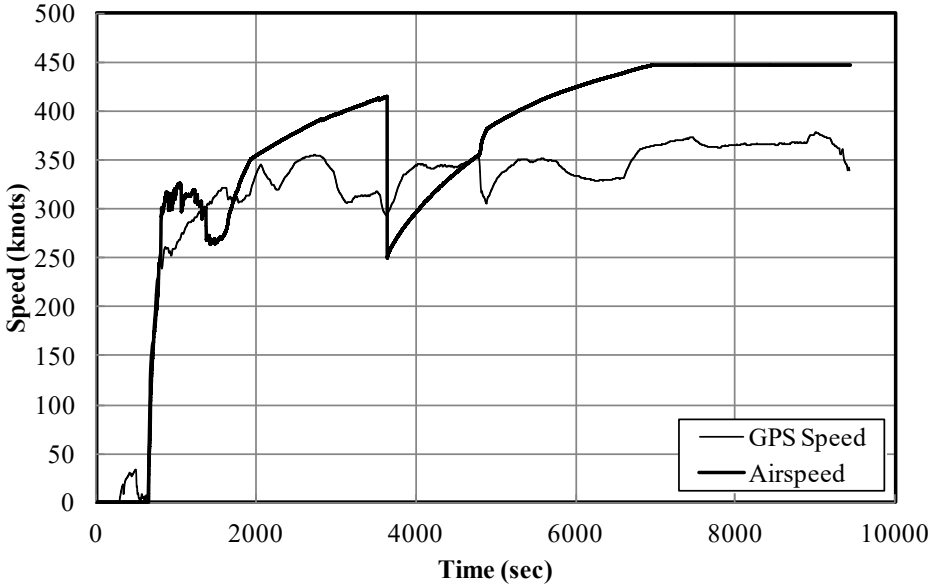

Figure 6. Example of drifting airspeed

In addition to the spikes in pressure altitude that were previously discussed, its recorded values differed significantly from the GPS altitude in a relatively large number of cases. Figure 7 shows an example in which comparison of the terrain elevation with the two altitudes proved the pressure altitude to be the one in error. It is unclear if such errors in the pressure altitude also impacted the accuracy of the recorded airspeeds, as shown for the same flight in Figure 8. Therefore, pressure altitude was not used in any of the analyses.

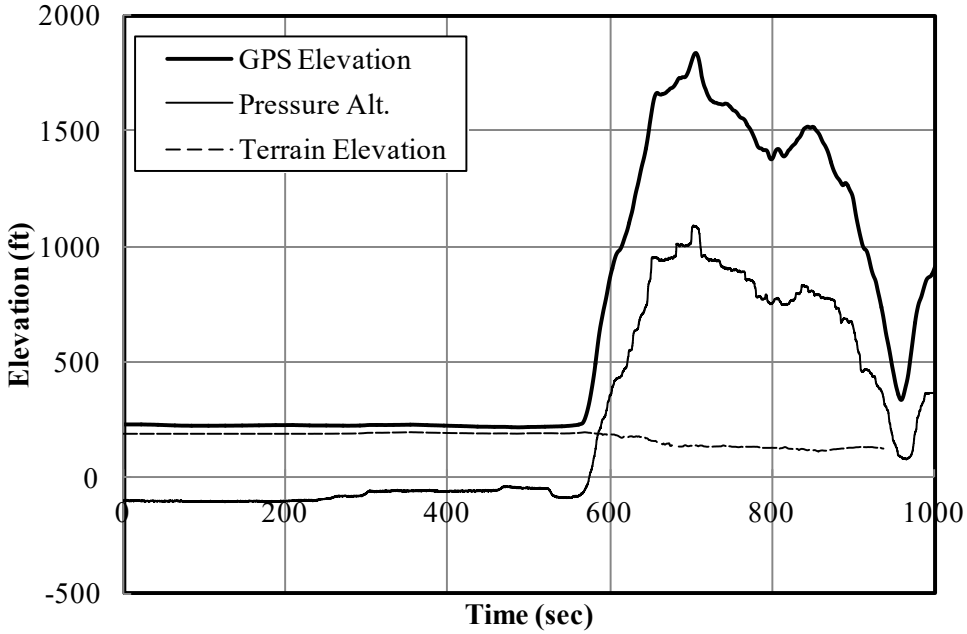

Figure 7. Example of erroneous pressure altitude

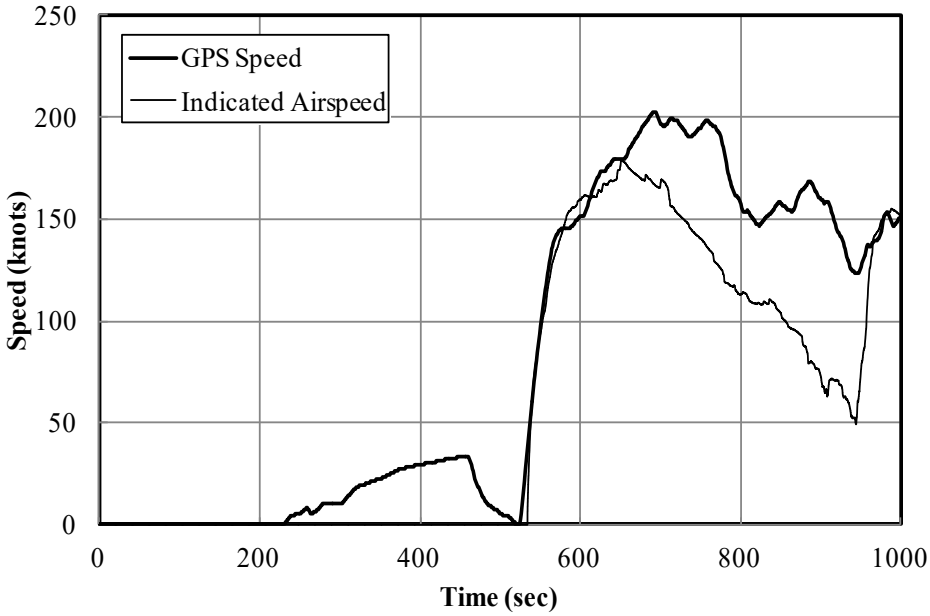

Figure 8. Example of erroneous airspeed

Another issue that appeared in many of the earlier flight files was apparent drifting of the pitch-and-roll attitude gyroscopes (see Figure 9). Files with this behavior were identified and removed from analysis. However, since this was a manual process, it is not clear if all such cases were captured. Representatives from Latitude indicated that this drifting of the gyroscopes was due to electromagnetic interference in the earlier years and that the issue was resolved in 2017. However, even in the 2017 data, there were cases where the recordings of these parameters appeared suspect. For this reason, no statistical analysis was performed of maximum/minimum pitch-and-roll angles. The remainder of the recorded data, such as the acceleration and air data, appeared to be unaffected.

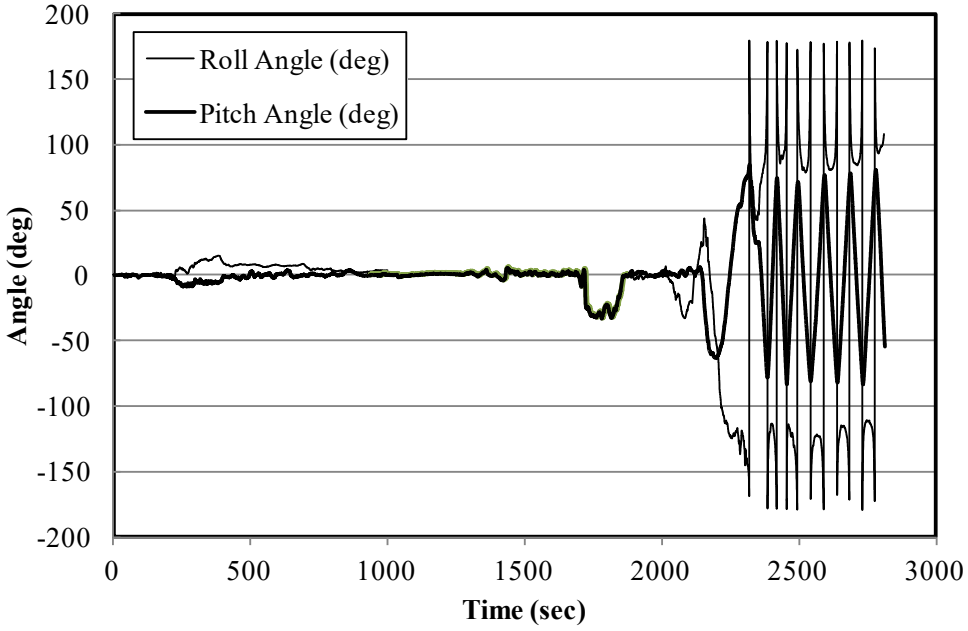

Figure 9. Example of drifting attitude indications

Due to many reasons already discussed, approximately 200 flight files were blocked from analysis, leaving slightly under 10,000 flight files to use. However, again, not all files provided useful information in every case. For example, because of the absence of information on terrain elevation, no AGL analysis could be performed for flights outside of the United States. Another example was the absence of indicated airspeed in a large of number of files, which prevented comparing this parameter with the airframe limitations. Therefore, a system of flags was devised to identify various anomalies. These codes were included in the output files, allowing the removal of suspect data from postprocessing where appropriate. Table 10 describes these codes.

It should be noted that CODE(4) was for identification of flight type, which does not qualify as an anomaly. This parameter assisted in grouping the results according to the missions flown. If a retardant drop was detected, the flight was marked as a firefighting mission. If no drops were detected and takeoff and landing points were more than 20 miles apart, the flight was marked as a ferry. This distance was obtained from the differences in the latitude and longitude, according to the method outlined in Appendix BAPPENDIX B—USAGE DATA PRESENTATION of

reference [15]. If no drop was detected and the takeoff and landing points were closer than 20 miles, the flight was assumed to be a maintenance/training flight.

Table 10. Codes used to flag various anomalies

Code	Interpretation
CODE(1) Airspeed	IAS = Recorded IAS IASD = |GPS speed – TAS| > 50 knots GPS = Missing IAS, GPS speed used instead
CODE(2) Spikes in Data Values	YES = Some spikes were removed NO = No spikes were present in the data
CODE(3) Terrain Elevation	YES = Available from NED NO = Unavailable from NED (set to -1000000)
CODE(4) Flight Type	FF = Firefighting flight FERY = Ferry flight MAIN = Maintenance flight
CODE(5) Aircraft Weight	REC = Recorded weight EST = Missing weight, estimated based on flight type
CODE(6) Complete Flight or Not	COM = Complete flight INC = Incomplete flight, missing takeoff or landing

4.3 DERIVED AND EXTRACTED PARAMETERS

4.3.1 Flight Duration and Distance

The flight duration was defined as the time from liftoff to touchdown. The flight distance was determined from integration of the GPS airspeed.

4.3.2 Sign Convention

Acceleration data was recorded in three directions: normal (z), longitudinal (x), and lateral (y). As shown in Figure 10, the positive z direction is up, and the positive x direction is forward.

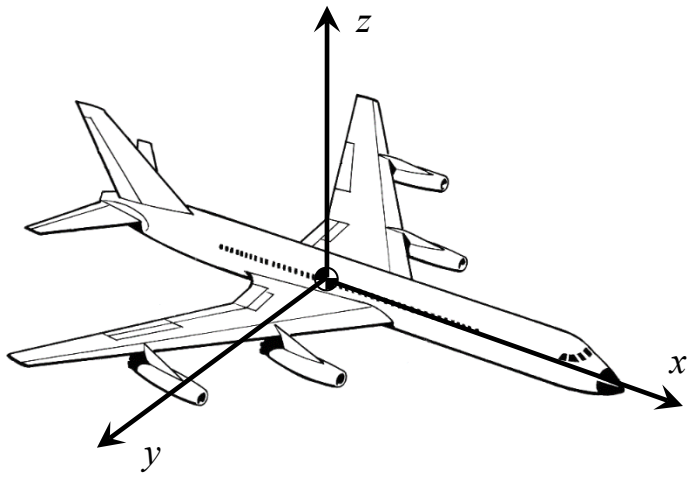

Figure 10. Sign convention for airplane accelerations

4.3.3 Peak and Valley Selection

Consistent with past practices, the peak-between-means method of reference[16] was used to select the peaks and valleys in the vertical acceleration. In this method, only one peak or valley is counted between two successive crossings of the mean. Figure 11 shows this schematically. A threshold zone (dead band) of ±0.05 g was used in the data reduction to omit irrelevant load variations around the mean. The same dead band values were used for gusts and maneuvers.

4.3.4 Separation of Maneuver and Gust Load Factors

Incremental vertical accelerations were separated into gust and maneuver loads using the two-second rule of reference [17]. This method was developed using data from a fleet of B-737 and MD-82/83 aircraft, and was deemed appropriate for the airframes under consideration. Therefore, a peak or a valley in the incremental load factor that lasted two seconds or longer was classified as a maneuver load.

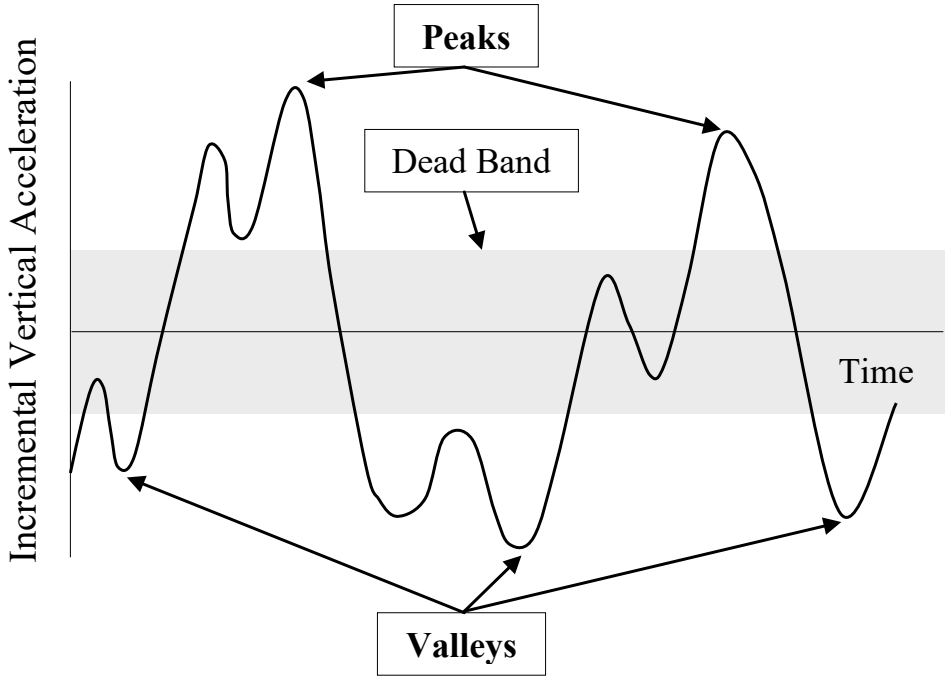

Figure 11. Peak-between-means classification of loads

Cumulative occurrences of incremental load factor were determined per nautical mile and per 1000 hours for Ground-Air-Ground (GAG) cycles. Flights were divided into phases and loads spectra were developed for each phase, as well as for the entire flight, for various altitude bands. Table 11 shows the altitude bands used. The same values were used for AGL and mean sea level (MSL) altitudes.

Table 11. MSL and AGL altitude bands

Bands	Altitude (ft)
1	< 500
2	501 – 1500
3	1501 – 4500
4	4501 – 9500
5	9501 – 14,500
6	14,501 – 19,500
7	19,501 – 24,500
8	> 24,501

4.3.5 Phases of Flight

The analysis was limited to airborne segments of each mission. Firefighting flights were divided into the following five phases:

- Cruise 1 — One minute after takeoff, climb to altitude and cruise to the drop zone

- Entry — Preparation for drop, including brief loiter and descent into the drop site
- Drop — The time when the retardant is leaving the aircraft
- Exit — Climbing out immediately following the drop
- Cruise 2 — Return trip to base until one minute before landing

Figure 12 shows these flight phases schematically in a time history of the altitude. Also, Figure 13 presents a typical flight time history, showing two drops, for comparison. The short cruise segments between drops were not included in flight phase analyses, but were part of the overall GAG cycle. Table 12 further elaborates on flight phase separation criteria. In cases of ferry and maintenance/training flights, only the overall GAG cycle was considered. The one minute after takeoff and before landing were not included.

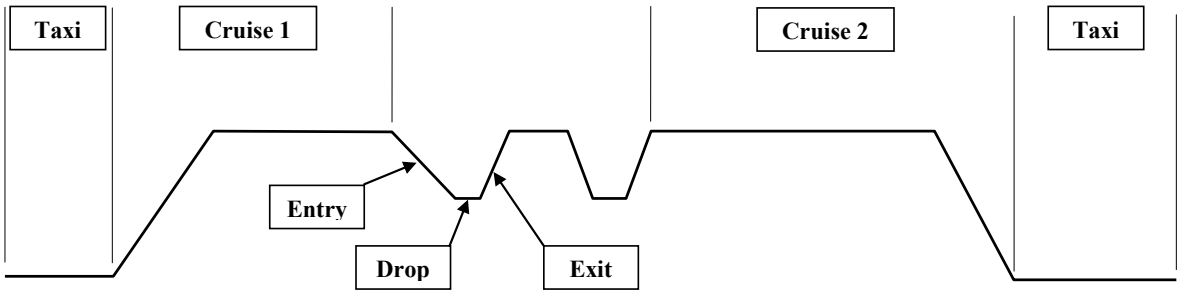

Figure 12. Schematic of various flight phases

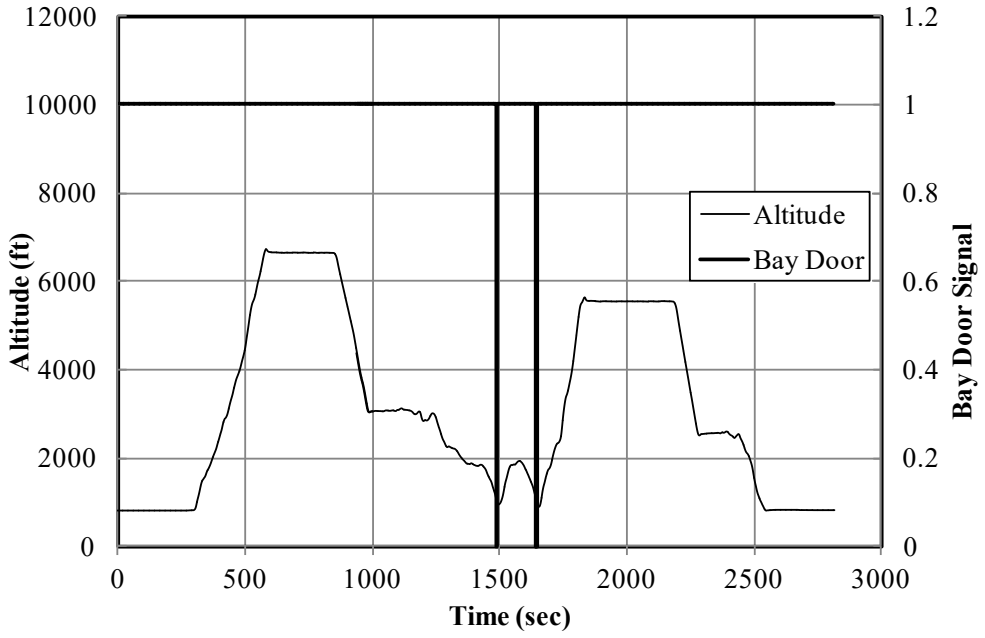

Figure 13. A typical flight time history with two drops

Table 12. Flight phase separation criteria

Flight Phase	Start Time (t_1) Identification	Stop Time (t_2) Identification
Cruise 1	One minute after takeoff	Three minutes before the start of the first drop
Entry	Flaps lowered prior to start of the drop or three minutes before the opening of the first bay door	Opening of the first bay door
Drop	Opening of the first bay door	Closing of the last bay door plus 0.5 second
Exit	End of the drop	Two flap movements after the end of the drop or ninety seconds past the end of the drop
Cruise 2	Three minutes past the end of the last drop	One minute before landing

4.3.6 Derived Gust Velocities

Derived gust velocities were calculated from measured normal accelerations, only for vertical gusts.

$$U_{de} = \frac{\Delta n_z}{\overline{C}} \tag{1}$$

where:

U_{de} = derived gust velocity (ft/s)

Δn_z = incremental vertical load factor (g)

The aircraft response factor, $\overline{C}$, was calculated from

$$\overline{C} = \frac{\rho_0 V_e C_{L_\alpha} S}{2W} K_g \tag{2}$$

where:

ρ_0 = 0.002377 slug/ft^3, standard sea level air density

V_e = equivalent airspeed (ft/s)

C_{L_α} = aircraft lift-curve slope (per radian)

S = wing reference area (ft^2)

W = instantaneous aircraft weight (lb)

$K_g = \frac{0.88\mu}{5.3+\mu}$, gust alleviation factor

$\mu = \frac{2W}{\rho g \bar{c} C_{L_\alpha} S}$, reduced mass

ρ = air density at altitude from equation 3 (slug/ft^3)

g = 32.17 ft/s^2, acceleration of gravity

$\bar{c}$ = wing mean geometric chord (ft)

The outside air temperature and pressure were among the recorded parameters. Therefore, the corresponding air density could be calculated from

$$\rho = \frac{P}{\overline{R}T} \tag{3}$$

where

P = static pressure in psf

$\overline{R}$ = 1,716.3 ft-lb/slug-R, specific gas constant for air

T = absolute temperature in Rankine

Following the procedure used in reference [18], aircraft lift-curve slope, C_{L_α}, was determined from

$$C_{L_\alpha} = C_{l_{\alpha,wb}} \left[1 + \frac{C_{l_{\alpha,t}}}{C_{l_{\alpha,wb}}} \frac{S_t}{S} \left(1 - \frac{\partial \varepsilon}{\partial \alpha} \right) \right] \tag{4}$$

where:

$C_{l_{\alpha,wb}}$ = wing lift-curve slope (per radian)

$C_{l_{\alpha,t}}$ = horizontal tail lift-curve slope (per radian)

S_t = horizontal tail area (ft^2)

S = wing area (ft^2)

$\frac{\partial \varepsilon}{\partial \alpha}$ = rate of change of downwash at the tail due to the wing, given by (reference [19])

$$\frac{\partial \varepsilon}{\partial \alpha} \approx \frac{0.349 C_{l_{\alpha,wb}}}{\lambda^{0.3} A_r^{0.725}} \left(\frac{3\bar{c}}{l_t'} \right)^{0.25} \tag{8}$$

where:

λ = wing taper ratio

A_r = wing aspect ratio

$\bar{c}$ = wing mean geometric chord (ft)

l_t' = distance between the wing and the horizontal tail aerodynamic centers (ft)

In all of the above expressions, from reference [20], assuming thin airfoils with lift-curve slopes of 2π per radian, the wing and the tail lift-curve slopes were calculated from

$$\left(C_{l_\alpha} \right)_{\text{Wing or tail}} = \frac{2\pi A_r}{\sqrt{2 + \left[4 + A_r^2 \beta^2 \left(1 + \frac{\tan^2 \Lambda}{\beta^2} \right) \right]}} \tag{9}$$

where:

A_r = b^2 / S, aspect ratio

b = span (ft)

β = $\sqrt{1 - M^2}$, compressibility effect

M = V_t / a, flight Mach number

Λ = wing half-chord sweep angle (degrees or radian)

V_t = true airspeed (ft/s)

a = $\sqrt{\gamma \bar{R} T}$, local speed of sound (ft/s)

γ = 1.4, ratio of specific heat coefficients for air

5. DATA PRESENTATION

5.1 AIRFRAME USAGE

APPENDIX B—USAGE DATA PRESENTATION contains the figures and tables associated with this section. Table B-1 contains the list of tables, followed by the list of figures in Table B-2 and Table B-3.

5.1.1 Ground-Air-Ground Usage – All Missions

Table B-4 lists the total number of flights by airframe, in addition to duration and distance flown by each, omitting references to specific aircraft. This table shows that data from over six thousand hours of flight time was available for analysis, although not all flights include all information needed for every figure or table. As a result, the number of flights, total duration, and total distance flown differ between figures and tables for each segment of the analysis.

Flights were divided into three categories—ferry, firefighting (Fire Ops), and maintenance/training (Maint.). Figure B-1 shows the number of flights based on duration in each category. It is clear from this figure that very few flights lasted longer than 80 minutes, and the average flight time was close to 40 minutes. This was slightly shorter than the 45-minute average for the legacy heavy airtankers, indicated in REFERENCES [5].

Figure B-2 shows the correlation between distance and duration. With the exception of a few ferry flights that were as long as five to six hours, the majority were under three hours. The relatively tight correlation between the distance and duration shown in this figure implies that the missions were not flown over a wide range of speeds. This may have been the case because the results were dominated by those from firefighting missions. It should be noted that the distances presented in all of these results are based on integrated ground speed (i.e., GPS speed).

Figure B-3 presents maximum MSL altitudes and corresponding flight distances. This figure also shows the altitude limits associated with the different aircraft types, although different revisions of REFERENCES [13] indicate 31,000 feet instead of 35,000 feet for the RJ-85. Based on these results, very few flights approached the limit altitude, with the majority remaining below 20,000 feet. Naturally, the longer distances were associated with higher maximum altitudes.

Figure B-4 and Figure B-5 show maximum altitudes and maximum indicated airspeeds. The results shown here are only from those cases with reliable recorded indicated airspeeds, which constituted 296 ferry, 6,543 firefighting, and 491 maintenance/training flights.

Figure B-4 shows maximum MSL altitudes and coincident indicated airspeeds. Depending on the revision of reference [13] used, maximum altitudes for the RJ-85 varied between 31,000 and 35,000 feet. Apparently, none of the flights took place above the latter limit. This figure also shows that the ferry flights were flown at the highest altitudes, followed by firefighting flights, and then maintenance/training flights. This was expected in that the average distance flown for ferry flights was about 410 nautical miles. The averages for firefighting and maintenance/training flight types were 146 and 84 nautical miles, respectively.

Figure B-5 shows maximum indicated airspeed and coincident altitudes. As indicated in this figure, the maximum indicated airspeeds of 295 and 300 KIAS were exceeded in a number of cases. However, in no case did the indicated airspeed exceeded V_{MO} by more than 10%. It appears in this figure that the majority of overspeeding cases were associated with firefighting flights. This is simply due to the fact that the vast majority of the flights fell into this category.

Normal load factors and coincident indicated airspeeds are shown in various parts of Figure B-6 and Figure B-7 for different flap settings. These figures show the maximum and minimum vertical load factors, and corresponding indicated airspeeds, and the maximum indicated airspeed and coincident vertical load factor for each flight. The limits shown in these figures are those for RJ-85 at sea level for maximum takeoff weight and very close to the minimum operating weight. These results are only for those cases where reliable indicated airspeed was available. Similar airspeed limits for BAe-146 were not available, but were expected to be close to those of RJ-85.

Data from reference [21] for stall speed at maximum landing weight was used to establish the maximum lift coefficient of each aircraft type. Table 13 shows these values, which were used to establish the stall boundaries for various flap settings in Figure B-6 and Figure B-7. REFERENCESeference [22] shows an almost linear variation of maximum lift coefficient with flap deflection for a NACA 65_3-118 airfoil, as shown in Figure 14. Therefore, a similar linear variation was used to estimate the maximum lift coefficient, and, therefore, the stall speeds for RJ-85 at different flap settings. The two circles in this figure represent the known values of maximum lift coefficient at the corresponding flap positions.

Table 13. Estimates of the maximum lift coefficient

Aircraft	Flaps (degrees)	Max. Landing Weight (pounds)	Stall Speed (knots)	Maximum Lift Coefficient
RJ-85	33	85,000	93	3.49
BAe-146	33	77,500	90	3.40

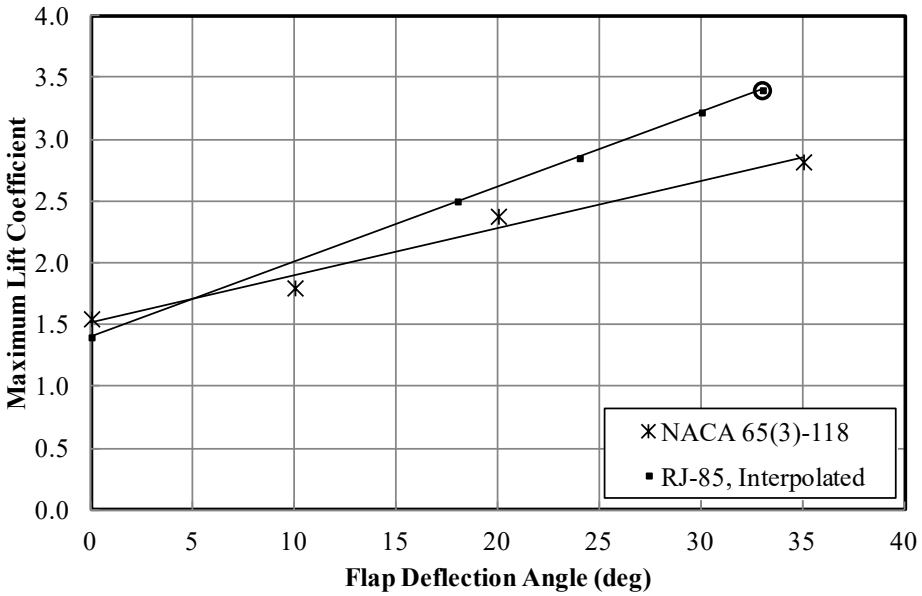

Figure 14. Estimate of maximum lift coefficient for RJ-85

When the flaps were retracted, the vertical load factor reached its limit of +2.5 g in one case, otherwise, this value was never exceeded. Maximum indicated airspeeds exceeded V_{MO} in a number of cases, consistent with those shown in Figure B-5, but always remained well below 10% above this value. This was not always true for cases when the flaps were deflected as can be seen in Figure B-6 and Figure B-7.

With the flaps deflected, in a number of cases, the maximum vertical load factor exceeded the FAR-prescribed value of +2.0 g, especially in the third detent. Many of these cases were traced to drop phases and were associated with the retardant release. Four such cases are shown in detail in Figure 15 and Figure 16 from different aircraft (two from BAe-146 and two from RJ-85). In two of these cases, Figure 15(a) and Figure 16(c), it is clear that an additional load factor of 1.2 g to 1.5 g occurred during the drop. Interestingly, in the other two cases, Figure 15(b) and Figure 16(d), it appears that the crew tried to unload the structure prior to the drop in anticipation of the ensuing positive load factor. The magnitudes of these loads are larger than one would expect as being associated with the sudden change in the aircraft mass, which would account for an added +0.5 g of incremental load factor. The authors speculate that some of the additional load factor is due to the change in the direction of the airflow around the aircraft due to the formation of the retardant plume. Since the duration of the drop is longer than two seconds, generally, these loads appear in the maneuver category. All of these traits have been observed previously in relation to other airtankers (e.g., reference [23]).

Figure B-8 shows the maximum and minimum load factors, as well as the maximum airspeeds and corresponding vertical load factor for times when the speed brake is deployed. Although there is no airspeed or load factor limit for deploying the speed brakes, this information may be of value in determining their maintenance and inspection intervals.

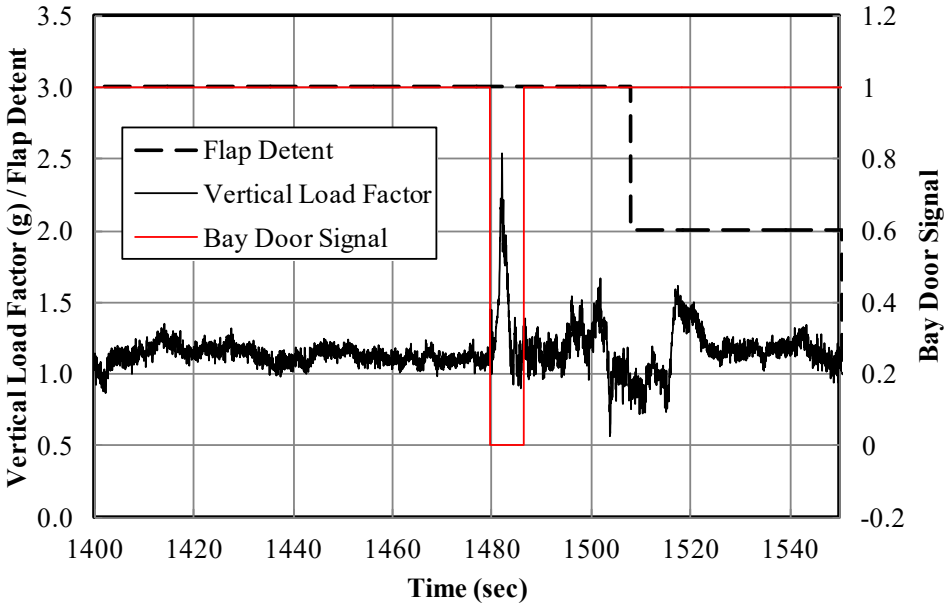

(a) Case 1

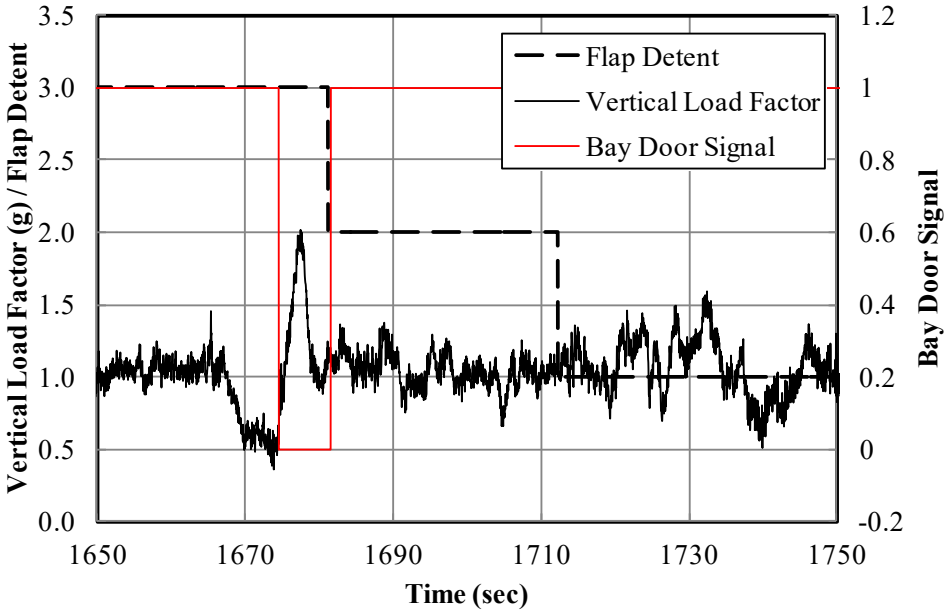

(b) Case 2

Figure 15. Typical peak load factors associated with the drop phase

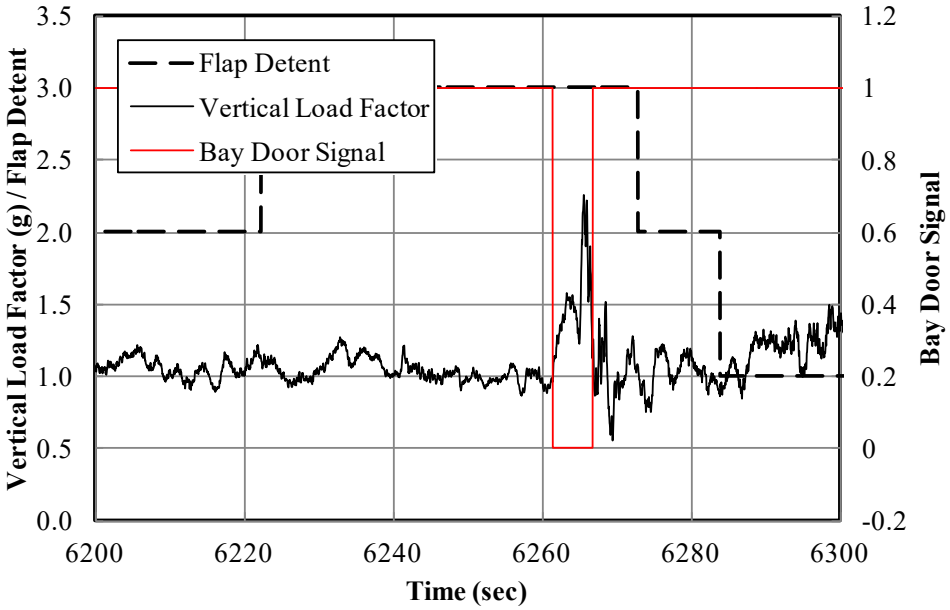

(c) Case 3

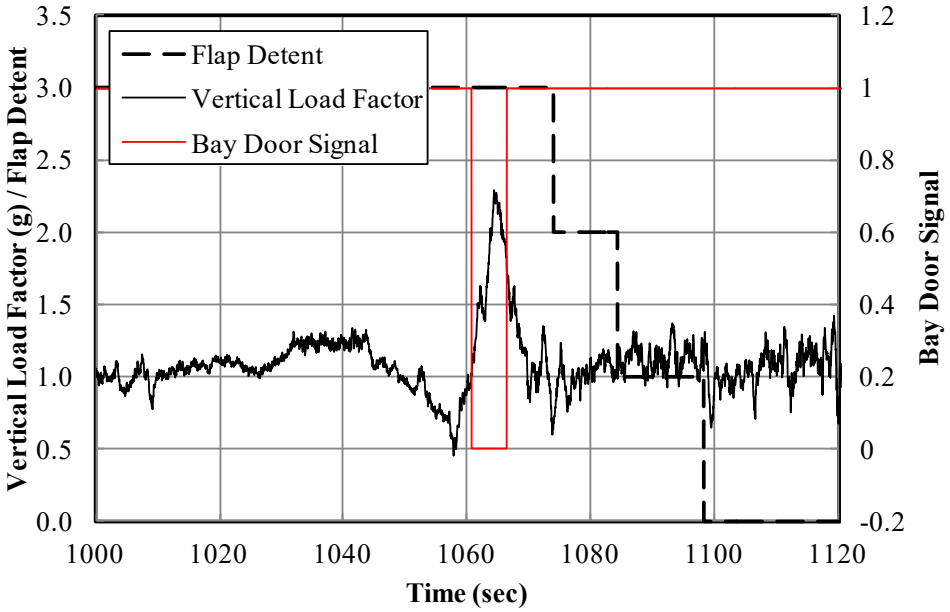

(d) Case 4

Figure 16. Typical peak load factors associated with the drop phase (continued)

The frequency of flap and speed brake deflections are shown in Table B-5 and presented in Figure B-9. In ferry flights, resembling the civil transport role of the airframes, the flaps were deployed 2-3 times per flight. However, in firefighting missions, flaps were deployed at almost twice that rate, especially in the third detent. This is a characteristic of firefighting operations in which the drop phase is flown with the flaps in the third detent. The number of flap extensions per flight for maintenance/training flights was somewhere in between those of the other types of missions. Table

B-6 shows that firefighting and maintenance/training flights have a larger percentage of flight time with the flaps and speed brake deflected.

Figure B-10 provides the number of drops per flight. As shown, the majority of the firefighting flights involve a single drop. Also, very few flights entail more than three drops. On average, drop phases account for just under seven seconds of total flight time. However, the longer durations shown in Figure B-11 are probably due to some flights having more than one drop phase or cycling of the bay doors. It is safe to assume that drops lasting less than two seconds were due to noise in the bay door signal that was not filtered out.

The probability distributions of takeoff and landing weights are shown in Table B-7 and in Figure B-12 and Figure B-13. Understandably, firefighting missions entail the largest difference between takeoff and landing weights, followed by ferry and maintenance/training operations. Again, these results pertain only to those cases where correct recording of the aircraft weight was available.

Table B-8 show the statistics for takeoff and landing indicated airspeeds and in different parts of Figure B-14 and Figure B-15. The results indicate that landing speeds were very close among different missions. However, the larger takeoff weights associated with firefighting missions necessitated higher takeoff speeds for these flights. In general, there was less variation in takeoff speeds than in landing speeds, as manifested by the larger standard deviation of the latter. Again, the results are only from those cases where reliable indicated airspeed was available.

Finally, maximum and minimum lateral and coincident vertical load factors at landing were examined. The lateral load factors were examined within ±2 seconds of landing, and the maximum and minimum values are presented against the vertical load factor at the landing point in Figure B-16. The lateral load factor exceeded -1.0 g once. However, the landing impact seems to result in many cases with vertical load factors in excess of +2.5 g, with one case exceeding +4.1 g. Note that, even though Figure B-16 shows that there are two data points in which vertical load factor was +4.1 g, both corresponded to the same flight, one each for the maximum and minimum lateral load factors for that flight. Detailed examination of the data from this mission suggests this value to be real and not caused by an erroneous spike.

5.1.2 Phase-Specific Usage – Firefighting Missions

To arrive at the results for cruise 1, all phases shorter than five minutes were removed from analysis. Also, when indicated airspeed was of interest, only those cases with a reliable value for this parameter were considered.

Figure B-17 shows the total number of cruise 1 phases, distributed by duration. It is obvious that the majority of cruise 1 phases lasted approximately 20 minutes, while very seldom did one last longer than one hour.

Figure B-18 provides the correlation of distance and duration for cruise 1. The tight distribution of the points shows a relatively constant flight speed that is characteristic of cruise phases. This behavior is also consistent with the correlation between maximum altitude and coincident distance, shown in Figure B-19. The maximum altitudes of the two types of aircraft also are marked in this figure. In no case did the maximum altitude by either aircraft type exceed the limit.

Figure B-20 shows the maximum altitude and the corresponding indicated airspeed. Again, only flights with reliable indicated airspeed were used to arrive at these results. Consequently, the number of cases shown in this figure is approximately 75% of those in the previous figures. In this figure, the maximum airspeed for the RJ-85 also is marked for reference. As previously discussed, in a number of cases, the limit indicated airspeed was exceeded, but always remained less than 10% over V_{MO}. This behavior is even clearer in maximum indicated airspeed and coincident MSL altitude as presented in Figure B-21. This figure clearly shows the airspeed limits of the two types of aircraft.

The total number of cruise 2 phases did not match that of cruise 1 phases for a variety of reasons, including incomplete flights and noisy squat switch signals flagging false landings. Again, for analyzing cruise 2 phases, flights shorter than five minutes were eliminated.

On average, cruise 2 phases were slightly shorter than cruise 1 phases, as indicated in Figure B-22. This could reflect the fact that cruise 1 could include some time in holding before entering the fire zone, while cruise 2 would be a direct flight back after the drop. As the figure indicates, the majority of the cruise 2 phases consisted of 10- to 20-minutes flights with an average duration of 12.5 minutes. Seldom did a cruise 2 phase last longer than 40 minutes.

Figure B-23 shows that good correlation of distance and duration was observed during cruise 2 phases. The tight correlation between these two parameters is indicative of direct flights back to base without much holding or maneuvering. Also, these phases, being much shorter than cruise 1, were flown at relative lower altitudes, as indicated in Figure B-24.

Figure B-25 shows maximum altitudes and corresponding indicated airspeeds. None of these flights approached the limit MSL altitude, although a few were flown faster than V_{MO}, as shown in Figure B-25 and Figure B-26. Again, these figures include only those cases where reliable indicated airspeed was available, which was approximately 75% of all cases.

The entry phases were those immediately before the start of a drop. The start of the entry was either three minutes or the last flap change before the start of the drop. Consequently, some entry phases were unreasonably short. Also, sometimes cycling of the bay doors in mid-flight resulted in false drop indications, leading to a false entry preceding it. These were identified by unusually high indicated airspeeds. Therefore, entry phases with distances less than 0.1 nautical miles or average airspeeds faster than 200 KIAS were removed from this analysis.

Figure B-27 shows the number of entry phases distributed by duration. Unlike similar figures for cruise 1 and cruise 2, the abscissa shows the durations in seconds. The last column to the right represents the number of entries that was based on the three-minute time limit. It is evident that typical entry phase lasted substantially less than three minutes, with an average of 84 seconds.

Generally, entry phases were flown with very precise airspeed control, reflected in the close correlation between distance and duration shown in Figure B-28. This also is evident in Figure B-30 and Figure B-31, showing a dense clustering of the data points about a mean indicated airspeed of 150 KIAS. These two figures represent only those cases where reliable indicated airspeed was available. Note that the results in Figure B-29 are for the maximum altitudes of the entry phases,

which could be substantially higher than that of the drop. Also, while the MSL altitudes were as high as 12,000 feet, the corresponding AGL altitudes were significantly lower.

Almost invariably, the drop phase is flown with the flaps extended to 30 degrees. Therefore, many of the entry phases are flown with flaps in the second or third detent. Also, some entry phases entail much maneuvering to position the aircraft precisely for the drop. Therefore, the maximum and minimum values of the vertical load factors in this phase were of interest. Figure B-32 contains the *V-n* diagrams pertaining to these two flap settings during the entry phases. Although this figure also shows the limit airspeed for the flaps lowered to 33 degrees, this flap setting was never used during the drop phase. Clearly, while the maximum airspeed was exceeded slightly in many cases, in no case did the vertical load factor exceed its limit of +2.0 g.

Figure B-33 provides the number of drop phases, distributed by their durations. Average drop duration of 6.0 seconds was prevalent. Drops shorter than two seconds were attributed to noise in the bay door signal and were not included in the results. Also, overly long drop durations were thought to be due to cycling of the bay doors in flight or leaving them open after a drop. Nonetheless, the majority of the firefighting missions involved a single drop lasting around six seconds.

Figure B-34 and Figure B-35 show the correlation between distance and duration and maximum drop altitudes. Clear correlation between the distance and duration is due to the fact that these phases were flown with great precision. Also, while Figure B-35 shows MSL altitudes reaching as high as 16,000 feet, the corresponding AGL altitudes were concentrated below 200-300 feet.

Much like the cases of entry phases, the airspeeds and altitudes were closely clustered around their mean values, as indicated in Figure B-36 and Figure B-37. The average indicated airspeed during this phase was about 145 KIAS, although the 170-knot limit airspeed for operating with flaps deflected by 30 degrees was exceeded in a large number of cases. This can be seen more clearly in the *V-n* diagram for this phase (Figure B-38). Also, consistent with the earlier discussion, the vertical load factor surpassed the 2.0-g limit for this flap setting on a noticeable number of occasions.

Finally, the number of exit phases distributed by duration is provided in Figure B-39. The criterion for the end of the exit phase was either two flap changes from the third detent or 90 seconds after the end of the drop phase, whichever occurred first. Clearly, from this figure, the majority of the exit phases concluded long before 90 seconds with an average of 43 seconds. However, there were many cases where the end of the exit phase had to be marked based on duration.

Figure B-40 through Figure B-43 show that there were many similarities between the exit phases and entry and drop phases. Much like the preceding phases, exit phases were flown below 12,000 feet in MSL altitude, with similar airspeeds, clustered around 155 KIAS. Again, the altitudes shown in Figure B-41 and Figure B-42 are the maximum MSL altitudes, which, in all likelihood, were encountered near the end of this phase.

The exit phases were likely to be flown with the flaps in the first, second, or third detent. Figure B-44 and Figure B-45 show the *V-n* diagrams for this phase for each flap setting. With flaps in the first detent, there was only one case with the maximum airspeed in excess of the prescribed limit.

However, the limit airspeeds for the second and the third flap detents were surpassed in a large number of cases. Also, in a handful of cases, the maximum vertical load factor went beyond the +2.0-g limit, but remained well below +2.5 g.

5.1.3 Summary of Usage

Results were shown for GAG (i.e., overall) airframe usage. Missions were divided into firefighting, ferry, and maintenance-training. Firefighting missions constituted the largest group of flights.

Overall average flight time was approximately 40 minutes, with relatively good correlation between distance and duration. MSL altitudes remained well within the prescribed limits, although maximum indicated airspeeds were exceeded in a large number of cases, but remained below 10% above the limit when flaps were retracted.

With the flaps extended, estimates were made of the stall speed for two weights nearing maximum takeoff and minimum operational values. Associated *V-n* diagrams were constructed for each flap setting. Maximum airspeed and maximum load factor exceeded the limits associated with the appropriate flap setting a number of times, especially during firefighting missions, with the latter associated with the drop phase. The majority of these load factors lasted longer than two seconds, and, therefore, were categorized as maneuvers.

When examining systems usage, frequency of flap deployment was shown to be higher during firefighting missions by approximately a factor of two. Data quality prevented examination of the pressurization cycles and pitch- and roll-excursions. The majority of firefighting missions involved one drop per flight. Total drop duration per flight averaged slightly less than 7 seconds.

Takeoff and landing weights were examined. The largest differences between the two were shown to be for firefighting missions, followed by ferry and maintenance/training flights. This analysis was limited to those cases with reliable recorded aircraft weight. Examination of landing indicated airspeeds showed them to be somewhat consistent among missions, although this could not necessarily be stated for takeoff. In addition, the estimates were based on data files with reliable recorded indicated airspeed.

Lateral and vertical load factors during landing were extracted, with a handful of the latter showing values well in excess of +2.5 g and the highest at just over 4.1 g. This is an issue worth pursuing further. Lateral load factors remained within ±1.0 g, with the exception of one case at negative 1.1 g.

Firefighting missions were divided into five types of flight phases—cruise 1, entry, drop, exit, and cruise 2. Airframe usage consisting of number of occurrences, duration, maximum MSL altitude, and maximum indicated airspeed, were studied and were shown to be within prescribed limits, with the exception of the last one exceeding V_{MO}. Also, *V-n* diagrams were constructed for entry, drop, and exit phases for the most likely flap settings. In all three phases, the maximum indicated airspeed exceeded its limit in a noticeable number of times. The maximum vertical load factors remained less than the limit, except for the drop phase where load factors as high as +2.4 g were detected.

5.2 FLIGHT LOADS

Past experience associated with analyzing firefighting operations showed a clear correlation between flight loads and AGL altitudes (reference [9]). Therefore, flight loads spectra per flight phase, including the entire flight, were sorted into AGL, as well as MSL, altitude bands. The results for the AGL altitude bands are discussed first, with the relevant figures and table presented in Appendix C. These results were extracted from flights that took place within the United States where terrain elevation could be obtained from NED. Appendix D is dedicated to the results sorted by MSL altitude bands. Since more data was available in this category, the total number of hours and the distances flown, as shown in appendix D, are slightly larger than those of appendix C. In each section, the results are presented from individual phases, followed by those from the overall airborne flights. Also, results from firefighting missions are discussed first, followed by those of ferry and maintenance/training missions. Table C-1 and Table C-2 provide the list of tables and figures available in appendix C.

5.2.1 Correlation with AGL Altitude

For firefighting flights, Table C-3 shows the number of phases and their associated durations and distances. The numbers of cruise 1 and cruise 2 phases do not match because not all flights were complete. Since many flights entailed multiple drops, the numbers of entry, drop, and exit phases exceed those of cruise 1 and cruise 2. In all, data from over 4,000 flight hours of firefighting operations was used to establish the results that follow.

The results from cruise 1 and cruise 2 phases are presented side by side for ease of their comparison. The distribution of the flight hours and distances per altitude band for cruise 1 phases are presented in Table C-4. The altitudes shown in this table are the ceilings of the associated bands. Therefore, it is evident that over 60% of these phases were flown at AGL altitudes below 4,500 feet and more than 95% below 14,500 feet.

Figure C-1 shows the cumulative occurrences of incremental vertical gust load factor, per 1000 hours and per nautical mile. The maximum incremental vertical load factors were spread over the range of ±1.0 g, with good correlation with altitude at lower heights. The frequencies of occurrence near 0 g's were quite comparable with those of lead planes, the results of which are shown in reference [9]. The cumulative occurrences of incremental vertical maneuver load factor are given in Figure C-2. Better correlation of frequencies with AGL altitude can be seen in this figure. The magnitudes of the load factor were below those of legacy heavy airtankers [5] and lead planes [9]. This was expected in that the former airframes were designed to MILSPEC, while the latter were FAR-23 aircraft, both with much higher design limit load factors. However, the frequencies near the center were comparable among all three types of aircraft.

Table C-5 presents the distances and durations, per AGL altitude band, for cruise 2. Again, 88% of these phases were flown below 9500 feet and 98% below 14,500 feet. Comparison of these results with those of cruise 1 shows that these phases were flown at a slightly higher average ground speed (272 knots compared with 258 knots). The combination of the higher flight speeds and lower wing-loading resulted in slightly higher gust load factors associated with this phase (Figure C-3) than those of cruise 1. However, the cumulative occurrences of the incremental vertical maneuver load factors, presented in Figure C-4, were comparable with those of cruise 1,

but with slightly higher counts, especially for negative values. In both cases, absence of sufficient data in the lowest altitudes, as well as above 14,500 feet, resulted in some scatter in the results in those altitude bands. Nonetheless, in both flight phases, the dependence of the frequency of occurrence of the load factors on AGL altitude was quite evident.

Table C-6 shows the distribution of the durations and the distances, per AGL altitude band, flown during the entry phases. In accordance with the phase separation criteria previously described, entry phases had a maximum duration of three minutes, although the majority were far shorter. During this phase, average ground speed was 155 knots, and the airplane was almost always flown below 4500 feet. Nonetheless, the cumulative occurrences of the incremental vertical gust and maneuver load factors, shown in Figure C-5 and Figure C-6, are almost void of information in higher altitude bands. In general, the gust load factors were smaller in magnitude than those of cruise 1, owing to the much lower average airspeeds. However, maneuver load factors, while smaller than those of cruise 1 in magnitude, were more frequent.

Table C-7 provides the distribution of the durations and distances by AGL altitude for the drop phases. Predictably, more than 90% of these phases were flown at altitudes below 1500 feet, with 83% below 500 feet. The average ground speed in this phase was 153 knots. The total time spent in this phase was under 20 hours for over 10,000 drops.

Figure C-7 and Figure C-8 present the cumulative occurrences of incremental vertical gust and maneuver load factors for the drop phases. The gust loads occurred at a slightly higher magnitude and frequency than those of the other phases. However, the maneuver loads occurred at noticeably higher magnitudes and frequencies, owing to the need for precision flying in this phase and the additional load factor due to retardant release. This trend was consistent with the results obtained from legacy airtankers [5]. The results from this phase also show the largest difference in the frequencies between positive and negative maneuver load factors near 0 g's. Due to scarcity of recorded accelerations at higher altitudes, significant scatter was present in their results.

The drop phases were flown almost exclusively with the flaps extended to 30 degrees. Per aircraft type certificate [13], normal load factors were limited to +2.0/0.0 g. In many cases, the positive limit was exceeded, but remained below +2.5 g. This exceedance was more prominent in maneuver loads than in gust loads, where the former was influenced by the additional load factor due to retardant release.

Table C-8 shows the summary of the durations and distances flown during the exit phases. Again, almost all exit phases were flown below AGL altitudes of 4,500 feet, with 75% below 1,500 feet. Cumulative occurrences of incremental vertical gust loads factors (Figure C-9) showed higher frequencies than the entry phases, but lower than those of the drop phase. Average flight speeds were comparable between entry and exit. However, the aircraft was significantly lighter during the latter phase, making it more responsive to atmospheric turbulence. The same relative trends were also observed in incremental vertical maneuver load factors, shown in Figure C-10. This was expected in that, generally, exiting the fire zone entails more aggressive maneuvering than entering it.

Combining the results from all phases led to exceedance spectra for the overall flight; that is for GAG cycles. The results for firefighting flights were obtained by simply adding those of the

individual phases. The results for ferry and maintenance/training flights also are presented individually by mission type.

Table C-9 shows the durations and distances for firefighting operations, with the corresponding spectra in Figure C-11 and Figure C-12. These results are representative of the firefighting missions as a whole and are useful in comparison with other missions, such as ferry and maintenance/training. Because of the addition of all phases, more data was available for each altitude band, resulting in less scatter in the corresponding results. Also, availability of more data from the longer cruise phases led to their dominance in the overall results. Nonetheless, the dependence of the frequency of occurrence of the incremental gust and maneuver loads on AGL altitude was more evident, as depicted in Figure C-11 and Figure C-12.

Ferry flights came closest to the missions for which the airframes were designed. By their nature, these flights took place at higher altitudes than the other two types of missions, with average ground speeds approaching 350 knots. Table C-10 provides the distribution of durations and distances from these missions. It is evident from this table that the flights were distributed among all altitude bands, with the highest percentages between 14,500 and 24,500 feet.

Figure C-13 shows the cumulative occurrences of the incremental vertical gust load factor for ferry flights. While ferry flights were flown at higher altitudes than firefighting mission, they also were flown at much higher average airspeeds and relatively lighter weights. On average, takeoff weights for ferry missions were approximately 20,000 pounds less than those of firefighting missions, while the landing weights for the two were comparable. Consequently, their frequencies of occurrence of incremental vertical gust load factors were slightly higher than those of firefighting missions. However, due to the nature of these missions, their incremental maneuver load factors did not extend to the larger values of the firefighting missions, as indicated in Figure C-14. Also, for these missions, the frequency of occurrence of the positive load factors was approximately one order of magnitude higher than the negative load factors.

A number of flights originated and ended at the same airport, without carrying retardant, and were flown at relatively low altitudes and short durations, with an average ground speed of 206 knots. These missions were deemed to be related to maintenance and training. Table C-11 summarizes their durations and distances. It is clear from these results that the majority of these flights did not occur above the AGL altitude of 4,500 feet. The cumulative occurrences of incremental gust and maneuver vertical load factors for these flights are shown in Figure C-15 and Figure C-16. These figures resembled those of the low-altitude cases of cruise 2. Obviously, there was not sufficient data available at higher altitudes to establish well-defined exceedance spectra for them.

5.2.2 Correlation with MSL Altitude

Appendix D contains the flight loads results, categorized by MSL altitudes bands. Table D-1 and Table D-2 provide the list of tables and figures available in appendix D.

Table D-3 presents the total durations and distance per phase for firefighting flights. These results include those from flights outside of the United States where ground elevation was not available. Therefore, the total number of hours and nautical miles are slightly higher than those presented in

appendix C. Nevertheless, the trends are the same in that cruise 1 and cruise 2 constituted the majority of the flight duration and distance.

Table D-4 summarizes the cruise 1 results, which are divided into MSL altitude bands. Whereas over 60% of the flights took place below AGL altitudes of 4,500 feet, only 20% were flown below the same MSL altitude. Also, availability of more data at higher altitudes resulted in a somewhat better defined curves for cumulative occurrences of incremental gust and maneuver vertical load factors presented in Figure D-1 and Figure D-2. The same could also be said about cruise 2, and those durations and distances are summarized in Table D-5. Again, availability of more data at higher altitudes resulted in well-defined exceedance spectra for MSL altitudes between 4,500 and 14,500 feet, at the expense of that for the lower altitudes, as indicated in Figure D-3 and Figure D-4. Having less than 2% of the flight time in MSL altitude bands below 1,500 feet did not lead to meaningful results for the lower altitudes.

Table D-6 summarizes the durations and distances flown in each MSL altitude band during entry phases. Again, the maximum MSL altitudes for these phases were much higher than the same in terms of AGL altitudes, as previously discussed. The majority of the entry phases were clustered around a narrow range of altitudes. Therefore, the cumulative occurrences of the incremental gust and maneuver vertical load factors, shown in Figure D-5 and Figure D-6, did not appear much different from those presented in Appendix C, except for a shift in the altitude bands.

Table D-7 shows that similar results were observed for drop phase and those durations and distances per altitude band. While the mean MSL altitudes were much higher than AGL altitude, the magnitudes of the associated load factors were the same, as demonstrated in Figure D-7 and Figure D-8. Only 4% of the drops occurred below MSL altitude of 500 feet, compared with 83% below the same AGL altitude. Much like the results shown in Appendix C, some of the incremental maneuver load factors approached values of +1.5 g.

Finally, the exit phases are summarized in Table D-8 and in Figure D-9 and Figure D-10. Again, the trends are unchanged from those presented in terms of AGL altitude bands, except now the predominant altitude bands, being relative to MSL, are higher.

Table D-9 provides durations and distances for firefighting flights for GAG cycles, divided into MSL altitude bands. Again, the total number of flight hours and distances shown here are slightly higher than those based on AGL altitude because of the inclusion of flights outside of the United States. The corresponding cumulative occurrences of the incremental gust and maneuver vertical load factor are shown in Figure D-11 and Figure D-12. Comparing these results with the corresponding ones based on AGL altitudes clearly shows the dependence of the loads spectra more on the latter than on MSL altitude. This dependence is especially evident in maneuver loads.

Table D-10 summarizes the same information for ferry flights, with the associated cumulative incremental gust and maneuver loads shown in Figure D-13 and Figure D-14. Interestingly, the results for ferry and maintenance/training flights, presented in Table D-11 and in Figure D-15 and Figure D-16, appear to show dependence on MSL altitude that is false. These flights were performed at low AGL altitudes and the distribution of their results on MSL altitude bands is solely due to terrain elevation. After all, it is difficult to explain why the crew would maneuver more

aggressively at higher MSL altitudes (4500-14,500 feet) than they would at lower altitudes (0-1500 feet). This would be contrary to all previous observations.

5.2.3 Summary of Flight Loads

Recorded vertical load factors were divided into gust and maneuver loads using the two-second rule. The number of occurrences of each type was counted using the method of peaks-between-means. The occurrences were then categorized according to their altitudes. Eight bands were used for AGL and MSL altitudes.

Prior experience showed better correlation of the loads with AGL altitude, especially in firefighting operations that are conducted at lower levels. Exceedance spectra, per 1000 hours and per nautical mile, were developed for cumulative occurrences of incremental gust and maneuver load factors based on AGL altitude and MSL altitude. For firefighting missions, the corresponding spectra were developed for each flight phase, as well as for the overall flight (i.e., GAG cycle).

The majority of cruise 1 and cruise 2 phases were shown to have been flown below AGL altitude of 4,500 feet. Incremental gust and maneuver load factors remained within ±1.0 g. However, for cruise 2, the combination of the higher flight speeds and lower wing-loading resulted in slightly higher gust load factors than were observed for cruise 1. Better correlation with AGL than MSL altitude was observed.

Almost all entry phases were flown below 4,500 feet AGL, and yet below 9,500 feet MSL. Consequently, lack of sufficient data at or above these altitudes prevented developing meaningful load spectra in that range. In general, the gust load factors were smaller than those of cruise 1 and cruise 2, owing to the much lower average airspeeds. However, maneuver load factors, while smaller than those of cruise 1 and cruise 2 in magnitude, were more frequent than both.

More than 80% of drop phases had maximum AGL altitudes below 1500 feet, but below 9,500 MSL altitudes. The gust loads occurred at a slightly higher magnitude and frequency than those of the other phases. The maneuver loads, which included the additional load factor due to retardant release, occurred at noticeably higher frequencies and magnitudes that many times exceeded the +2.0-g limit associated with flap deflections in that phase.

Almost all exit phases were concluded before reaching AGL altitude of 4,500 feet, with 75% below 1,500 feet. Only 45% of the exit phases were completed below MSL altitude of 4,500 feet. Average flight speeds were comparable between entry and exit. However, the aircraft was significantly lighter during the latter phase, making it more responsive to atmospheric turbulence. Maneuver loads were more frequent during the exit phase, as leaving the fire zone entails more aggressive maneuvering than entering it.

Overall gust and maneuver loads spectra were developed for the firefighting, ferry, and maintenance/training missions. Availability of more data from cruise phases led to their dominance in the overall results for firefighting missions. The majority of the maintenance/training flights were flown under 4,500 feet AGL. In all three cases, better correlation of the loads with AGL than MSL altitudes was evident.

5.3 DERIVED GUST VELOCITIES

Appendix E outlines the results for derived gust velocities in the form of exceedance spectra. Table E-1 and Table E-2 provide a list of tables and figures pertaining to this material.

This information is limited to the data recorded by some of the BAe-146 fleet. Due to erroneous weight recordings in the RJ-85 data, derived gust velocities could not be determined for those flights with any degree of reliability. Furthermore, some of the earlier data recorded from the BAe-146 fleet did not contain aircraft weight. Finally, the analysis had to be limited to those cases with accurately recorded indicated and equivalent airspeeds, which are necessary for finding the derived gust velocities. The combination of these limiting issues resulted in a very small proportion of the data being useful for the current analysis.

Because the cumulative occurrences of the derived gust velocities per 1000 hours and per nautical mile are very similar in nature, in the interest of brevity, only the latter forms are presented here. This form of presentation also allows side-by-side comparison of the results categorized by AGL and MSL altitude bands.

5.3.1 Firefighting Phases

Table E-3 summarizes the number of phases, and duration and distance in each phase for firefighting flights. This table shows two sets of results, one for AGL altitudes, and a second for MSL altitudes. The differences between the two sets stem from flights outside of the United States where terrain elevation was not available from NED. Nonetheless, the differences between the two sets are quite small. Altogether, a little over 900 hours of firefighting flights were available for extraction of the derived gust velocities.

Table E-4 shows that cruise 1 comprises almost half of the data available for analysis. This table also shows the distribution of the flight time among different altitude bands. Whereas 20% of cruise 1 phases were flown below AGL altitude of 1,500 feet, the percentage was slightly over 5% for MSL altitudes. This resulted in a much better correlation of the derived gust velocities with AGL altitude bands, as shown in Figure E-1. In this figure, the results from the third and the fourth MSL altitude bands are almost coincident, while they are clearly different when placed in AGL altitude bands. The magnitudes and the frequencies of the derived gust velocities for this phase were comparable with those of other aircraft in firefighting operations in the same range of altitudes.

Table E-5 provides the durations and distances for cruise 2. Altitude dependence in this phase was almost identical to that of cruise 1, but total available flight time was almost half. This was also apparent when considering the airframe usage, which did include a much larger set of data. It is believed that the difference is due to the fact that flying to the fire zone took place at slightly lower speeds and included some time in holding prior to the drop. On the other hand, once the retardant was released, the crew would fly back to the base directly and at a somewhat higher speed and altitude. The derived gust velocities, as presented in Figure E-2, were not much different from those of cruise 1. However, in this case, lack of sufficient data at the lowest altitudes prevented a clear definition of the derived gust velocities in that regime.

Table E-6 shows the durations and distances of the entry phases, sorted into AGL and MSL altitude bands. Again, comparing the two parts of this table better highlights the ground proximity of these phases. Figure E-3 presents the corresponding cumulative occurrences of the derived gust velocities. The dependence of the frequency of occurrence on AGL altitude is clearly visible in this figure. Also, comparing these results with those from cruise 1 and cruise 2 revealed the presence of higher-derived gust velocities in this phase of flight. Again, this was expected due to lower AGL altitudes.

Table E-7 and Figure E-4 summarize the results from the drop phases. While these results are based on only 4.3 hours of flight time, they represent over 2,500 drops. This amount of data resulted in well-defined exceedance spectra.

The first part of Table E-7 clearly shows the low-level nature of the drop phases, which is lost in the second part. This can also be observed in the first part of Figure E-4. The derived gust velocities extracted from this phase were the highest seen in firefighting operations, both in magnitude and in frequency. Multiple hand calculations were performed to ensure the accuracy of these results. Unfortunately, instrumentation difficulties on legacy heavy airtankers prevented comparison of those results with the present ones. There are some questions about the applicability of the Pratt formula (references [24] and [25] and equations 1 and 2) to a modern air transport aircraft [26]. This matter is worth investigating in a separate effort. Suffice it to say that the results shown here have been thoroughly vetted for accuracy and consistency with past practices.

Table E-8 contains the summary of the durations and distances associated with the exit phases, distributed by AGL and MSL altitudes. There is much in common between these results and those from the entry phases in distribution among various altitude bands. However, the cumulative time spent in exit phases was roughly half of that for the entries. These similarities also extended into the cumulative occurrences of the derived gust velocities, as shown in Figure E-5. Again, clear correlation of the results with AGL altitude was observed.

5.3.2 Overall Flights

The results from all firefighting phases were combined to develop the composite exceedance spectra for these missions. Table E-9 and Figure E-6 present the outcomes. Both of these clearly show the low-altitude nature of firefighting missions. Also, the first part of Figure E-5 reveals the clear correlation of the derived gust velocities with AGL altitude. Understandably, those parts of this figure related to lower AGL altitudes, such as the first two bands, are heavily influenced by the results from the entry, drop, and exit phases. Similarly, results from cruise 1 and cruise 2 phases dominated the behavior of the exceedance curves at higher AGL altitudes.

In comparison with firefighting missions, very little data was available for ferry and maintenance/training flights (43 and 33 hours, respectively, compared with 900 hours) for the present analysis. Consequently, a large amount of scatter could be seen in their exceedance spectra.

Table E-10 provides the durations and the distances for ferry flights, separated into various AGL and MSL altitude bands. It is clear from this material that all altitude bands were almost equally represented in the data. This resulted in very little data in each altitude band, and, therefore, the absence of well-defined trends in Figure E-7. Nonetheless, the results closely resembled those of

reference [27], but with slightly higher frequencies. Also, these results had the same frequencies as those of cruise 1 of firefighting flights for all altitudes except for the very lowest. However, the largest magnitudes remained below those of cruise 1.

Maintenance/training results were considered last. Table E-11 provides their distributions of durations and distances, with the corresponding spectra in Figure E-8. Although the available data is this case was less than that of ferry flights, they were distributed more closely in lower altitude bands. Consequently, the cumulative occurrences of their derived gust velocities, distributed among only five altitude bands, were quite well defined. Nonetheless, their magnitudes and frequencies proved to be very similar to those of ferry missions.

5.3.3 Summary of Derived Gust Velocities

Derived gust velocities were estimated for all flights with reliable recorded aircraft weight and indicated airspeed. Results were presented in the form of cumulative occurrences per nautical mile for this parameter, divided into AGL and MSL altitude bands.

Individual flight phases for firefighting missions were examined. Clear correlation with AGL altitude bands was present in the results. The results for cruise 1 and cruise 2 phases were very similar, although the amount of data in the latter phase was almost half of that from the former. The magnitudes and the frequencies of the derived gust velocities were much higher for entry, drop, and exit, with the drop phase having the highest magnitudes. Due to the magnitudes of the derived gust velocities observed during the drop phase, questions were raised about the applicability of the method to estimate the derived gust velocities.

Results were also presented for GAG cycles for all missions. Those for the firefighting missions consisted of combining the phase-specific results. Firefighting missions proved to have the highest derived gust velocities at lower altitudes, driven by the entry, drop, and exit phases. Their results at higher altitudes were very similar to those of ferry and maintenance/training missions. Absence of sufficient data for ferry flights resulted in considerable scatter in those exceedance spectra. Since the majority of the maintenance/training flights were flown at lower altitudes, the resulting cumulative occurrences of derived gust velocities were well defined.

5.4 COMPARISONS WITH OTHER SOURCES

This section is dedicated to the comparison of the cumulative occurrences of loads and derived gust velocities with other sources. The results are presented in Appendix F, with the figures summarized in Table F-1. The results from all altitude bands were combined to enable comparisons with those from various references.

For firefighting missions, the influence of flight phase on cumulative occurrences of incremental vertical gust and maneuver load factors are shown in Figure F-1 and Figure F-2. The first figure indicates that the highest frequencies of gust loads were associated with the drop phase, followed by cruise 2 and exit, and then entry and cruise 1. The composite distribution of the gust loads almost matched that of ferry flights. These results were consistent with the details discussed earlier. The drop phases were flown at the lowest altitude and closest to the fire zone, subjecting the airframe to the highest levels of atmospheric turbulence. Cruise 2 phases were flown at nearly the lowest weights and higher speeds, making the aircraft respond more vigorously to gusts. On the

other hand, cruise 1 and entry phases entailed the largest weights, reducing the airframe's response to gust velocities.

Examination of the maneuver loads in Figure F-2 revealed the trends to be quite different from those of the gust loads. In this case, the highest load factors were associated with the drop phase, followed by exits, and then the other phases. Higher maneuver load factors during the drop phase were driven by the necessity for precise flight path control and the additional load factor due to retardant release. The higher load factors during the exit phases were in all likelihood driven by the crew's desire to exit the area expeditiously and the increased aircraft response due to the reduction in weight. However, the latter effect also resulted in reduced structural loads at the same load factors. In any case, the combined maneuver load factors, representing the GAG cycle, were almost one order of magnitude more frequent than those of ferry flights.

Unlike in the case of the lead aircraft [9], the maneuver load factors occurred almost two orders of magnitude less frequently than did the gust loads. Therefore, when combining all loads, the occurrence of the latter dominated the results. This is shown in Figure F-3, where the overall loads are compared with those of Boeing 737-400 [28], Airbus A-320 [29] and Civil Aircraft Airworthiness Data Recording Program (CAADRP)-2 [30]. The fact that the removal of the maneuver load factors did not influence the results much is evident in Figure F-4, which is limited to gust loads only. In any event, the occurrences of the combined vertical load factors were two to three orders of magnitude more frequent than the civil transport aircraft. The difference is simply a reflection of the environment in which these airframes are used.

To prove the above point, cumulative occurrences of the incremental vertical gust load factors are compared with those of lead aircraft from reference [9] in Figure F-5. While Beechcraft King Airs flown as lead planes are very different in configuration layout, size, speed, and weight, they are operated in the same environment as the airtankers. The lower wing loading of these aircraft translated into higher gust loads than on the airtankers. Nonetheless, good agreement between the results of the two operations reaffirms the above point.

In Figure F-6, the maneuver loads spectra from various missions are compared with those of commercial transports. It is clear that firefighting missions entailed the largest and the most frequent maneuver load factors, consistent with the earlier discussions. Also, the differences between the current results and those from Boeing 737-400 and Airbus A-320 were not surprising in that commercial transports are flown with occupant comfort in mind, with little maneuvering and avoiding turbulent air as much as possible. However, the differences between the results from the two transport aircraft and those of CAADRP were unexpected.

Next, the cumulative occurrences of the incremental maneuver load factors were compared with those from the legacy airtankers, namely P2V and P3A [5]. This is presented in Figure F-7. It is clear from this figure that the positive maneuver loads associated with firefighting occurred with nearly the same magnitude and frequency for incremental load factors below +0.5 g. Beyond this point, the difference became much larger. At incremental load factor of +1.5 g, the frequencies of occurrence were almost an order of magnitude higher for the P3A and more than two orders of magnitude for the P2V. Also, the incremental maneuver load factors on the P2V extended beyond +2.0 g, while those of the present aircraft and P3A did not go beyond +1.5 g. The negative maneuver load factors occurred with almost equal frequency for all aircraft and all missions.

Finally, the cumulative occurrences of the derived gust velocities from different missions were compared with those from Boeing 737-400 and Airbus A-320. Figure F-8 shows the results of this comparison. In order to avoid clutter, each part of this figure pertains to comparison with one of the two transport aircraft. In the case of Boeing 737-400, the cumulative occurrences of the derived gust velocities agreed well with those from firefighting and maintenance/training missions when the flaps were extended. However, the magnitudes and the frequencies differed considerably with those of retracted flaps. The results from ferry missions fell somewhere in between. It should be noted that in the present analysis no distinction was made of the gust velocities with the flaps retracted or extended in that the atmospheric turbulence was not deemed to depend on this parameter. It can only be speculated that the two cases for Boeing 737-400 differed so much because in commercial operations, flaps are extended only at lower altitudes, similar to those of firefighting and maintenance/training missions. The same trends also held in comparing the results with those of Airbus A-320. However, in this case, derived gust velocities occurred less frequently than those of Boeing 737-400. The difference could be attributed to the load alleviation system on A-320 [31].

To summarize, comparison of the flight phases showed that in firefighting operations, the drop phase incurred the most severe and the most frequent gust and maneuver loads on the airframe. While the maneuver loads during exit phases were also large and frequent, the drastic reduction in the aircraft weight rendered them less taxing on the structure.

Vertical load factors were shown to be significantly more frequent than those of commercial operations, but were very similar to those of other aircraft flown in support of aerial firefighting. This observation was applicable to both gust and maneuver load factors.

The incremental maneuver load factors were also compared with those of legacy airtankers and were shown to agree well with them for relatively small values. However, at large values of incremental load factors, the legacy airtankers were shown to have been flown more aggressively.

Finally, the cumulative derived gust velocities were compared with those of two aircraft in commercial operations with and without flap deflection. The derived gust velocities agreed well with those with flaps extended, but were much larger and more frequent than those with the flaps retracted. It was stipulated that the differences were due to flight altitudes, as opposed to the state of the flaps.

6. SUMMARY AND CONCLUSION

6.1 SUMMARY

Recorded data from 16 next-generation heavy airtankers flown in support of the USFS aerial firefighting operations were analyzed. The fleet consisted of eight each of BAe-146 and RJ-85 airframes. This data was used to arrive at statistical airframe usage and flight loads spectra from actual in situ operations. The similarity between the two airframe types justified combining their results. All subsequent analyses were limited to airborne flight phases.

IONode™ DFDRs supported by Latitude Technologies Corporation were used to record the information. Recordings from all channels were transformed into a uniform 32-Hz format and were stored in a central repository maintained by HBM-nCode Federal LLC. This sample rate was up

to four times higher than what was used in previous similar investigations. The data was downloaded by the WSU team and examined for accuracy. A range of anomalies in the recorded data was identified and outlined in the report.

The recorded vertical load factors contained higher frequencies typical of the structural modes. Various filters were considered for cleaning this data and the effects of each on the gust and maneuver load factors spectra were presented. An eighth-order, low-pass Butterworth filter with an 8-Hz cutoff frequency was chosen to eliminate the higher modes. All subsequent analyses were performed using the filtered values of the vertical load factor.

Missions were divided into three categories—firefighting, ferry, and maintenance/training. Firefighting missions were further divided into five individual phases— cruise 1, entry, drop, exit, and cruise 2. Airframe and systems usage were examined for each flight phase of firefighting flights, as well as for the GAG cycle for all missions.

Statistical results of the airframe usage were presented and compared with aircraft limitations such as maximum altitude, maximum indicated airspeed, and load factor limits. Overall average flight time was shown to be approximately 40 minutes. Maximum altitudes remained well within the limits. However, maximum indicated airspeeds were shown to be above the prescribed limits in a large number of cases. When flaps were retracted, maximum indicated airspeeds remained well below $1.1V_{MO}$. However, when flaps were deployed, maximum indicated airspeeds were in excess of this value in a noticeable number of cases.

Likewise, maximum vertical load factors remained within the prescribed limits when the flaps were retracted. However, in a large number of cases, they were shown to be in excess of the +2.0-g limit when flaps were deployed. Detailed examination of the data revealed that these occur mostly during the drop phase.

Other information pertaining to airframe usage included duration and distance, number of retardant drops per flight, flap cycling frequency, takeoff and landing weights, and landing impact load factors. Frequency of flap deployment was shown to be over twice as much for firefighting missions as it was for other flight types. On a handful of flights, the vertical load factors at landing impact were in excess of +2.5 g, with the largest value approaching +4.2 g. Lateral load factors at landing remained within ±1.1 g. The errors in the recorded pitch-and-roll angles and cabin pressure prevented examination of these parameters.

For developing flight loads spectra, vertical load factors were divided into gust and maneuver loads using the two-second rule and their occurrences were counted using the method of peaks-between-means. The load counts were further divided according to the altitudes at which they occurred. Eight altitude bands were used for MSL and AGL altitudes and exceedance spectra were developed for each.

For firefighting missions, cumulative occurrences of gust and maneuver loads were developed for each flight phase. The majority of cruise 1 and cruise 2 phases were flown below AGL altitude of 4,500 feet and their incremental vertical load factors remained within ±1.0 g. However, cruise 2 phases showed slightly higher vertical load factors, which was speculated to be due to the slightly higher speeds and lower wing loadings than in cruise 1. Entry phases showed smaller load factors

than either of the cruise phases, but the maneuver load factors occurred at a higher frequency. The drop phases had slightly higher magnitudes and frequencies of gust load factors, but significantly higher maneuver load factors than any other flight phase. It was speculated that the latter was influenced by the increased load factor during the drop, as previously discussed. During exit phases, gust and maneuver load factors were higher in magnitude and frequency than those of all other segments of flight except for the drop phases. It is believed that this was due to the lower wing loadings and the necessity to exit the fire zones expeditiously.

Flight loads spectra were also developed for GAG cycles of all three mission types. For firefighting missions, they were obtained simply from summing the counts for individual phases. The results from various missions compared favorably, noting that those for firefighting missions were dominated by the larger volume of data from cruise phases. Throughout, the flight loads spectra showed a clearer dependence on AGL altitude than on MSL altitude.

For cases with reliable recorded aircraft weight, derived gust velocities were determined and presented in the form of cumulative occurrences per nautical mile. Again, the data was presented for AGL and MSL altitude bands, even though better correlation with altitude was evident in the former set. Firefighting missions proved to have the highest derived gust velocities at lower altitudes, driven by the entry, drop, and exit phases. At higher altitudes, the results of all three mission types were comparable.

Finally, these results have been compared to those of the legacy airtankers and other aircraft flown in support of firefighting missions and as civil transport. The gust load factor spectra are shown to be similar to other USFS aircraft being flown in the same environment. The maneuver load factor spectra indicate smaller loads than those of legacy airtankers, but considerably exceeding in frequency those of civil transport.

6.2 CONCLUSIONS

1. The number of anomalies and the missing or unreliable information in the recorded data decreased as the seasons proceeded. However, the anomalies identified in this report have to be addressed and be remedied. It is critical to ensure accurate and consistent recordings of all parameters.
2. Some systems usage, such as flap deployment and retraction and perhaps pressurization cycles, are more frequent in firefighting operations than in civil transport flights. Adjustment of the inspection frequency of these systems is in order.
3. The presence of the structural modes in the data calls for filtering of the data prior to storing it in the nCode library. The most robust type of filter was used for the present analysis, requiring significant computational effort. It is possible that a lower-order filter would suffice for the purpose of extracting flight loads spectra from operational data. The present report contains ample evidence of the type of low-pass filter needed and the required cutoff frequency.
4. The comparison of the flight phases in firefighting operations showed that the drop phase incurred the most severe and the most frequent gust and maneuver loads on the airframe. While the maneuver loads during exit phases were also large and frequent, the drastic reduction in the aircraft weight rendered them less taxing on the structure.

5. Cumulative occurrences of the incremental vertical gust loads proved to be very similar to those from ASM/Lead aircraft being operated in the same environment, despite the differences in aircraft types. Perhaps the results from the latter group can be used as a benchmark for future life-cycle analysis.
6. Occurrences of relatively large load factors with the flaps in the third detent have to be addressed.
7. The maneuver load factor spectra showed much smaller loads than those on legacy airtankers, but exceeded in frequency those of FAR 25 certified aircraft flown as civil transport by two to three orders of magnitude. Therefore, continued operational load monitoring of the next generation airtankers is highly recommended.

7. REFERENCES

1. National Transportation Safety Board. (2004). Safety Recommendations A-04-29 through -33.

2. US Forest Service Fire and Aviation Management. (2009). Special Mission Airworthiness Assurance Plan for Aerial Firefighting for FY 2010-2015.

3. Kliment, L. K., Rokhsaz, K., Nelson, J., and Newcomb, J. (2010). *Operational Loads on Heavy Air Tankers.* Presented at the 2010 Aircraft Airworthiness and Sustainment Conference, Austin, TX, May 10-13, 2010.

4. Rokhsaz, K., Kliment, L. K., Nelson, J., and Newcomb, J. (2014). Operational Assessment of Heavy Air Tankers. *AIAA Journal of Aircraft, 51*(1), 62–77.

5. FAA Report. (2011). Usage and Maneuver Loads Monitoring of Heavy Air Tankers. (DOT/FAA/AR-11/7).

6. Kliment, L.K., Rokhsaz, K., Nelson, J., Terning, B., and Weinstein, E.M. (2015). Usage and Flight Loads Analysis of King Airs in Aerial Firefighting Missions. *AIAA Journal of Aircraft, 52*(3), 910–916.

7. Kliment, L.K., Rokhsaz, K., Nelson, J., Terning, B., and Weinstein, E.M. (2013). *Usage and Flight Loads Analysis of King Airs in USFS Service.* (AIAA-2013-4407), Presented at 2013 Aviation Technology, Integration, and Operations Conference.

8. Menon, A., Kliment, L.K., Rokhsaz, K., Nelson, J., and Terning, B. (2015). *Flight Loads and Atmospheric Turbulence Analysis from a Fleet of ASM/Lead Aircraft.* (AIAA-2015-1845), Presented at 56th AIAA/ASCE/AHS/ASC Structures, Structural Dynamics, and Materials Conference.

9. FAA Report. (2017). Further Airframe Usage and Operational Loads Monitoring of ASM/Lead Aircraft. (DOT/FAA/TC-17/40).

10. USDA Forest Service (2012). *Large Airtanker Modernization Strategy*, Final Version Released February 10, 2012.

11. US Forest Service Fire and Aviation Management. (2010). *Special Mission Airworthiness Assurance Guide for Aerial Firefighting and Natural Resource Aircraft*.

12. Rokhsaz, K. and Kliment, L. K. (2017). Errors and Uncertainties in Derived Gust Velocities Extracted from Flight Data. *AIAA Journal of Aircraft*, *54* (2), 802–806.

13. Department of Transportation, Federal Aviation Administration. (2018).*Type Certificate Data Sheet No. A49EU – Revision 19*,.

14. USGS National Elevation Dataset (NED). Retrieved from https://gishubdata.nd.gov/dataset/usgs-national-elevation-dataset-ned, last accessed May 2018.

15. FAA Report. (2005). Statistical Data for the Boeing-747-400 Aircraft in Commercial Operations. (DOT/FAA/AR-04/44).

16. ASTM Standard E 1049-85 (Reapproved 2005) "Standard Practices for Cycle Counting in Fatigue Analysis." ASTM International, West Conshohocken, PA, 2003, DOI: 10.1520/C0033-03, www.astm.org.

17. FAA Report. (1999). An Evaluation of Methods to Separate Maneuver and Gust Load Factors from Measured Acceleration Time Histories. (DOT/FAA/AR-99/14).

18. Etkin, B. (1982). *Dynamics of Flight, Stability and Control* – Second Edition, New York, NY: John Wiley & Sons.

19. Dommasch, D. O., Sherby, S. S., and Connolly, T. F. (1967). *Airplane Aerodynamics* – Fourth Edition, New York, NY: Pitman Publishing Corporation.

20. Roskam, Jan. (2001). *Airplane Flight Dynamics and Automatic Flight Controls – Part I*, Third Printing, Lawrence, KS: DARcorporation.

21. Paul Jackson, Editor in Chief. (2000). *Jane's all the World's Aircraft, 1999-2000 Edition*, Alexandria, VA: Jane's Information Group, Inc.

22. Abbott, I. A. and von Doenhoff, A. E. (1959). *Theory of Wing Sections*, New York, NY: Dover Publications, Inc.

23. FAA Report. (2016). Preliminary Comparison of Agricultural and Single-Engine Air Tanker Operational Loads. (DOT/FAA/TC-16/9).

24. NACA Report. (1953). A Revised Formula for the Calculation of Gust Loads. (NACA-TN-2964).

25. NACA Report. (1953). A Revised Gust-Load Formula and Re-Evaluation of V-G Data Taken on Civil Transport Airplanes from 1933 to 1950. (NACA-TR-1206).

26. Rokhsaz, K. and Kliment, L. K. (2017). *Higher Order Estimations of Load Factor from Derived Gust Velocity*. AIAA-2017-1362. Presented at 58th AIAA/ASME/ ASCE/AHS/ASC Structures, Structural Dynamics, and Materials Conference, AIAA Science and Technology Forum and Exposition 2017, Grapevine, TX.

27. FAA Report. (2017). Flight Loads Analysis of Business Jets. (DOT/FAA/TC-16/10).

28. FAA Report. (1996). Flight Loads Data for a Boeing 737-400 in Commercial Operation (DOT/FAA/AR-95/21).

29. FAA Report. (2002). Statistical Loads Data for the Airbus A-320 Aircraft in Commercial Operations. (DOT/FAA/AR-02/35).

30. King, G.E. (1970). Civil Aircraft Airworthiness Data Recording Programme – Manoeuvre Loads During Training and Test Flying, C.P. No. 1176, Aeronautical Research Council. (replaces RAE Technical Report 70226 – ARC 32850).

31. NASA Report. (2012). Survey of Applications of Active Control Technology for Gust Alleviation and New Challenges for Lighter-weight Aircraft. (NASA/TM—2012–216008).

APPENDIX A—FILTERING VERTICAL ACCELERATIONS

A.1. BACKGROUND

The first generation of digital flight data recorders (DFDRs) used by United States Forest Service (USFS) was custom-made by Systems and Electronics, Inc. (SEI) in which data was collected at unequal recording rates. In this system, several channels were given the authority to trigger a line of output when their reading changed by more than a pre-specified amount. Therefore, data was recorded at unequal intervals, and sometimes multiple lines of output were associated with the same timestamp. This resulted in a great deal of difficulty in working with the data and the unavailability of any information concerning the frequency content of various channels.

Subsequently, this system was abandoned in favor of a compact, low-cost, digital system. The new units, GAU-2000, were manufactured and supported by Appareo Systems, LLC. This unit had the sample rate of 128 Hz, while its output could be tailored to a much lower rate. In the initial phases of employing this unit, a balance had to be reached between the fidelity of the recorded information for further analysis and the needed storage volume. Therefore, most of these units were set to record the information at a constant rate of 8 Hz.

Concerns over the possibility of missing the extreme values of the recorded information and aliasing, coupled with availability of larger storage capacity led to recording the data at higher rates. In the initial phases, some airframes were equipped with two GAU-2000 units; one recording all channels at 8 Hz, and a second recording the accelerations at 32 Hz. The two units were time correlated, although their outputs were filtered differently. Per communications with technical staff at Appareo Systems, LLC, the authors were instructed that:

- *GAU 2000 units sampling at 8 Hz do not implement any sort of low-pass or band-pass filtering for the accelerometer data.*

- *However, the 32 Hz units do apply filtering prior to recording the accelerometer data. A 9th-order digital FIR filter with a cutoff of approximately 16 Hz is implemented in software to attenuate higher frequencies. The use of this filter applies a small DC gain (32890/32768, or approximately 1.0037) to all raw recorded data samples. Our postprocessing tools are configured to apply a correction to remove this gain, so typically this does not need to be otherwise adjusted for.*

While the data collected by the GAU-2000 system was robust and free of anomalies, the system was severely limited by the number of analog input channels. This limitation prevented recording of a number of important parameters, such as instantaneous flap position or retardant quantity. Therefore, a third generation of DFDRs emerged as the alternative. Presently, most operators are switching to IONode100, which is marketed and supported by Latitude Technologies Corp. The units currently in operation record all channels at the constant rate of 32 Hz.

While the data collected at 32 Hz increased the fidelity of the recorded information, an additional concern was introduced. Preliminary examination of this data revealed the existence of what appeared to be structural modes, in the recorded accelerations. Figure A-1 shows an example of the frequency content from a flight segment recorded on one of the airtankers using two GAU-2000 units. It is doubtful that frequencies above approximately 10 Hz are due to gust loads. A

close-up view of the time history of the vertical acceleration over a short time span is also shown in Figure A-2, which clearly shows the influence of the structural vibration in the recorded vertical accelerations. These higher frequencies will not affect the calculations of structural strength from loads and are likely from internal localized structural vibration within the aircraft. Nonetheless, collection of data at frequencies above 10-12 Hz is necessary for improving the quality of the gust load spectra.

One of the prime objectives of the Operational Loads Monitoring program is the accurate extraction of gust and maneuver loads spectra from flight data. It is speculated that the presence of the structural modes would greatly, and artificially, increase the frequency of occurrence of gust load factors. Therefore, in order to arrive at accurate flight loads spectra, it is necessary to filter out the structural modes prior to any analysis. However, any filtering of the data will result in dampening of the peaks in the recorded accelerations. Therefore, any filtering has to be performed judiciously to ensure no loss of pertinent information. The goal of the present document is to report on the efficacy of various filters to remove structural modes without loss of critical information.

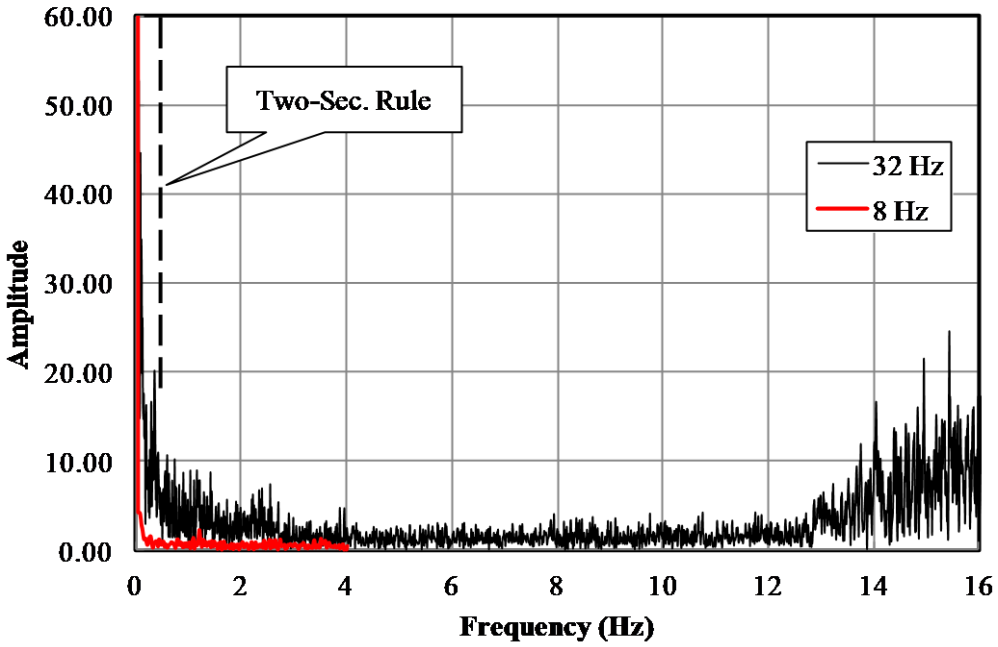

Figure A-1. Typical frequency content of normal acceleration

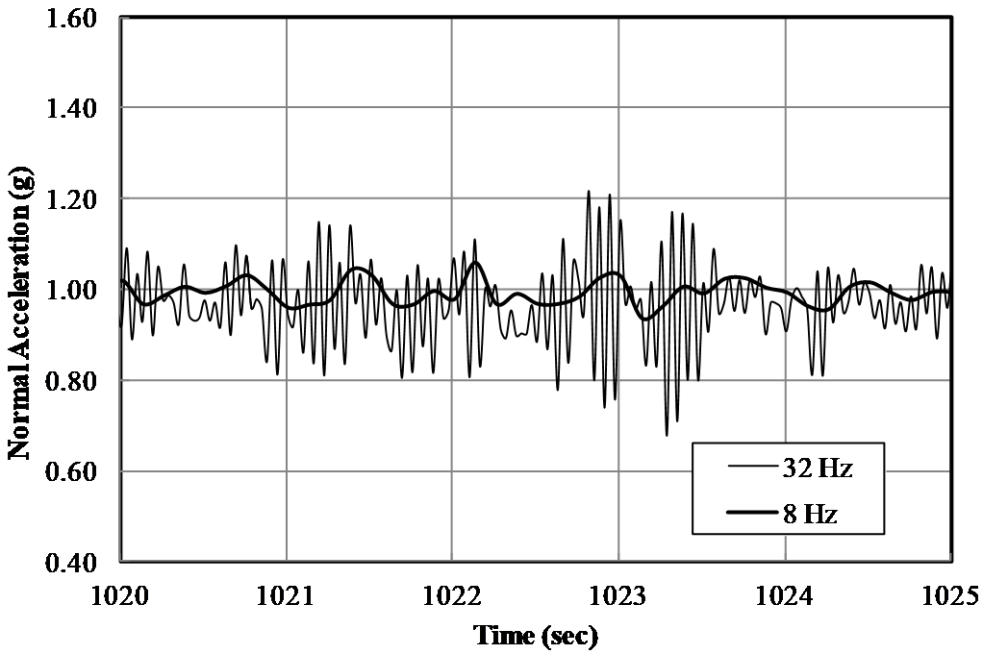

Figure A-2. Close-up view of time history of vertical acceleration

A.2. METHOD OF ANALYSIS

Filters applied in the frequency domain allow precise choosing of the cutoff frequencies at the expense of additional computation time. To apply these filters, it is necessary to transform the data into the frequency domain, apply the algorithm, and back-transform the data into the time domain. Furthermore, to take advantage of the speed offered by the Fast Fourier Transform (FFT) algorithms, the number of points transformed in each step has to be a power of 2. This means breaking up the files into segments to be transformed individually and ignoring the last segment of the original file. The required transforms can add a significant overhead to the computation time when processing thousands of flight files. File segments 4096 lines long offered the best compromise between speed and left-over parts that at most consisted of 128 second at the end of the file.

On the other hand, filters applied in the time domain can be executed very rapidly, but may require some trial and error in determining the cutoff frequencies. Two such filters were used; data skipping, and averaging. A simple explanation of each type of filter is given below.

A.2.1 Butterworth Filter

This is a classical filter applied in the frequency domain. First, the data is transformed from the time domain into the frequency domain using FFT. The following gain is then applied:

$$G(\omega) = \frac{G_0(\omega)}{\sqrt{1+\left(\frac{\omega}{\omega_c}\right)^{2n}}} \tag{A-1}$$

where; $G(\omega)$ = filtered amplitude

$G_0(\omega)$ = amplitude prior to filtering

ω = frequency

ω_c = cutoff frequency

n = order of the filter

Once the data is filtered, it is transformed back into the time domain for extracting the flight loads spectra. Identifying the appropriate filter order, n, and the cutoff frequency, ω_c, were part of the present investigation. Figure A-3 and Figure A-4 show the effects of filter order and the cutoff frequency on the data. In each case, the first part of the figure shows the gains, while the second part shows the effect on the time history of a short segment of the data. In these figures, the original 8-Hz and 32-Hz data refer to the data as recorded by the GAU-2000 units.

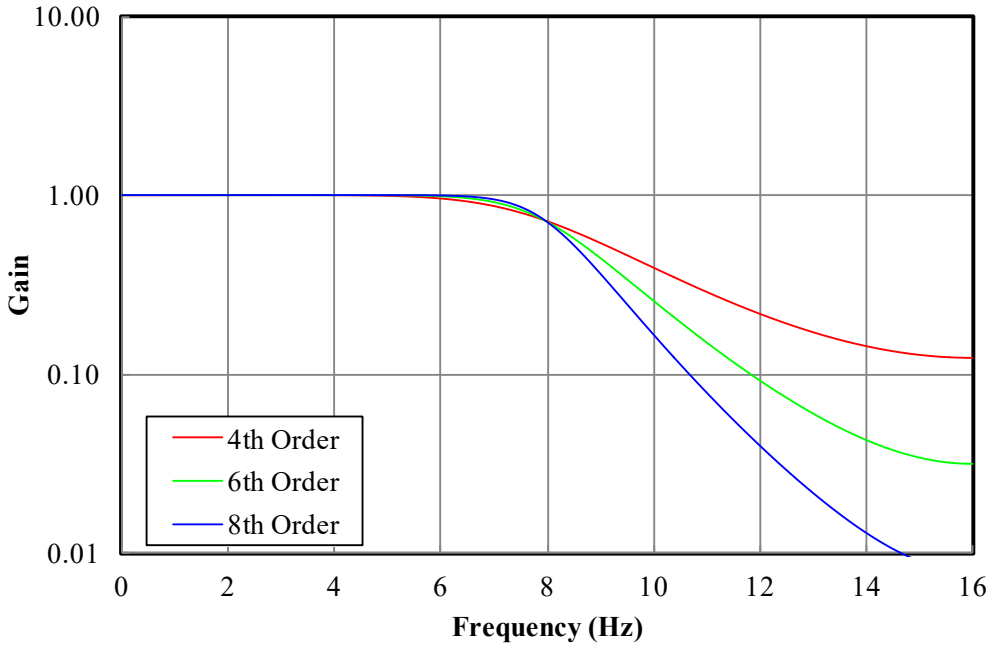

(a)

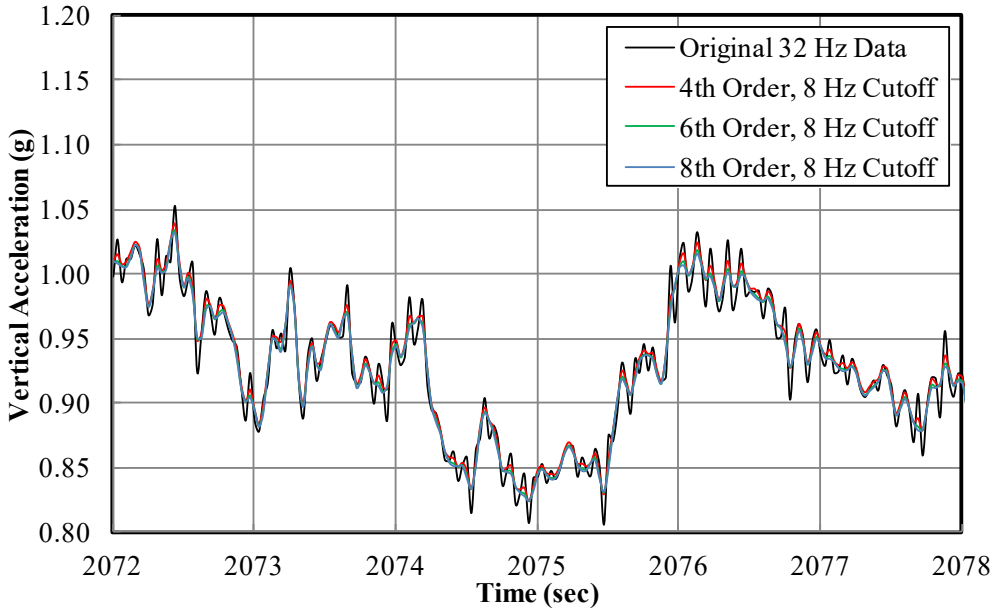

(b)

Figure A-3. Effect of filter order on gain and time history - ω_c = 8 Hz (a) gain (b) sample time history

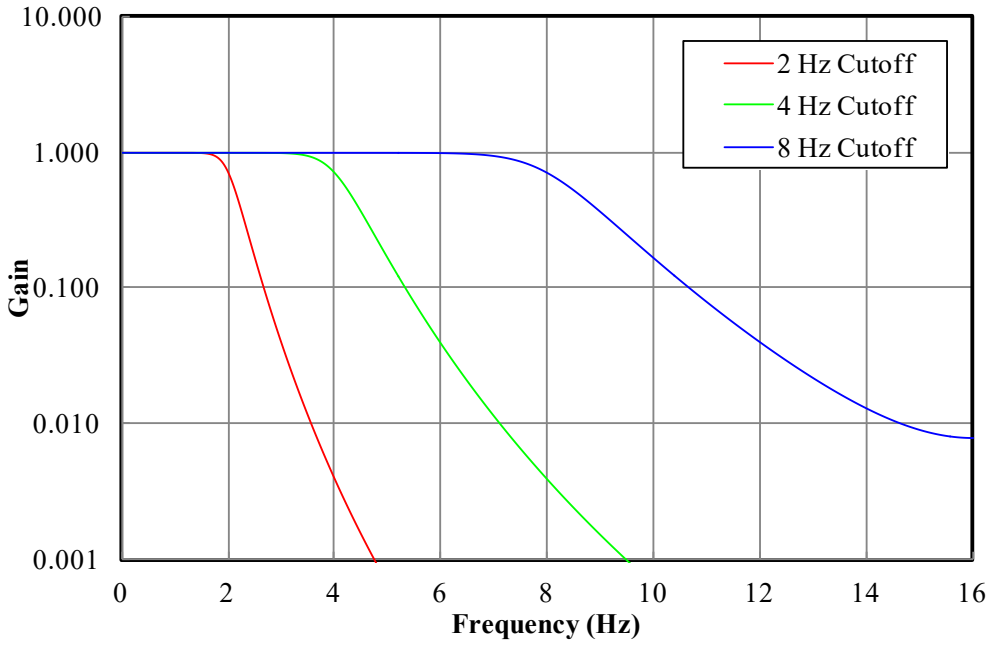

(a)

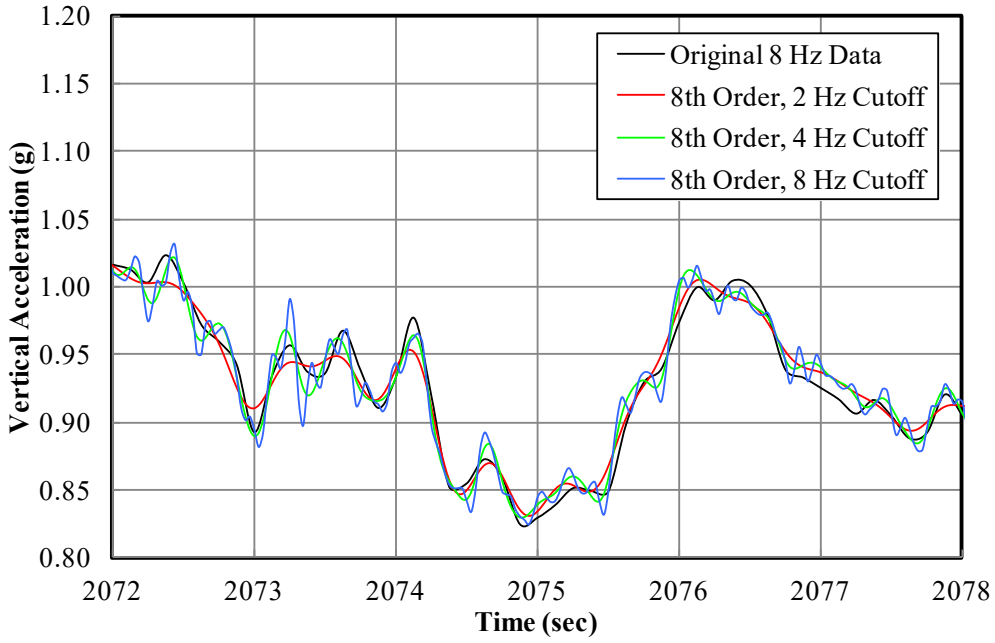

(b)

Figure A-4. Effect of cutoff frequency on gain and time history – eighth-order filter (a) gain (b) sample time history

A.2.2 Finite Impulse Response Filter

These filters operate in the discrete-time domain, which removes the necessity to transform the data into the frequency domain and back into the time domain. The general form of a finite impulse response (FIR) filter is:

$$y(n) = \sum_{k=-M_1}^{M_2} a_k x(n-k) \tag{A-2}$$

where; $y(n)$ = filtered signal at time step n

M_1, M_2 = number of time steps before and after n

a_k = arbitrary weight associated with time step k

$x(n)$ = original signal at time step n

The simplest form of a FIR filter is averaging of several time steps, such as

$$y(n) = \frac{1}{3}\left[x(n-1) + x(n) + x(n+1)\right] \tag{A-3}$$

The above expression results in a three-term centered filter with equal weight for each term. For the present study, two centered FIR filters were investigated; a five-term, and a seven-term. The results, when applied to a limited amount of data are shown in Figure A-5 and Figure A-6.

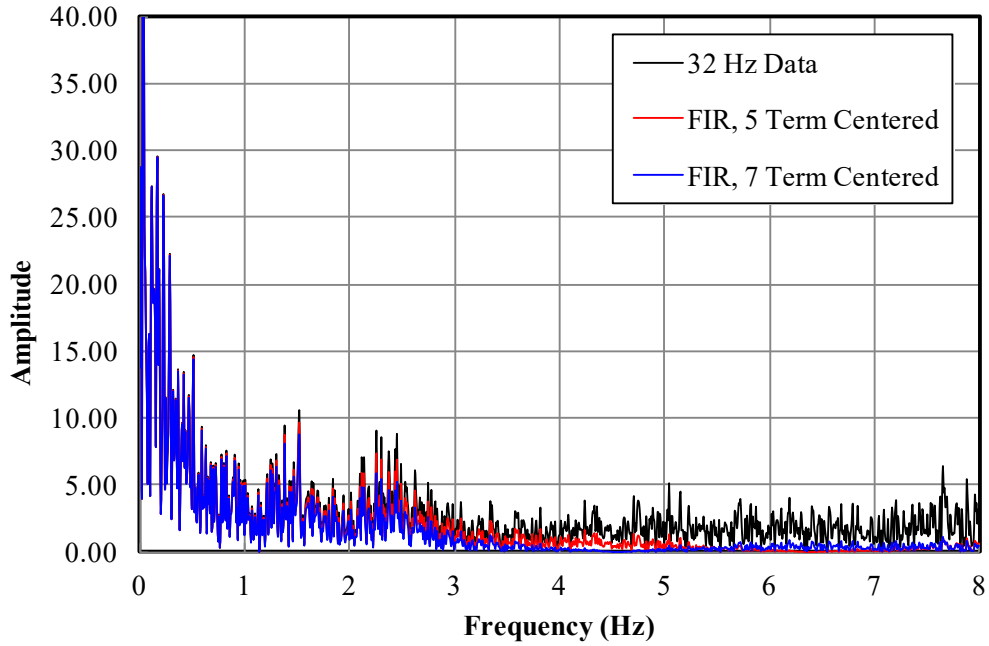

(a) Effect of Filtering on Frequency Content

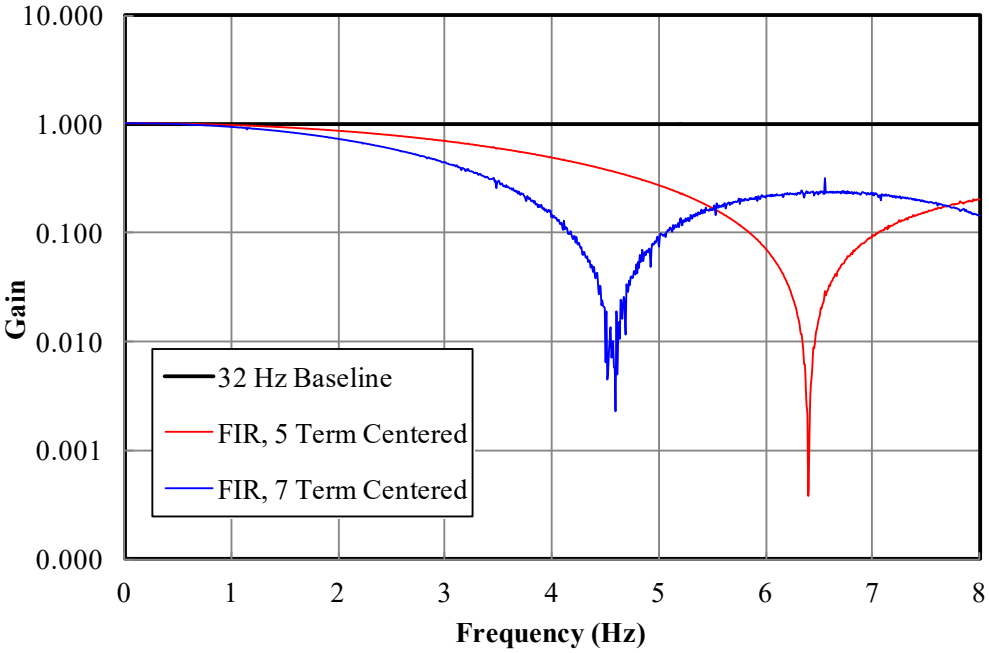

(b) Gain

Figure A-5. Effect of FIR filters on gain and time history

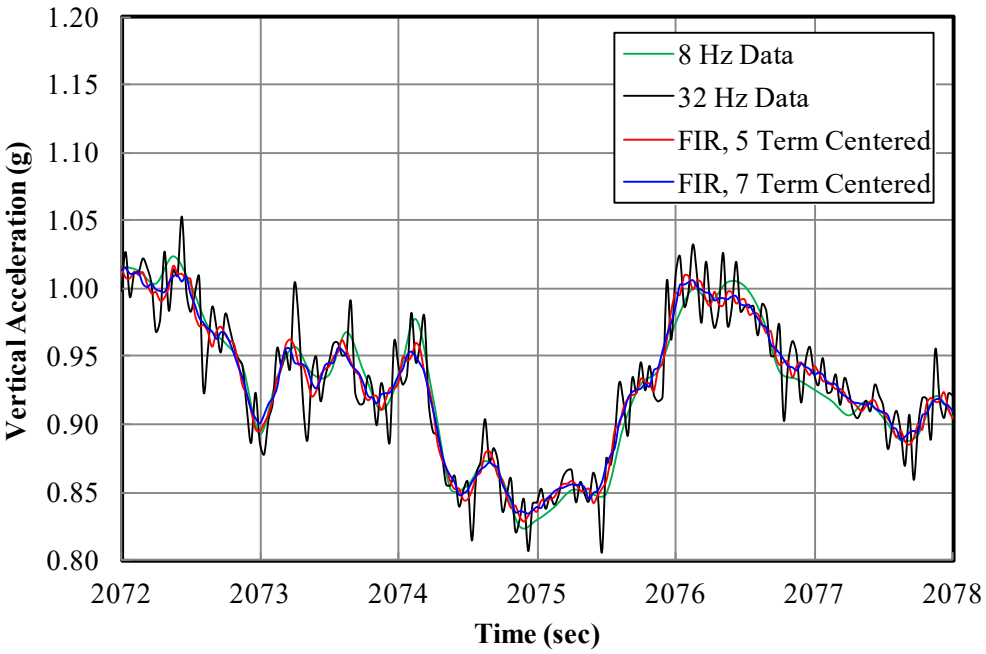

(c) Sample Time History

Figure A-6. Effect of FIR filters on gain and time history (continued)

As indicated in part (b) of Figure A-5, these filters appeared to act as a notch filter, with minimum gains at frequencies of 4.6 and 6.4, respectively. However, even at their peaks beyond these frequencies, they offered nearly one decibel of reduction in gain.

A.2.3 Data Skipping

This is the simplest form of filtering and simulates data recorded at a lower sample rate. Ideally, if the two GAU-2000 units were time correlated, and if neither signal was filtered prior to recording, the results of data skipping would match those recorded at 8 Hz. However, as can be seen from Figure A-7, this was not case when applied to a small sample of the data. There could be multiple reasons for this disagreement.

First, as previously mentioned, the 32-Hz data was filtered to remove higher frequencies, which could have affected some of the lower frequencies as well. Secondly, depending on which point was taken to be the starting value, different peaks and valleys would be skipped. This is shown in a close-up view of the data from Figure A-7 in Figure A-8. Finally, the difference in the locations of the two recorders could have resulted in sensing different accelerations.

In any event, the root mean squared (RMS) of the deviation from the average value over 128 seconds of data remained quite stable. In this case, the RMS was defined as:

$$RMS = \frac{1}{N}\sqrt{\sum_{n=1}^{N}\left[x(n)-\bar{x}\right]^2} \qquad \text{(A-4)}$$

where; N = total number of points (1024 in this case)

$x(n)$ = filtered data

$\overline{x}$ = average of the 32-Hz data over the same period

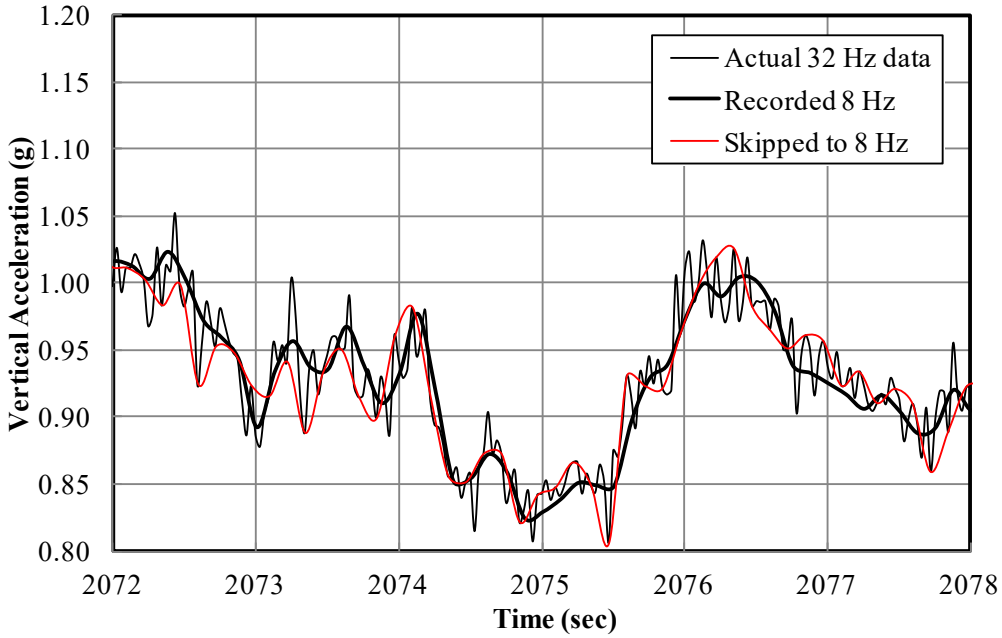

Figure A-7. Effect of data skipping on signal time history

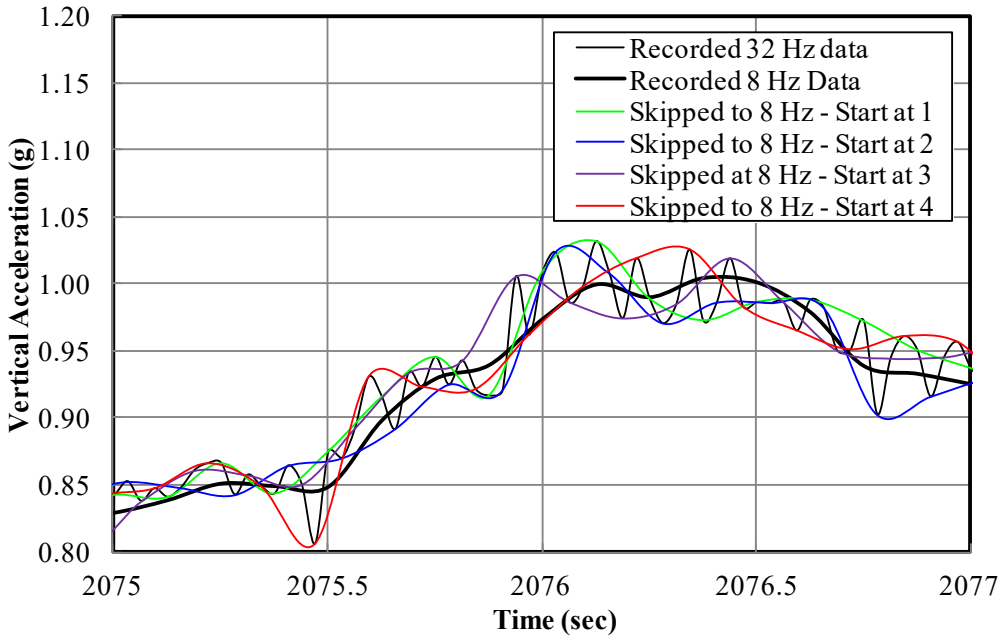

Figure A-8. Close-up view of a segment of data from Figure A-7

Table A-1 shows the averages and the RMS values of the data over the 128-second sample data. The values in this table indicate that various schemes of data skipping altered neither the average, nor the RMS errors significantly. Therefore, despite the graphical deviations shown in Figure A-8, in aggregate, data skipping may be a viable and rapid method of filtering the data.

Table A-1. Effect of data skipping on RMS values of deviation from average acceleration over 128 seconds of sample data

	Recorded		Skipped to 8 Hz			
	8-Hz	32-Hz	Start @1	Start @2	Start @3	Start @4
Average (g)	0.99786	0.99836	1.00078	0.99684	0.99783	0.99801
RMS (g)	---	---	0.00192	0.00188	0.00193	0.00192

A.3. RESULTS AND DISCUSSION

A small sample of flight data was used to examine the effect of various filters on the resulting flight loads spectra. Nineteen files from three different airframes were chosen, ensuring that they all contained complete missions. A small number of files pertained to ferry flights, while the majority showed at least one retardant drop. Approximately 27.4 hours of operation were included in this analysis.

Gust and maneuver loads were separated using the two-second rule. Loads spectra were developed for the entire data without removing the ground phases. It was speculated that the inclusion of the ground phases could impact the gust loads counts slightly, but not the frequency of occurrence of the maneuver loads.

A.3.1. Unfiltered Data

In order to establish a baseline, gust and maneuver loads spectra were developed for the unfiltered recorded data first. The results, shown in Figure A-9, highlight some important issues. As expected, the inclusion of the structural modes interfered significantly with the frequency of occurrence of the gust loads, with the difference being one order of magnitude. Furthermore, maximum gust load factors recorded by the 32-Hz system were much larger than those from the 8-Hz system due to the higher peaks associated with the structural modes. However, the maneuver load factors, associated with frequencies below 0.5 Hz (i.e., two-second rule) proved rather insensitive to the recording rate. The largest difference between the results from the two systems was approximately a factor of two to four, mostly in negative load factors.

These curves will be shown on all subsequent exceedance spectra for reference.

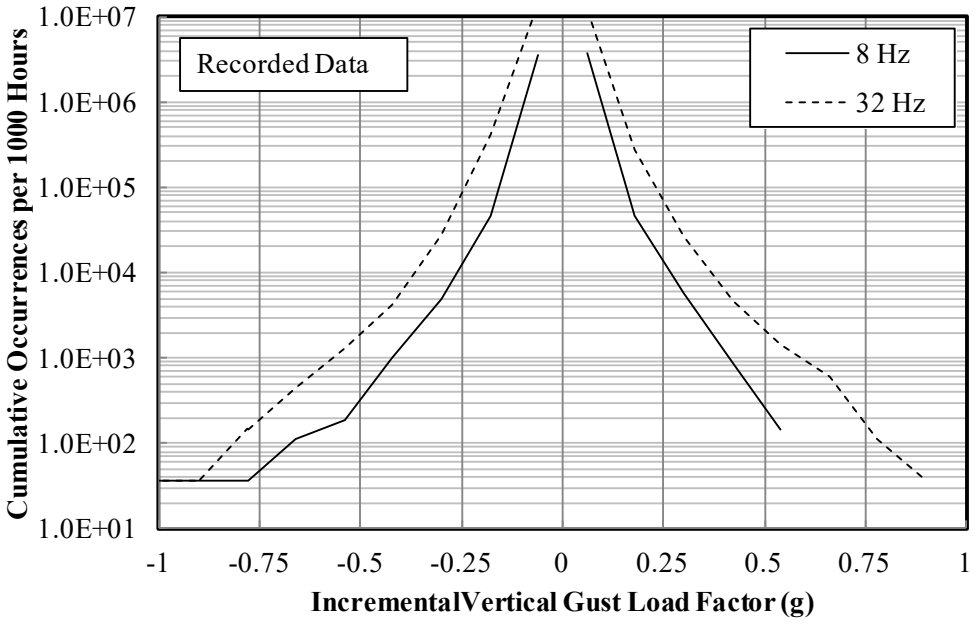

(a) Gust Loads

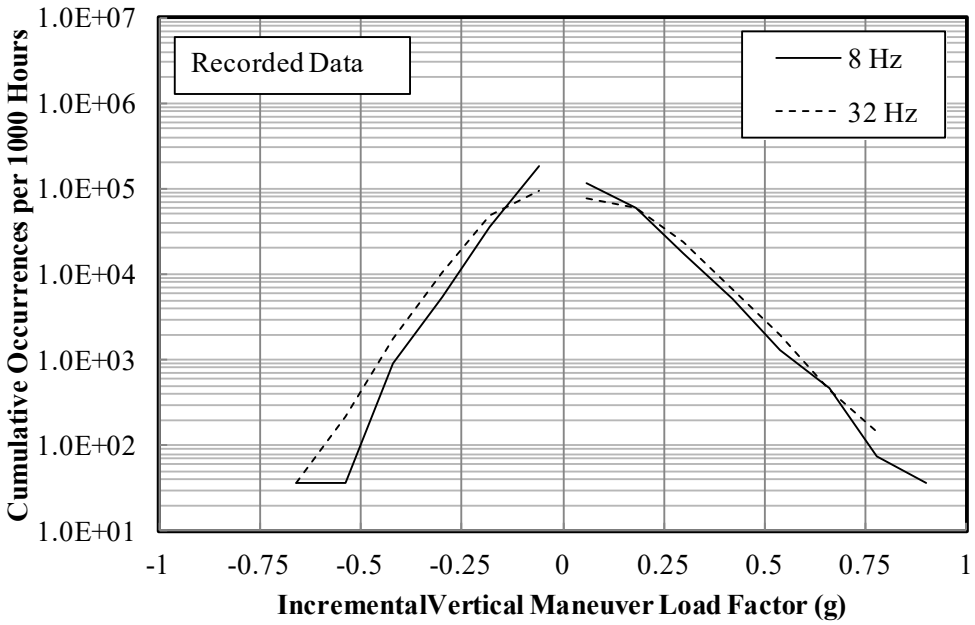

(b) Maneuver Loads

Figure A-9. Cumulative occurrence of incremental vertical load factor as recorded

A.3.2 Butterworth Filter

This filter offered two parameters that could be chosen; the filter order, and the cutoff frequency. The effect of the filter order was examined first, with a cutoff frequency of 8 Hz. Cutoff frequencies of 2 and 4 Hz also were examined for each filter order with similar results.

The incremental gust and maneuver loads spectra for various filter orders are shown in Figure A-10. It is clear from this figure that the filter order had minimal impact on the frequency of occurrence of the load factors. However, filtering out frequencies above 8 Hz did result in lowering the frequency of occurrence of the gust load factors by almost a factor of four. Positive maneuver load factors remained unchanged relative to the 32-Hz unfiltered data. The frequency of occurrence of the negative load factors was reduced and became closer to that of the unfiltered 8-Hz data at higher load factors.

Effects of cutoff frequency on the cumulative occurrences of incremental vertical load factor are shown in Figure A-11 for an eighth-order filter. In almost every case, the cutoff frequency of 2 Hz placed the cumulative occurrences of the load factor below the unfiltered 8-Hz recorded data. As the cutoff frequency increased, so did the cumulative occurrences. At higher load factors, for the cutoff frequency of 8 Hz, the cumulative counts per 1000 hours were approximately twice as many of those from the unfiltered 8-Hz data. However, the effect of the cutoff frequency was mostly limited to the cumulative occurrences of the gust load factors. The maneuver load factors, for the most part, remained insensitive to the magnitude of the cutoff frequency.

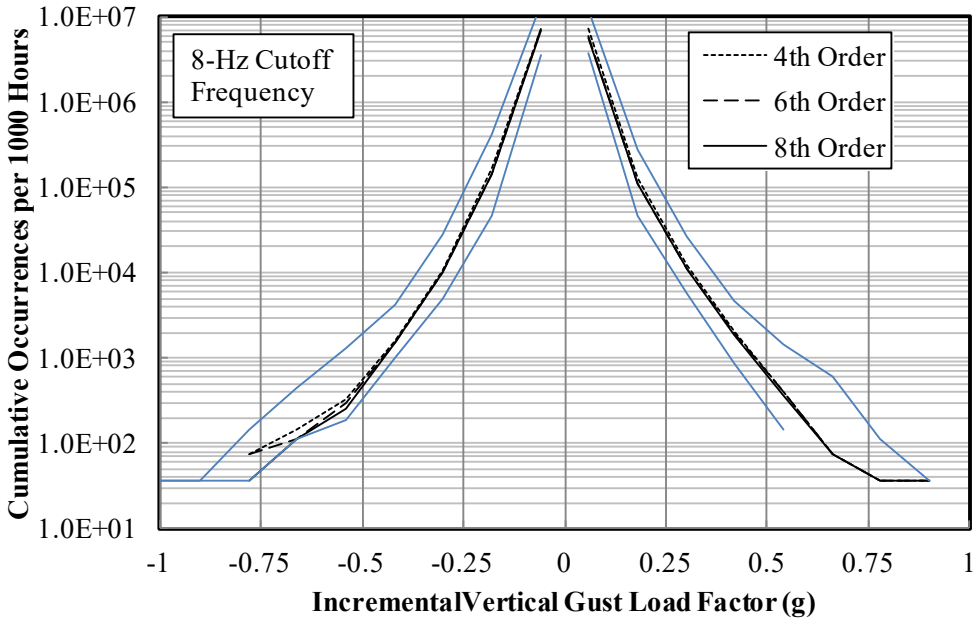

(a) Gust Loads

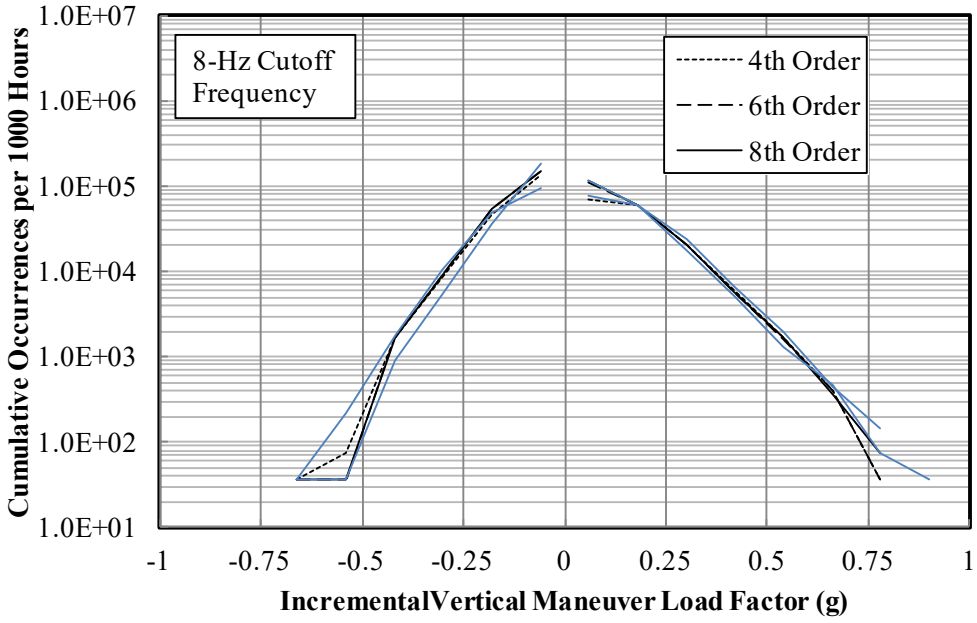

(b) Maneuver Loads

Figure A-10. Cumulative occurrence of incremental gust and maneuver vertical load factor – effect of Butterworth filter order

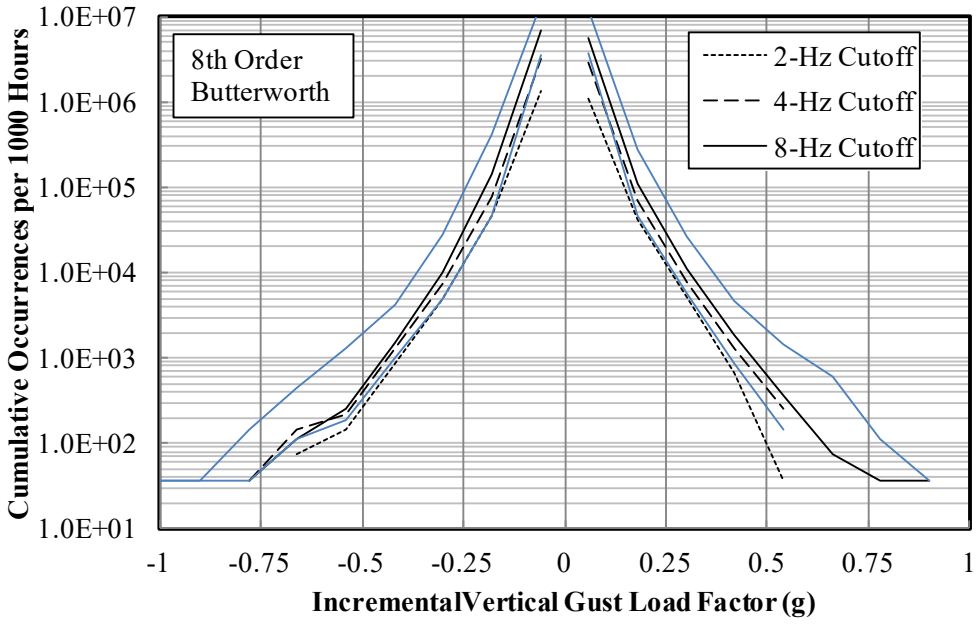

(a) Gust Loads

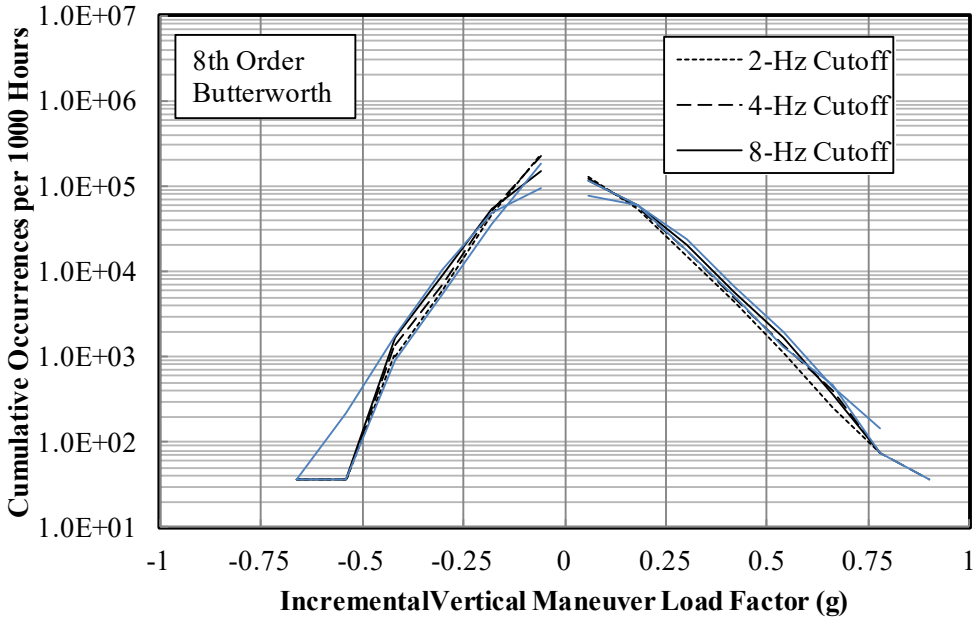

(b) Maneuver Loads

Figure A-11. Cumulative occurrence of incremental gust and maneuver vertical load factor – effect of Butterworth filter cutoff frequency

A.3.3 Finite Impulse Response Filter

As indicated previously, two centered, equally weighted FIR filters were investigated; a five-term, and a seven-term. This resulted in

$$y(n) = \frac{1}{5}\left[x(n-2) + x(n-1) + x(n) + x(n+1) + x(n+2)\right] \quad \text{(A-5)}$$

for the fifth-order and

$$y(n) = \frac{1}{7}\left[x(n-3) + x(n-2) + x(n-1) + x(n) + x(n+1) + x(n+2) + x(n+3)\right] \quad \text{(A-6)}$$

for the seventh-order filters. The effect of these filters was essentially to average either five or seven terms around the point of interest.

Figure A-12 indicates that the filtered data showed a very good agreement with the loads counts with those of the data recorded at 8 Hz, with the fifth-order filter showing slightly higher counts.

A.3.4 Data Skipping

This was the last filter described above in which the 32-Hz data is down-sampled to 8 Hz. In this case, data skipping was started with the first point, although it is suspected that starting with other points would result in similar cumulative occurrences of the load factors.

The results shown in Figure A-13 show the same trends as those of the previous filters. The cumulative occurrences of the incremental vertical gust loads fell in between those of the recorded 32-Hz and 8-Hz data, but the maneuver load counts proved insensitive to the filtering.

A.3.5 Comparison of Various Filters

In the previous sections, the effect of each filter was examined individually. However, a comparison of the effects of various filters on the same figure may be of interest. In order to avoid clutter, a single figure is used to compare the effects of the following filters with those of the data recorded at 32 Hz and 8 Hz:

- Eighth-order Butterworth filter with cutoff frequency of 8 Hz
- Fifth-order FIR filter
- Down-sampled data using data skipping

The results are shown in Figure A-14, which led to the following observations regarding cumulative occurrences of gust loads:

- The 32-Hz recorded data significantly overpredicted the counts.
- Excellent agreement was evident between the results of the fifth-order FIR filter and the 8-Hz recorded data.
- Very good agreement was present between the results from data skipping and eighth-order Butterworth filter with 8-Hz cutoff frequency.

This figure also shows that the cumulative occurrences of the maneuver load factors were quite insensitive to the filtering scheme.

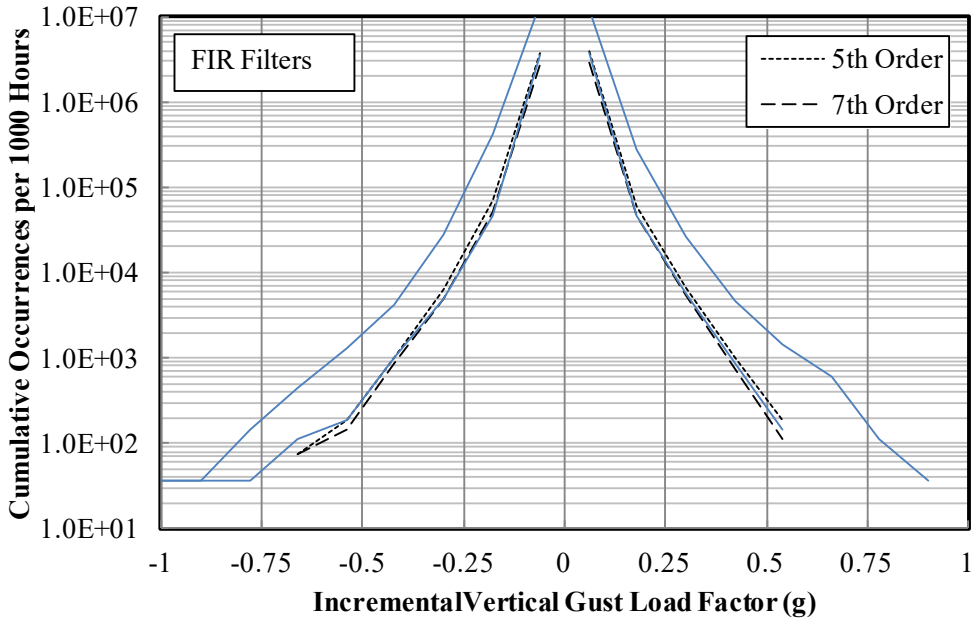

(a) Gust Loads

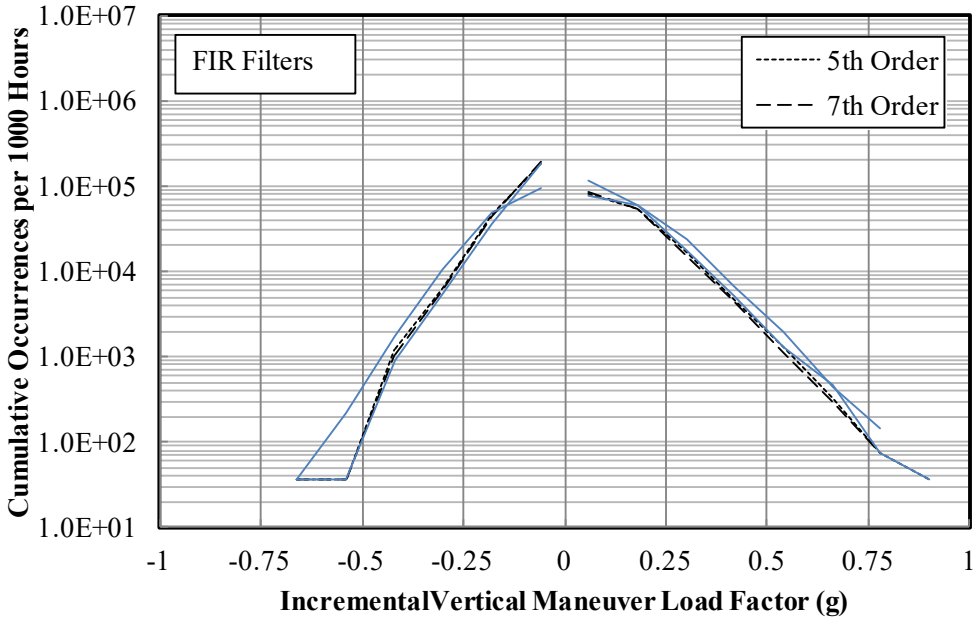

(b) Maneuver Loads

Figure A-12. Cumulative occurrence of incremental gust and maneuver vertical load factor – effect of fir filters

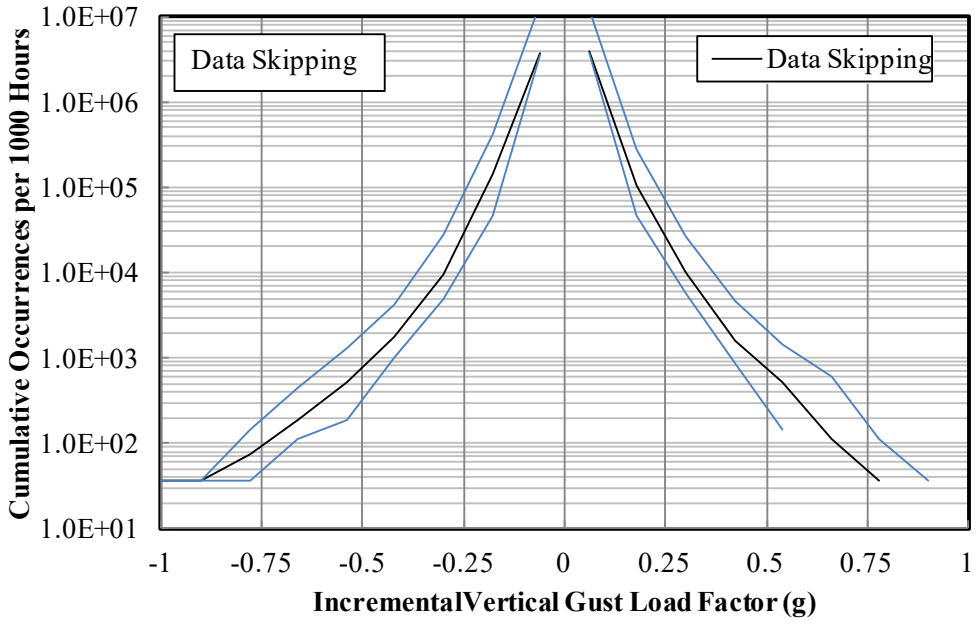

(a) Gust Loads

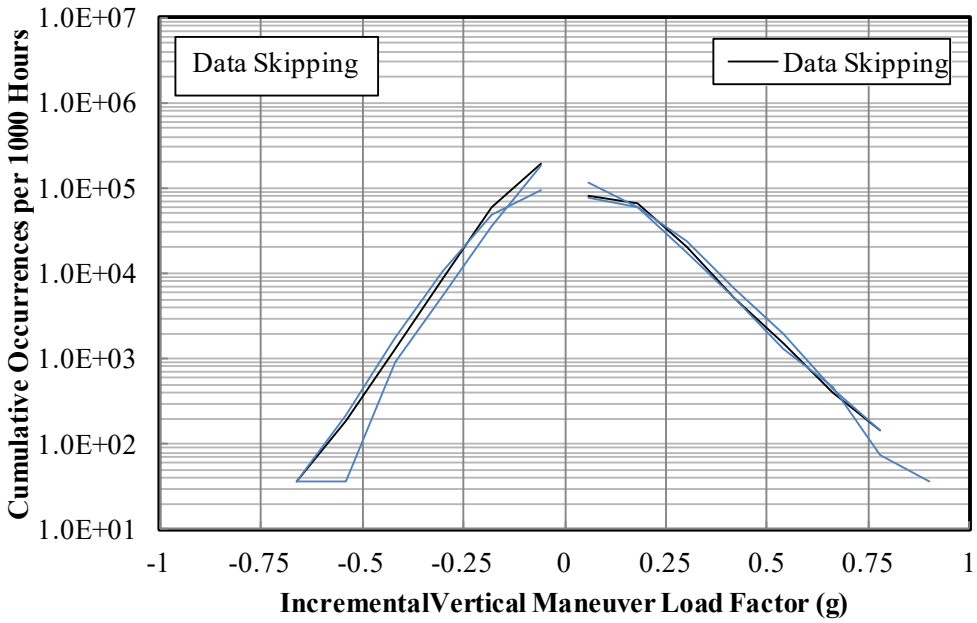

(b) Maneuver Loads

Figure A-13. Cumulative occurrence of incremental gust and maneuver vertical load factor – effect of data skipping

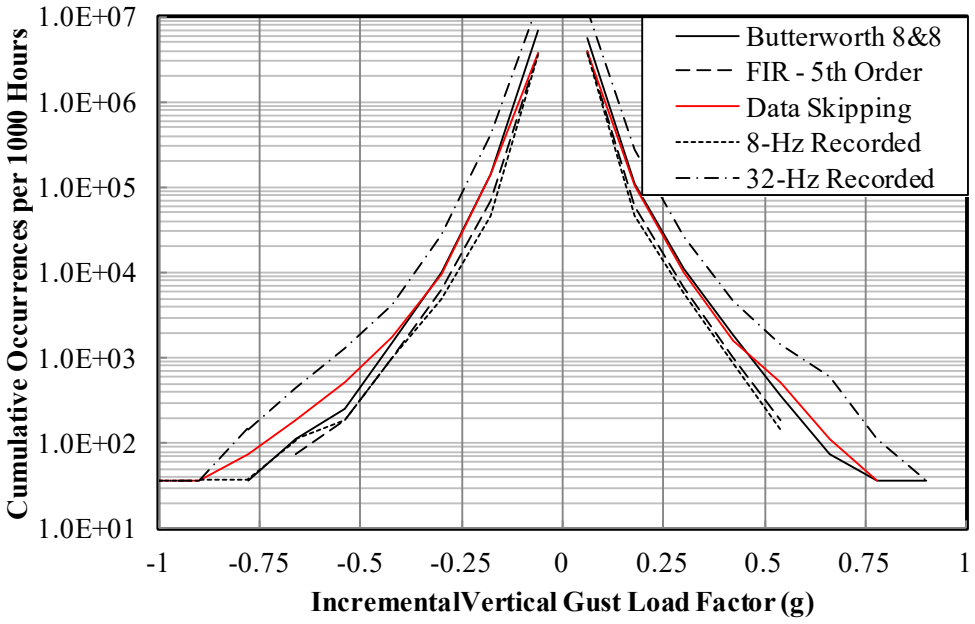

(a) Gust Loads

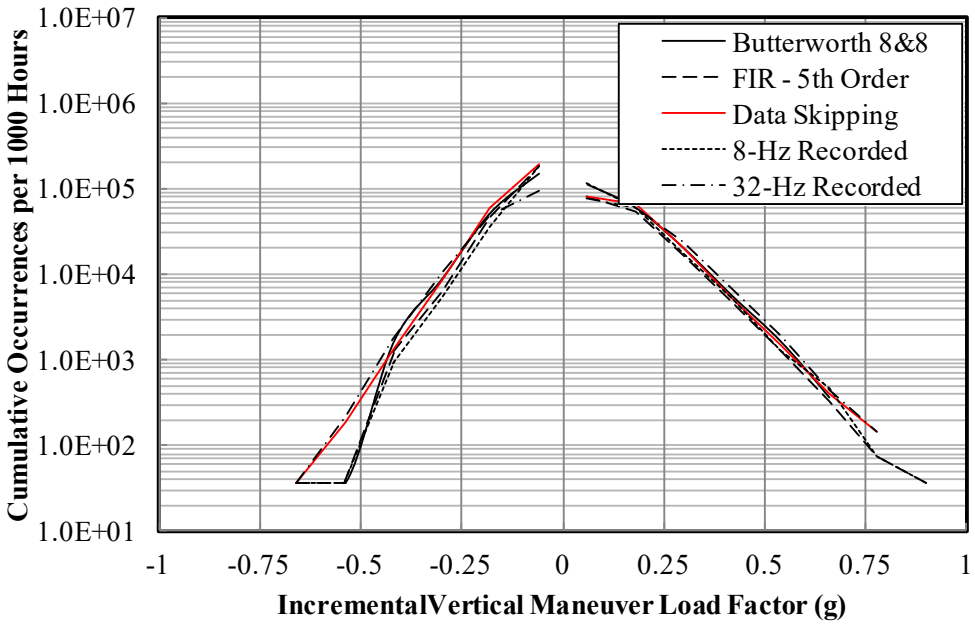

(b) Maneuver Loads

Figure A-14. Cumulative occurrence of incremental gust and maneuver vertical load factor – comparison of various filters

Another comparison presented here is that of the raw numbers of counts per 1000 hours for various filters. While graphical results afford quick comparison of results, they can also be misleading, especially when presented using logarithmic scale. These results are shown in Table A-2 and Table A-3, for incremental gust and maneuver load factors, respectively. Each band covered a width of 0.12 g, with the dead band in the center of ±0.05 g. The incremental load factors shown here

represent the values the center of each band (e.g. a value of 0.78 g represented a load factor range of 0.72 g to 0.84 g). Therefore, the bands labeled as ±0.06 g were partially covered by the dead band.

Examination of these results led to the following observations:

- The frequency of occurrence of the gust loads from the 32-Hz recorded data led to excessive number of counts. This was consistent with the earlier graphical observations.
- The cumulative occurrences of the incremental maneuver vertical load factor were somewhat insensitive to the method of filtering.
- Gust load results from eighth-order Butterworth with 4-Hz cutoff, fifth-order FIR, data skipping, and 8-Hz recorded data resembled each other greatly.

Table A-2. Cumulative occurrences of incremental vertical gust load factor per 1000 hours

Inc. Load Factor (g)	8th Order Butterworth Filters			FIR Filters		Data Skipping	8-Hz Recorded	32-Hz Recorded
	2-Hz Cutoff	4-Hz Cutoff	8-Hz Cutoff	5th Order	7th Order			
-1.02	0	0	0	0	0	36	37	37
-0.90	0	0	0	0	0	36	37	37
-0.78	0	37	37	0	0	73	37	147
-0.66	74	147	110	73	73	182	110	442
-0.54	147	221	258	182	146	510	184	1,288
-0.42	884	1,288	1,509	984	875	1,786	994	4,233
-0.30	4,970	7,510	9,903	6,235	4,886	9,479	4,970	27,536
-0.18	45,206	77,565	141,140	67,705	51,189	142,700	46,936	422,906
-0.06	1,316,574	3,265,003	6,967,122	3,807,790	2,800,999	3,756,796	3,576,992	14,126,665
Dead Band								
0.06	1,105,232	2,850,638	5,687,250	3,929,200	2,917,013	3,880,464	3,727,004	12,126,955
0.18	40,973	68,325	109,629	60,049	46,595	106,715	47,268	279,152
0.30	5,154	7,878	10,970	6,781	5,432	9,990	5,816	26,689
0.42	663	1,288	1,841	1,021	729	1,604	847	4,565
0.54	37	258	368	182	109	510	147	1,436
0.66	0	0	74	0	0	109	0	589
0.78	0	0	37	0	0	36	0	110
0.90	0	0	37	0	0	0	0	37
1.02	0	0	0	0	0	0	0	0

Table A-3. Cumulative occurrences of incremental vertical maneuver load factor per 1000 hours

Inc. Load Factor (g)	8th Order Butterworth Filters			FIR Filters		Data Skipping	8-Hz Recorded	32-Hz Recorded
	2-Hz Cutoff	4-Hz Cutoff	8-Hz Cutoff	5th Order	7th Order			
-1.02	0	0	0	0	0	0	0	0
-0.90	0	0	0	0	0	0	0	0
-0.78	0	0	0	0	0	0	0	0
-0.66	37	37	37	36	36	36	36	37
-0.54	37	37	37	36	36	182	36	221
-0.42	1,031	1,362	1,657	1,203	1,057	1,313	911	1,730
-0.30	6,037	6,884	9,019	6,235	5,979	8,568	5,287	10,565
-0.18	45,206	50,802	53,636	45,757	44,663	58,261	35,876	48,630
-0.06	236,117	219,441	153,068	187,693	194,985	190,425	180,909	96,229
Dead Band								
0.06	127,152	122,992	114,046	79,700	87,248	81,267	114,444	77,307
0.18	52,826	56,949	61,072	54,543	53,778	64,350	60,194	58,569
0.30	14,872	17,449	20,321	16,370	15,021	20,125	17,354	23,744
0.42	4,381	5,007	5,632	4,630	4,412	5,250	5,068	6,626
0.54	1,141	1,362	1,657	1,313	1,094	1,495	1,313	1,951
0.66	258	405	368	328	292	401	474	442
0.78	74	74	74	73	73	146	73	147
0.90	0	37	0	36	0	0	36	0
1.02	0	0	0	0	0	0	0	0

Finally, the total number of occurrences of gust and maneuver loads per 1000 hours over the entire 27.4 hours of operation are shown in Figure A-15. It was shown earlier that the order of the Butterworth filter did not influence the results much. Therefore, only the results from the eighth-order Butterworth filter are shown here. These results support the observations made earlier. Furthermore, it is obvious in this figure that as the filtering of the data reduced the occurrence of the gust loads, it increased that of the maneuver loads.

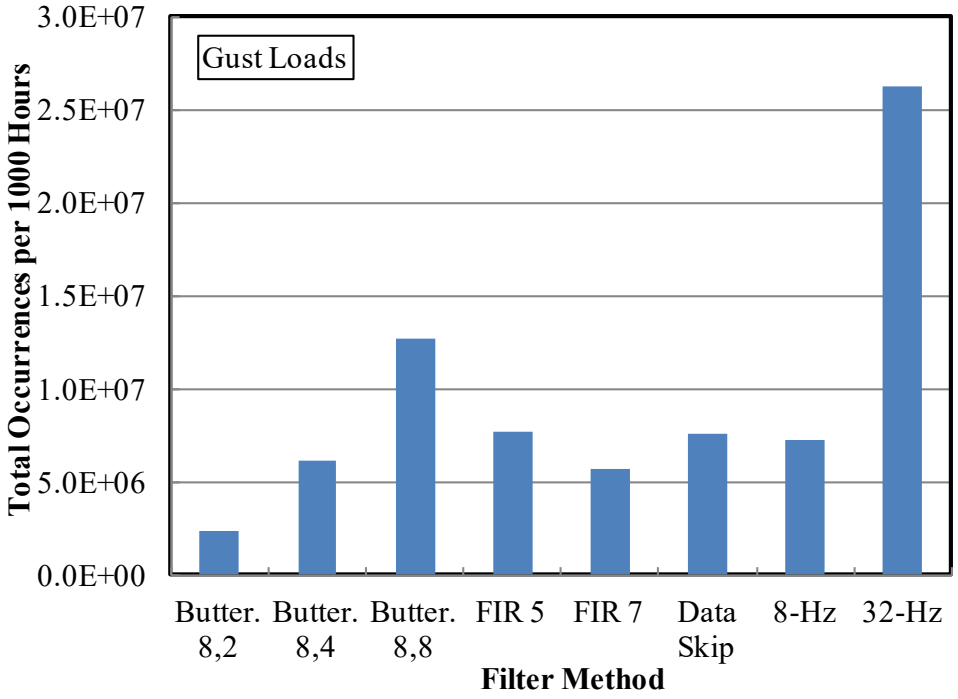

(a) Gust Loads

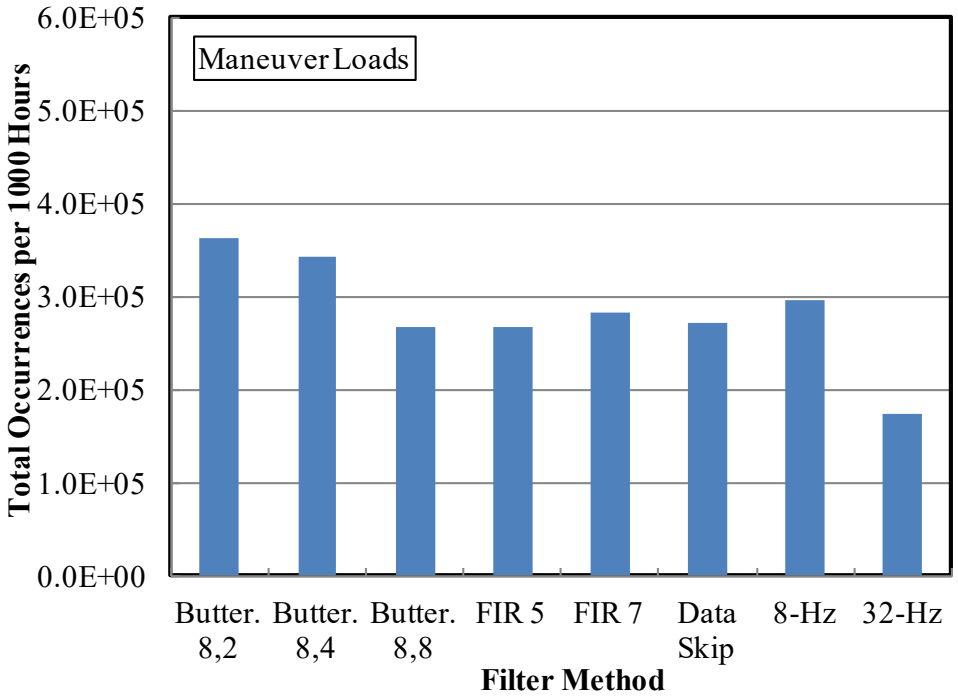

(b) Maneuver Loads

Figure A-15. Total number of loads per 1000 hours over 27.4 hours of operation

A.4. SUMMARY AND CONCLUSIONS

Operational data from three airframes, amounting to 27.4 hours of operations, were used to examine the effectiveness of various filters in minimizing the influence of the structural modes on the extracted gust and maneuver loads spectra. One filter in the frequency domain and two types of filter in the time domain were examined in this process. Data recorded by Appareo GAU-2000 units at 8 Hz and 32 Hz on the same airframes were used for comparison. It was demonstrated that the acceleration resulting from structural vibration could greatly and artificially increase the cumulative occurrences of the incremental vertical gust loads.

The standard Butterworth filter was used in the frequency domain. It was demonstrated that the results were not affected by the order of the filter, but depended on the cutoff frequency. Cutoff frequencies of 2, 4, and 8 Hz were used in the analysis. While frequency of 2 Hz is well below that of any structural mode, cutoff frequencies above 8 Hz could allow some of the lower structural modes to interfere with the data. Consequently, with this filter, a cutoff frequency of 8 Hz would be recommended.

FIR filters were also investigated. They were centered, equally-weighted, fifth- and seventh-order averaging schemes. Both proved effective at removing the higher frequencies.

The last filter consisted of skipping every three lines of the 32-Hz data for down-sampling it to 8 Hz. This method produced results very similar to that of an eighth-order Butterworth filter with cutoff frequency of 8 Hz.

While all of the above filters proved effective at reducing the influence of the structural vibration on the resulting loads spectra, the authors recommended to FAA and USFS the following schemes in the order of preference:

1. A fifth-order centered FIR filter offers adequate filtering of the data in the time domain. Consequently, it can be implemented directly as part of the analysis in extracting loads spectra, with minimal computational overhead.
2. Any order Butterworth filter with a cutoff frequency of 4 Hz could serve the purpose. The results proved insensitive to the order of the filter. Cutoff frequency of 2 Hz appeared to remove too many of the gust occurrences, while frequencies above 8 Hz allowed too many of the structural modes to affect the data. This technique offers the most analytically robust method of filtering the data. However, its implementation requires transforming the data into the frequency domain, filtering it, and back-transforming into the time domain. These transformations increase the computational overhead, which can be significant when analyzing large volumes of data.
3. Down-sampling the data using data skipping, while apparently crude, seemed to be equally effective as the above two filters. This technique can also be implemented in the time domain with minimal computational overhead. However, this method leaves open the question of whether or not the correct peaks and valleys are included in the results.

During a joint FAA/USFS/WSU meeting, it was determined that the Butterworth filter would be used for this project due to the robustness of this method. The cutoff frequency of 8 Hz was chosen to ensure elimination of higher structural modes.

APPENDIX B—USAGE DATA PRESENTATION

Table B-1. Statistical formats – usage data

Usage Data	Table
Summary of Flights, Durations, and Distances	Table B-4
Frequency of Flap and Speed Brake Deflections	Table B-5
Flight Time with Flap or Speed Brake Deflection	Table B-6
Takeoff and Landing Weights	Table B-7
Takeoff and Landing Indicated Airspeeds	Table B-8

Table B-2. Statistical formats – usage data

Usage Data	Figure
OVERALL FLIGHTS	
Number of Flights Based on Duration	Figure B-1
Distances and Durations	Figure B-2
Maximum MSL Altitudes and Corresponding Flight Distance	Figure B-3
Maximum MSL Altitude and Coincident Indicated Airspeed	Figure B-4
Maximum Indicated Airspeed and Coincident MSL Altitude	Figure B-5
V-n Diagram Compared with Sea-Level Limits	Figure B-6
V-n Diagram with Speed Brake Deployed	Figure B-8
Frequency of Flap and Speed Brake Deployment	Figure B-9
Number of Drops per Flight	Figure B-10
Distribution of Total Drop Duration per Flight	Figure B-11
Probability Distribution of Takeoff and Landing Weights	Figure B-12

Probability Distribution of Takeoff and Landing Airspeeds	Figure B-14
Maximum Lateral Load Factor and Coincident Vertical Load Factor at Landing	Figure B-16
CRUISE 1	
Number of Occurrences by Duration – Cruise 1	Figure B-17
Correlation of Distance and Duration – Cruise 1	Figure B-18
Maximum MSL Altitude and Corresponding Distance – Cruise 1	Figure B-19
Maximum MSL Altitude and Coincident Indicated Airspeed – Cruise 1	Figure B-20
Maximum Indicated Airspeed and Coincident MSL Altitude – Cruise 1	Figure B-21

MSL = Mean sea level

Table B-3. Statistical formats – usage data (continued)

Usage Data	Figure
CRUISE 2	
Number of Occurrences by Duration – Crusie 2	Figure B-22
Correlation of Distance and Duration – Cruise 2	Figure B-23
Maximum MSL Altitude and Corresponding Distance – Cruise 2	Figure B-24
Maximum MSL Altitude and Coincident Indicated Airspeed – Cruise 2	Figure B-25
Maximum Indicated Airspeed and Coincident MSL Altitude – Cruise 2	Figure B-26
ENTRY	
Number of Occurrences by Duration – Entry	Figure B-27
Correlation of Distance and Duration – Entry	Figure B-28
Maximum MSL Altitude and Corresponding Distance – Entry	Figure B-29
Maximum MSL Altitude and Coincident Indicated Airspeed – Entry	Figure B-30
Maximum Indicated Airspeed and Coincident MSL Altitude – Entry	Figure B-31
V-n Diagram – Entry	Figure B-32
DROP	
Number of Occurrences by Duration – Drop	Figure B-33
Correlation of Distance and Duration – Drop	Figure B-34
Maximum MSL Altitude and Corresponding Distance – Drop	Figure B-35
Maximum MSL Altitude and Coincident Indicated Airspeed – Drop	Figure B-36
Maximum Indicated Airspeed and Coincident MSL Altitude – Drop	Figure B-37
V-n Diagram – Drop	Figure B-38

EXIT	
Number of Occurrences by Duration – Exit	Figure B-39
Correlation of Distance and Duration – Exit	Figure B-40
Maximum MSL Altitude and Corresponding Distance – Exit	Figure B-41
Maximum MSL Altitude and Coincident Indicated Airspeed – Exit	Figure B-42
Maximum Indicated Airspeed and Coincident MSL Altitude – Exit	Figure B-43
V-*n* Diagram – Exit	Figure B-44

Table B-4. Summary of flights, durations, and distances

Model	Tanker Number	Number of Good Flights	Duration (min)	Duration (hr)	Distance (nm)
BAe-146	1	1040	37,132	619	155,085
	2	515	19,425	324	80,189
	3	646	24,512	409	99,595
	4	515	20,897	348	84,147
	5	818	24,889	415	99,160
	6	329	14,066	234	56,848
	7	820	32,074	535	130,954
	8	974	37,558	626	152,777
RJ-85	9	781	30,615	510	119,056
	10	377	15,811	264	63,917
	11	588	23,682	395	97,008
	12	767	29,459	491	116,646
	13	596	21,802	363	85,780
	14	337	18,623	310	80,765
	15	171	8,189	136	36,174
	16	428	17,320	289	67,762
Total	---	9,702	376,052	6,268	1,525,862

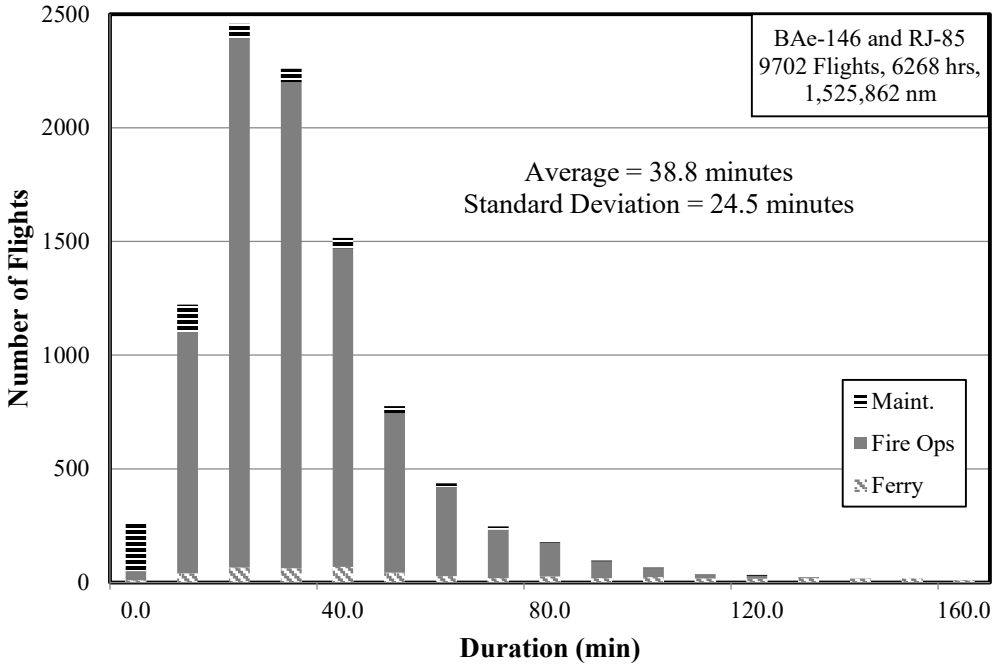

Figure B-1. Number of flights based on duration

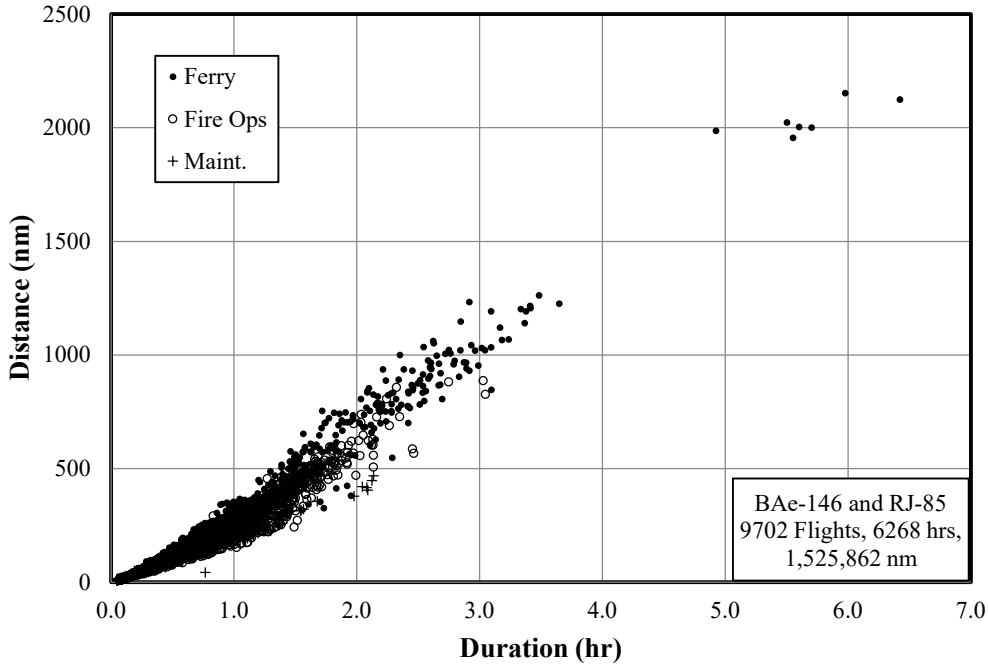

Figure B-2. Distances and durations

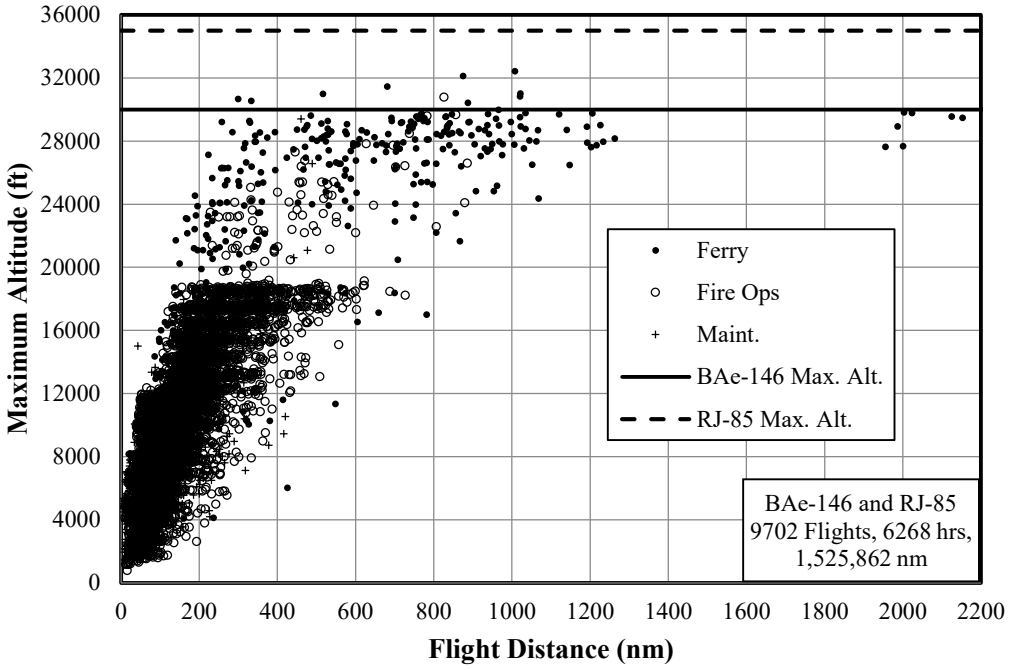

Figure B-3. Maximum MSL altitudes and corresponding flight distance

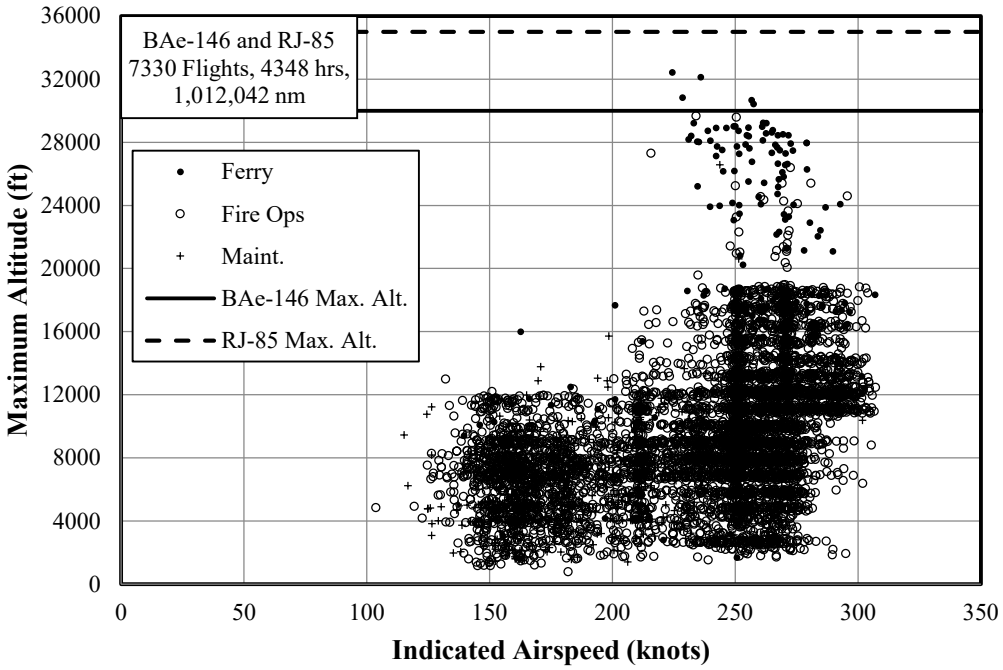

Figure B-4. Maximum MSL altitude and coincident indicated airspeed

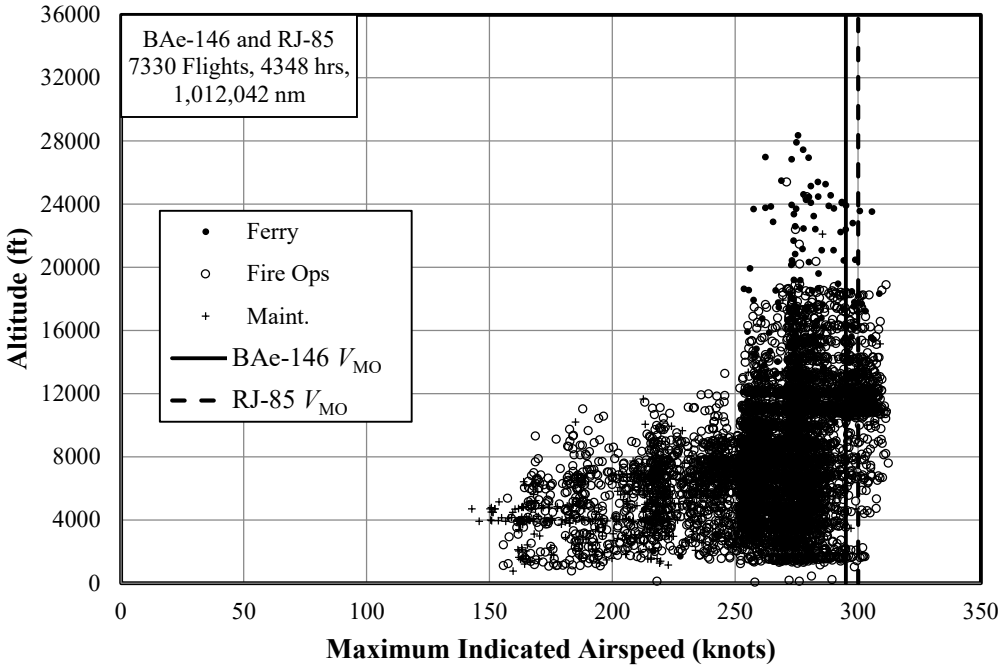

Figure B-5. Maximum indicated airspeed and coincident MSL altitude

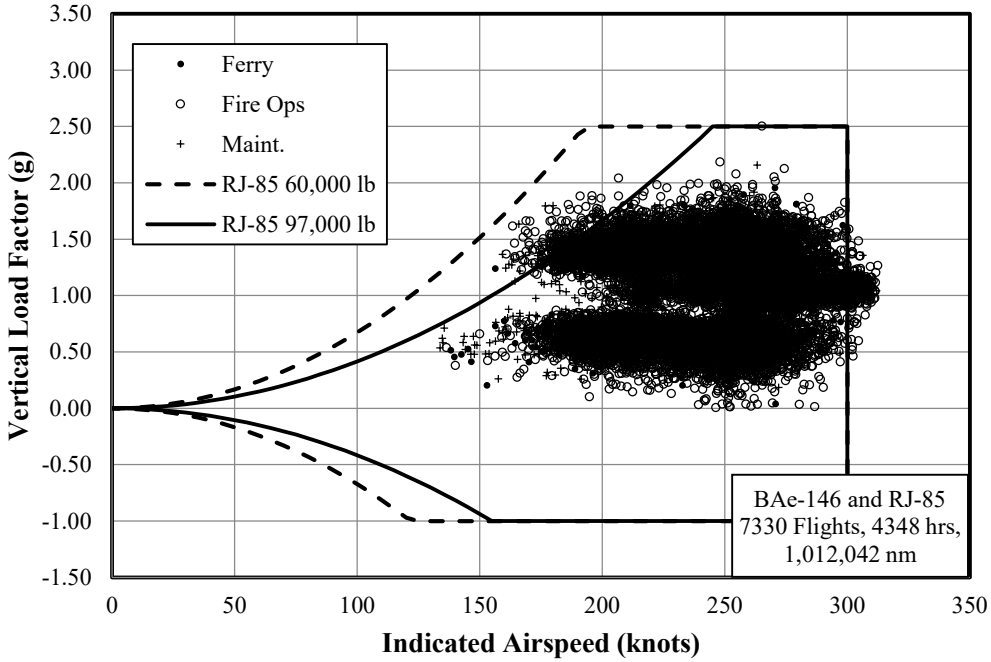

(a) FlapsRetracted

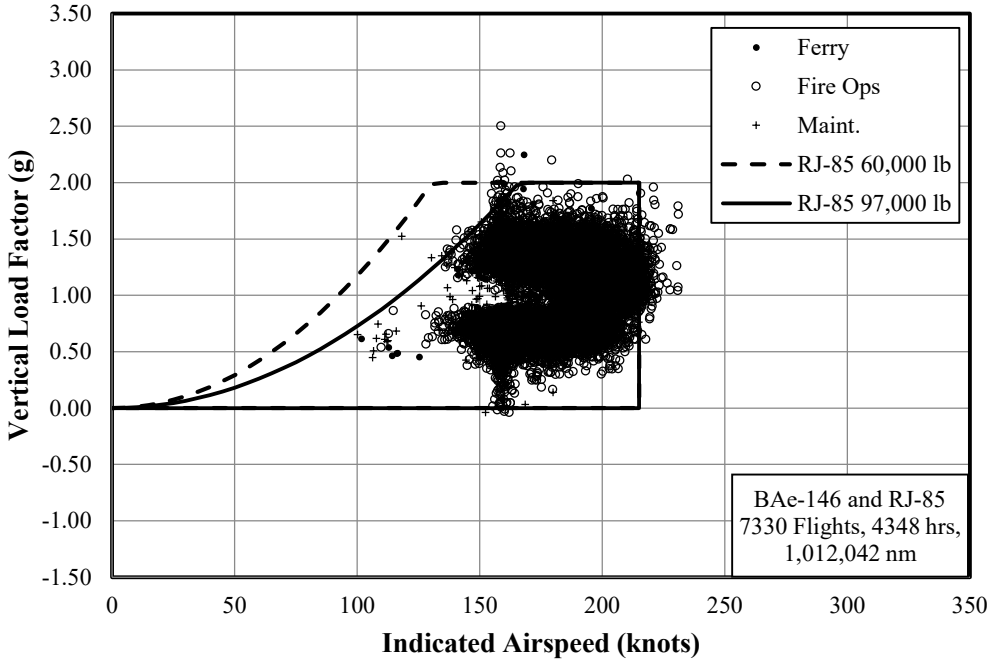

(b) Flaps in the First Detent

Figure B-6. *V-n* diagram compared with sea-level limits

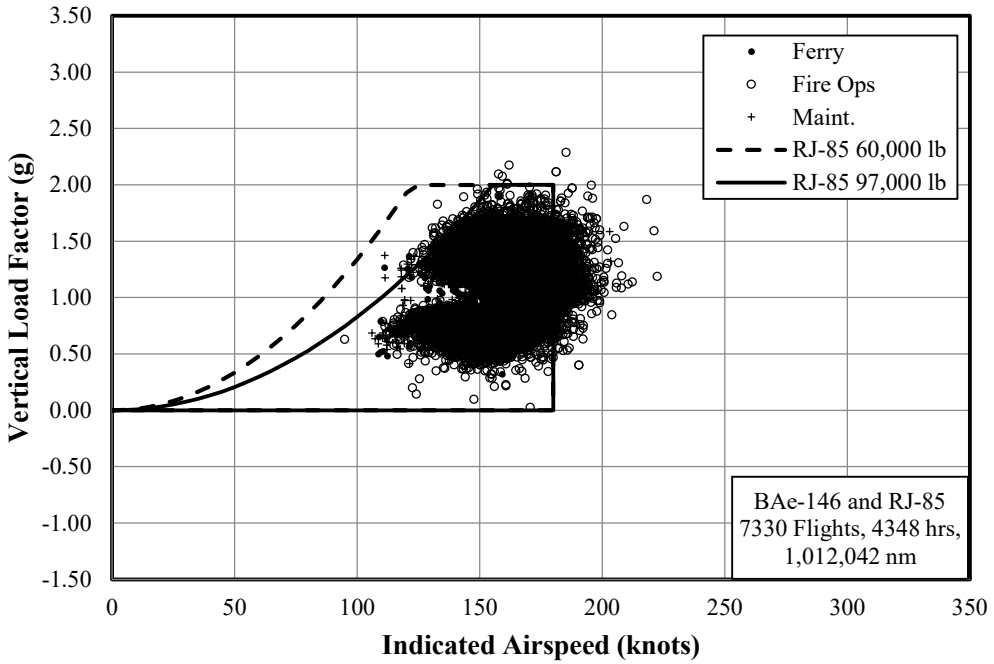

(c) Flaps in the Second Detent

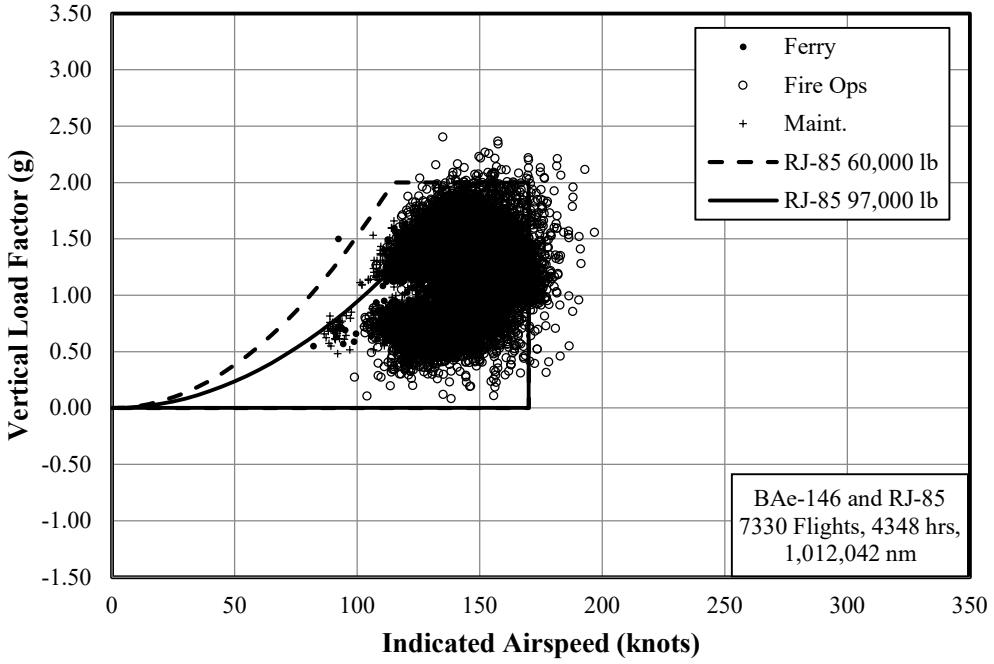

(d) Flaps in the Third Detent

Figure B-7. *V-n* diagram compared with sea-level limits (continued)

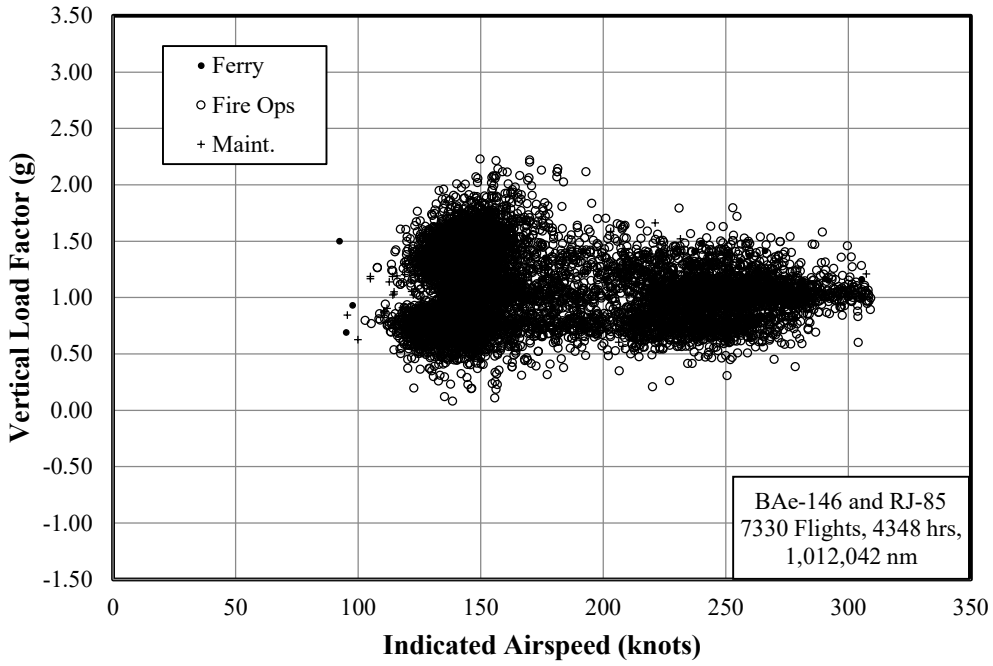

Figure B-8. *V-n* diagram with speed brake deployed

Table B-5. Frequency of flap and speed brake deflections

	Total Number of Deflections			Average Deflections per Flight		
Flap/Speed Brake	Ferry	Fire Ops	Maint.	Ferry	Fire Ops	Maint.
First Detent	1533	30,314	1737	2.84	3.53	2.98
Second Detent	1190	33,300	1781	2.20	3.88	3.06
Third Detent	1390	48,085	1993	2.57	5.60	3.42
Speed Brake	543	20,038	425	1.01	2.34	0.73

Based on 540 ferry, 8580 firefighing, and 582 maintenance/training flights

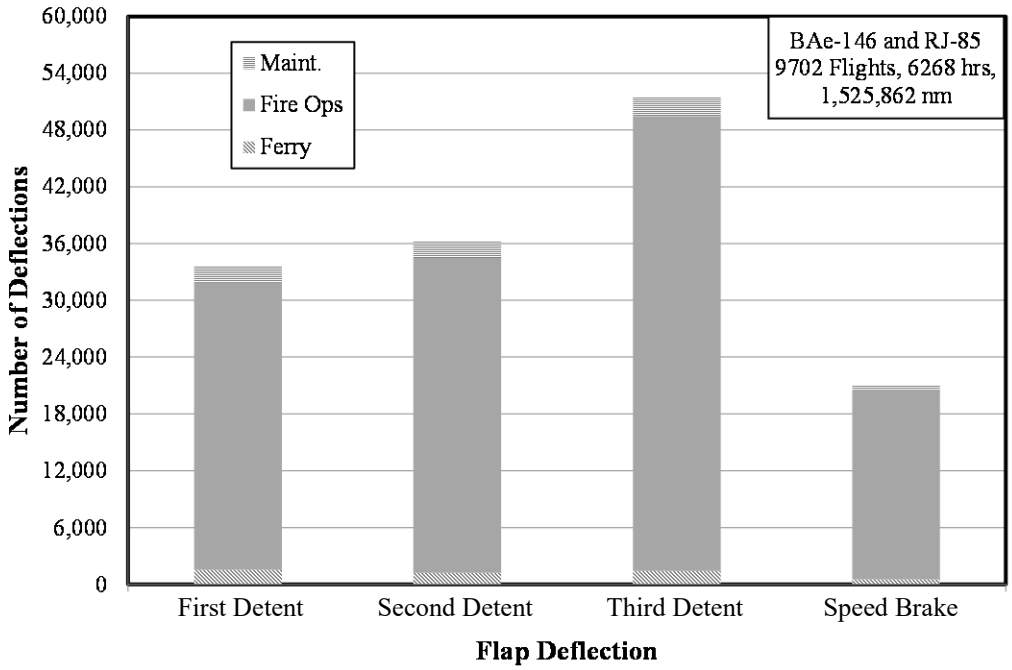

Figure B-9. Frequency of flap and speed brake deployment

Table B-6. Flight time with flap or speed brake deflection

	Total Deflection Time			Percentage of Flight Time		
Flap/Speed Brake	Ferry	Fire Ops	Maint.	Ferry	Fire Ops	Maint.
Flaps Retracted	617	3116	120	93.2	61.7	52.7
First Detent	23	706	54	3.5	14.0	23.8
Second Detent	11	842	32	1.6	16.7	14.2
Third Detent	11	390	21	1.6	7.7	9.2
Speed Brake	7	143	4	1.1	2.8	1.9

Based on 662 hours of ferry, 5055 hours of firefighting, and 227 hours of maintenance/training flights

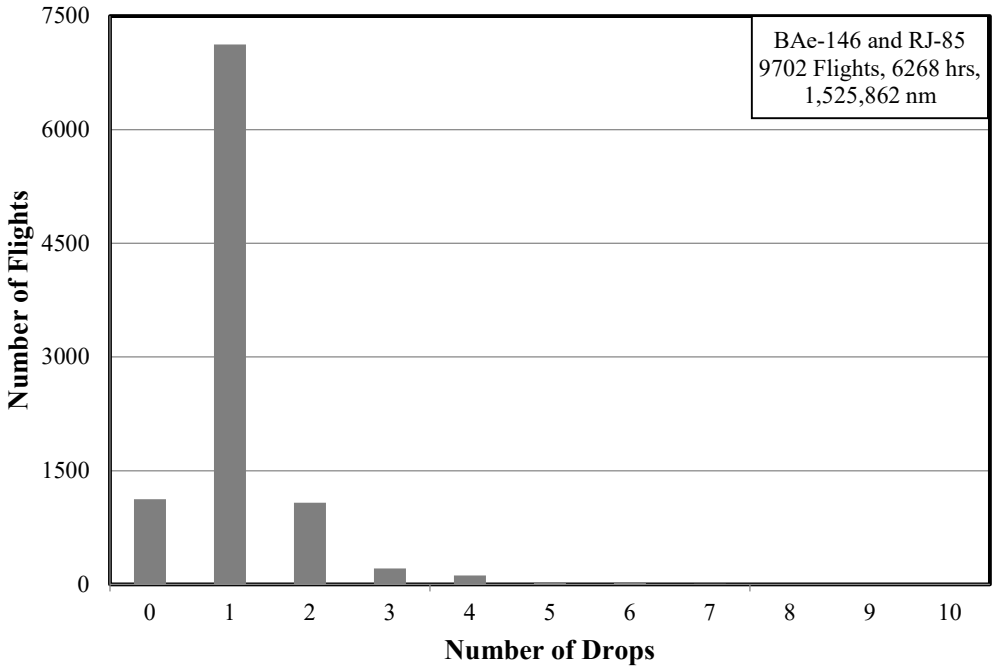

Figure B-10. Number of drops per flight

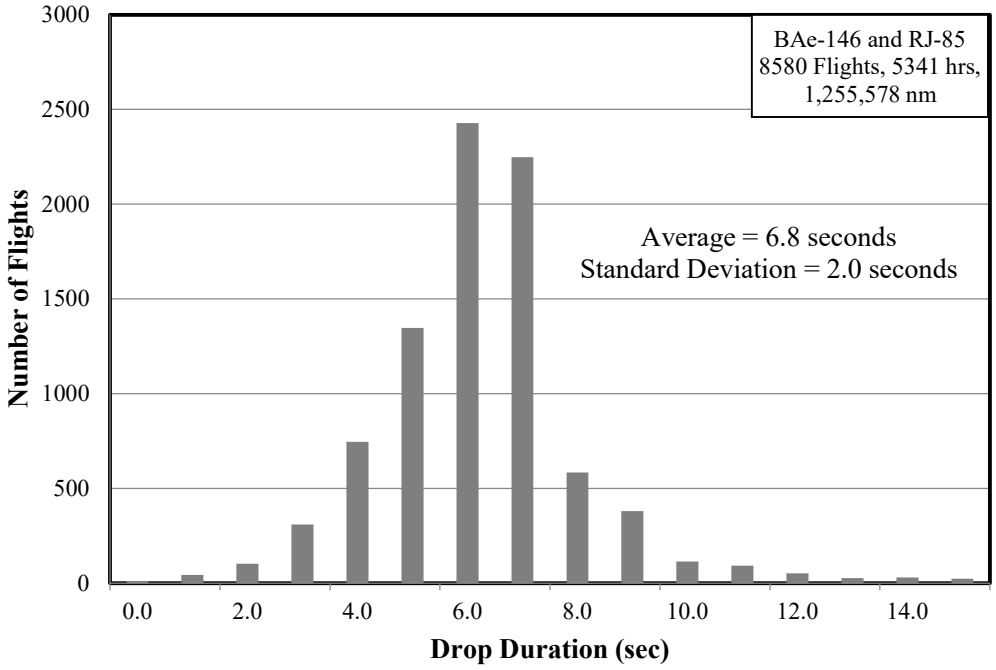

Figure B-11. Distribution of total drop duration per flight

Table B-7. Takeoff and landing weights

Missions	Takeoff		Landing	
	Average (pounds)	Standard Deviation (pounds)	Average (pounds)	Standard Deviation (pounds)
Ferry	67,638.1	6389.4	62,095.4	6778.1
Firefighting	87,447.0	2866.7	58,882.8	3109.6
Maint/Training	72,184.7	9443.9	70,124.8	8910.5

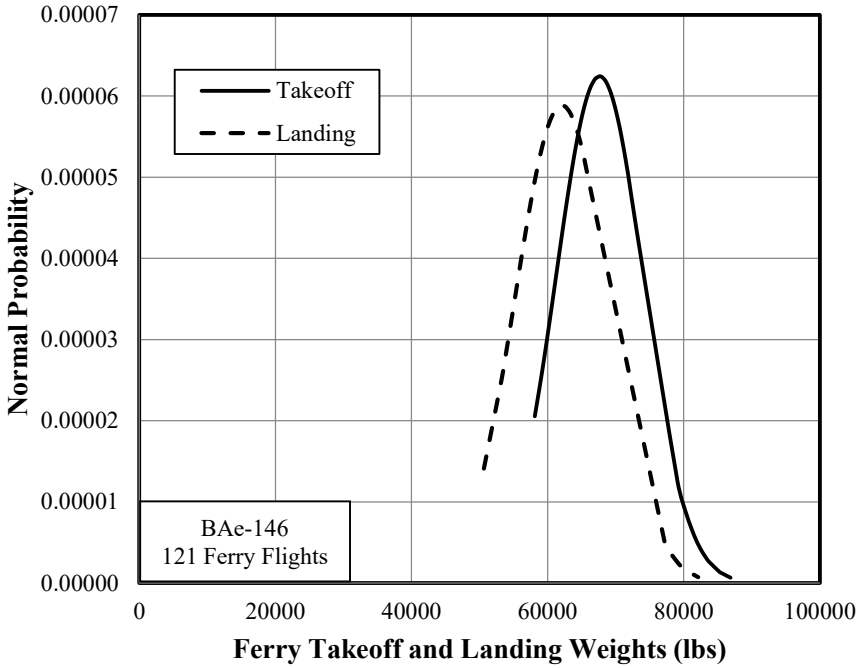

(a) Ferry Flights

Figure B-12. Probability distribution of takeoff and landing weights

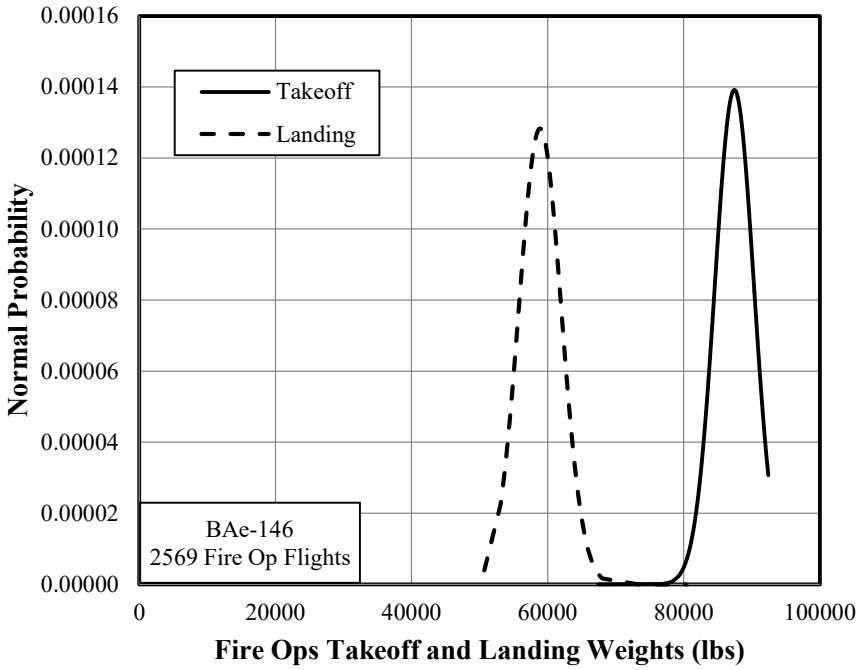

(b) Firefighting Flights

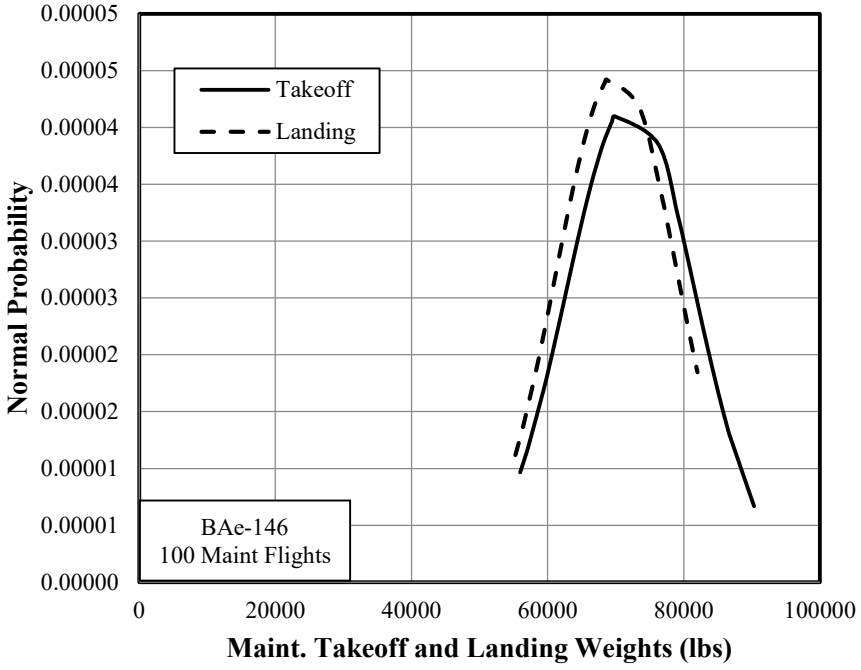

(c) Maintenance/Training Flights

Figure B-13. Probability distribution of takeoff and landing weights (continued)

Table B-8.Takeoff and landing indicated airspeeds

Missions	Takeoff		Landing	
	Average (KIAS)	Standard Deviation (KIAS)	Average (KIAS)	Standard Deviation (KIAS)
Ferry	127.2	7.9	102.4	15.9
Firefighting	134.9	9.3	101.9	20.2
Maint/Training	125.8	8.0	104.0	12.3

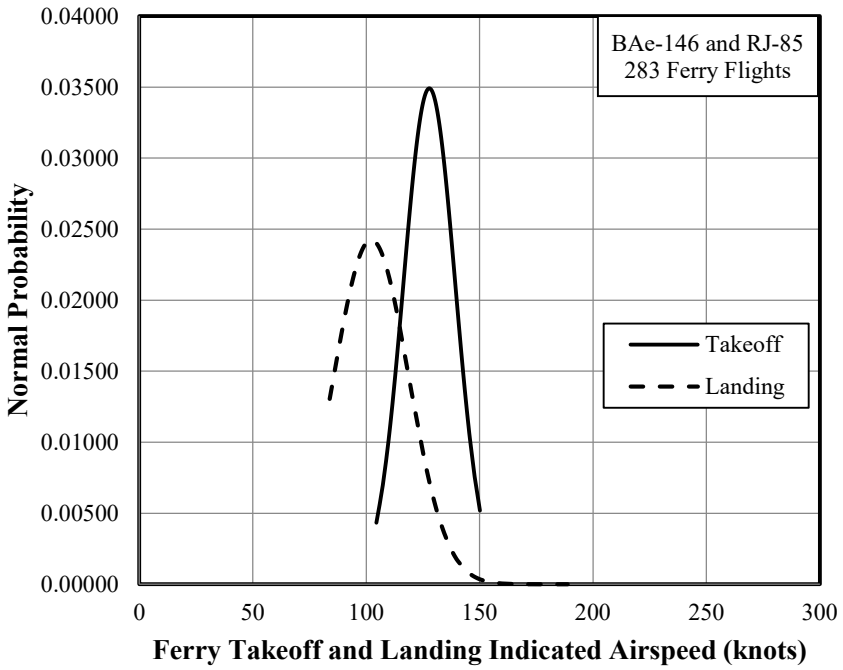

(a) Ferry Flights

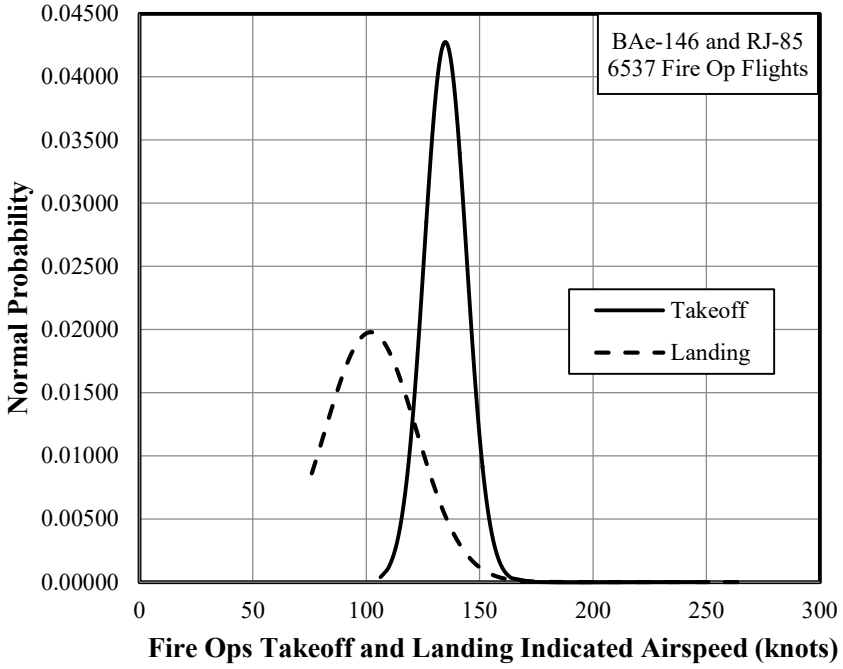

(b) Firefighting Flights

Figure B-14. Probability distribution of takeoff and landing airspeeds

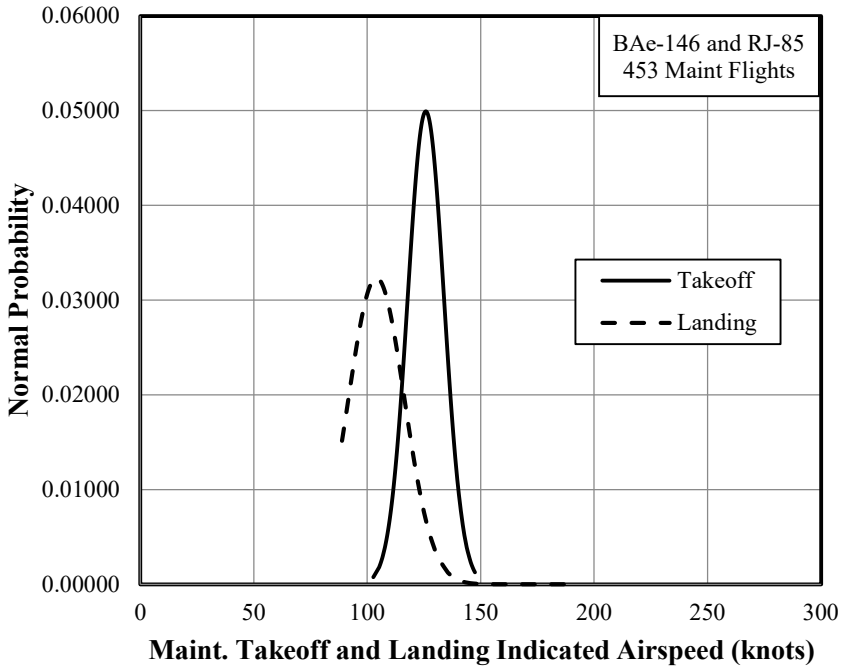

(c) Maintenance/Training Flights

Figure B-15. Probability distribution of takeoff and landing airspeeds (continued)

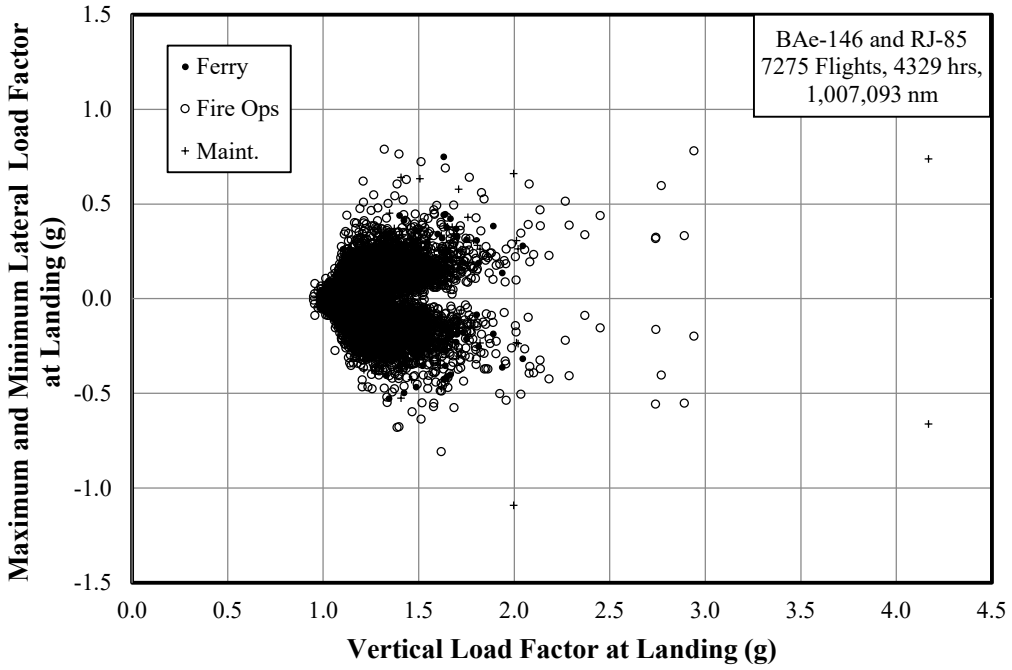

Figure B-16. Maximum and minimum lateral load factor and coincident vertical load factor at landing

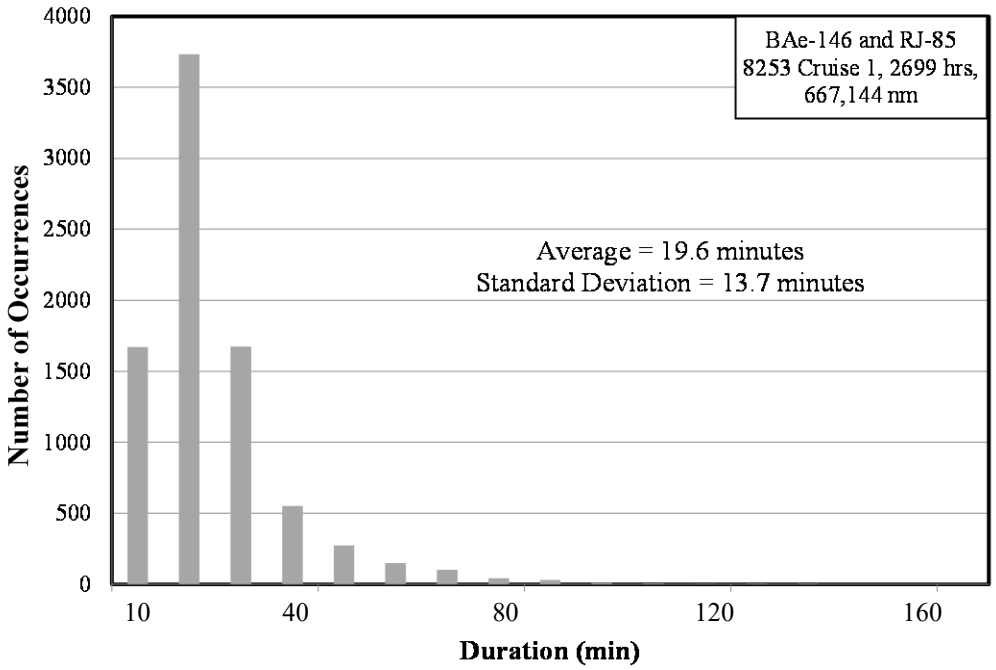

Figure B-17. Number of occurrences by duration – cruise 1

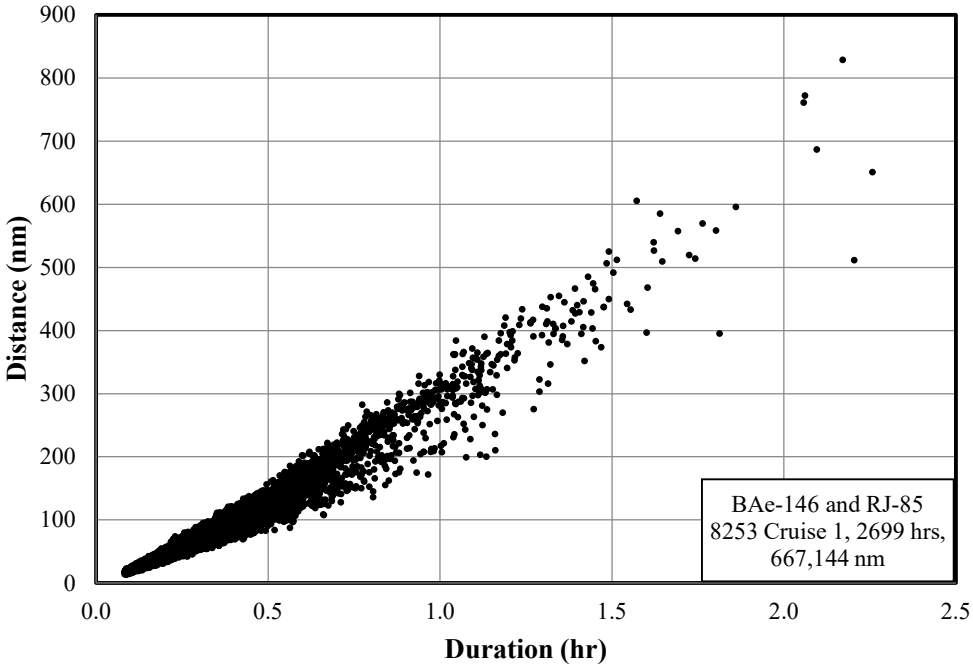

Figure B-18. Correlation of distance and duration – cruise 1

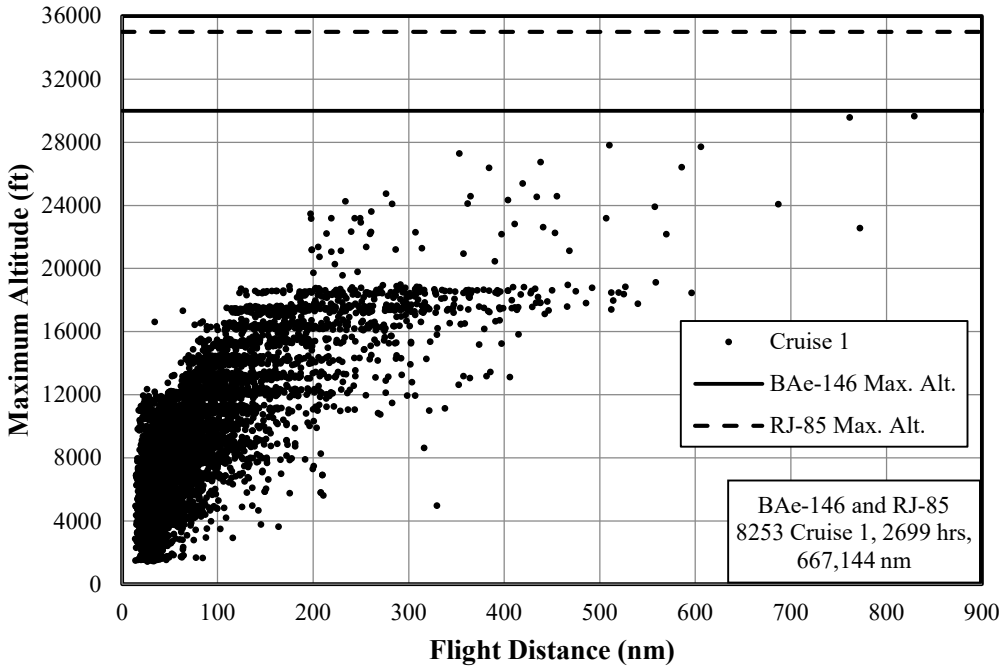

Figure B-19. Maximum MSL altitude and corresponding distance – cruise 1

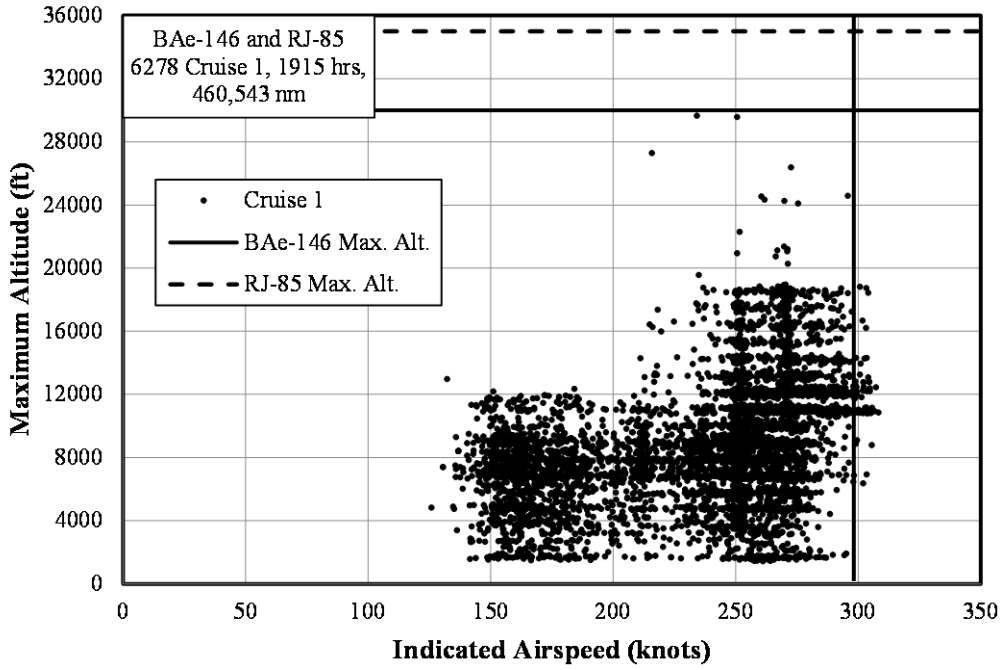

Figure B-20. Maximum MSL altitude and coincident indicated airspeed – cruise 1

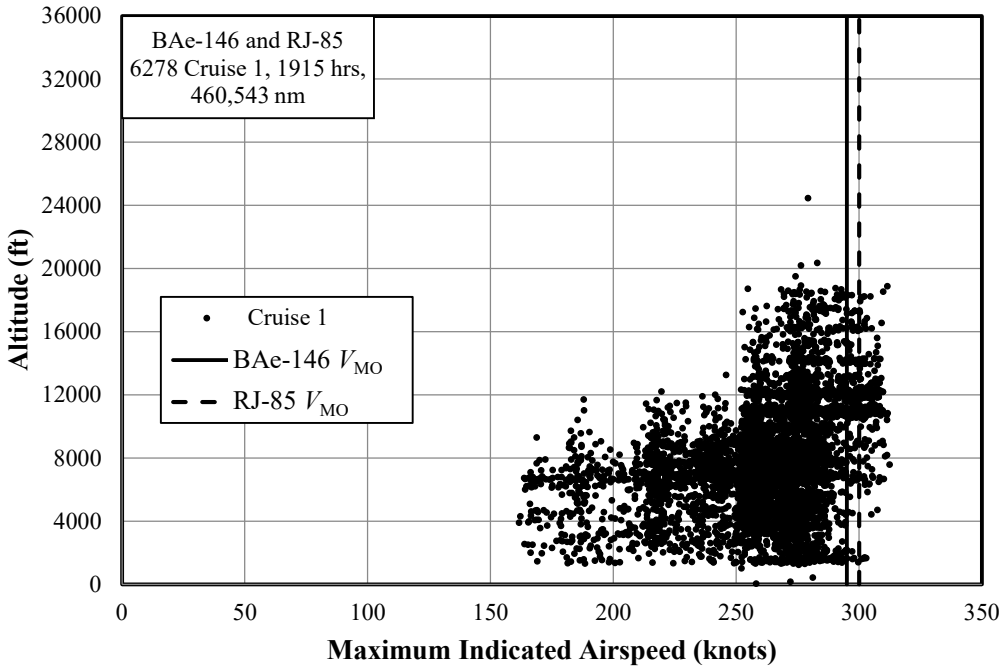

Figure B-21. Maximum indicated airspeed and coincident MSL altitude – cruise 1

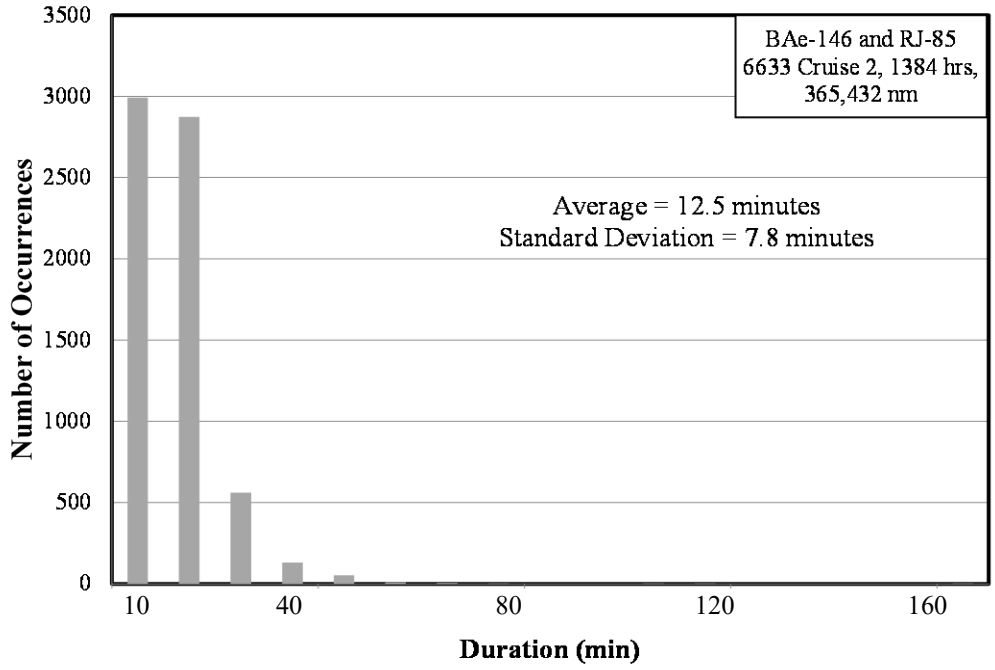

Figure B-22. Number of occurrences by duration – cruise 2

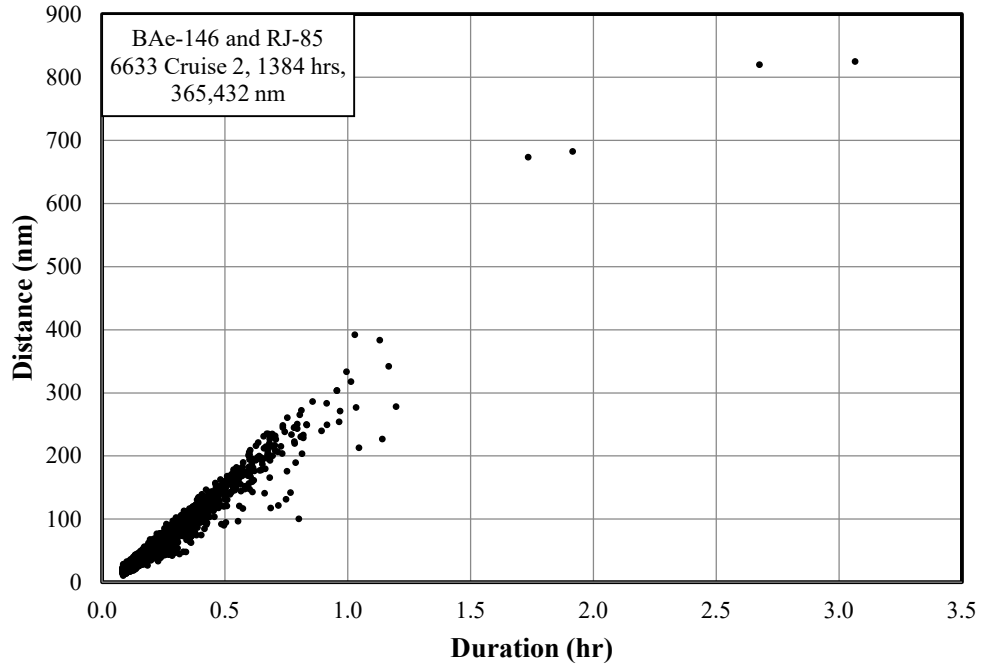

Figure B-23. Correlation of distance and duration – cruise 2

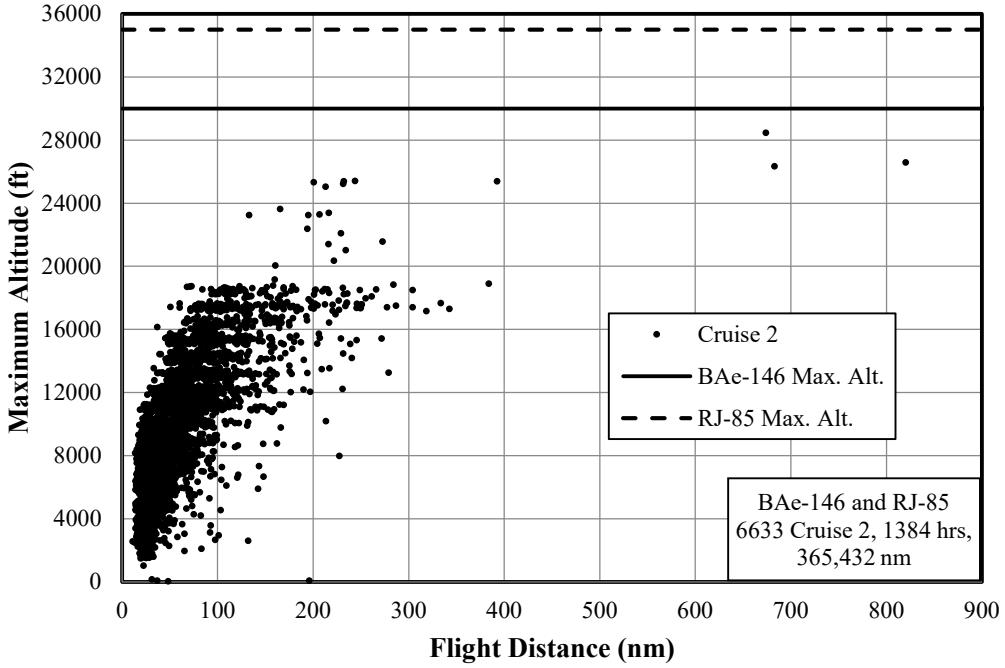

Figure B-24. Maximum MSL altitude and corresponding distance – cruise 2

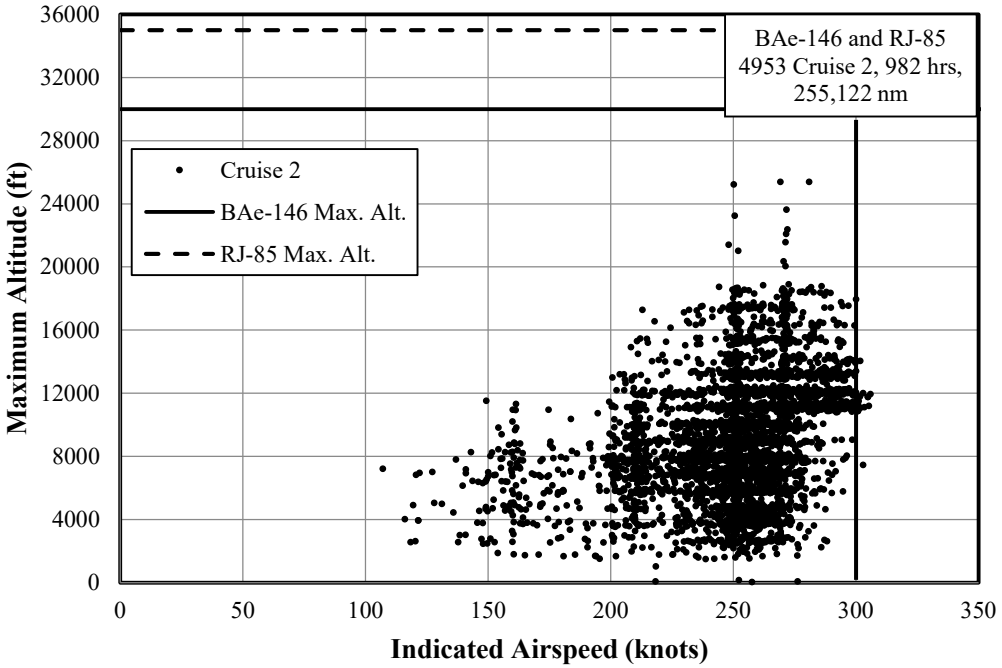

Figure B-25. Maximum MSL altitude and coincident indicated airspeed – cruise 2

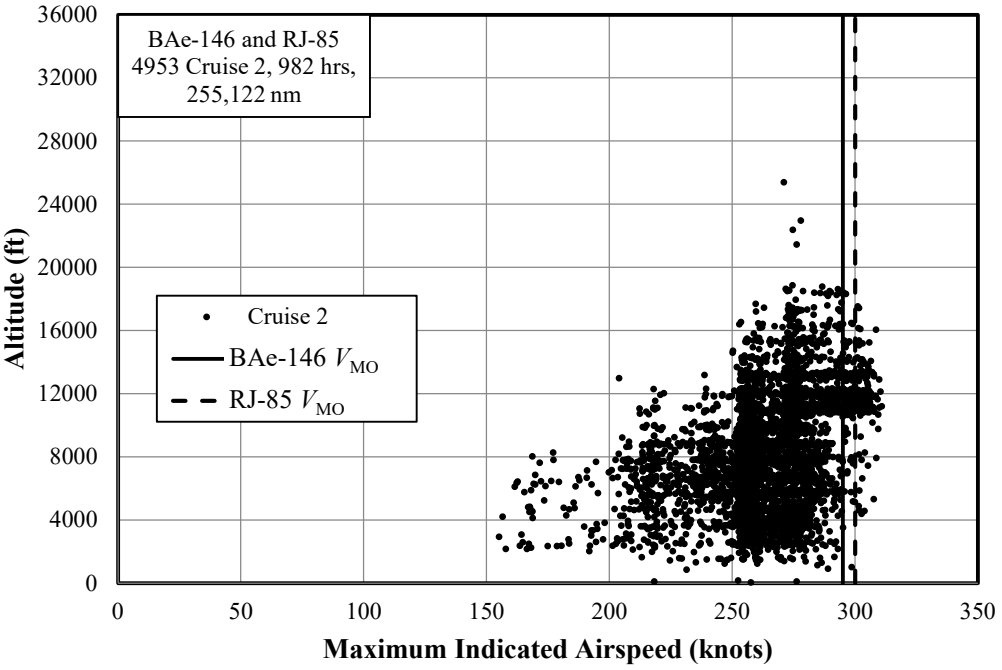

Figure B-26. Maximum indicated airspeed and coincident MSL altitude – cruise 2

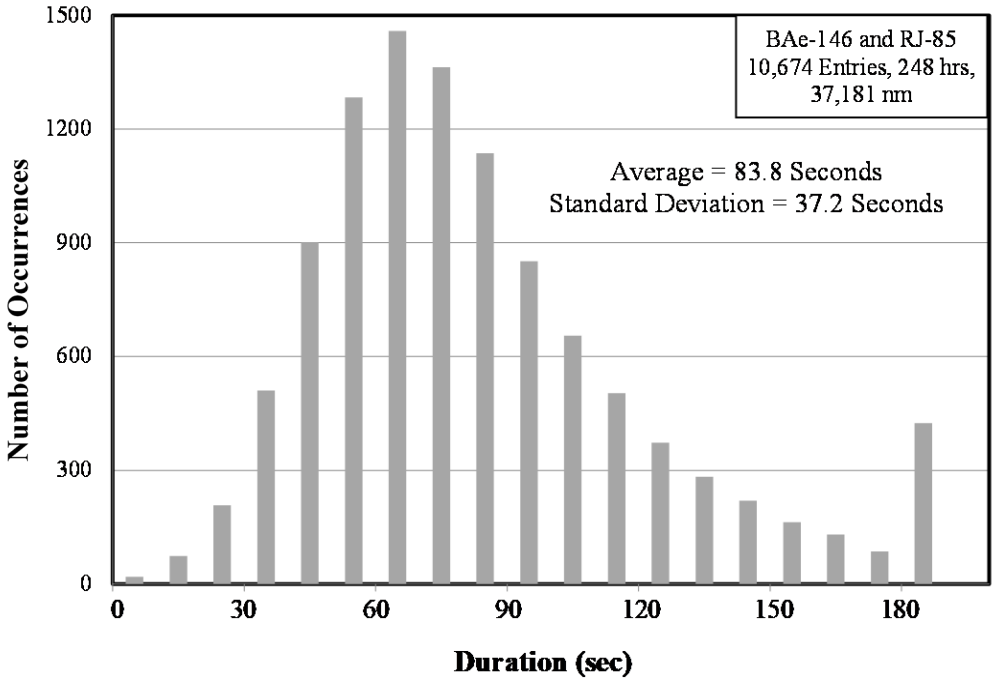

Figure B-27. Number of occurrences by duration – entry

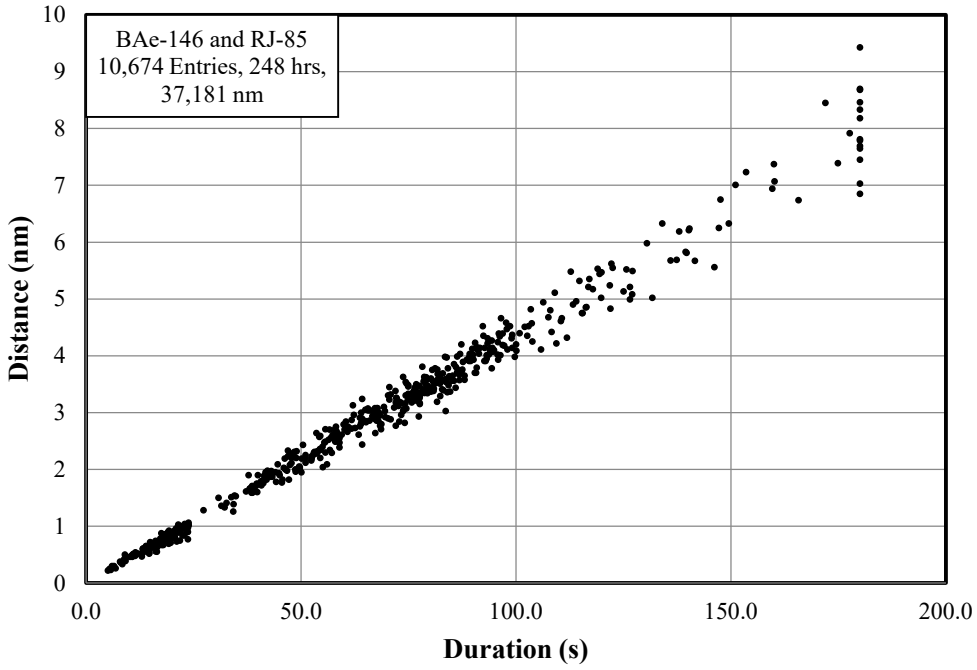

Figure B-28. Correlation of distance and duration – entry

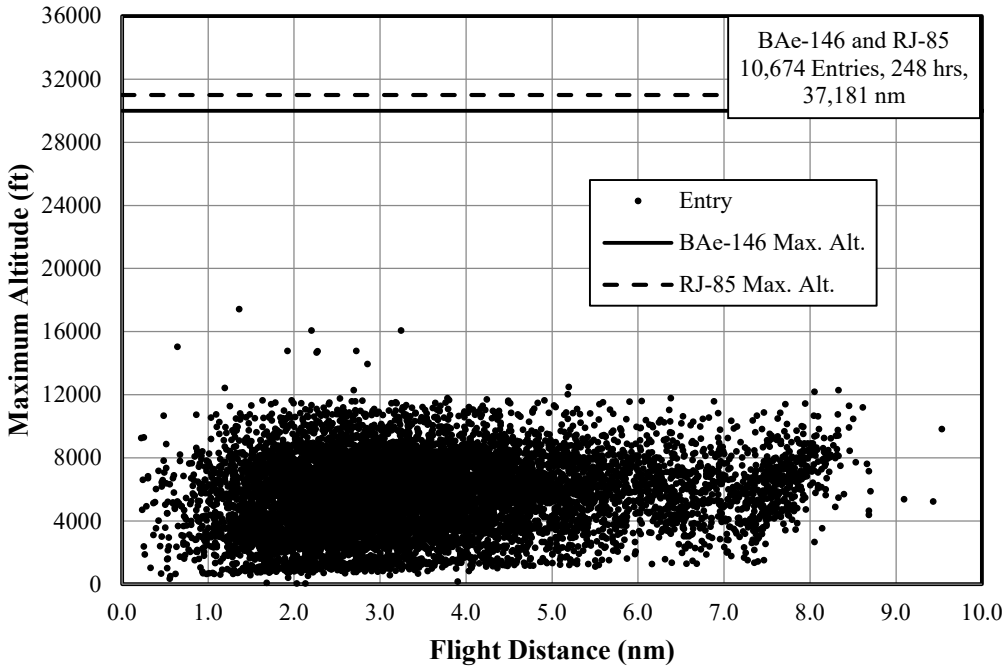

Figure B-29. Maximum MSL altitude and corresponding distance – entry

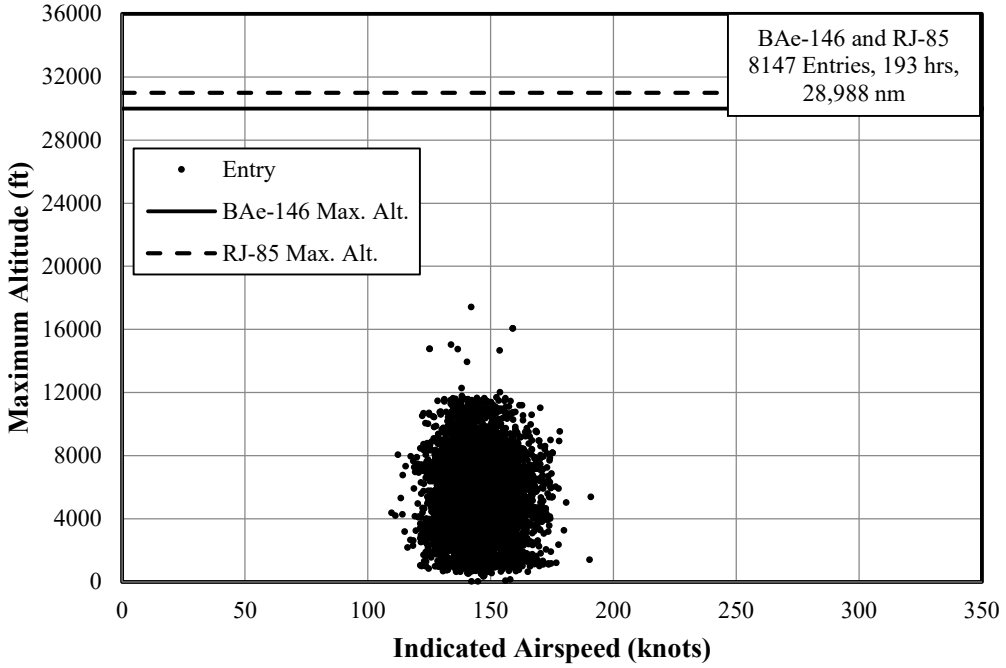

Figure B-30. Maximum MSL altitude and coincident indicated airspeed – entry

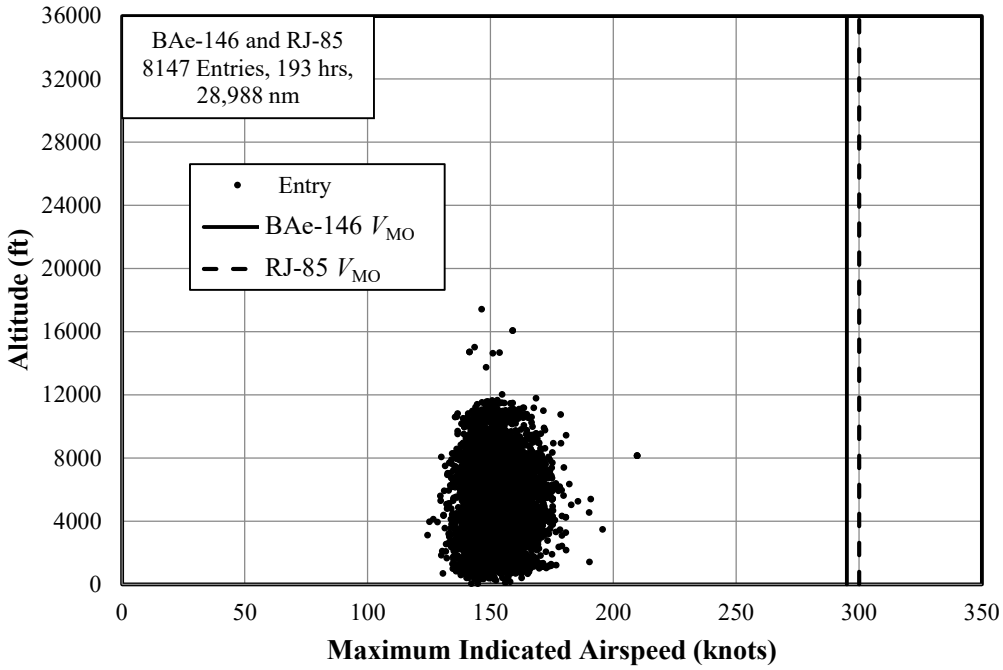

Figure B-31. Maximum indicated airspeed and coincident MSL altitude – entry

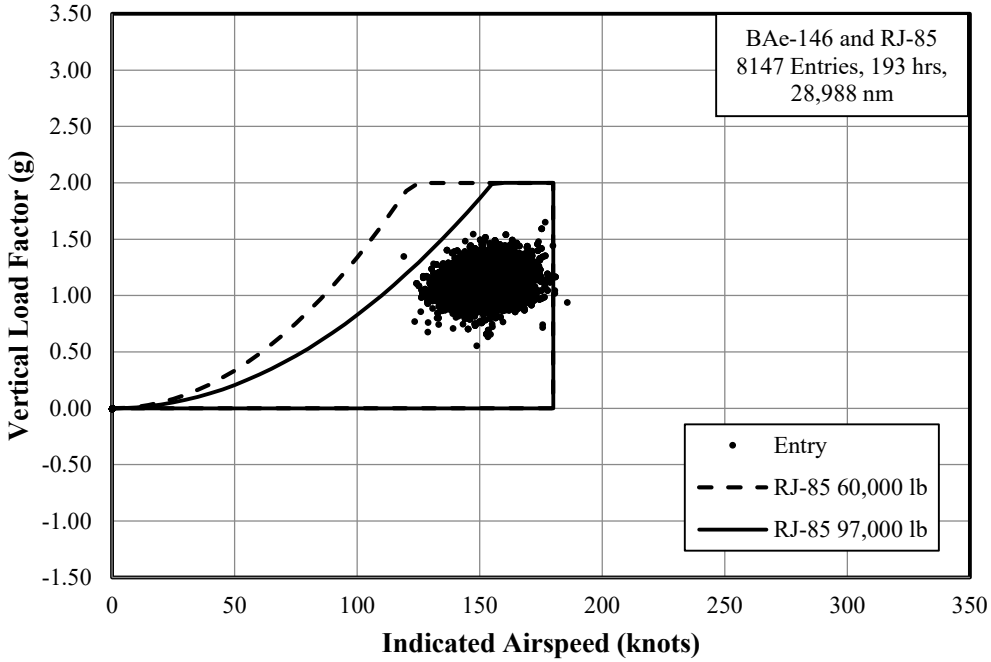

(a) Flaps in the Second Detent

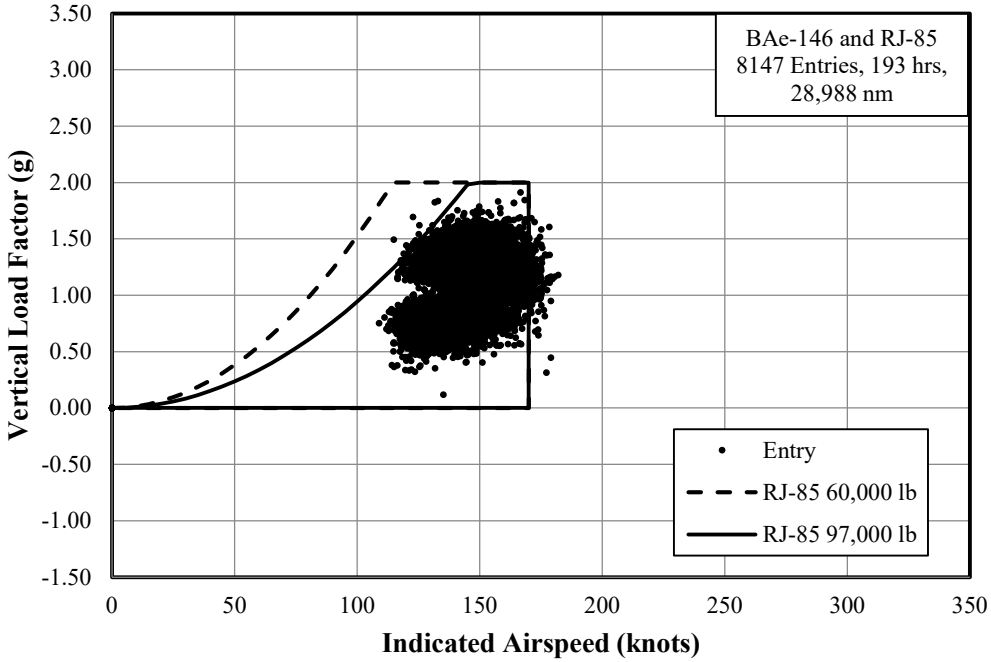

(b) Flaps in the Third Detent

Figure B-32. *V-n* diagram – entry

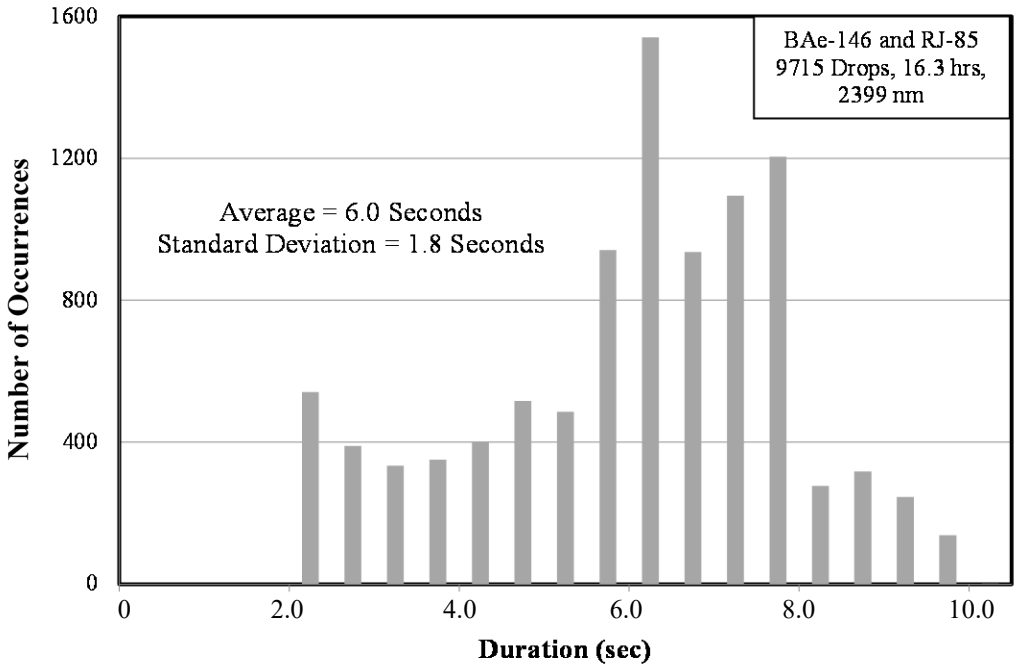

Figure B-33. Number of occurrences by duration – drop

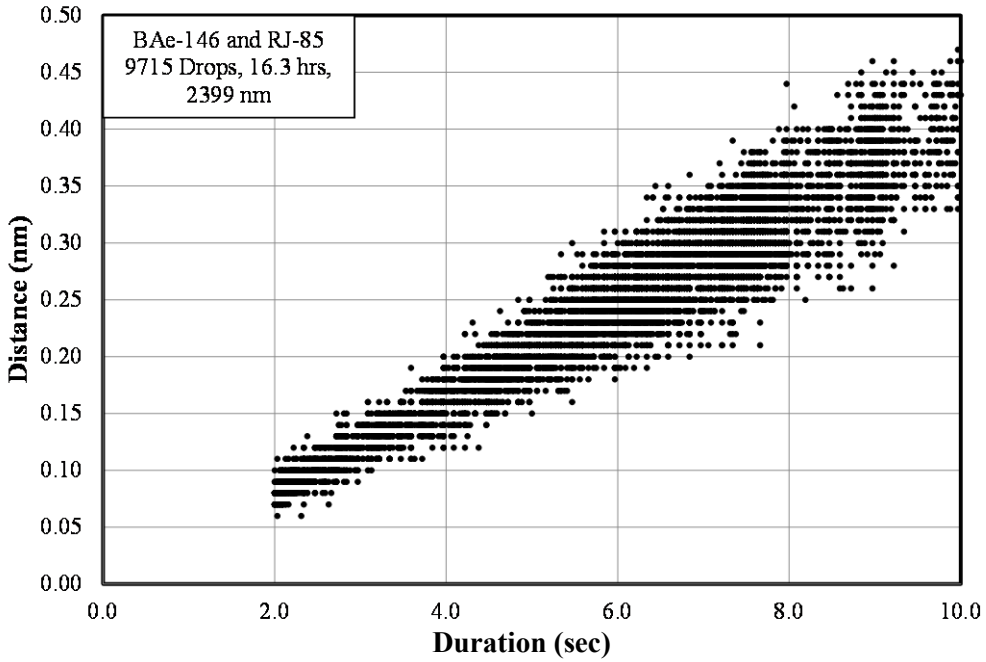

Figure B-34. Correlation of distance and duration – drop

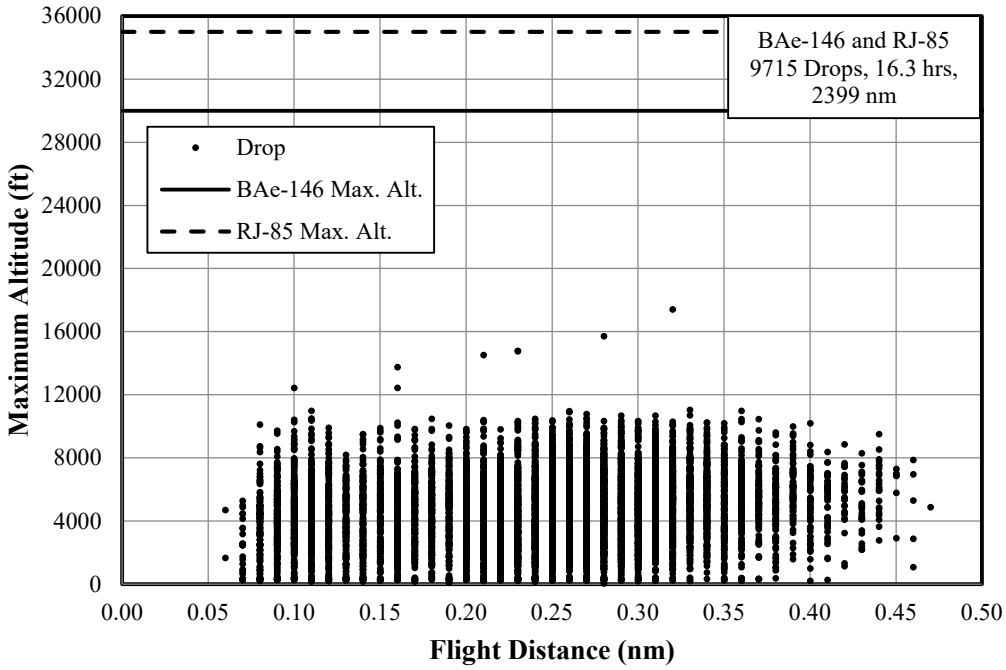

Figure B-35. Maximum MSL altitude and corresponding distance – drop

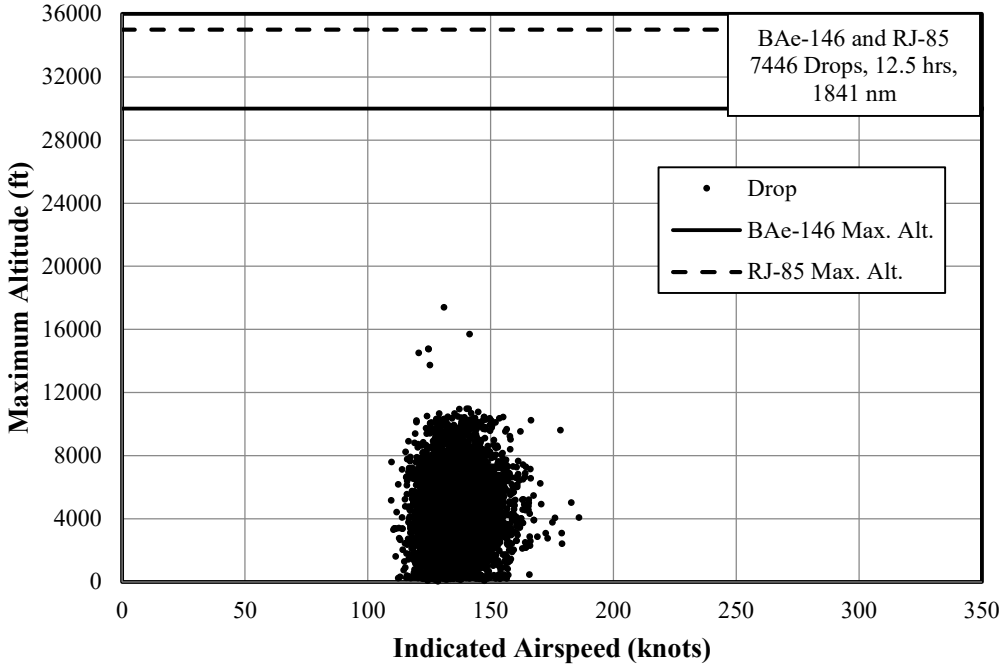

Figure B-36. Maximum MSL altitude and coincident indicated airspeed – drop

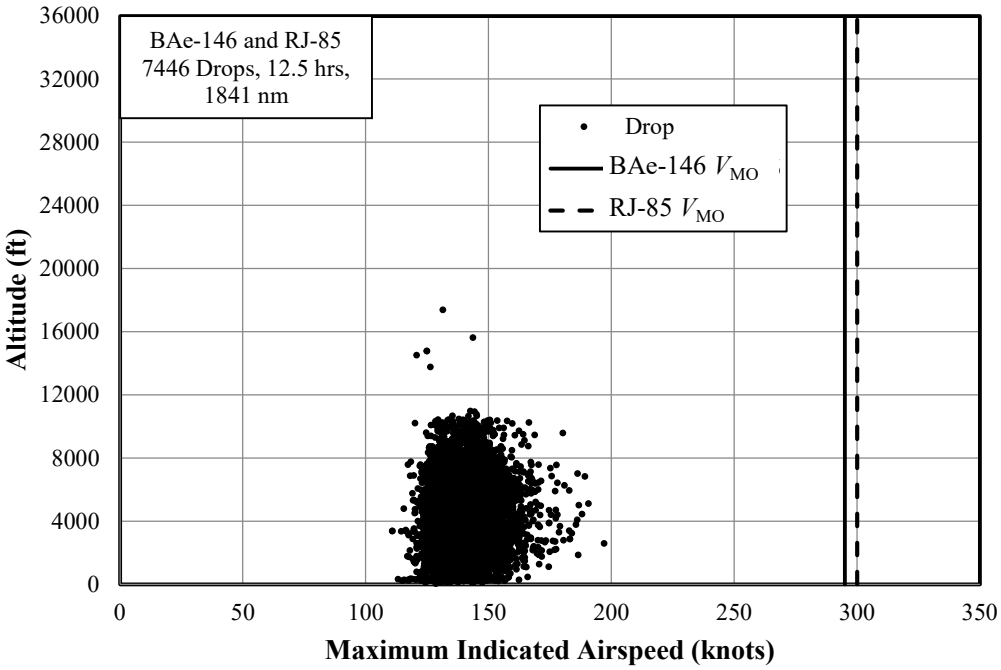

Figure B-37. Maximum indicated airspeed and coincident MSL altitude – drop

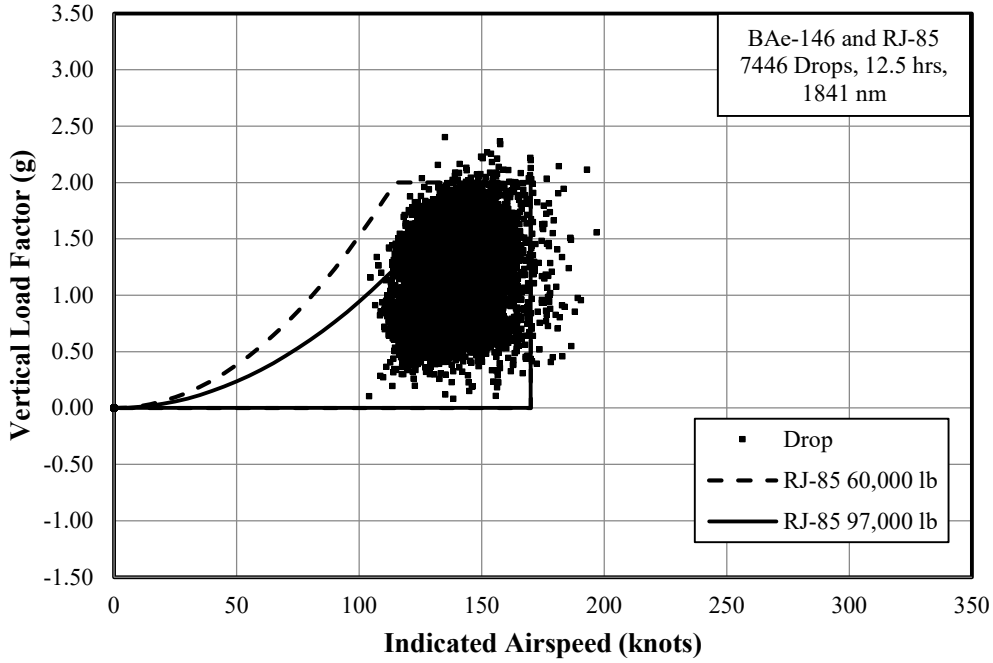

Figure B-38. *V-n* diagram – drop

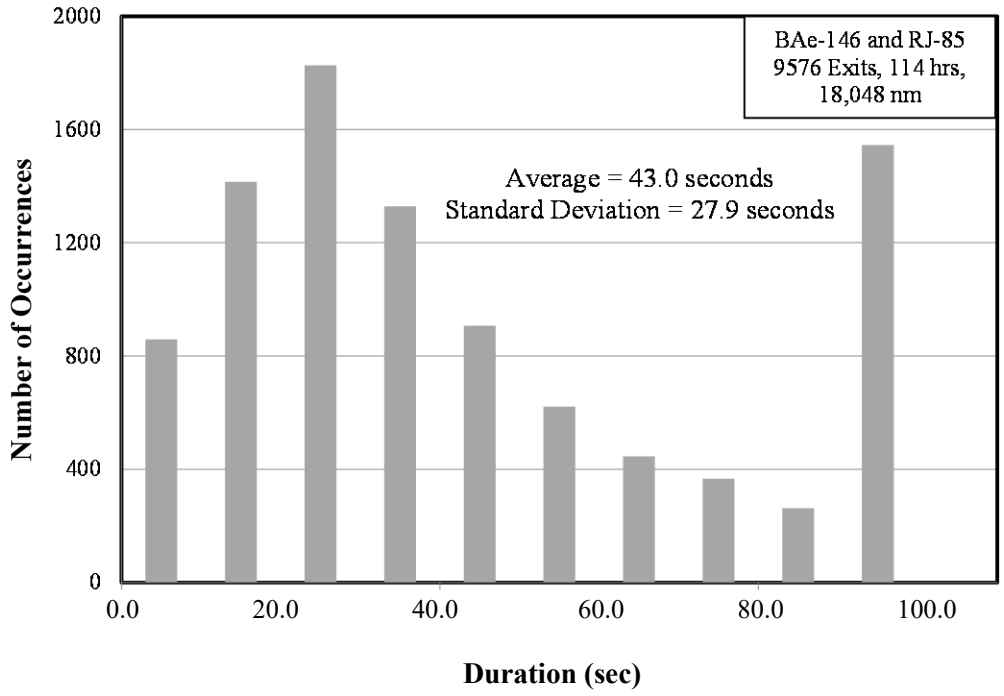

Figure B-39. Number of occurrences by duration – exit

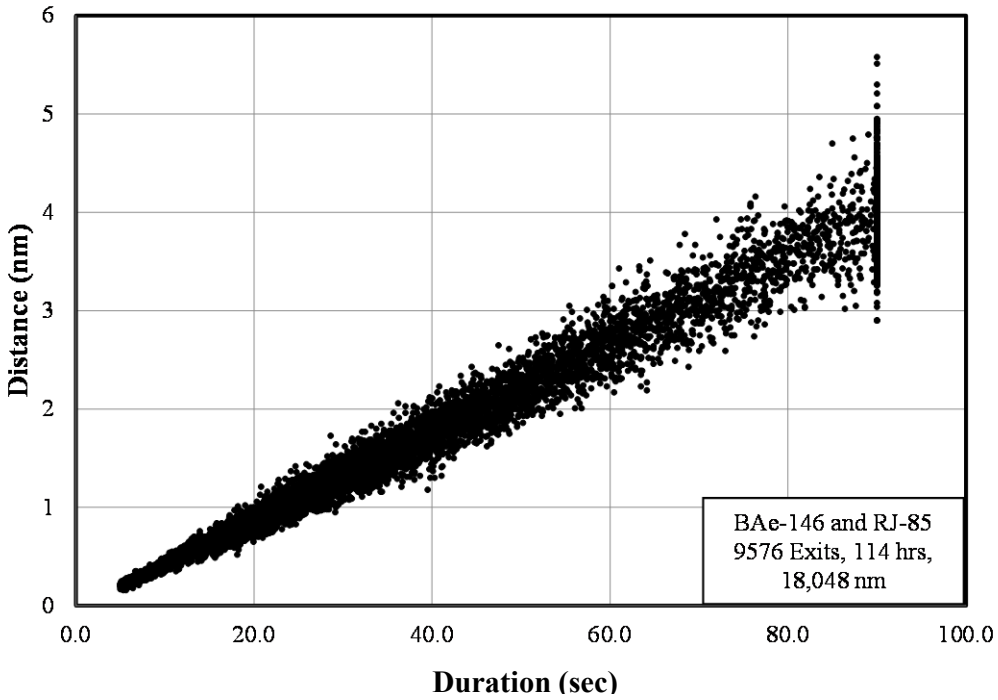

Figure B-40. Correlation of distance and duration – exit

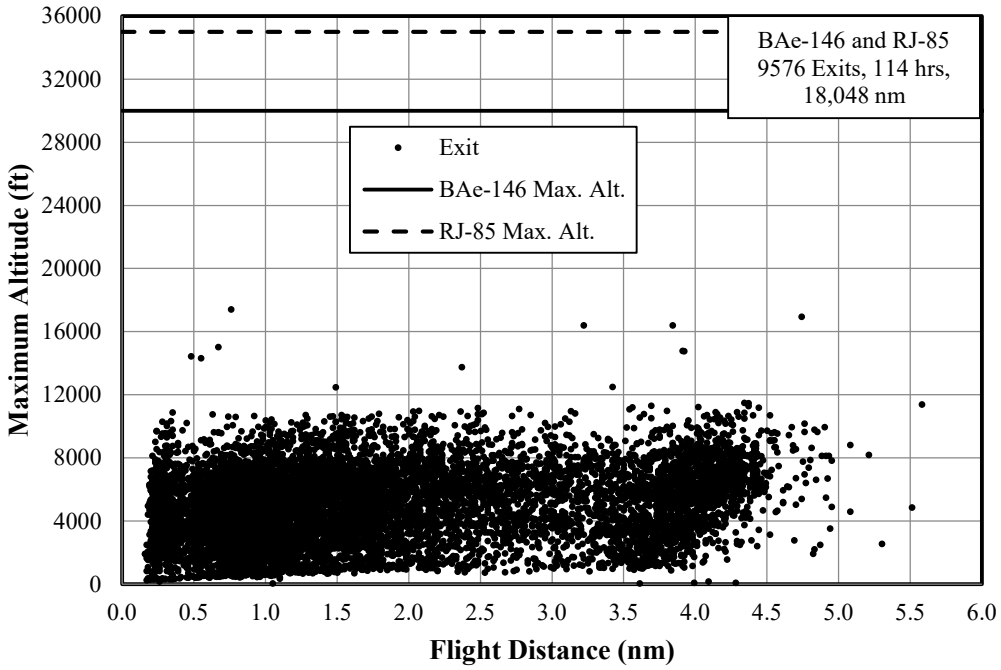

Figure B-41. Maximum MSL altitude and corresponding distance – exit

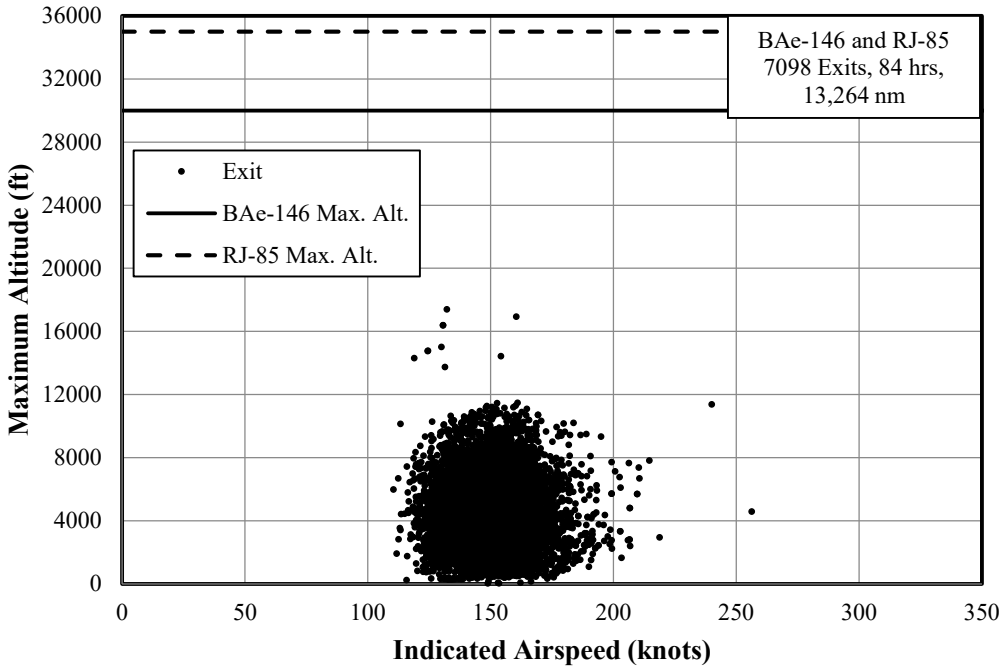

Figure B-42. Maximum MSL altitude and coincident indicated airspeed – exit

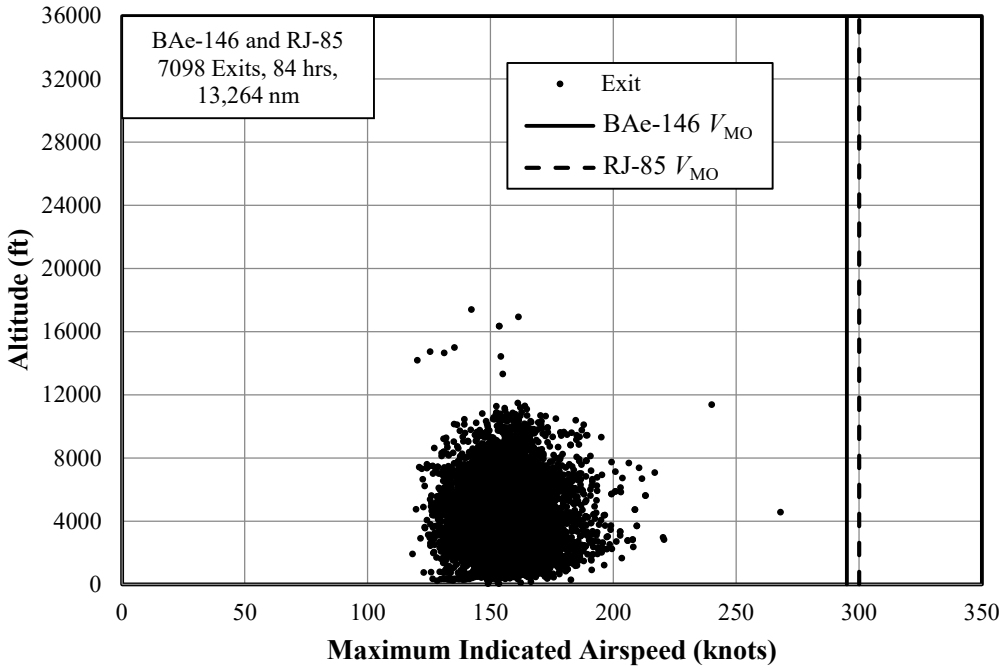

Figure B-43. Maximum indicated airspeed and coincident MSL altitude – exit

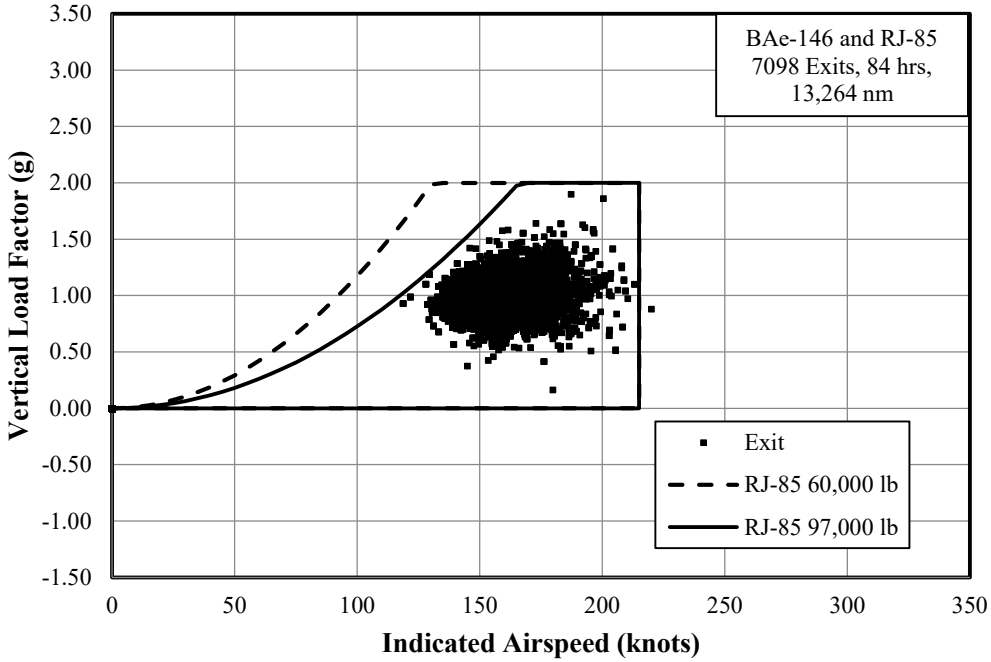

(a) Flaps in the First Detent

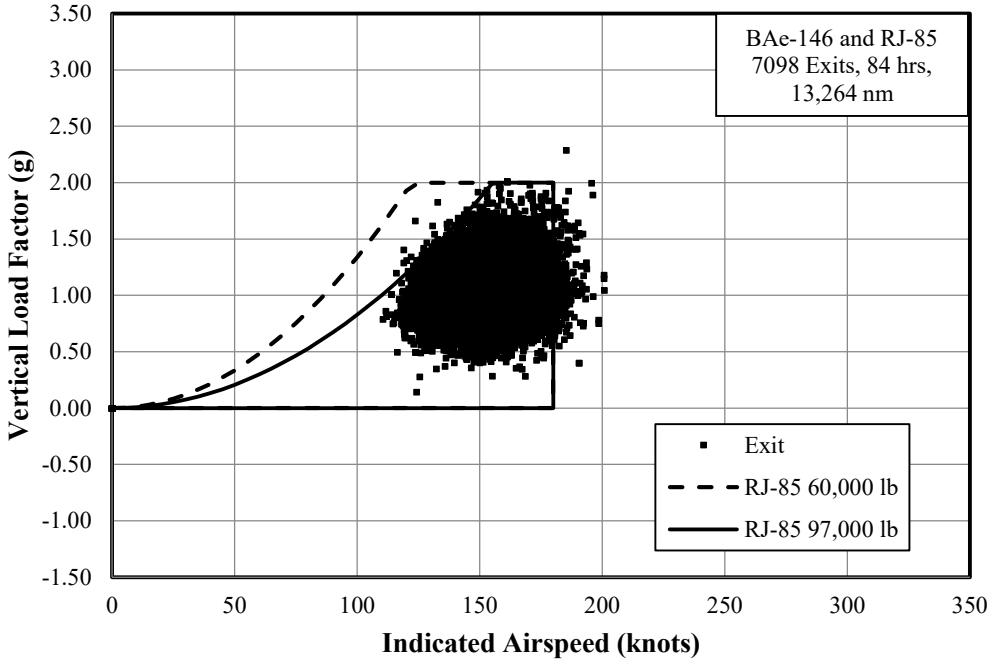

(b) Flaps in the Second Detent

Figure B-44. *V-n* diagram – exit

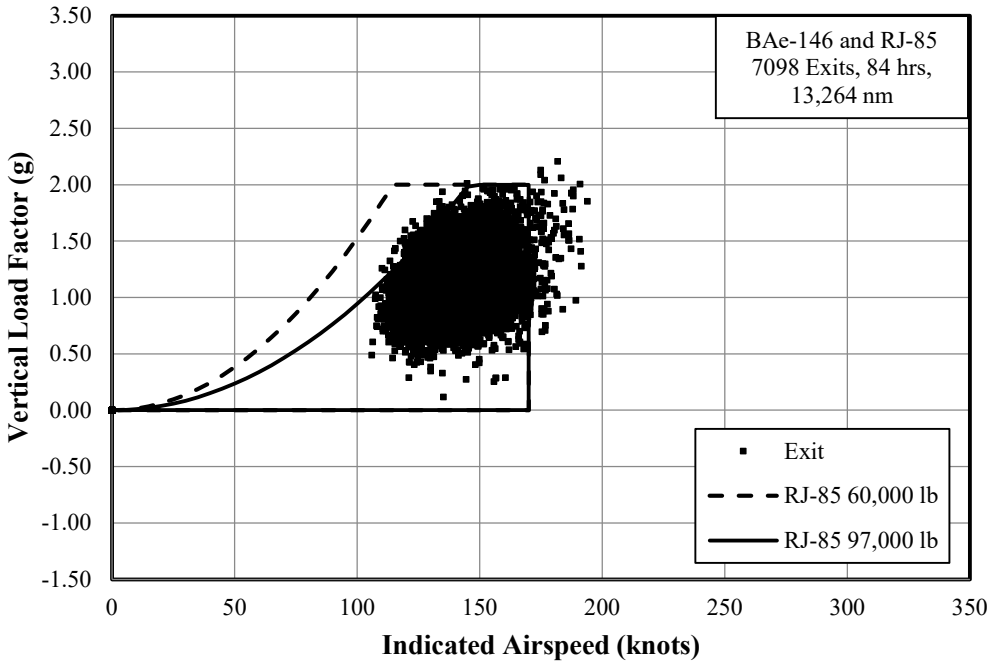

(c) Flaps in the Third Detent

Figure B-45. *V-n* diagram – exit (continued)

APPENDIX C—FLIGHT LOADS BY ABOVE GROUND LEVEL ALTITUDE

Table C-1. Statistical formats – flight loads data by above ground level (AGL) altitude

Flight Loads Data	Table
Summary of Durations and Distances for All Flight Phases	Table C-3
Summary of Durations and Distances – Cruise 1	Table C-4
Summary of Durations and Distances – Cruise 2	Table C-5
Summary of Durations and Distances – Entry	Table C-6
Summary of Durations and Distances – Drop	Table C-7
Summary of Durations and Distances – Exit	Table C-8
Summary of Durations and Distances for Firefighting Flights	Table C-9
Summary of Durations and Distances for Ferry Flights	Table C-10
Summary of Durations and Distances for Maintenance/Training Flights	Table C-11

Table C-2. Statistical formats – flight loads data by AGL altitude

Flight Loads Data	Figure
CRUISE 1 PHASE	
Cumulative Occurrences of Incremental Vertical Gust Load Factor – Cruise 1	Figure C-1
Cumulative Occurrences of Incremental Vertical Maneuver Load Factor – Cruise 1	Figure C-2
CRUISE 2 PHASE	
Cumulative Occurrences of Incremental Vertical Gust Load Factor – Cruise 2	Figure C-3
Cumulative Occurrences of Incremental Vertical Maneuver Load Factor – Cruise 2	Figure C-4
ENTRY PHASE	
Cumulative Occurrences of Incremental Vertical Gust Load Factor – Entry	Figure C-5
Cumulative Occurrences of Incremental Vertical Maneuver Load Factor – Entry	Figure C-6
DROP PHASE	
Cumulative Occurrences of Incremental Vertical Gust Load Factor – Drop	Figure C-7
Cumulative Occurrences of Incremental Vertical Maneuver Load Factor – Drop	Figure C-8
EXIT PHASE	
Cumulative Occurrences of Incremental Vertical Gust Load Factor – Exit	Figure C-9
Cumulative Occurrences of Incremental Vertical Maneuver Load Factor – Exit	Figure C-10
FIREFIGHTING FLIGHTS	
Cumulative Occurrences of Incremental Vertical Gust Load Factor, Firefighting Flights	Figure C-11
Cumulative Occurrences of Incremental Vertical Maneuver Load Factor, Firefighting Flights	Figure C-12
FERRY FLIGHTS	
Cumulative Occurrences of Incremental Vertical Gust Load Factor, Ferry Flights	Figure C-13
Cumulative Occurrences of Incremental Vertical Maneuver Load Factor, Ferry Flights	Figure C-14
MAINTENANCE/TRAINING FLIGHTS	

Cumulative Occurrences of Incremental Vertical Gust Load Factor, Maintenance/Training Flights	Figure C-15
Cumulative Occurrences of Incremental Vertical Maneuver Load Factor, Maintenance/Training Flights	Figure C-16

Table C-3. Summary of durations and distances for all firefighting flight phases

Phase	Number of Occurrences	Duration (hr)	Distance (nm)
Cruise 1	8232	2576	666,299
Cruise 2	8129	1391	379,059
Entry	10,132	237	36,697
Drop	10,132	19	2925
Exit	10,132	113	18,631
Total		4336	1,103,611

Table C-4. Summary of durations and distances – cruise 1

Altitude Band Ceiling (ft)	Duration (hr)	Distance (nm)
500	87.4	14,108.0
1500	303.0	59,922.6
4500	1203.9	275,123.5
9500	629.0	190,059.7
14,500	271.7	96,047.0
19,500	70.9	26,926.2
24,500	9.1	3557.8
Above 24,500	1.4	554.6
Total	2576.4	666,299.4

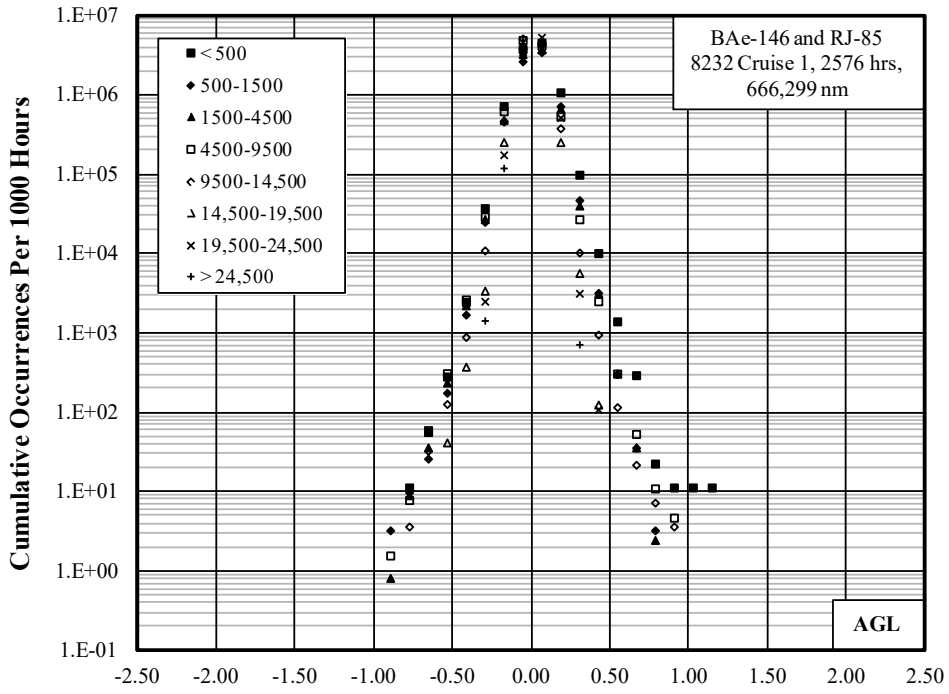

(a) Per 1000 Hours

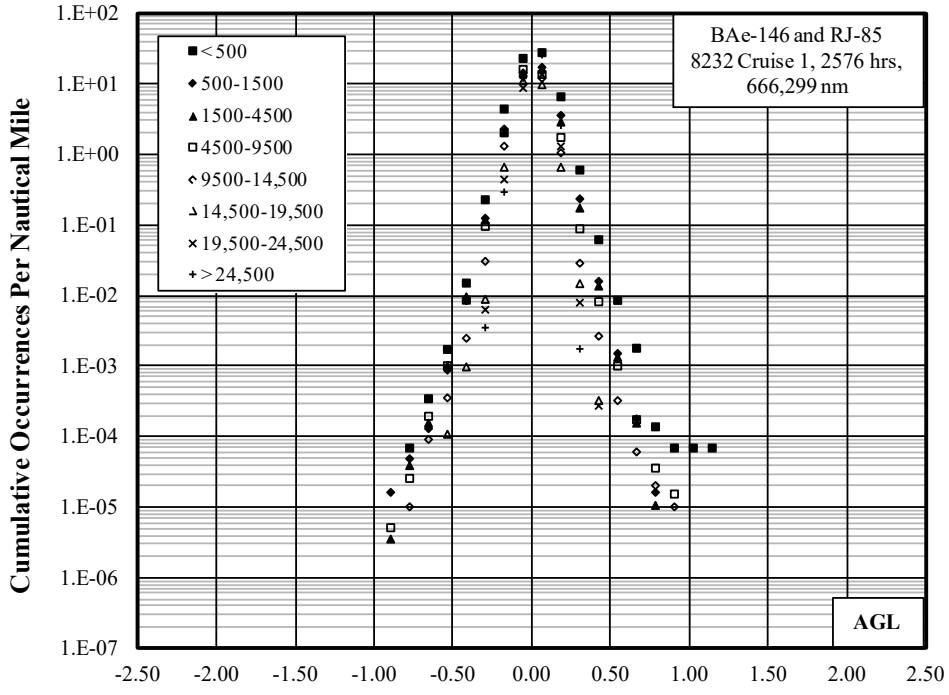

(b) Per Nautical Mile

Figure C-1. Cumulative occurrences of incremental vertical gust load factor – cruise 1

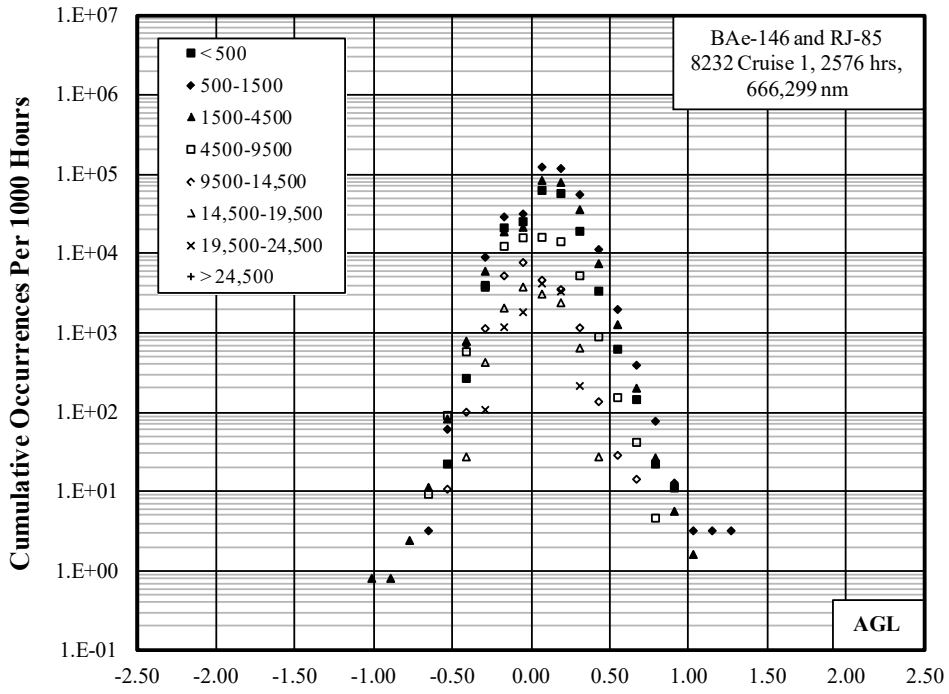

(a) Per 1000 Hours

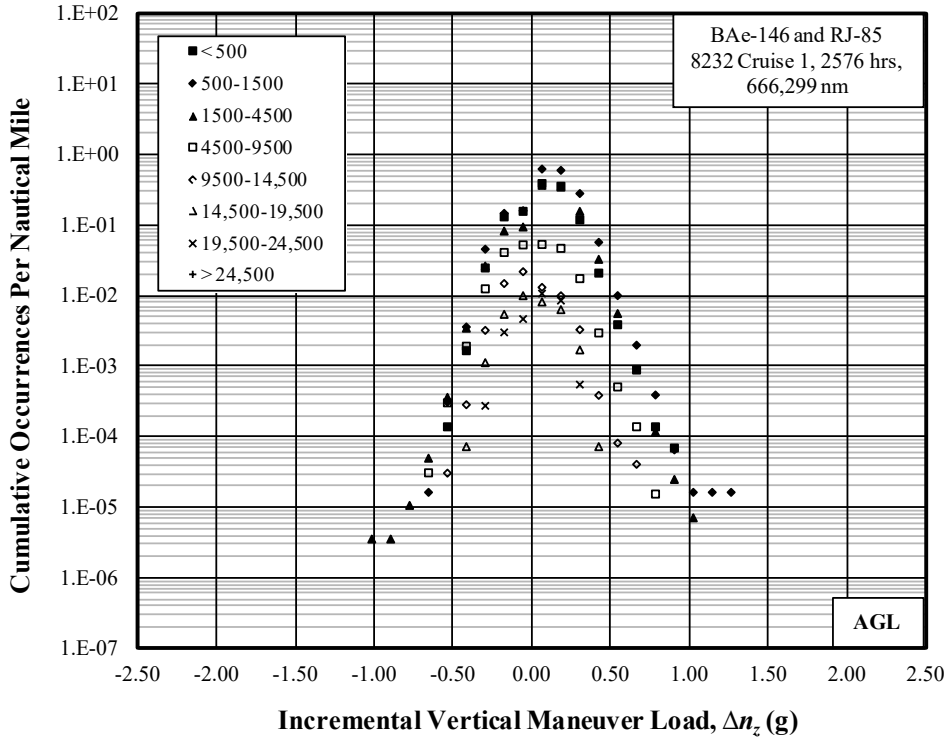

(b) Per Nautical Mile

Figure C-2. Cumulative occurrences of incremental vertical maneuver load factor – cruise 1

Table C-5. Summary of durations and distances – cruise 2

Altitude Band Ceiling (ft)	Duration (hr)	Distance (nm)
500	3.6	667.1
1500	168.3	29,782.3
4500	591.5	146,262.2
9500	457.3	142,093.5
14,500	141.3	49,158.4
19,500	22.7	8453.3
24,500	4.4	1887.4
Above 24,500	1.8	754.2
Total	1390.8	379,058.5

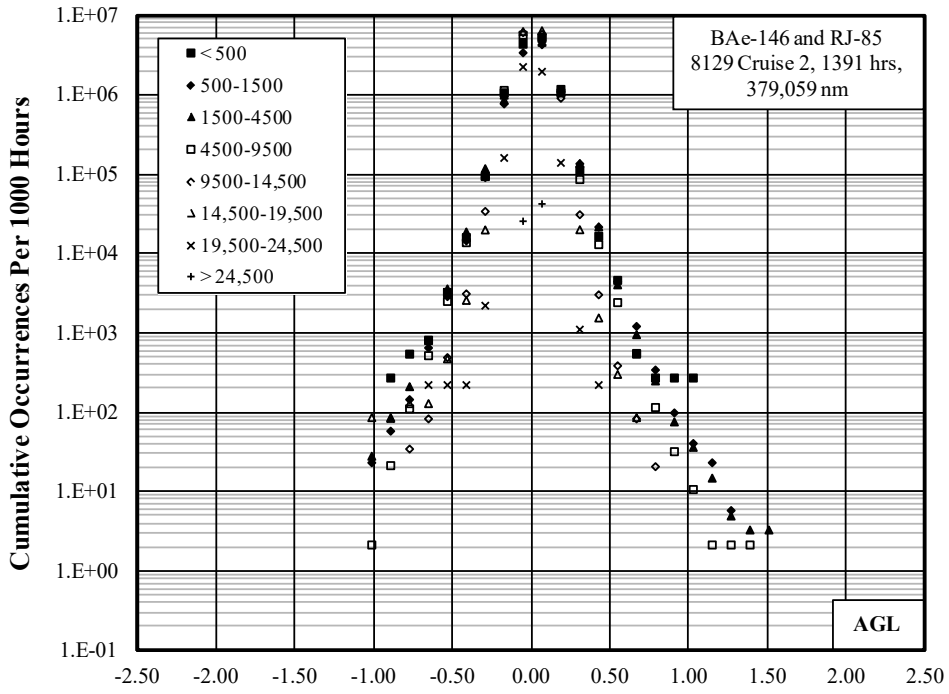

(a) Per 1000 Hours

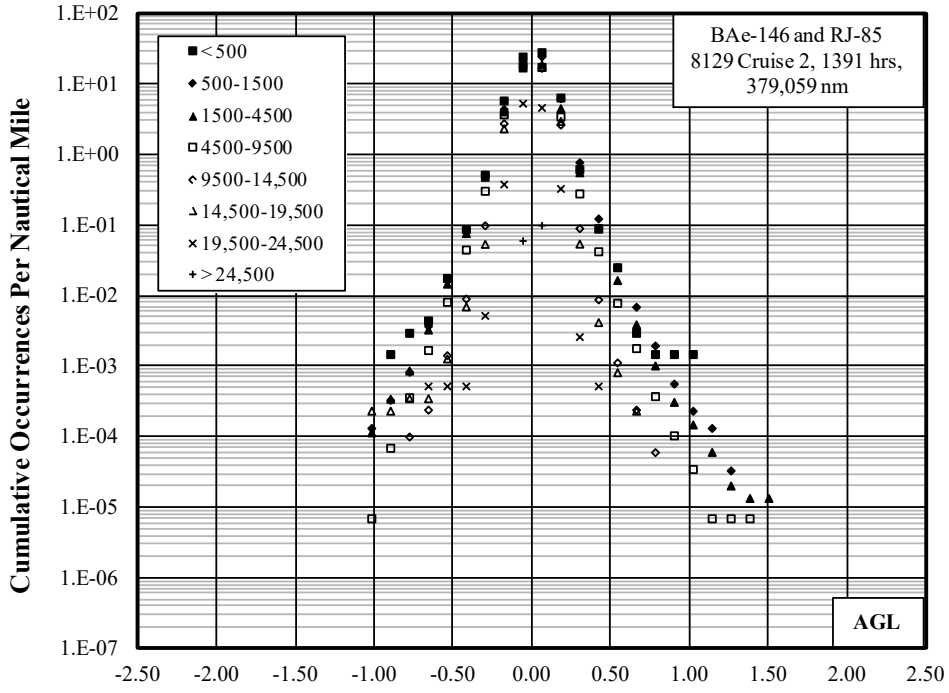

(b) Per Nautical Mile

Figure C-3. Cumulative occurrences of incremental vertical gust load factor – cruise 2

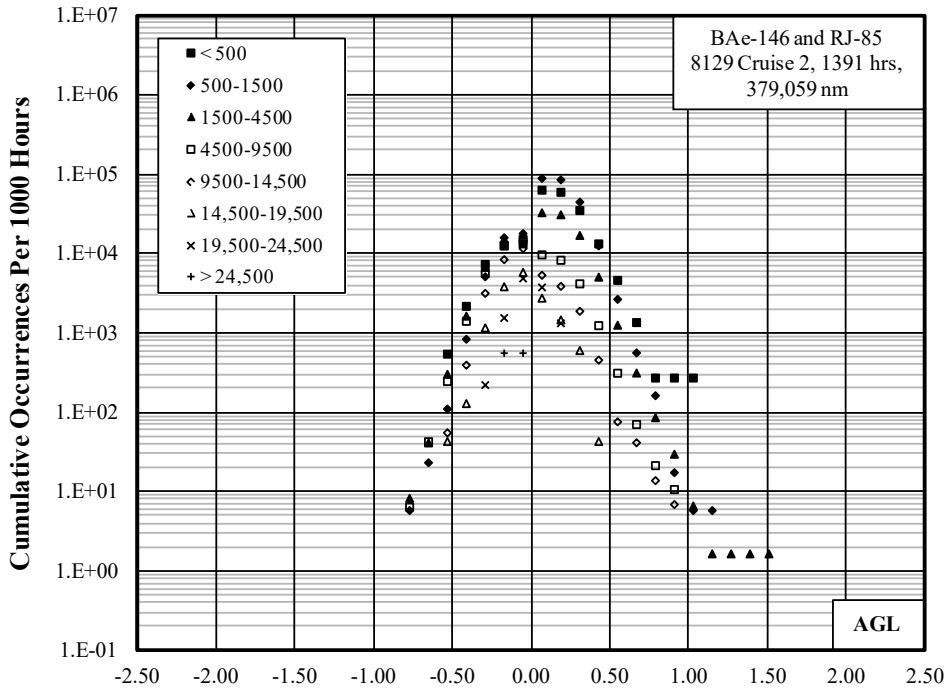

(a) Per 1000 Hours

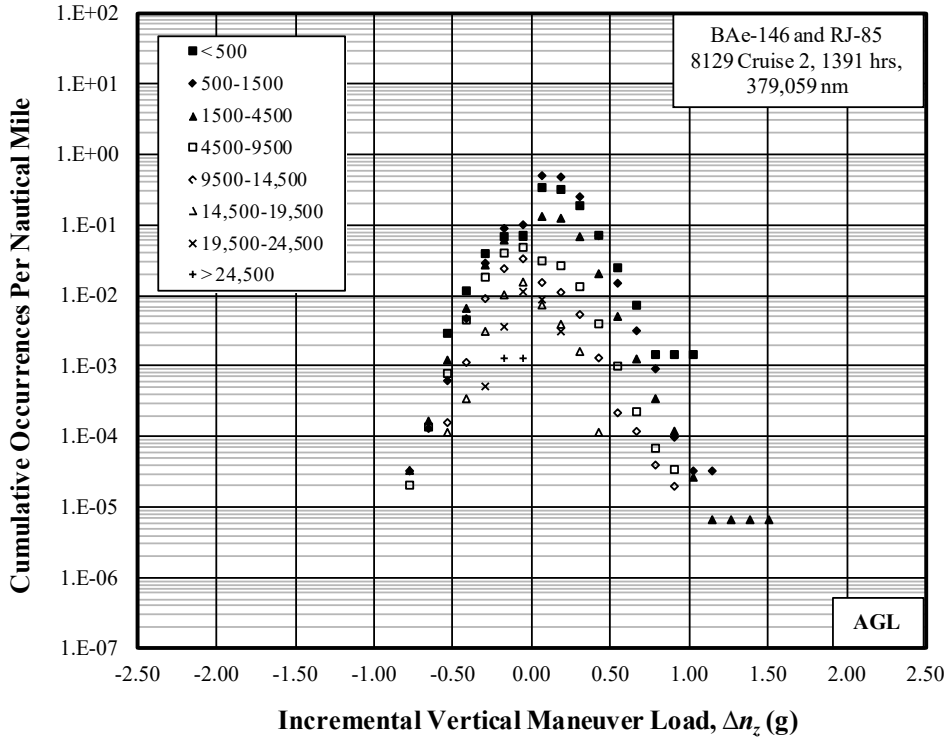

(b) Per Nautical Mile

Figure C-4. Cumulative occurrences of incremental vertical maneuver load factor – cruise 2

Table C-6. Summary of durations and distances – entry

Altitude Band Ceiling (ft)	Duration (hr)	Distance (nm)
500	35.5	5258.4
1500	117.6	17,969.8
4500	82.0	13,058.2
9500	1.8	348.4
14,500	0.3	62.4
19,500	0	0
24,500	0	0
Above 24,500	0	0
Total	237.3	36,697.2

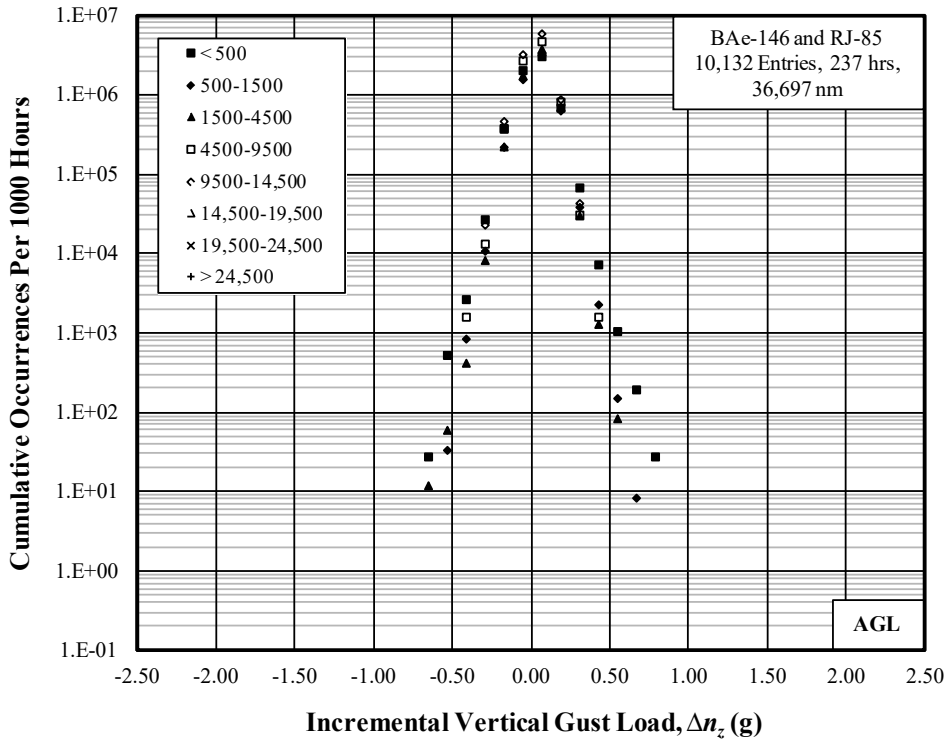

(a) Per 1000 Hours

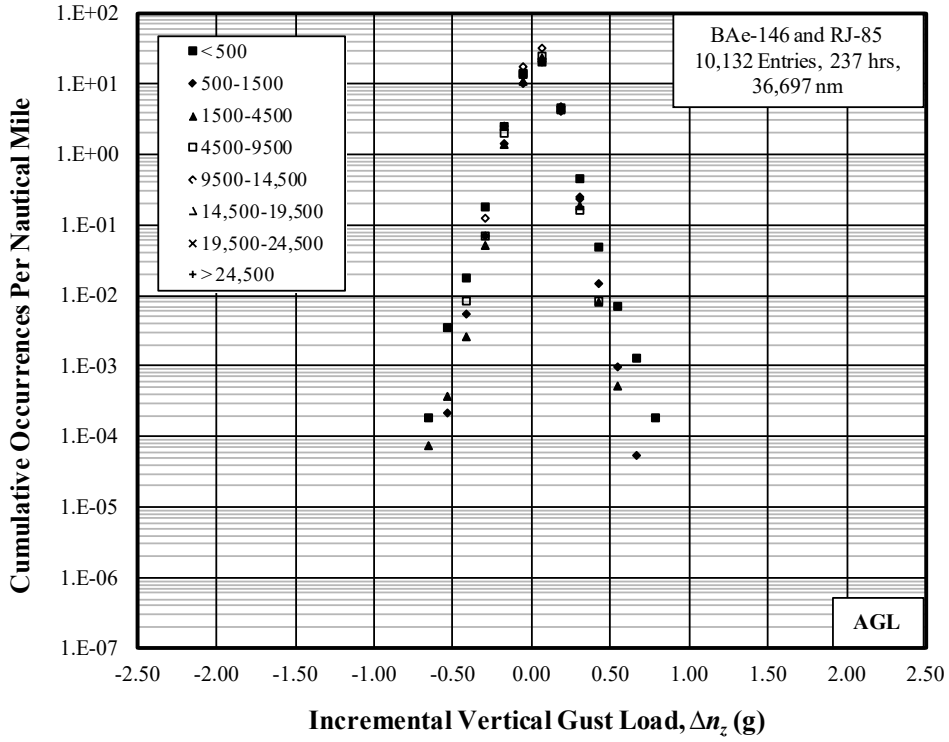

(b) Per Nautical Mile

Figure C-5. Cumulative occurrences of incremental vertical gust load factor – entry

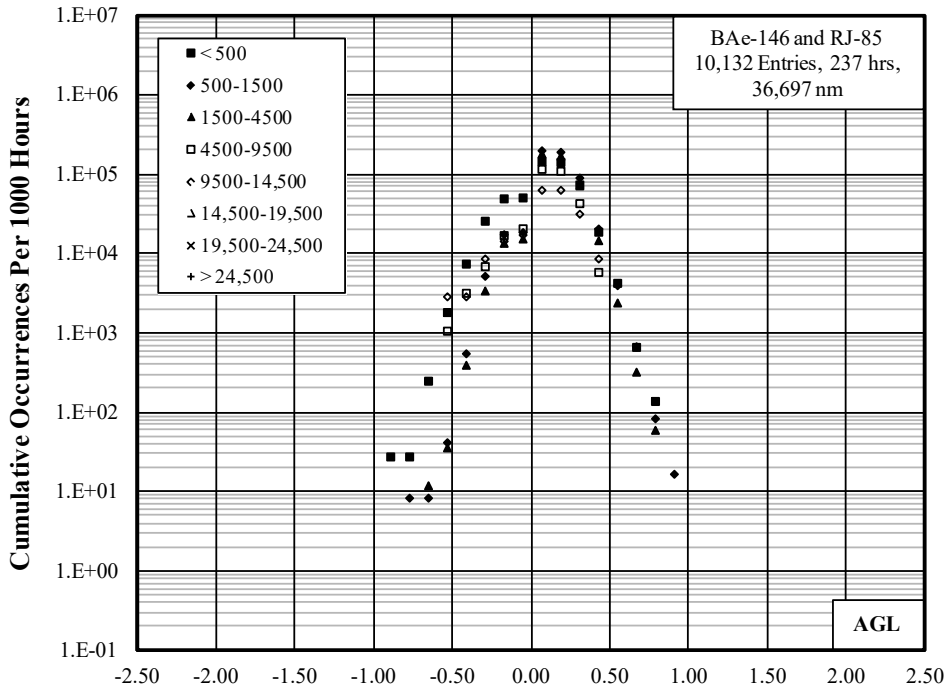

(a) Per 1000 Hours

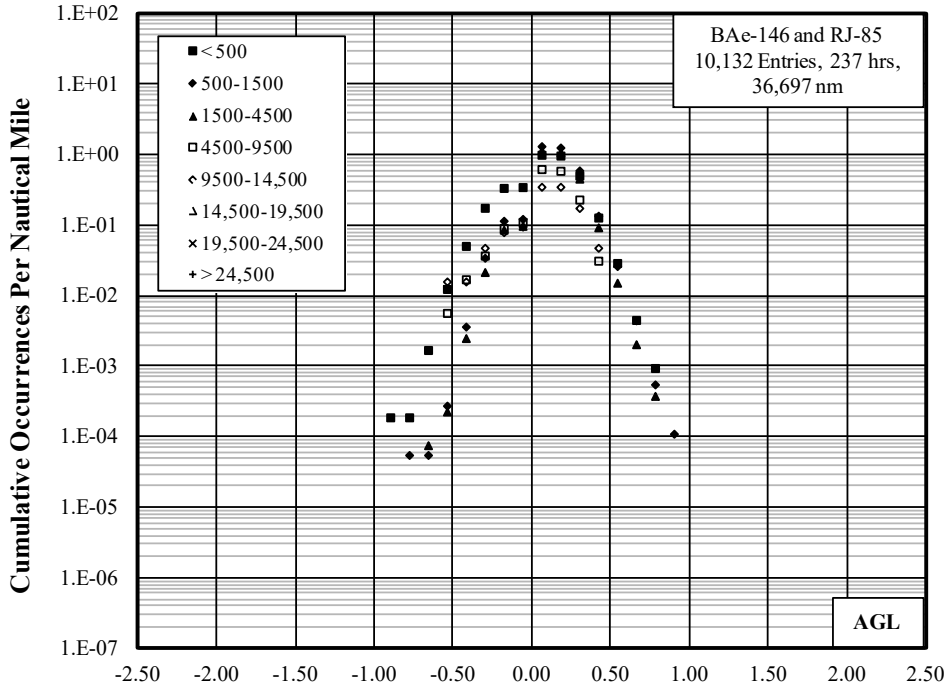

(b) Per Nautical Mile

Figure C-6. Cumulative occurrences of incremental vertical maneuver load factor – entry

Table C-7. Summary of durations and distances – drop

Altitude Band Ceiling (ft)	Duration (hr)	Distance (nm)
500	15.91	2364.4
1500	1.85	295.7
4500	0.87	167.6
9500	0.39	89.3
14,500	0.04	8.0
19,500	0	0
24,500	0	0
Above 24,500	0	0
Total	19.1	2924.8

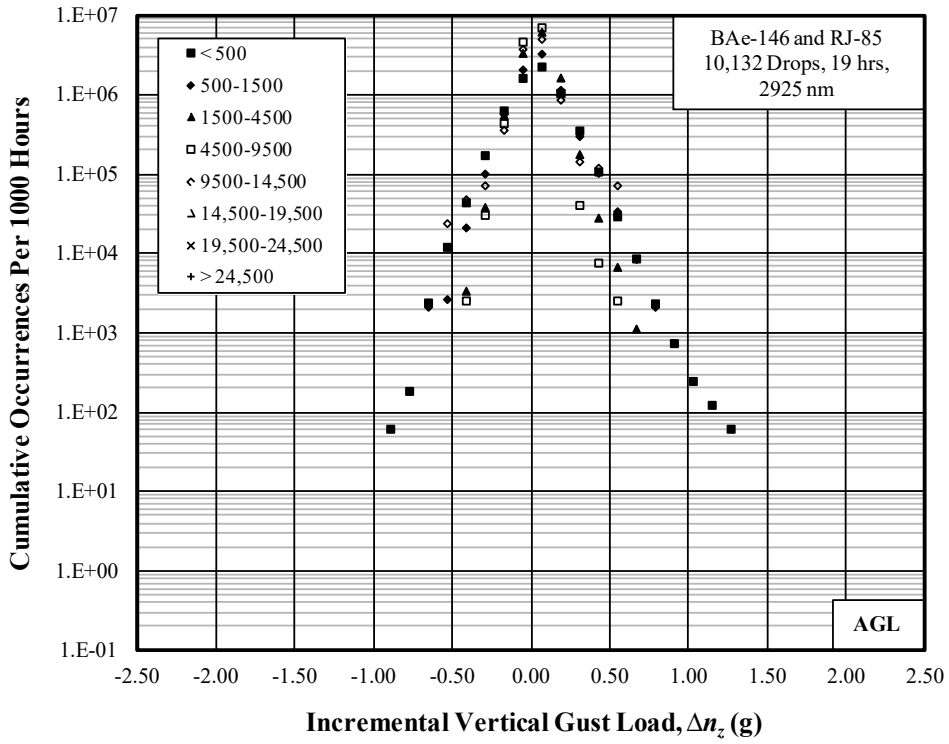

(a) Per 1000 Hours

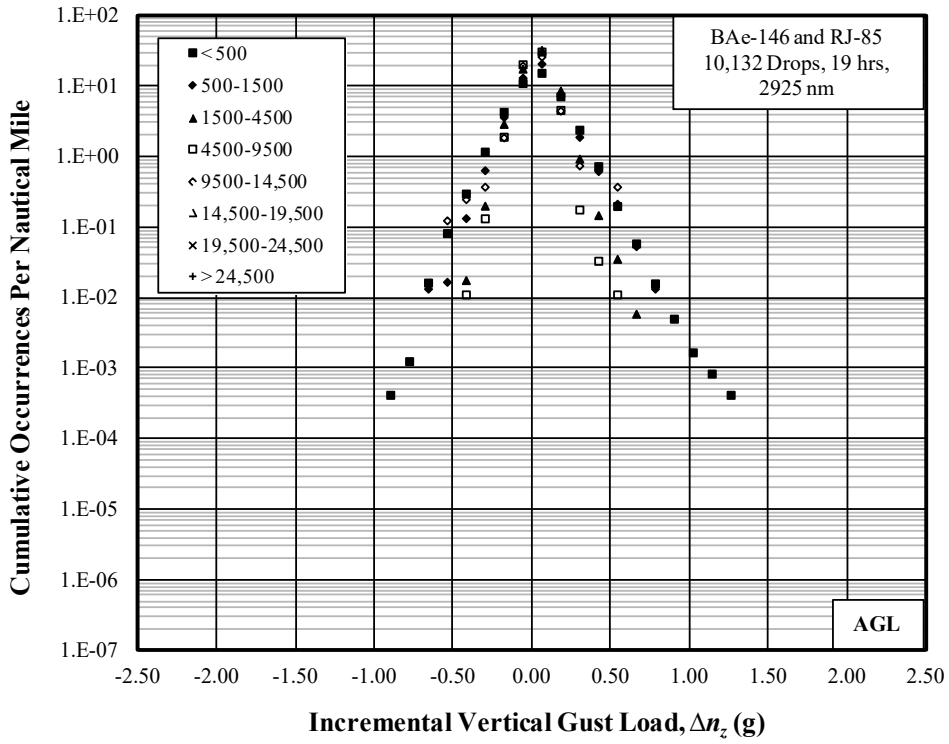

(b) Per Nautical Mile

Figure C-7. Cumulative occurrences of incremental vertical gust load factor – drop

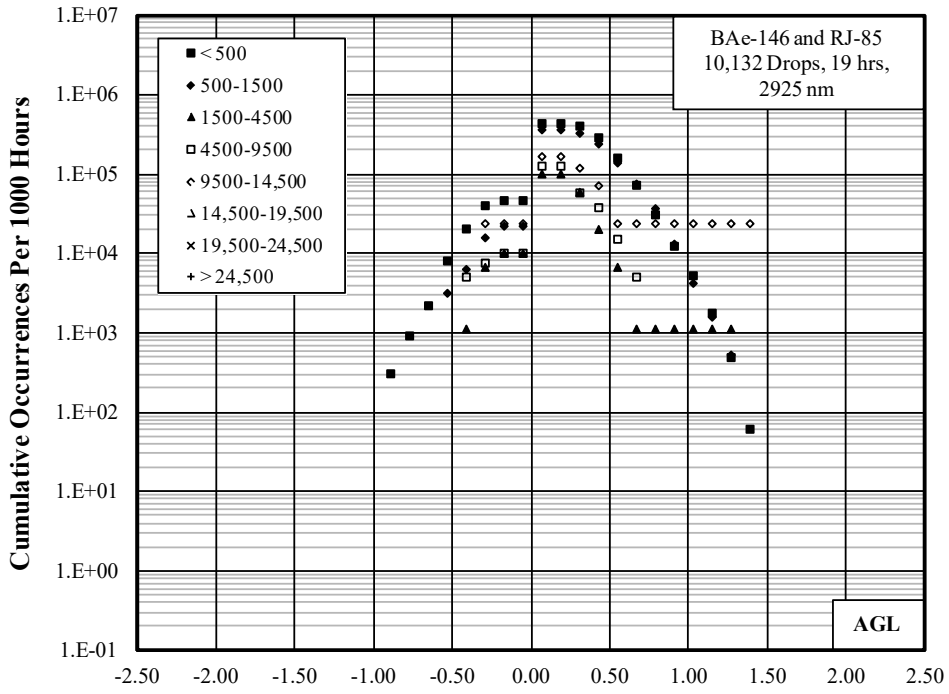

(a) Per 1000 Hours

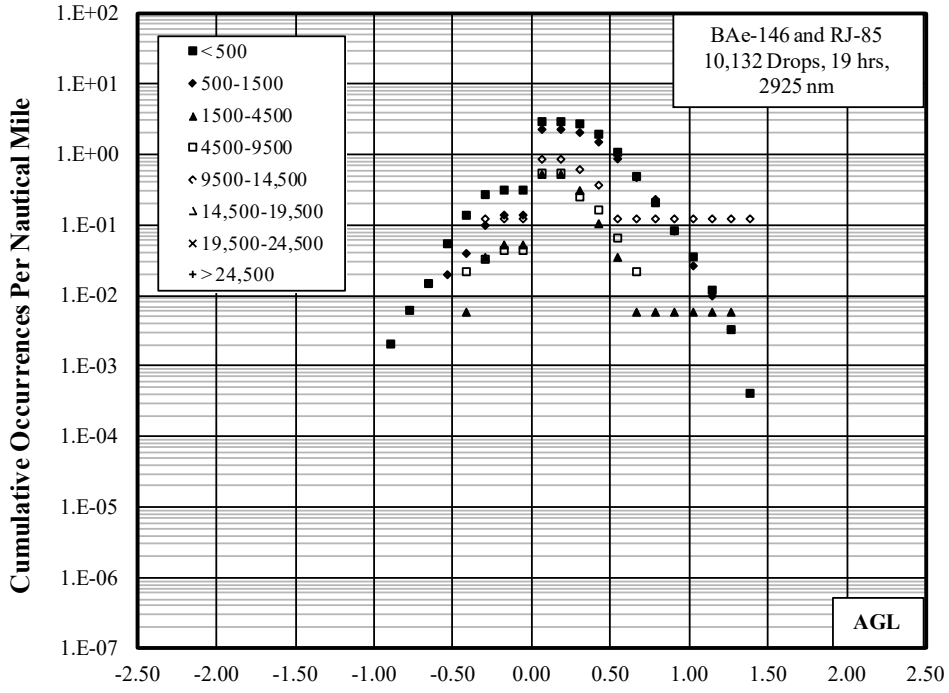

(b) Per Nautical Mile

Figure C-8. Cumulative occurrences of incremental vertical maneuver load factor – drop

Table C-8. Summary of durations and distances – exit

Altitude Band Ceiling (ft)	Duration (hr)	Distance (nm)
500	28.6	4391.9
1500	55.9	9241.0
4500	28.0	4824.9
9500	0.7	140.7
14,500	0.2	32.0
19,500	0	0
24,500	0	0
Above 24,500	0	0
Total	113.4	18,630.5

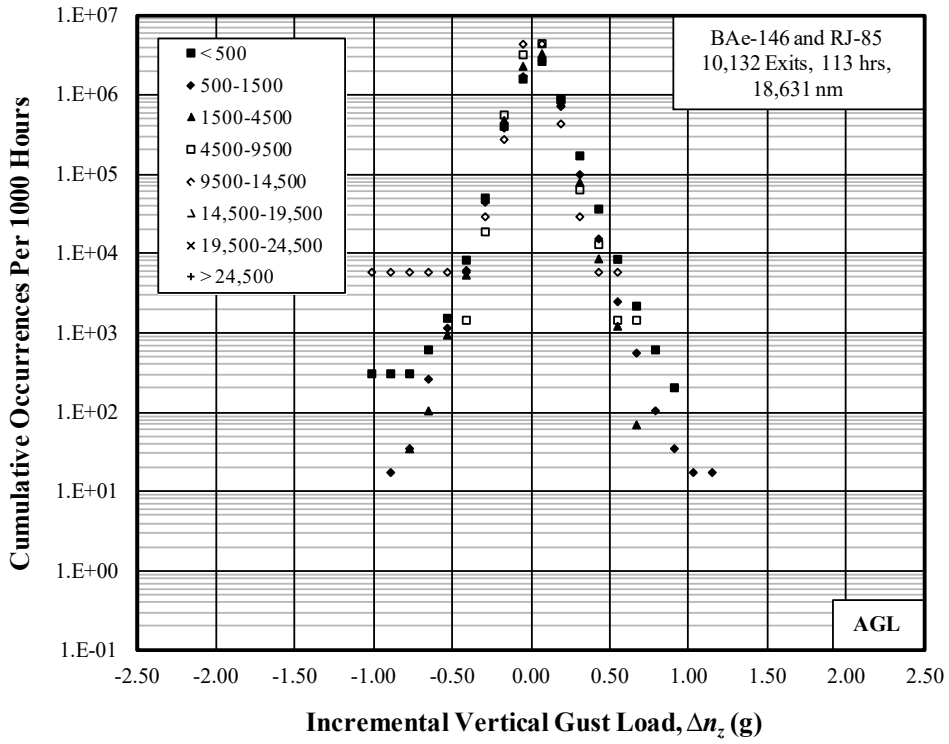

(a) Per 1000 Hours

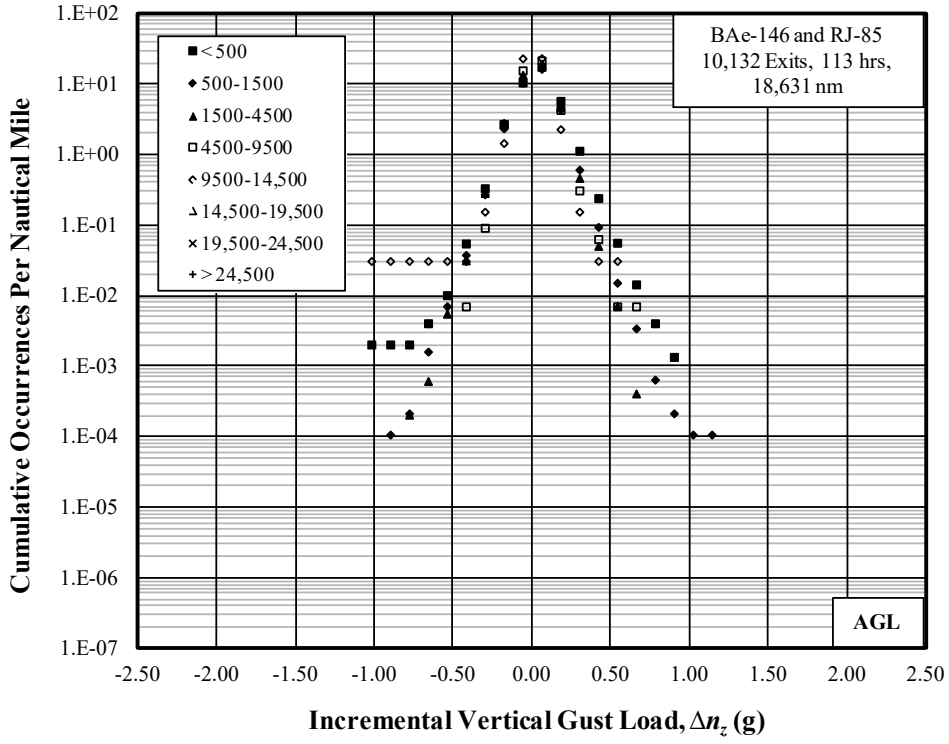

(b) Per Nautical Mile

Figure C-9. Cumulative occurrences of incremental vertical gust load factor – exit

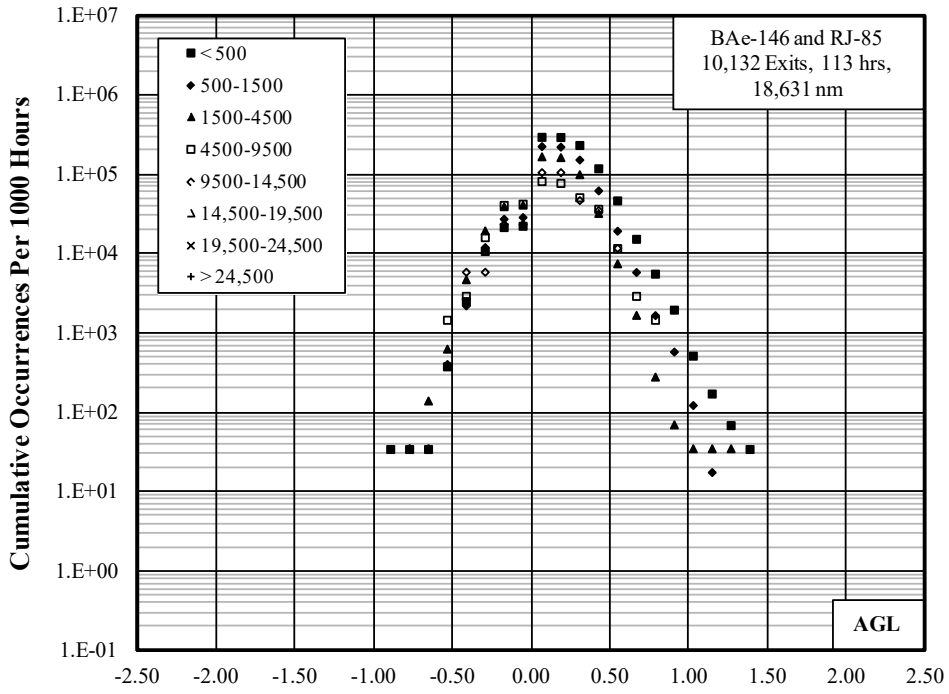

(a) Per 1000 Hours

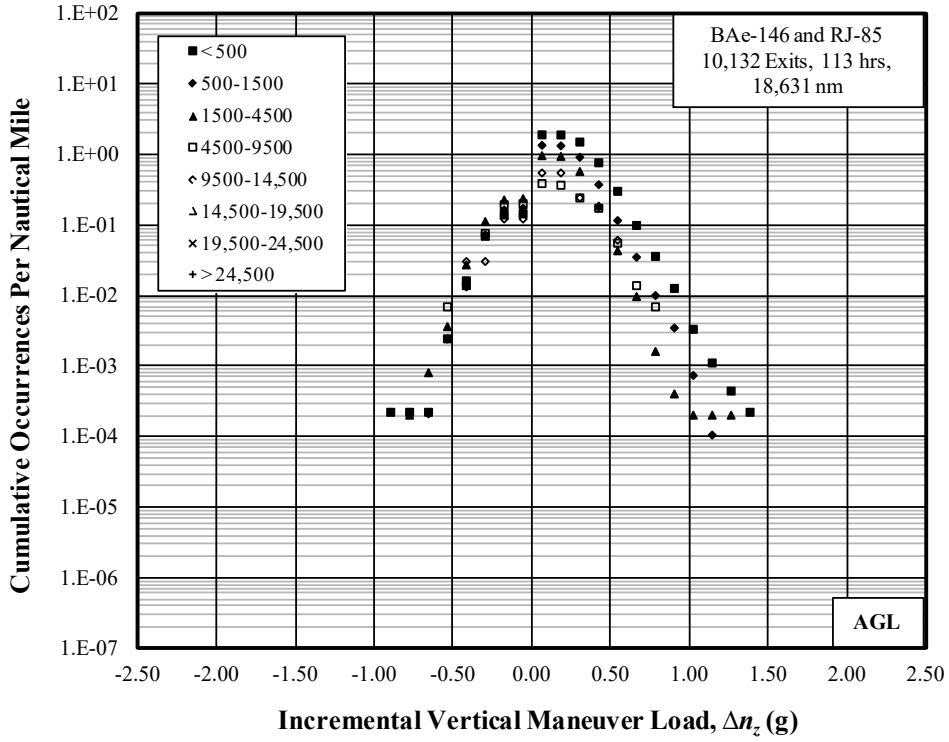

(b) Per Nautical Mile

Figure C-10. Cumulative occurrences of incremental vertical maneuver load factor – exit

Table C-9. Summary of durations and distances for firefighting flights

Altitude Band Ceiling (ft)	Duration (hr)	Distance (nm)
500	171.1	26,789.8
1500	646.7	117,211.4
4500	1906.3	439,436.4
9500	1089.2	332,731.5
14,500	413.5	145,307.8
19,500	93.6	35,379.5
24,500	13.5	5445.2
Above 24,500	3.1	1308.8
Total	4337.0	1,103,610.4

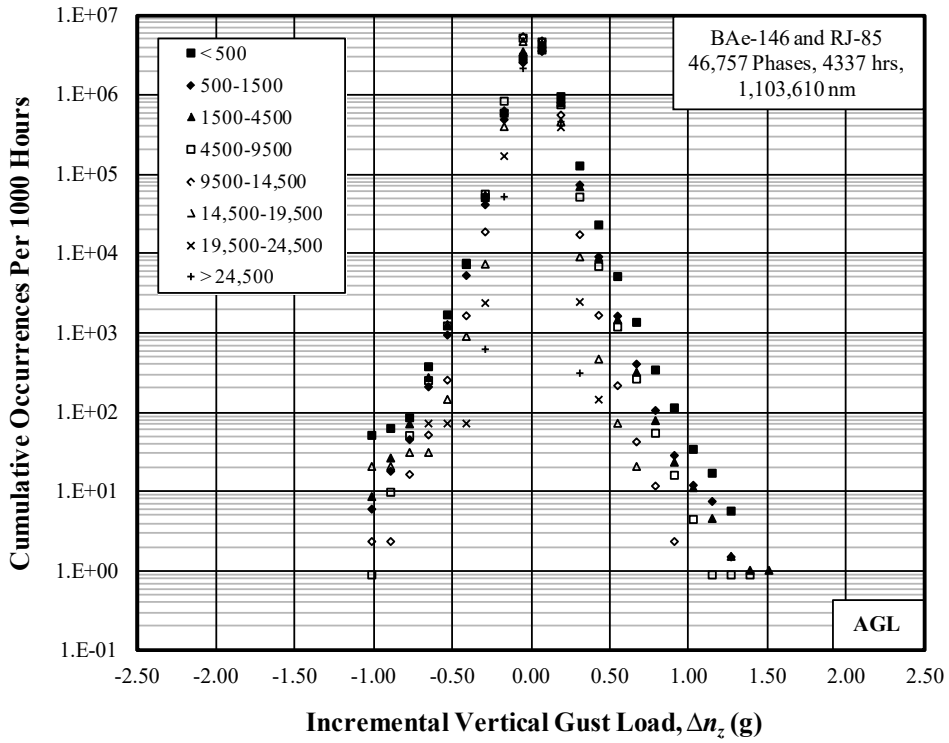

(a) Per 1000 Hours

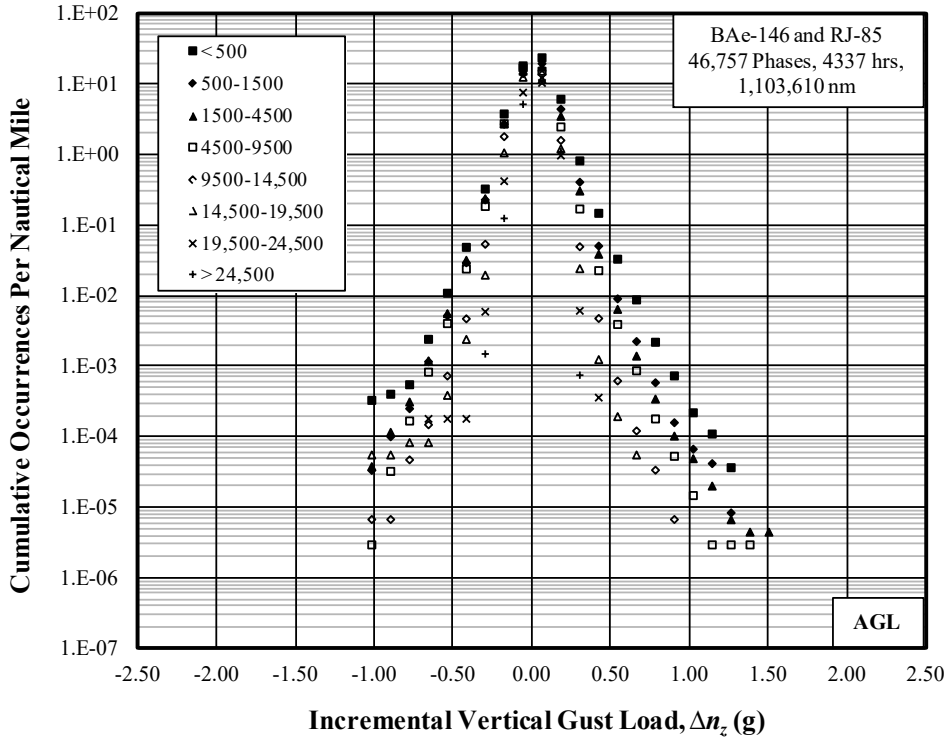

(b) Per Nautical Mile

Figure C-11. Cumulative occurrences of incremental vertical gust load factor, firefighting flights

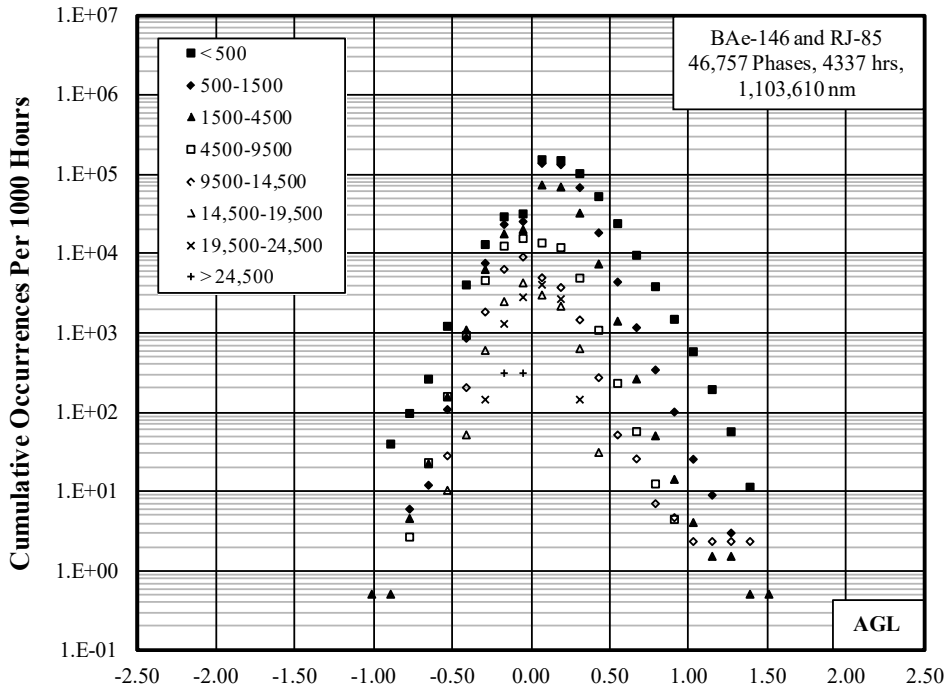

(a) Per 1000 Hours

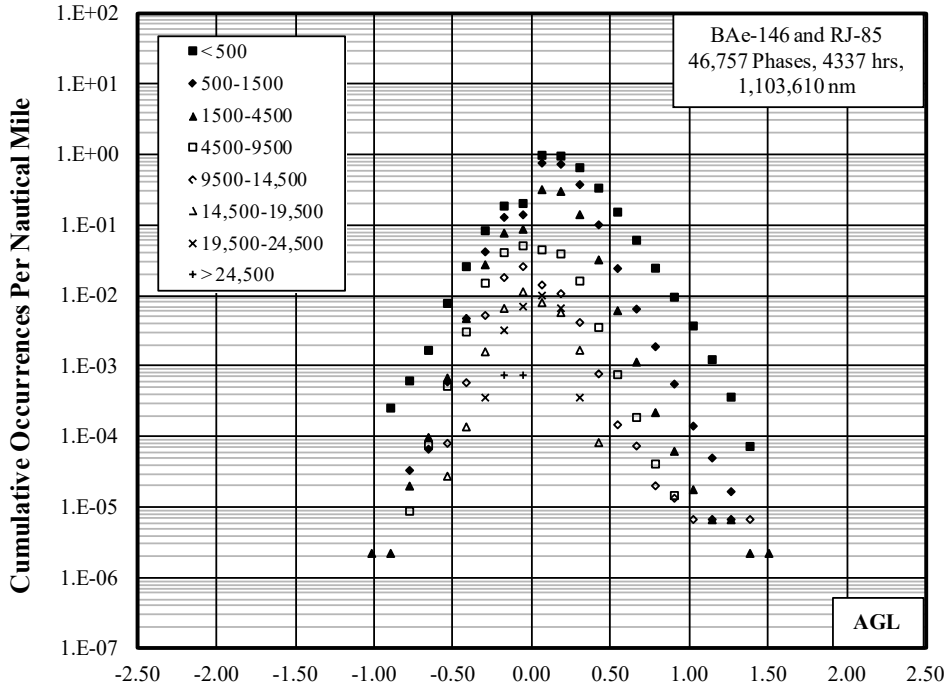

(b) Per Nautical Mile

Figure C-12. Cumulative occurrences of incremental vertical maneuver load factor, firefighting flights

Table C-10. Summary of durations and distances for ferry flights

Altitude Band Ceiling (ft)	Duration (hr)	Distance (nm)
500	0.9	128.9
1500	12.8	2057.4
4500	69.3	15,322.5
9500	82.4	24,016.9
14,500	75.6	26,054.6
19,500	88.4	34,237.5
24,500	150.6	62,234.8
Above 24,500	65.1	27,216.4
Total	545.1	191,268.9

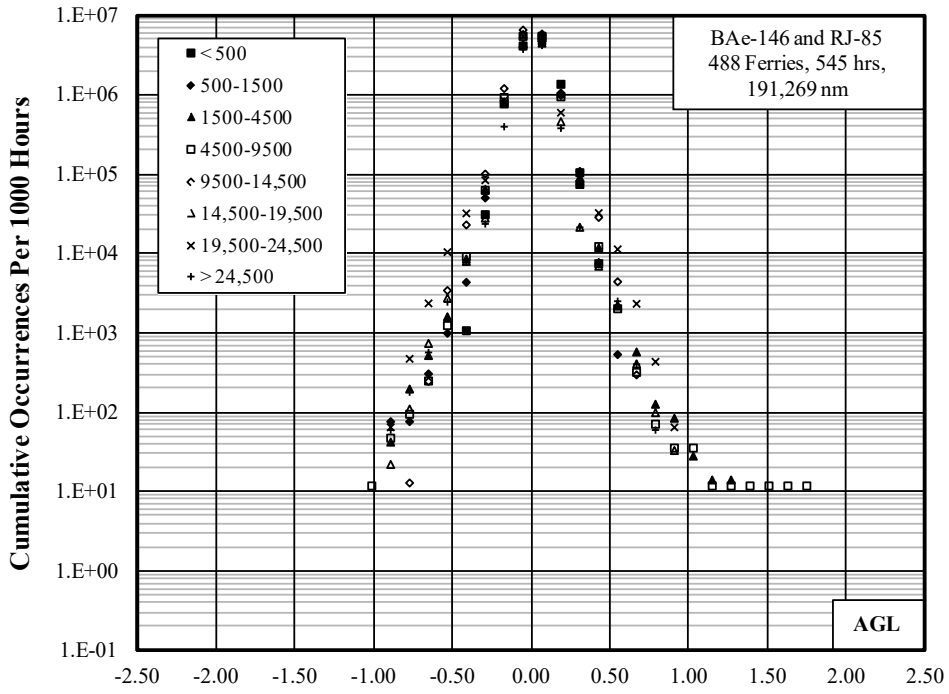

(a) Per 1000 Hours

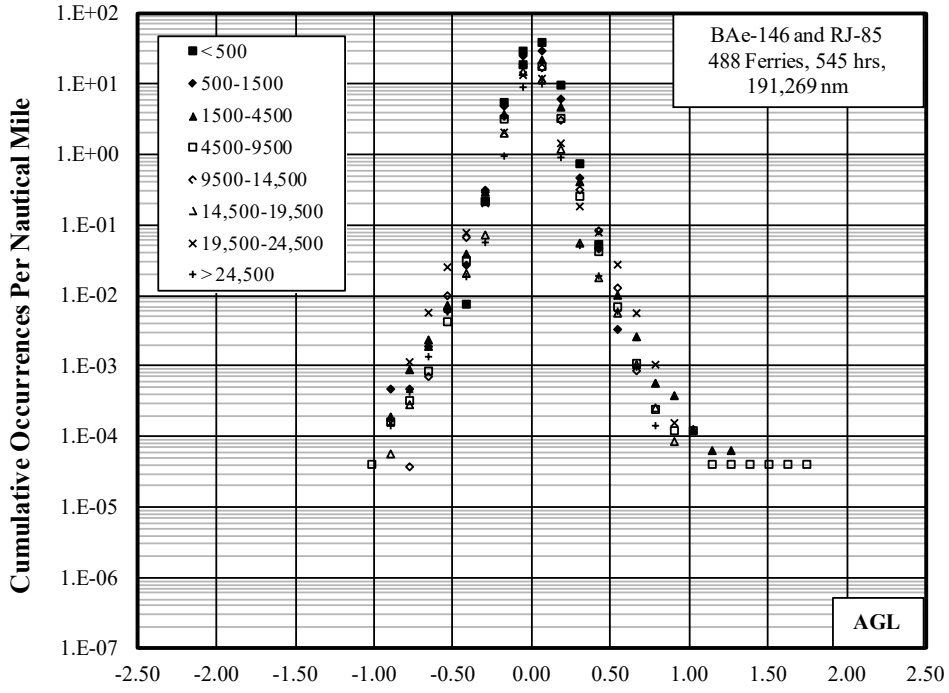

(b) Per Nautical Mile

Figure C-13. Cumulative occurrences of incremental vertical gust load factor, ferry flights

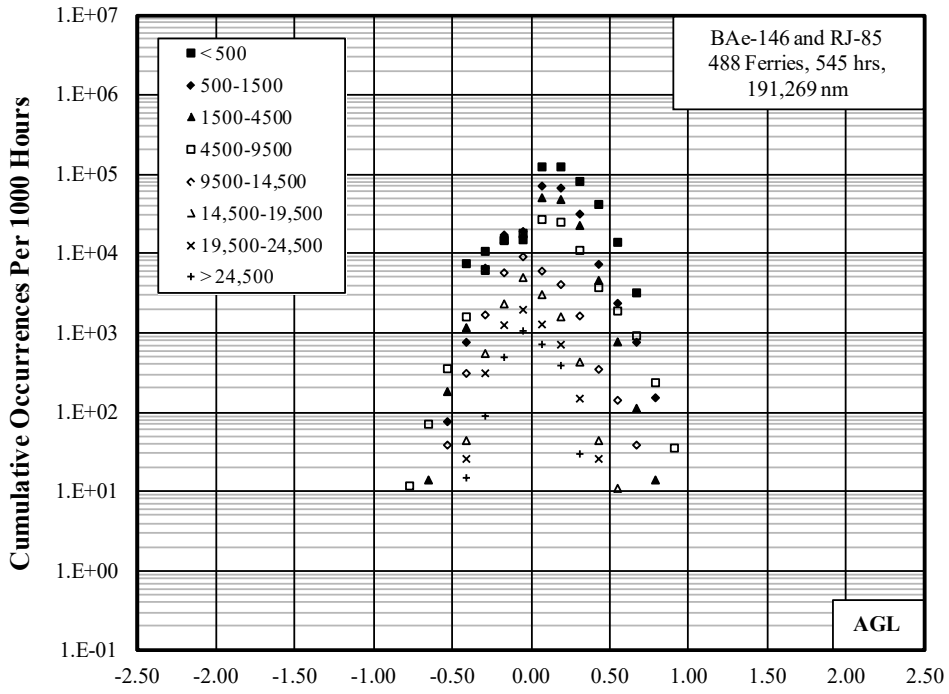

(a) Per 1000 Hours

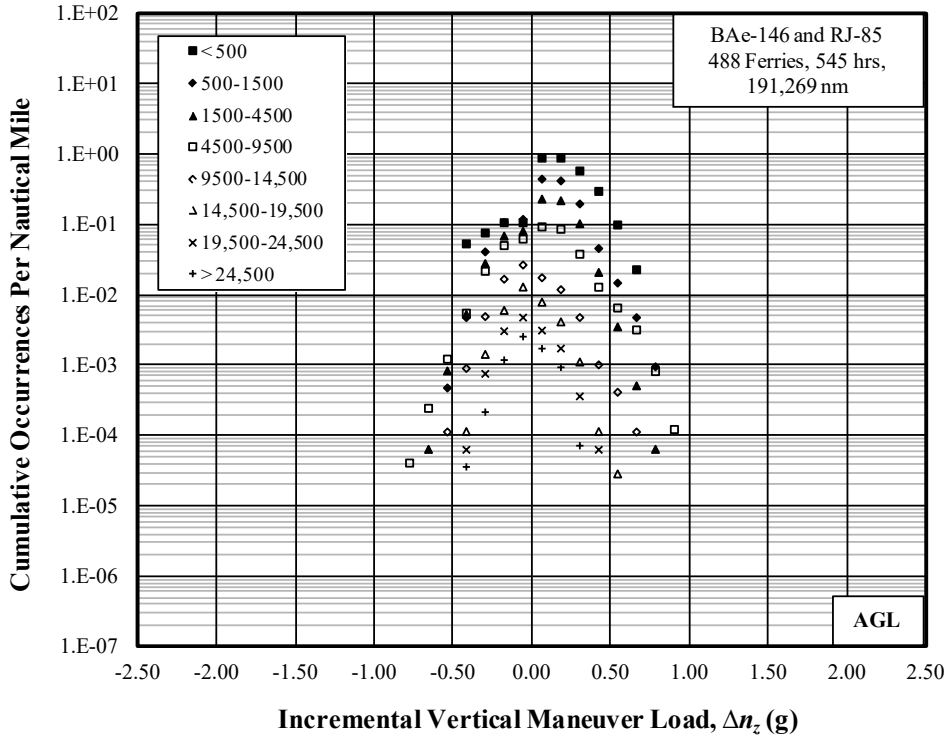

(b) Per Nautical Mile

Figure C-14. Cumulative occurrences of incremental vertical maneuver load factor, ferry flights

Table C-11. Summary of durations and distances for maintenance/training flights

Altitude Band Ceiling (ft)	Duration (hr)	Distance (nm)
500	7.8	1215.1
1500	29.7	4631.6
4500	126.1	25,340.6
9500	54.6	13,436.3
14,500	4.9	1366.8
19,500	1.0	286.6
24,500	0	0
Above 24,500	0	0
Total	224.1	46,277.0

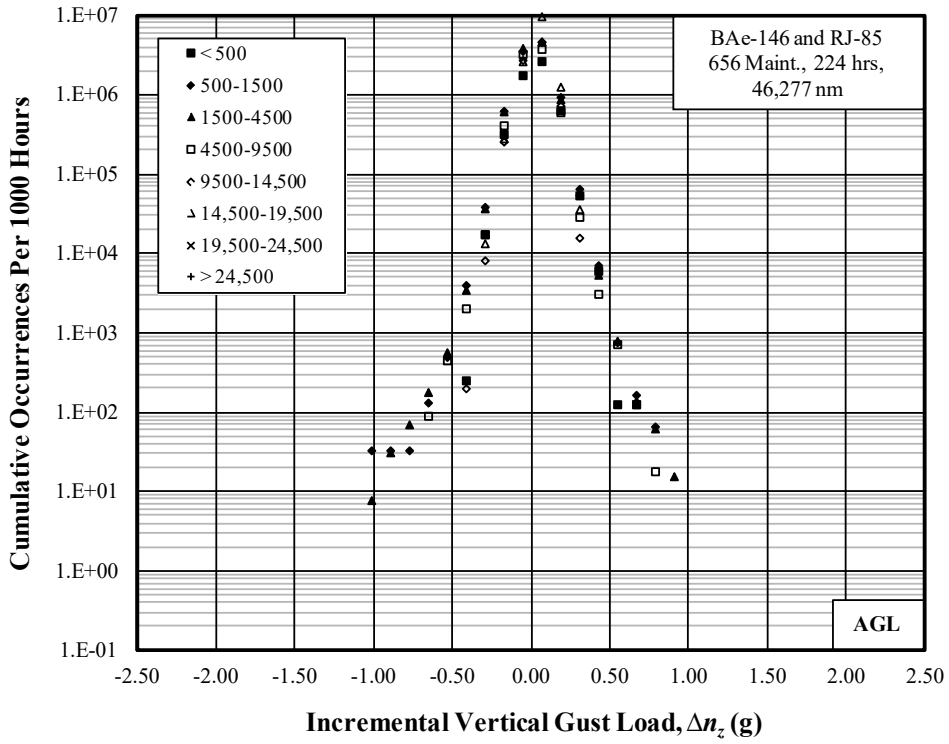

(a) Per 1000 Hours

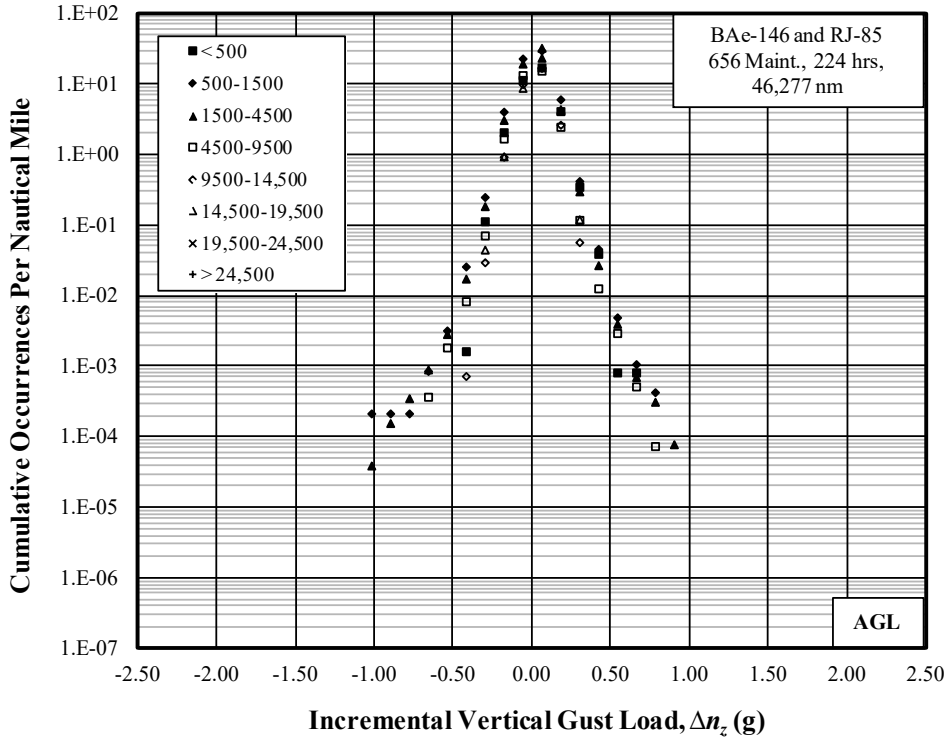

(b) Per Nautical Mile

Figure C-15. Cumulative occurrences of incremental vertical gust load factor, maintenance/training flights

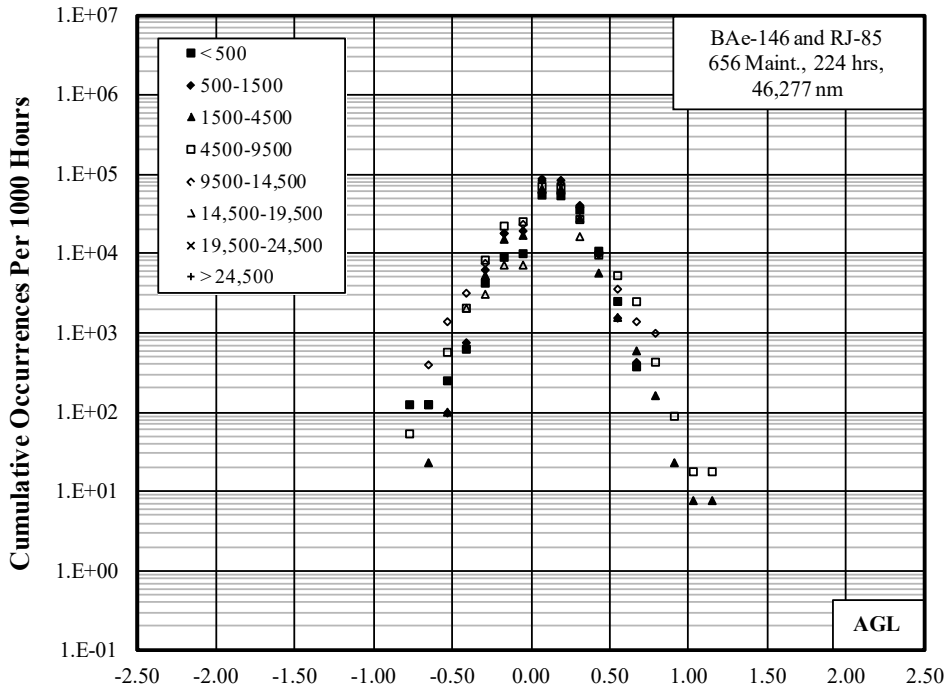

(a) Per 1000 Hours

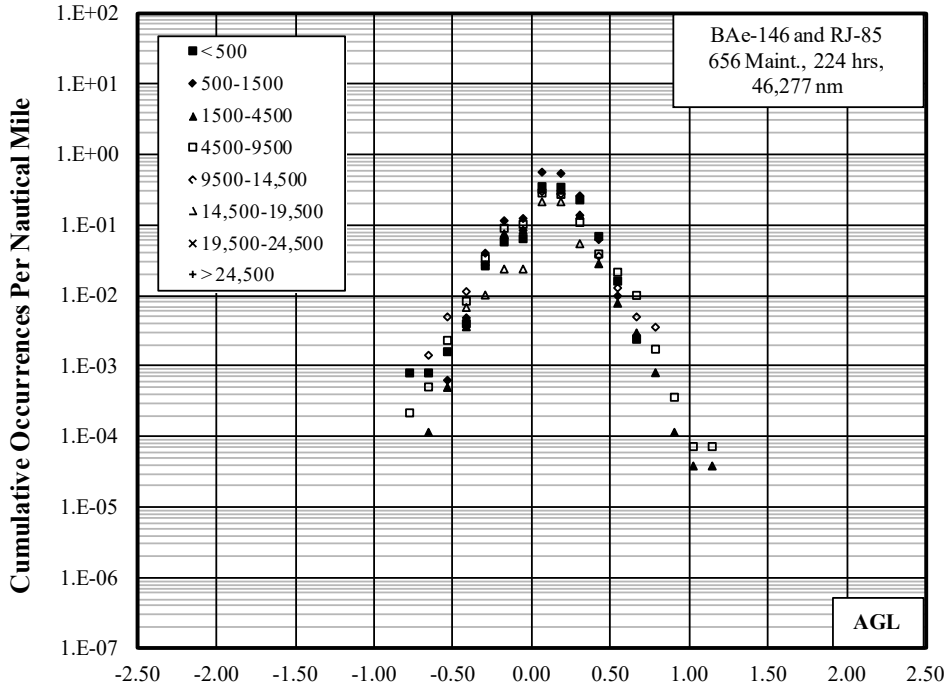

(b) Per Nautical Mile

Figure C-16. Cumulative occurrences of incremental vertical maneuver load factor, maintenance/training flights

APPENDIX D—FLIGHT LOADS BY MSL ALTITUDE

Table D-1. Statistical formats – flight loads data by mean sea level (MSL) altitude

Flight Loads Data	Table
Summary of Durations and Distances for All Flight Phases	Table D-3
Summary of Durations and Distances – Cruise 1	Table D-4
Summary of Durations and Distances – Cruise 2	Table D-5
Summary of Durations and Distances – Entry	Table D-6
Summary of Durations and Distances – Drop	Table D-7
Summary of Durations and Distances – Exit	Table D-8
Summary of Durations and Distances for Firefighting Flights	Table D-9
Summary of Durations and Distances for Ferry Flights	Table D-10
Summary of Durations and Distances for Maintenance/Training Flights	Table D-11

Table D-2. Statistical formats – flight loads data by MSL altitude

Flight Loads Data	Figure
CRUISE 1 PHASE	
Cumulative Occurrences of Incremental Vertical Gust Load Factor – Cruise 1	Figure D-1
Cumulative Occurrences of Incremental Vertical Maneuver Load Factor – Cruise 1	Figure D-2
CRUISE 2 PHASE	
Cumulative Occurrences of Incremental Vertical Gust Load Factor – Cruise 2	Figure D-3
Cumulative Occurrences of Incremental Vertical Maneuver Load Factor – Cruise 2	Figure D-4
ENTRY PHASE	
Cumulative Occurrences of Incremental Vertical Gust Load Factor – Entry	Figure D-5
Cumulative Occurrences of Incremental Vertical Maneuver Load Factor – Entry	Figure D-6
DROP PHASE	
Cumulative Occurrences of Incremental Vertical Gust Load Factor – Drop	Figure D-7
Cumulative Occurrences of Incremental Vertical Maneuver Load Factor – Drop	Figure D-8
EXIT PHASE	
Cumulative Occurrences of Incremental Vertical Gust Load Factor – Exit	Figure D-9
Cumulative Occurrences of Incremental Vertical Maneuver Load Factor – Exit	Figure D-10
FIREFIGHTING FLIGHTS	
Cumulative Occurrences of Incremental Vertical Gust Load Factor – Firefighting Flights	Figure D-11
Cumulative Occurrences of Incremental Vertical Maneuver Load Factor – Firefighting Flights	Figure D-12
FERRY FLIGHTS	
Cumulative Occurrences of Incremental Vertical Gust Load Factor – Ferry Flights	Figure D-13
Cumulative Occurrences of Incremental Vertical Maneuver Load Factor – Ferry Flights	Figure D-14
MAINTENANCE/TRAINING FLIGHTS	

Cumulative Occurrences of Incremental Vertical Gust Load Factor – Maintenance/Training Flights	Figure D-15
Cumulative Occurrences of Incremental Vertical Maneuver Load Factor – Maintenance/Training Flights	Figure D-16

Table D-3. Summary of durations and distances for all firefighting flight phases

Phase	Number of Occurrences	Duration (hr)	Distance (nm)
Cruise 1	8574	2718	702,052
Cruise 2	8461	1478	402,385
Entry	10,716	249	38,481
Drop	10,716	20	3057
Exit	10,716	116	19,076
Total		4581	1,165,050

Table D-4. Summary of durations and distances – cruise 1

Altitude Band Ceiling (ft)	Duration (hr)	Distance (nm)
500	11.6	1877.5
1500	71.3	13,039.1
4500	452.9	94,587.7
9500	1337.7	313,770.1
14,500	542.8	168,773.4
19,500	270.3	97,890.0
24,500	22.4	8717.8
Above 24,500	8.3	3396.2
Total	2717.5	702,051.8

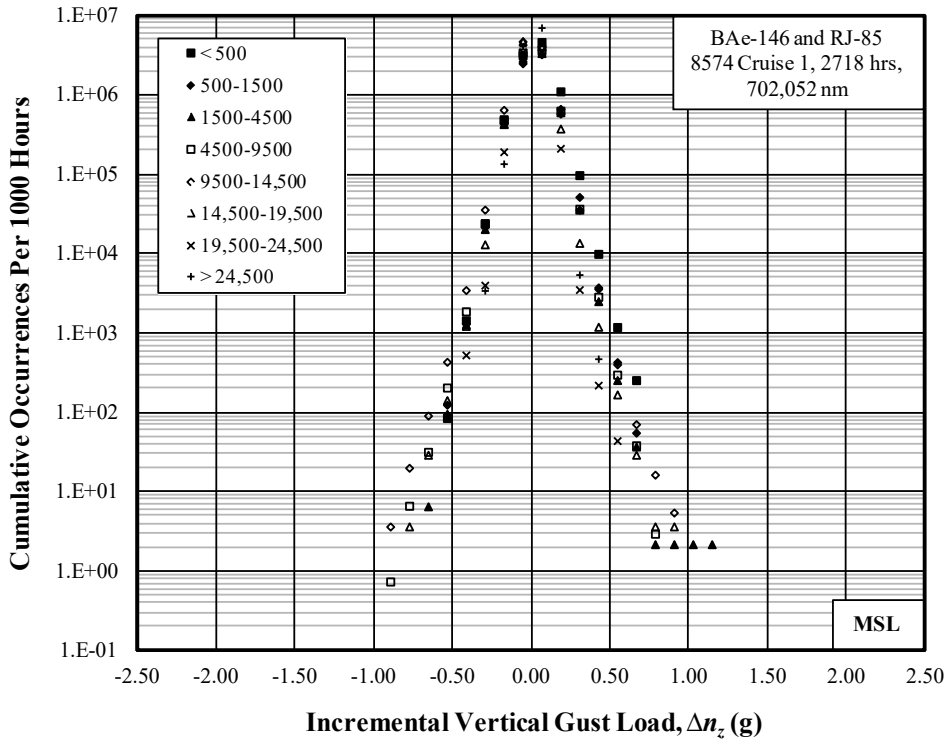

(a) Per 1000 Hours

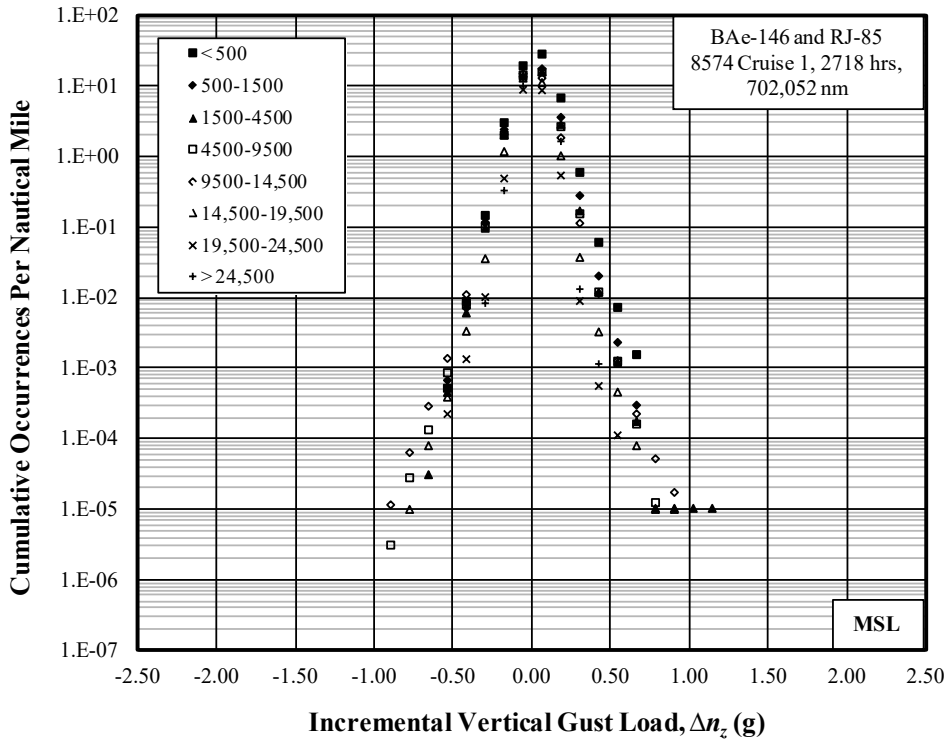

(b) Per Nautical Mile

Figure D-1. Cumulative occurrences of incremental vertical gust load factor – cruise 1

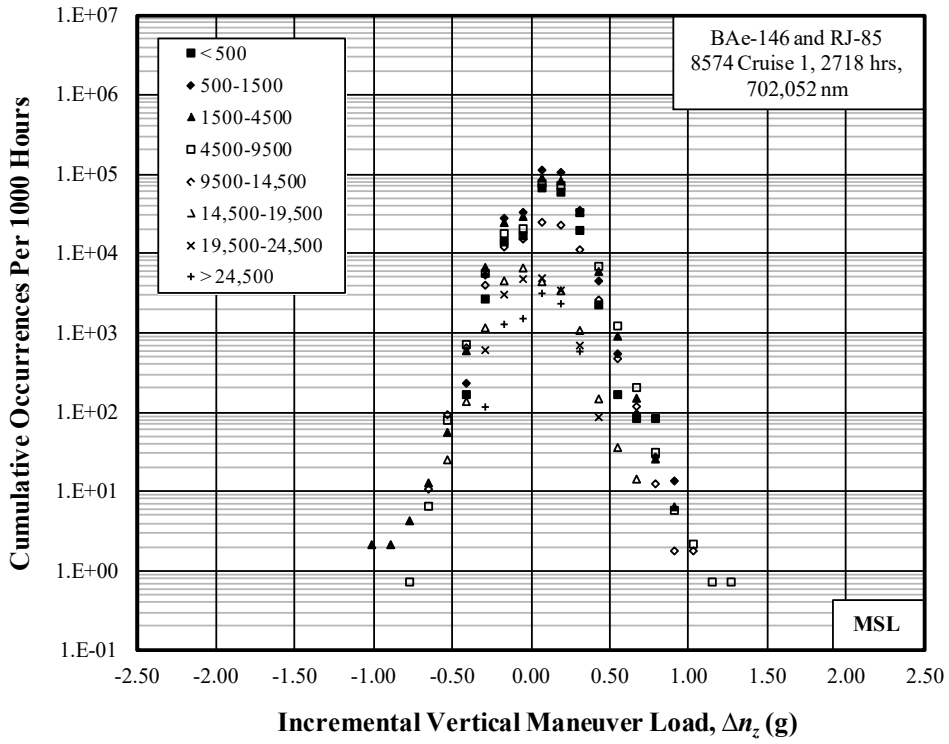

(a) Per 1000 Hours

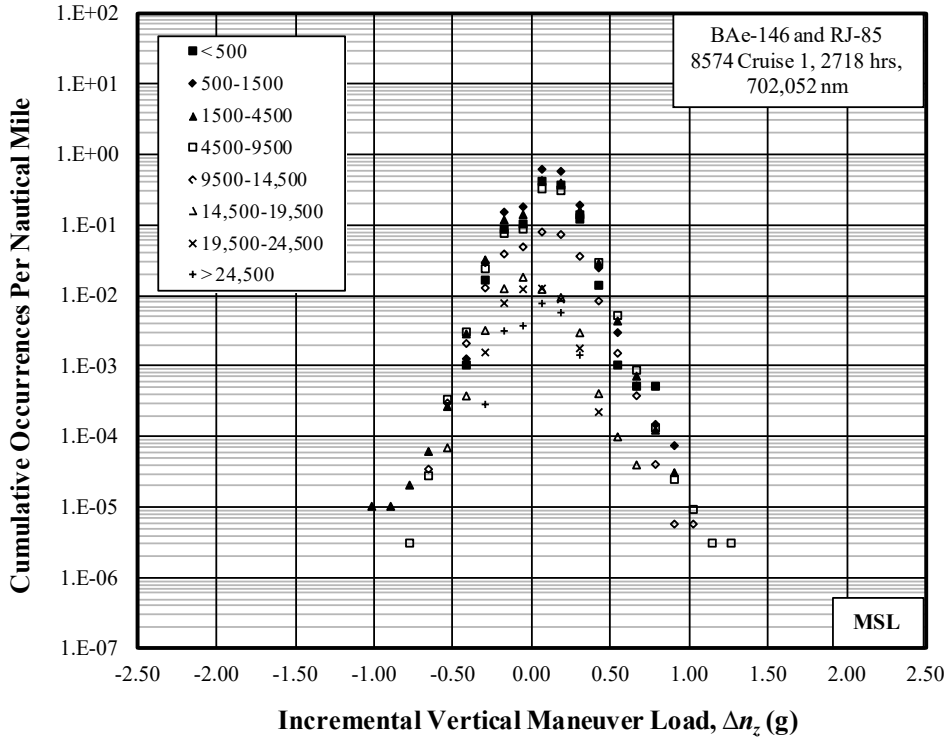

(b) Per Nautical Mile

Figure D-2. Cumulative occurrences of incremental vertical maneuver load factor – cruise 1

Table D-5. Summary of durations and distances – cruise 2

Altitude Band Ceiling (ft)	Duration (hr)	Distance (nm)
500	1.5	358.8
1500	22.3	3458.2
4500	295.0	62,303.9
9500	617.7	157,083.3
14,500	402.8	129,551.0
19,500	127.2	45,445.3
24,500	5.1	1908.2
Above 24,500	6.4	2725.9
Total	1477.9	402,834.6

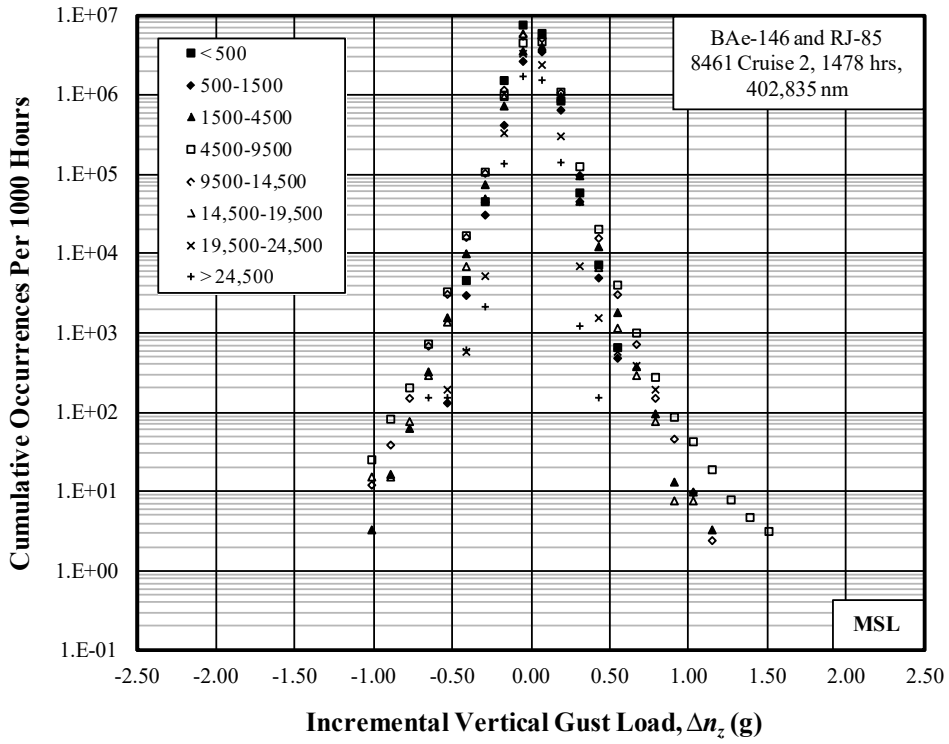

(a) Per 1000 Hours

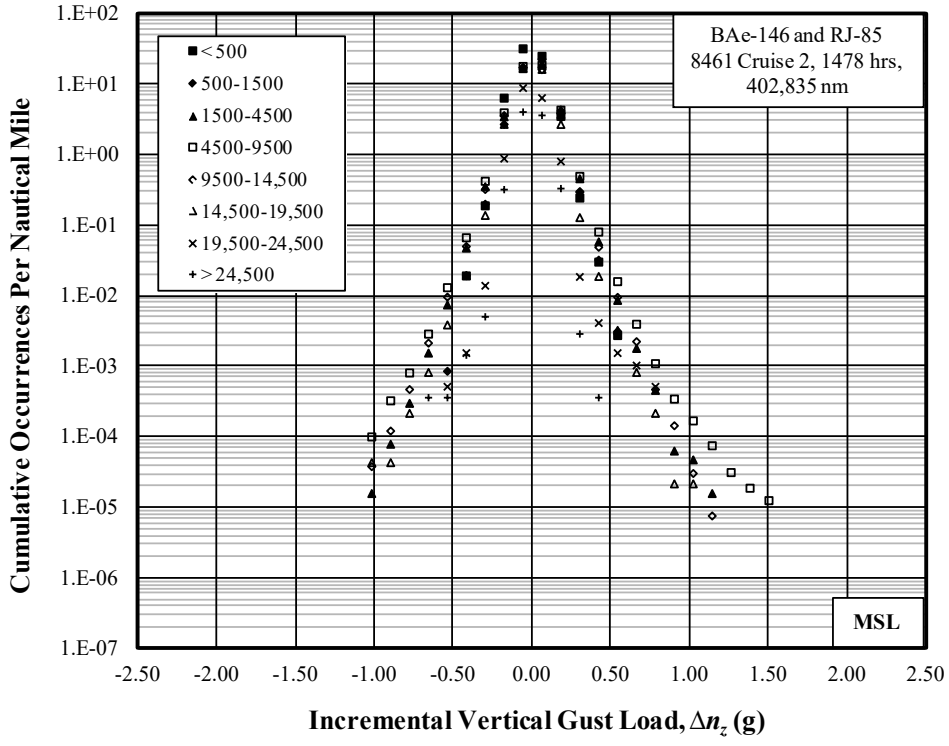

(b) Per Nautical Mile

Figure D-3. Cumulative occurrences of incremental vertical gust load factor – cruise 2

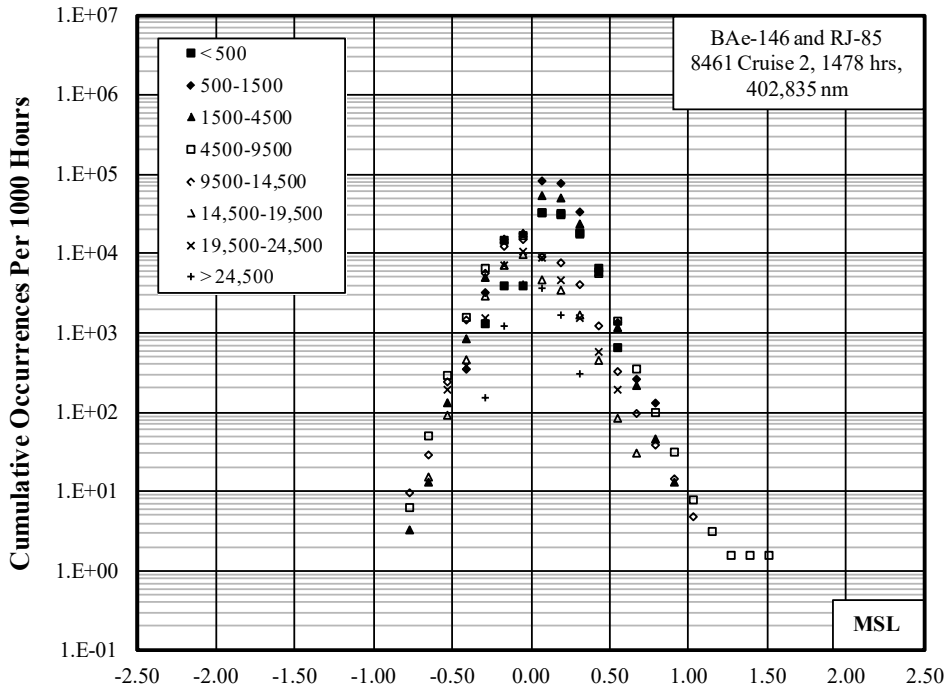

(a) Per 1000 Hours

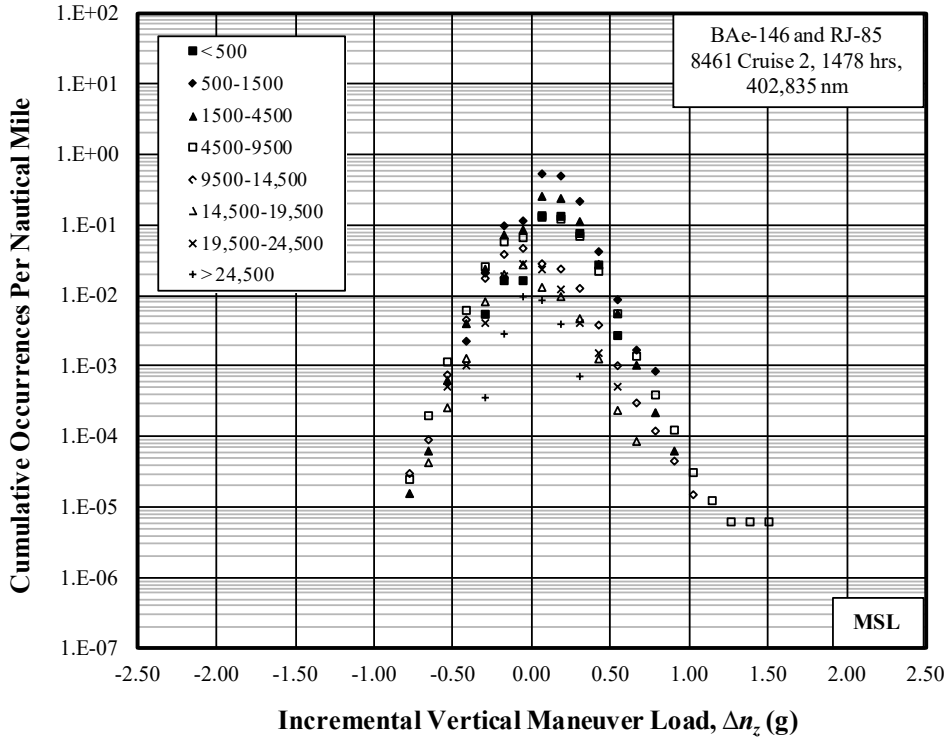

(b) Per Nautical Mile

Figure D-4. Cumulative occurrences of incremental vertical maneuver load factor – cruise 2

Table D-6. Summary of durations and distances – entry

Altitude Band Ceiling (ft)	Duration (hr)	Distance (nm)
500	1.9	254.7
1500	11.6	1658.5
4500	77.6	11,507.5
9500	149.9	23,646.3
14,500	8.2	1385.8
19,500	0.1	28.0
24,500	0.0	0.0
Above 24,500	0.0	0.0
Total	249.3	38,480.7

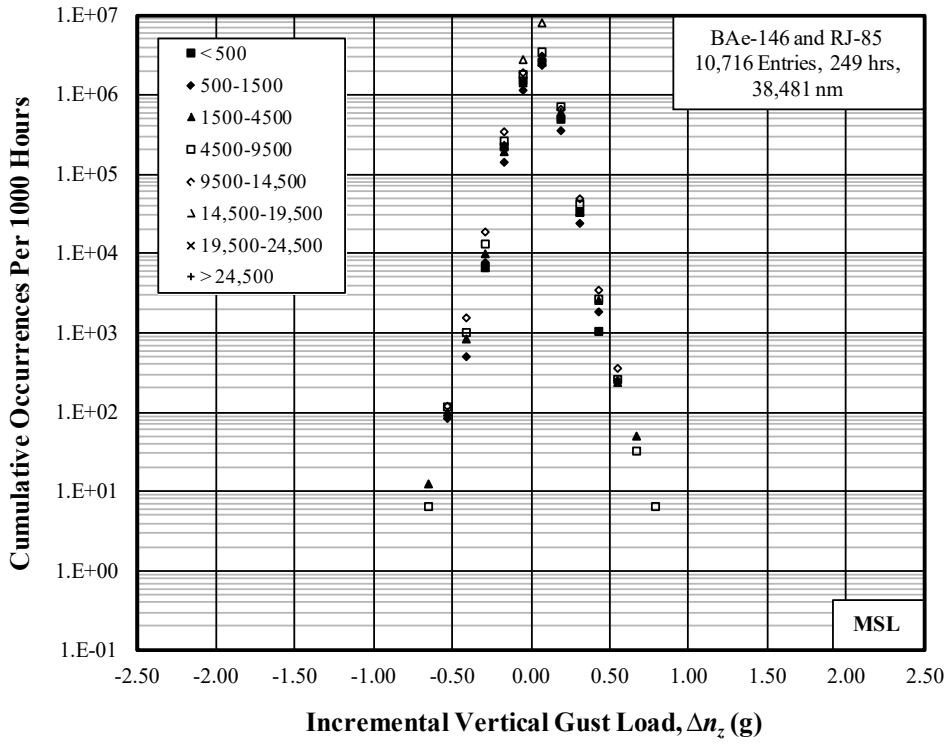

(a) Per 1000 Hours

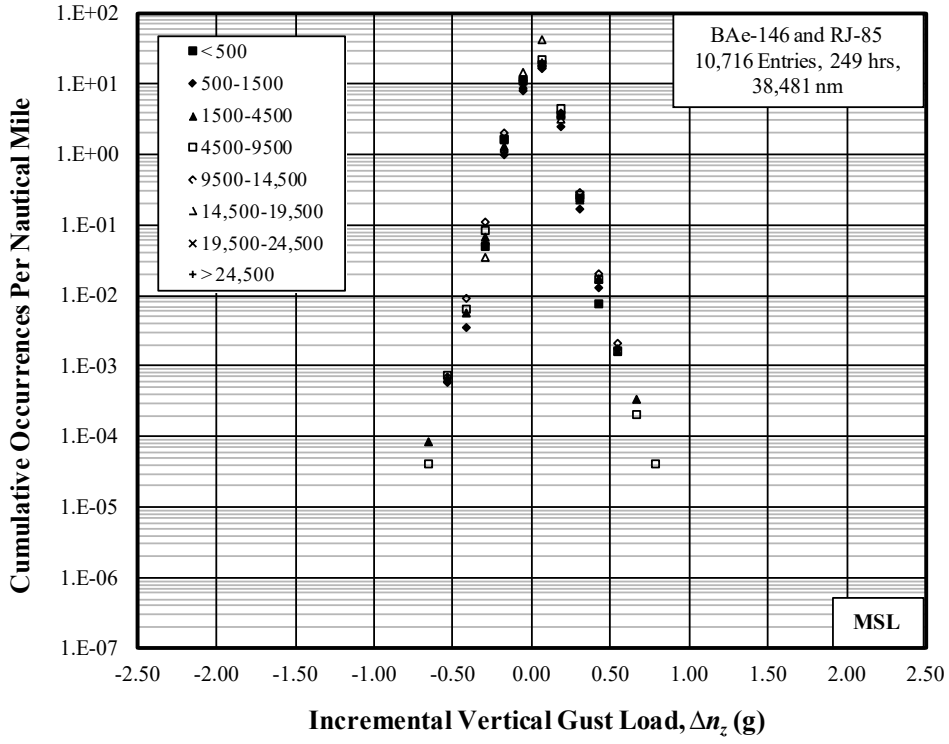

(b) Per Nautical Mile

Figure D-5. Cumulative occurrences of incremental vertical gust load factor – entry

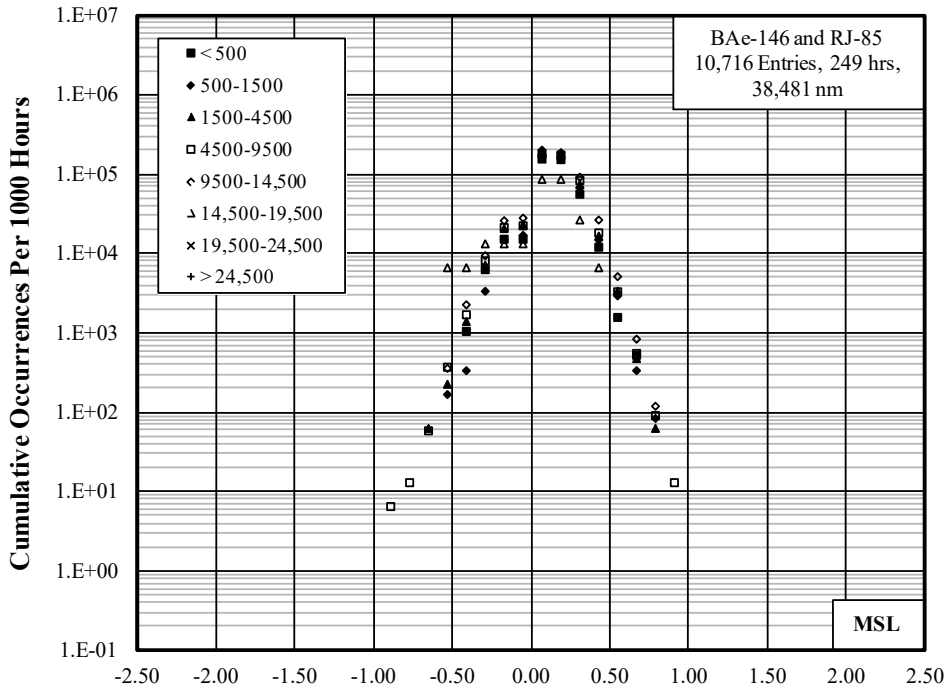

(a) Per 1000 Hours

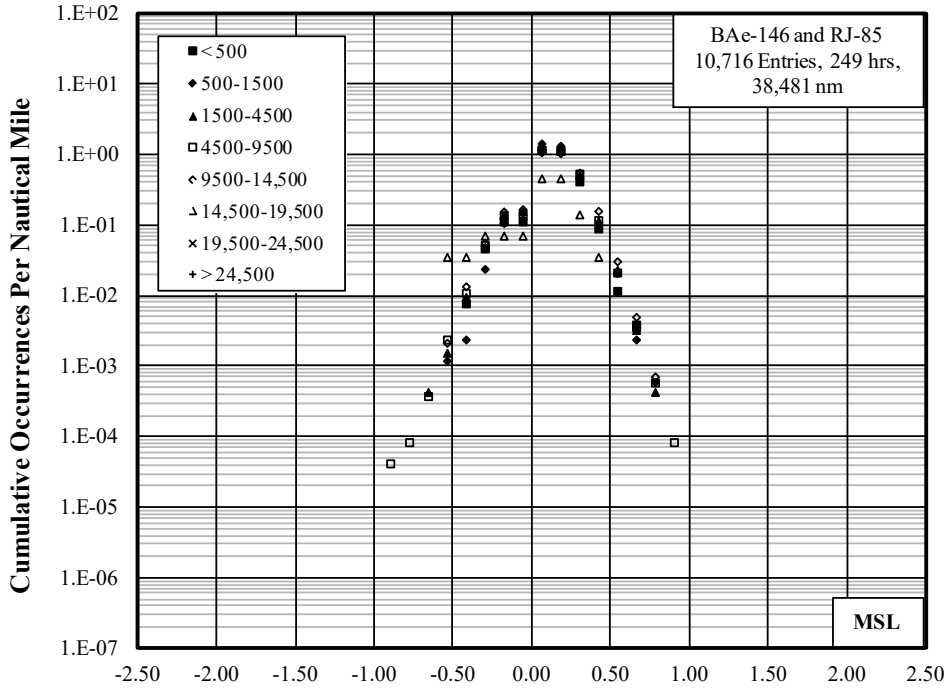

(b) Per Nautical Mile

Figure D-6. Cumulative occurrences of incremental vertical maneuver load factor – entry

Table D-7. Summary of durations and distances – drop

Altitude Band Ceiling (ft)	Duration (hr)	Distance (nm)
500	0.8	103.0
1500	1.2	172.9
4500	7.7	1156.8
9500	9.8	1522.8
14,500	0.5	98.2
19,500	0.0	3.4
24,500	0.0	0.0
Above 24,500	0.0	0.0
Total	19.9	3057.0

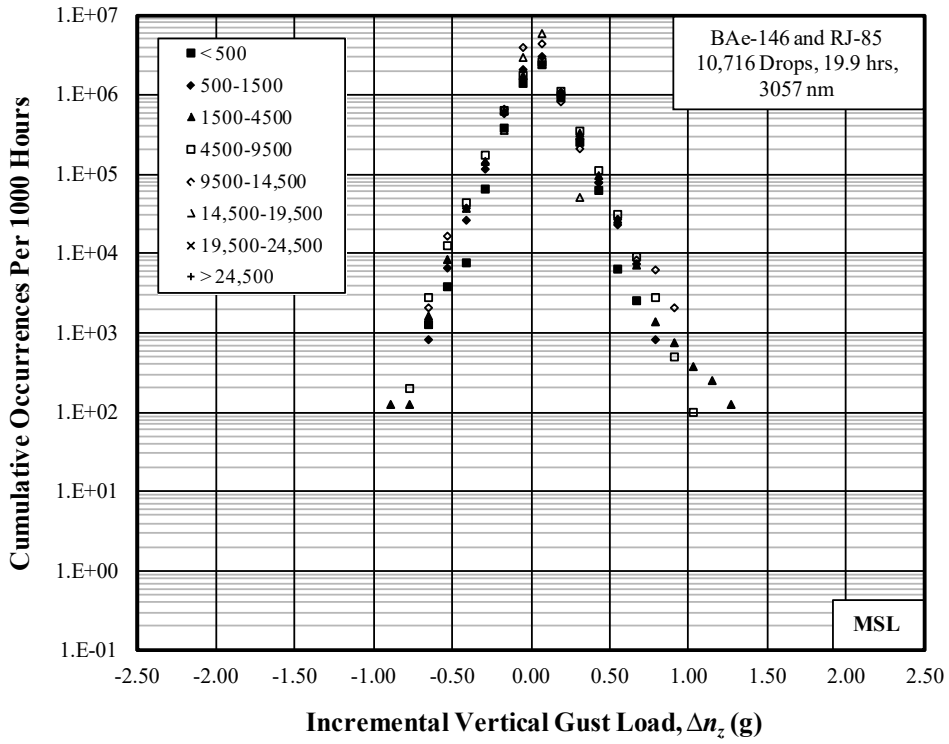

(a) Per 1000 Hours

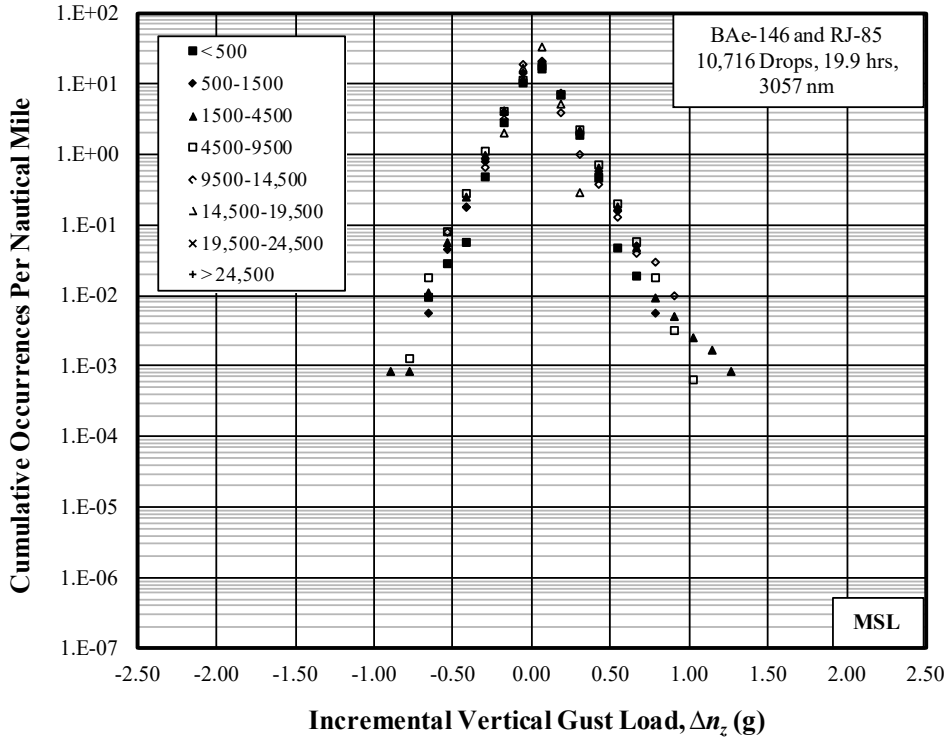

(b) Per Nautical Mile

Figure D-7. Cumulative occurrences of incremental vertical gust load factor – drop

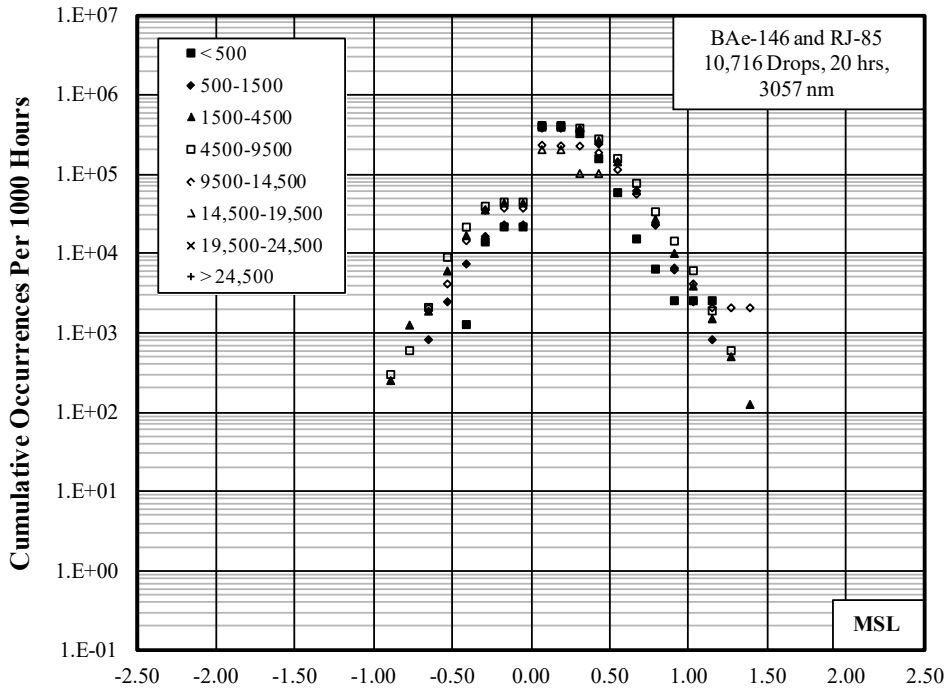

(a) Per 1000 Hours

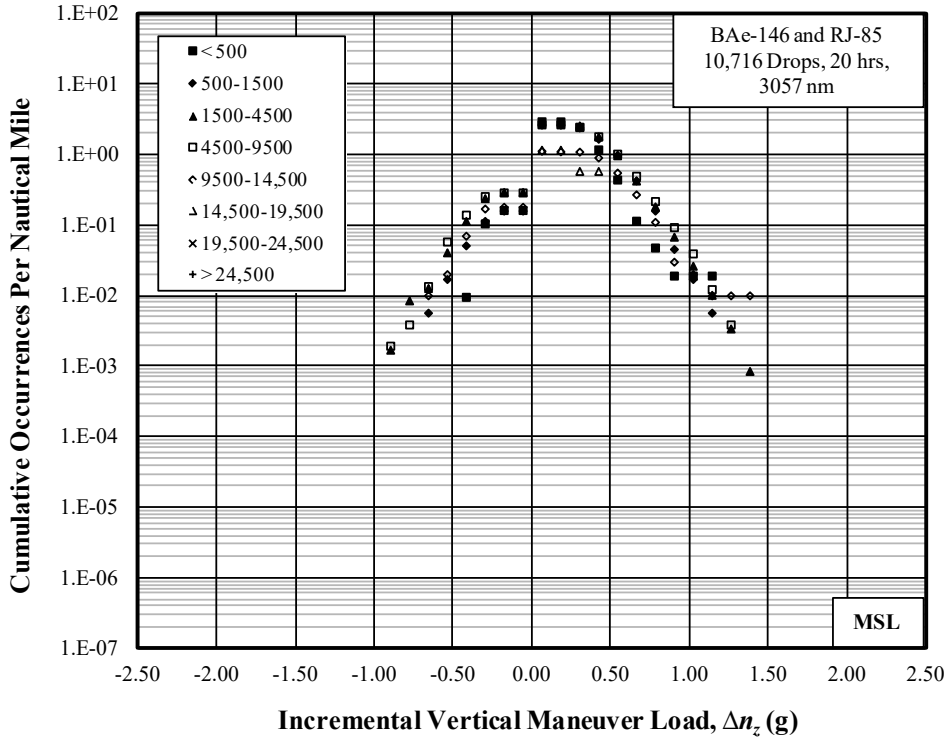

(b) Per Nautical Mile

Figure D-8. Cumulative occurrences of incremental vertical maneuver load factor – drop

Table D-8. Summary of durations and distances – exit

Altitude Band Ceiling (ft)	Duration (hr)	Distance (nm)
500	2.0	272.0
1500	7.7	1185.5
4500	42.2	6742.8
9500	61.9	10,414.5
14,500	2.3	439.0
19,500	0.1	22.2
24,500	0.0	0.0
Above 24,500	0.0	0.0
Total	116.3	19,076.0

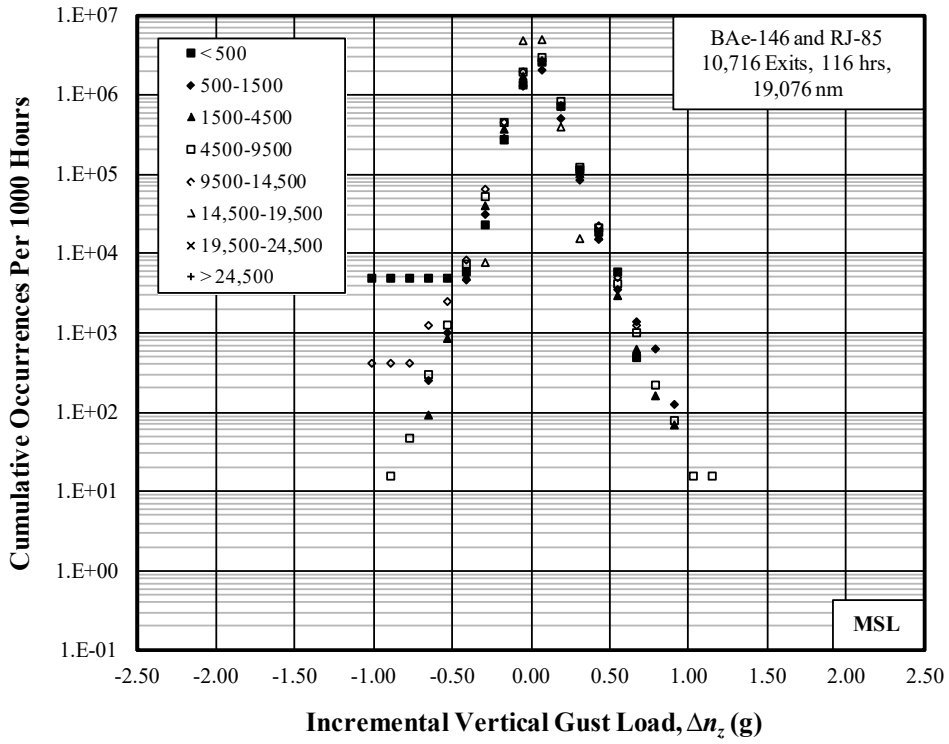

(a) Per 1000 Hours

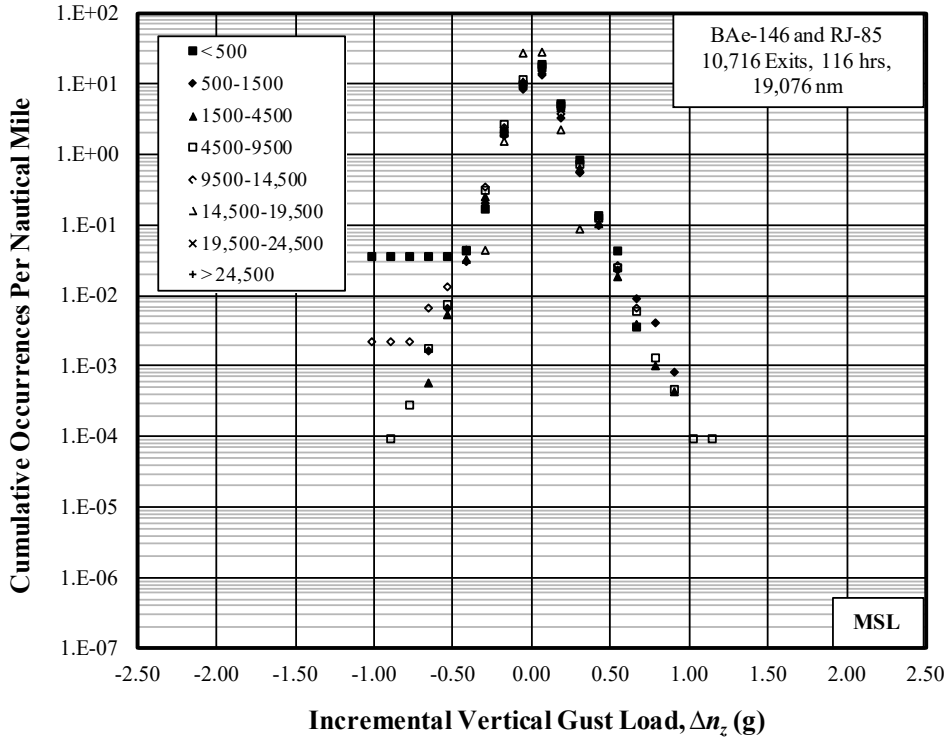

(b) Per Nautical Mile

Figure D-9. Cumulative occurrences of incremental vertical gust load factor – exit

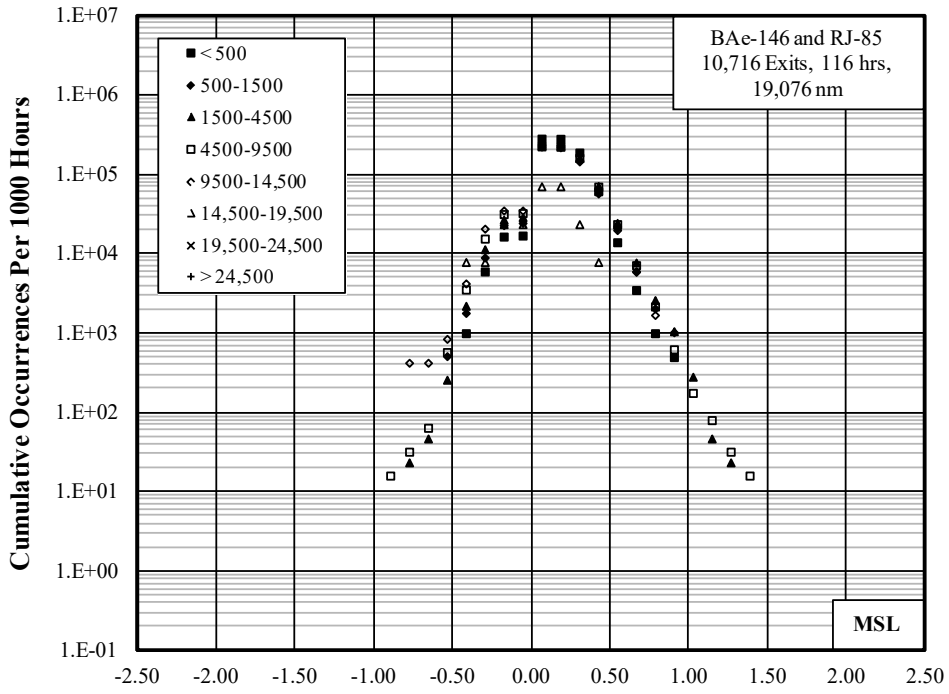

(a) Per 1000 Hours

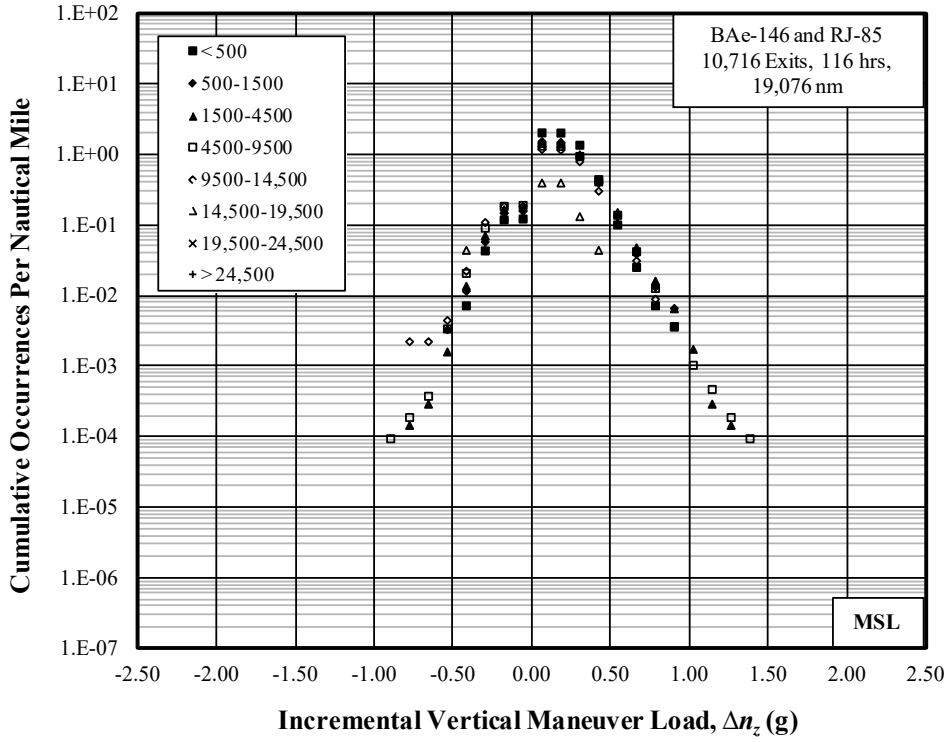

(b) Per Nautical Mile

Figure D-10. Cumulative occurrences of incremental vertical maneuver load factor – exit

Table D-9. Summary of durations and distances – firefighting flights

Altitude Band Ceiling (ft)	Duration (hr)	Distance (nm)
500	17.7	2866.0
1500	114.2	19,514.1
4500	875.5	176,298.8
9500	2176.9	506,437.0
14,500	956.6	300,247.4
19,500	397.8	143,388.8
24,500	27.5	10,626.1
Above 24,500	14.7	6122.1
Total	4581.0	1,165,500.1

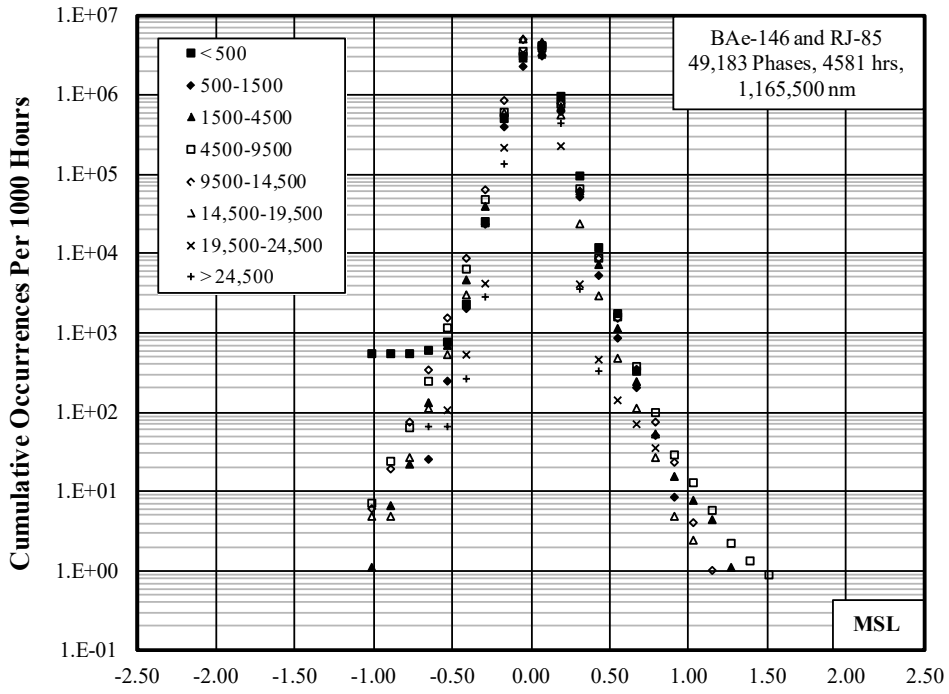

(a) Per 1000 Hours

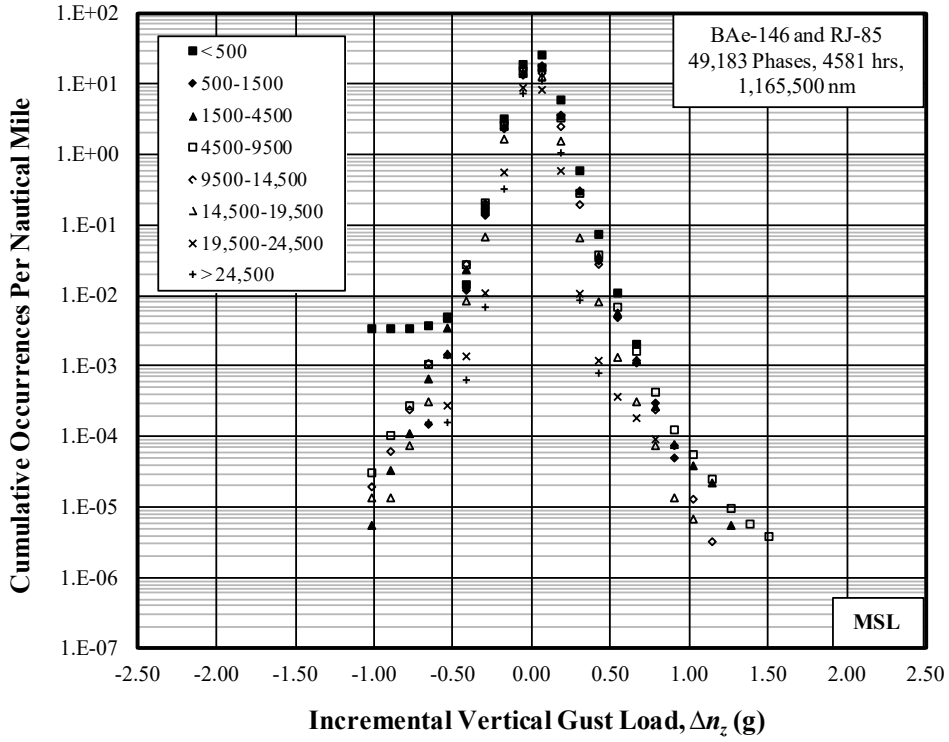

(b) Per Nautical Mile

Figure D-11. Cumulative occurrences of incremental vertical gust load factor – firefighting flights

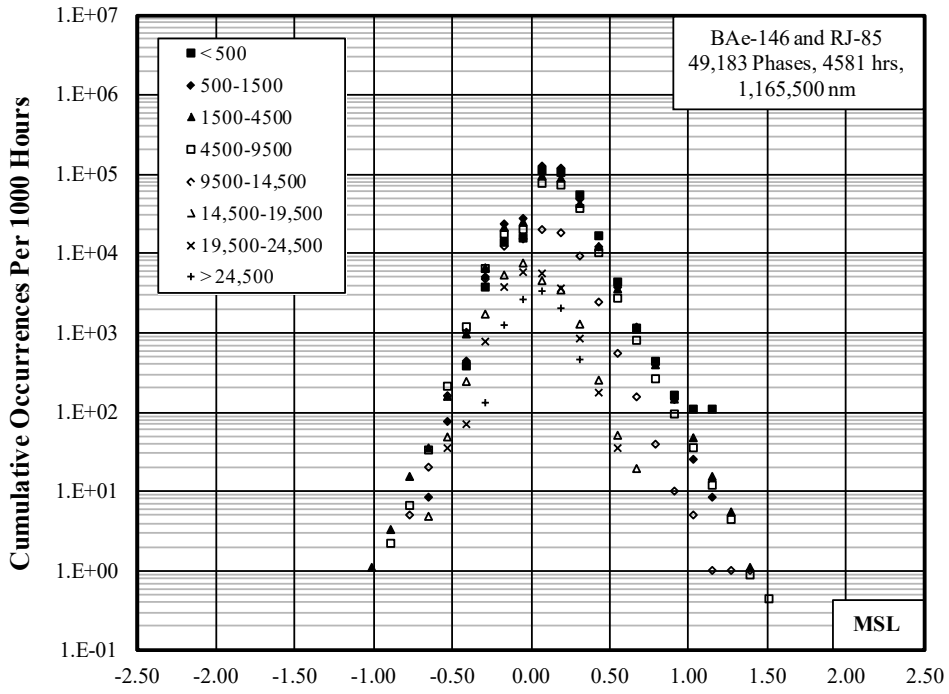

(a) Per 1000 Hours

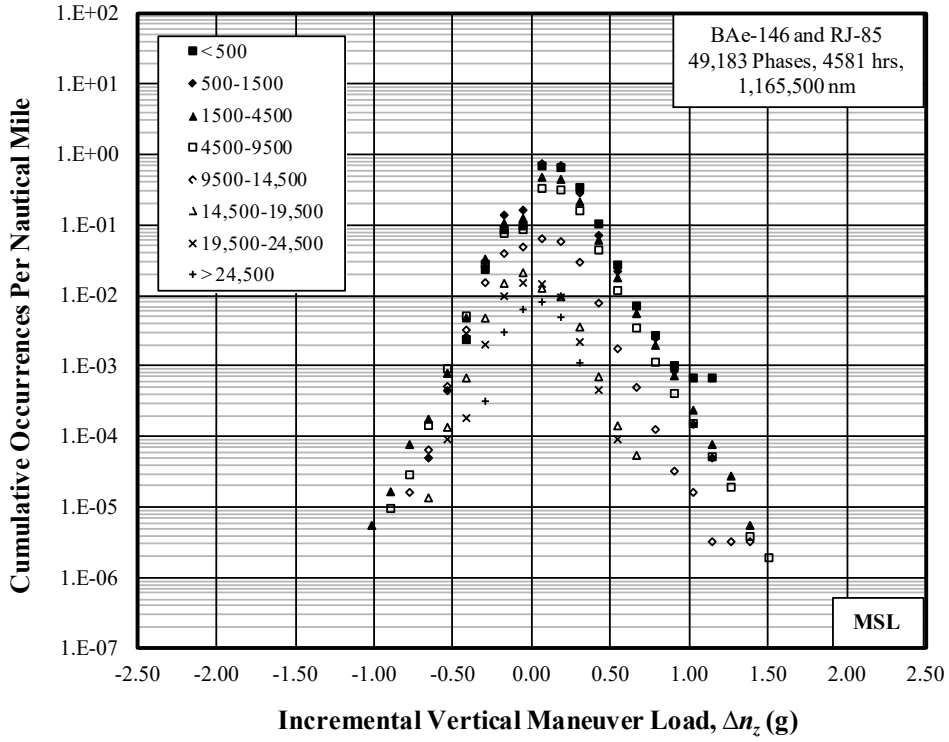

(b) Per Nautical Mile

Figure D-12. Cumulative occurrences of incremental vertical maneuver load factor – firefighting flights

Table D-10. Summary of durations and distances – ferry flights

Altitude Band Ceiling (ft)	Duration (hr)	Distance (nm)
500	0.1	10.2
1500	3.0	416.8
4500	50.0	9841.4
9500	73.2	18,413.6
14,500	68.5	21,180.8
19,500	92.0	32,444.9
24,500	78.5	30,466.8
Above 24,500	296.8	122,077.7
Total	662.1	234,852.3

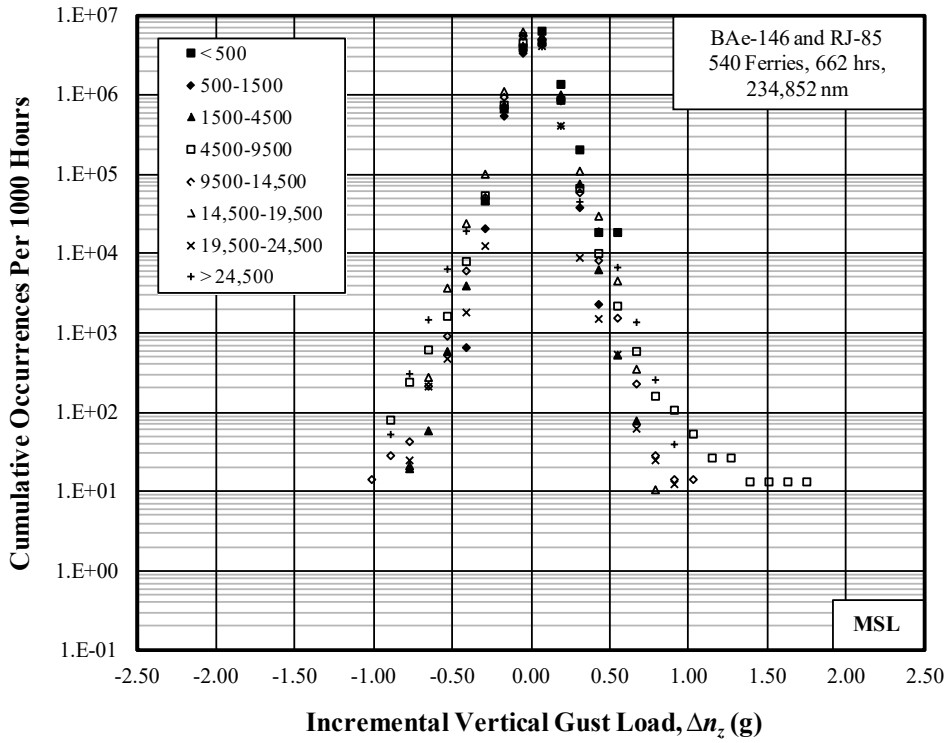

(a) Per 1000 Hours

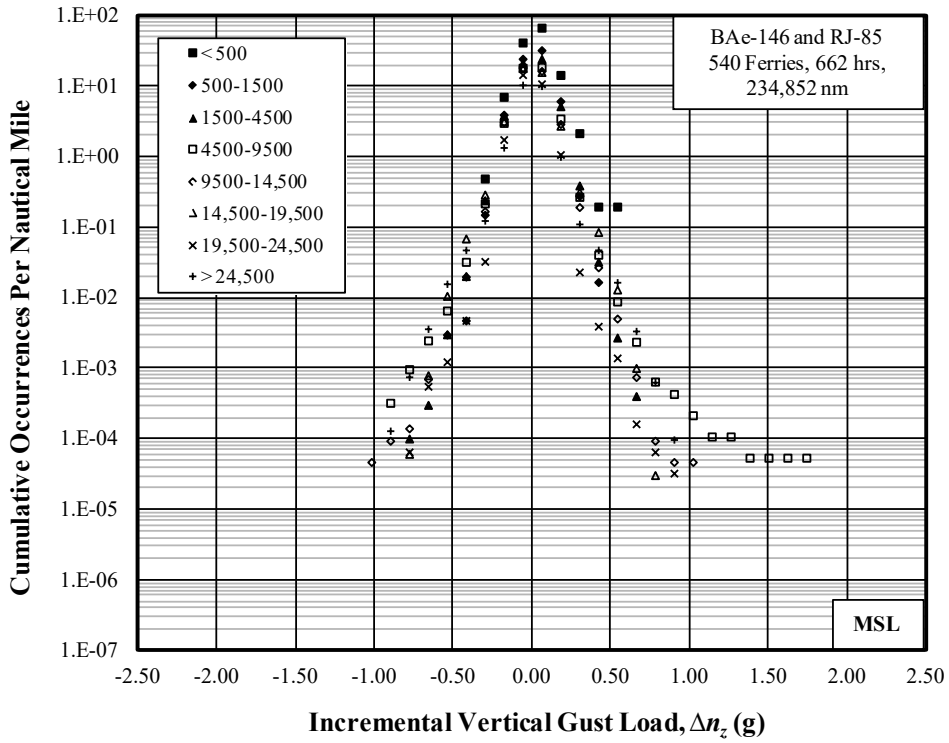

(b) Per Nautical Mile

Figure D-13. Cumulative occurrences of incremental vertical gust load factor – ferry flights

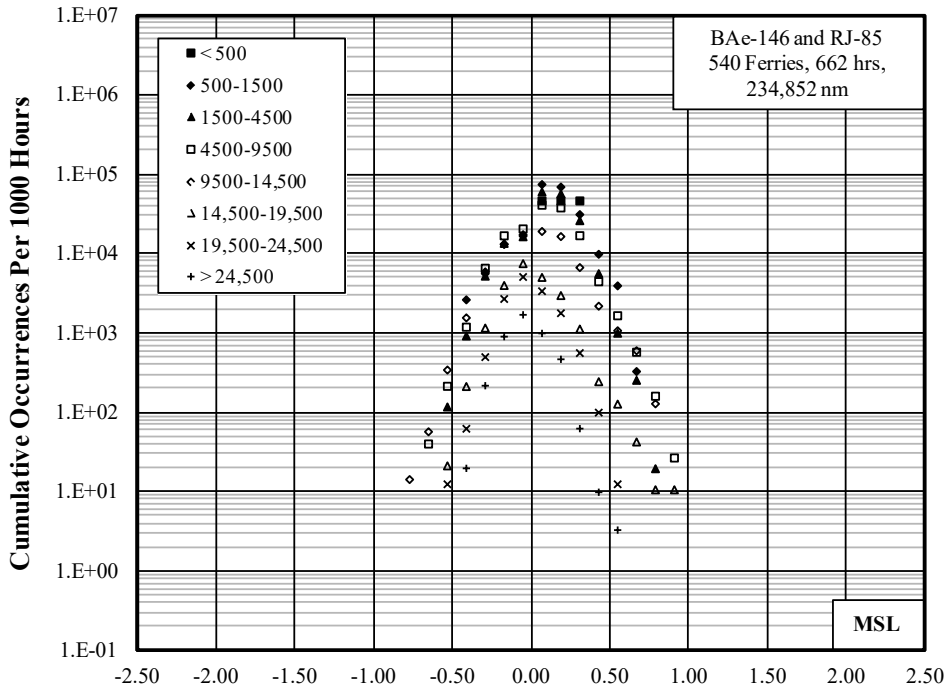

(a) Per 1000 Hours

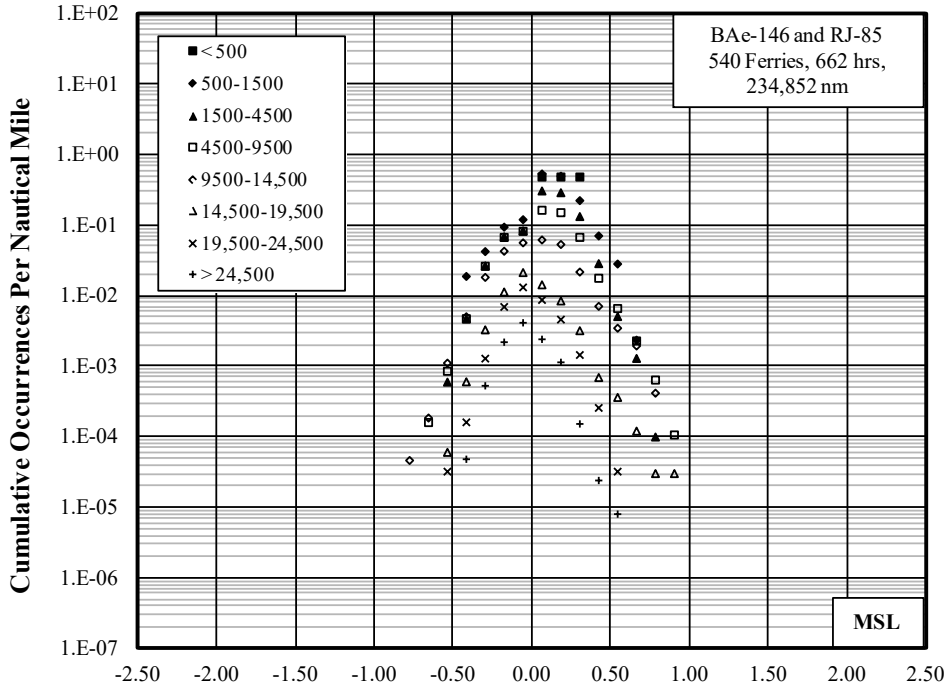

(b) Per Nautical Mile

Figure D-14. Cumulative occurrences of incremental vertical maneuver load factor – ferry flights

Table D-11. Summary of durations and distances – maintenance/training flights

Altitude Band Ceiling (ft)	Duration (hr)	Distance (nm)
500	3.8	680.0
1500	4.8	633.6
4500	80.2	14,296.9
9500	104.2	22,383.8
14,500	32.4	8382.2
19,500	3.4	1054.9
24,500	1.0	334.8
Above 24,500	1.0	408.7
Total	230.9	48,174.9

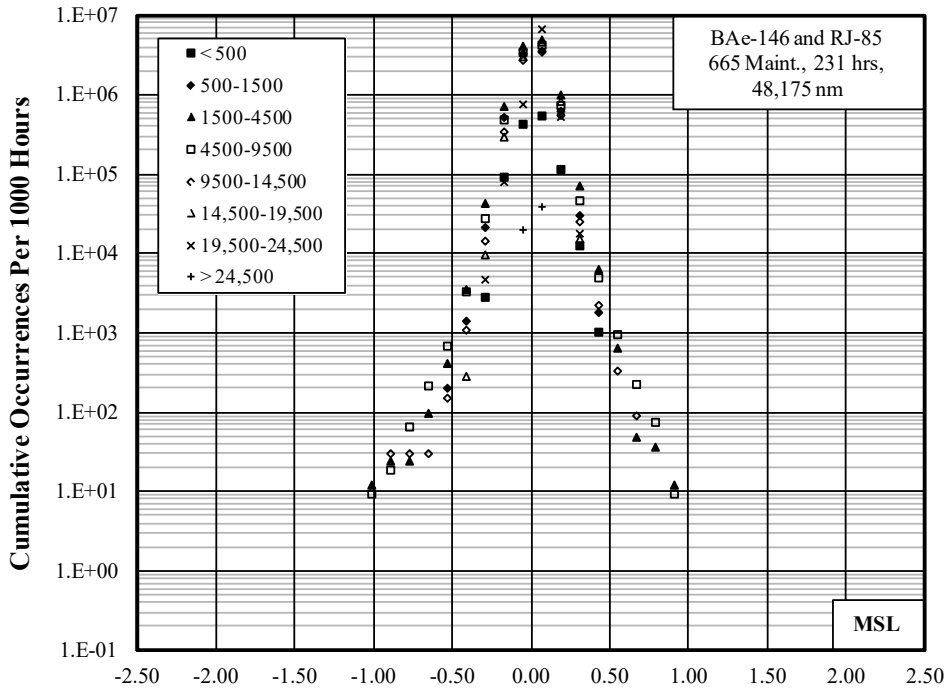

(a) Per 1000 Hours

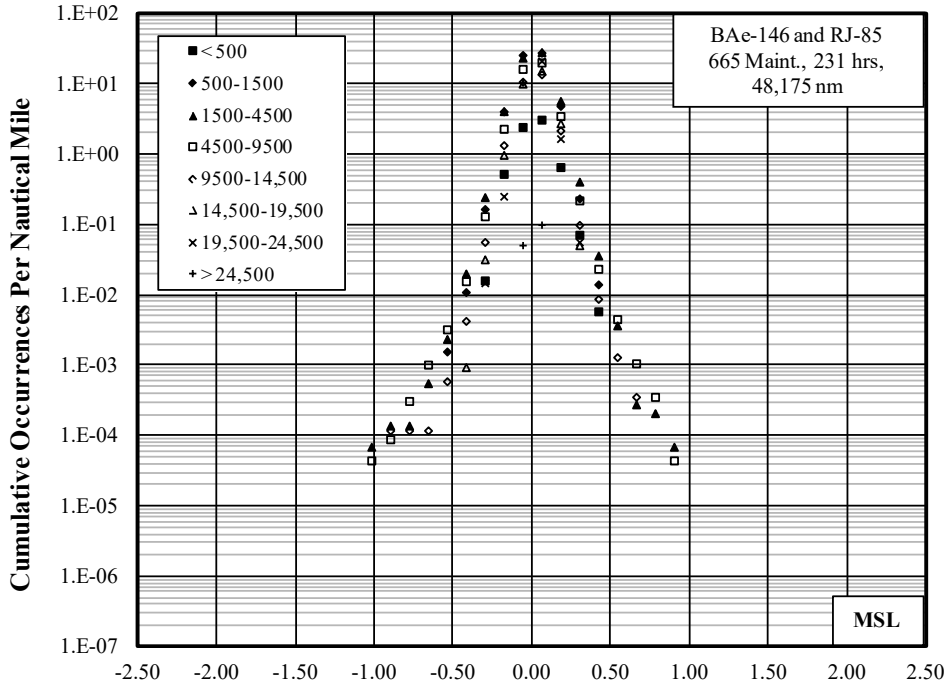

(b) Per Nautical Mile

Figure D-15. Cumulative occurrences of incremental vertical gust load factor – maintenance/training flights

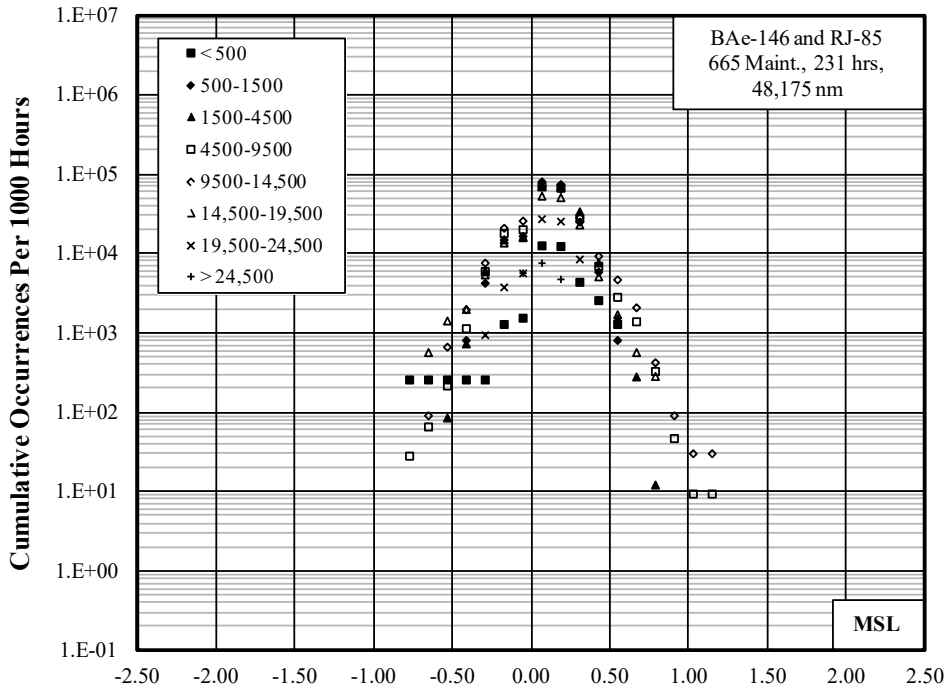

(a) Per 1000 Hours

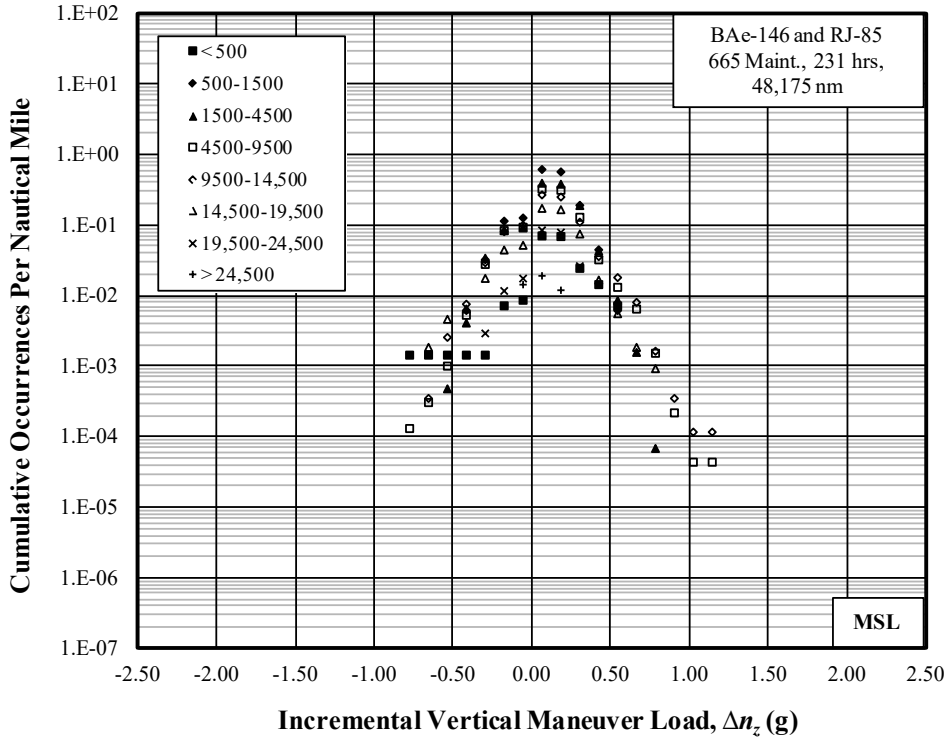

(b) Per Nautical Mile

Figure D-16. Cumulative occurrences of incremental vertical maneuver load factor – maintenance/training flights

APPENDIX E—DERIVED GUST VELOCITIES

Table E-1. Statistical formats – derived gust velocities by above ground level (AGL) and mean sea level (MSL) altitude

Flight Loads Data	Table
Summary of Durations and Distances for All Firefighting Flight Phases	Table E-3
Summary of Durations and Distances – Cruise 1	Table E-4
Summary of Durations and Distances – Cruise 2	Table E-5
Summary of Durations and Distances – Entry	Table E-6
Summary of Durations and Distances – Drop	Table E-7
Summary of Durations and Distances – Exit	Table E-8
Summary of Durations and Distances for the Overall Firefighting Flights	Table E-9
Summary of Durations and Distances for Ferry Flights	Table E-10
Summary of Durations and Distances for Maintenance Flights	Table E-11

Table E-2. Statistical formats – derived gust velocities by AGL and MSL altitude

Derived Gust Velocities	Figure
Cumulative Occurrences of Derived Gust Velocity – Cruise 1	Figure E-1
Cumulative Occurrences of Derived Gust Velocity – Cruise 2	Figure E-2
Cumulative Occurrences of Derived Gust Velocity – Entry	Figure E-3
Cumulative Occurrences of Derived Gust Velocity – Drop	Figure E-4
Cumulative Occurrences of Derived Gust Velocity – Exit	Figure E-5
Cumulative Occurrences of Derived Gust Velocity, Overall Flight with All Phases	Figure E-6
Cumulative Occurrences of Derived Gust Velocity, Ferry Flights	Figure E-7

Cumulative Occurrences of Derived Gust Velocity, Maintenance Flights	Figure E-8

Table E-3. Durations and distances for all firefighting flight phases

	Phase	Number of Occurrences	Duration (hr)	Distance (nm)
By AGL Altitude	Cruise 1	2070	535.1	134,200.0
	Cruise 2	2046	283.3	75,134.8
	Entry	2503	54.6	8538.9
	Drop	2503	4.3	664.5
	Exit	2503	29.5	4826.1
	Total		906.7	223,364.2
By MSL Altitude	Phase	Number of Occurrences	Duration (hr)	Distance (nm)
	Cruise 1	2071	536.0	134,483.4
	Cruise 2	2047	283.6	75,228.4
	Entry	2504	54.6	8542.4
	Drop	2504	4.3	664.8
	Exit	2504	29.5	4828.5
	Total		908.0	223,747.5

Table E-4. Summary of durations and distances – cruise 1

	Altitude Band Ceiling (ft)	Duration (hr)	Distance (nm)
By AGL Altitude	500	24.6	3999.9
	1500	88.1	18,378.2
	4500	281.1	65,994.2
	9500	101.5	31,274.2
	14,500	35.9	13,082.4
	19,500	3.9	1471.2
	24,500	0	0
	35,000	0	0
	Total	535.1	134,200.0
	Altitude Band Ceiling (ft)	Duration (hr)	Distance (nm)
By MSL Altitude	500	3.5	544.3
	1500	25.7	5059.2
	4500	106.7	23,257.1
	9500	288.3	68,743.7
	14,500	82.1	25,808.8
	19,500	29.4	10,965.2
	24,500	0.3	105.2
	35,000	0	0
	Total	536.0	134,483.4

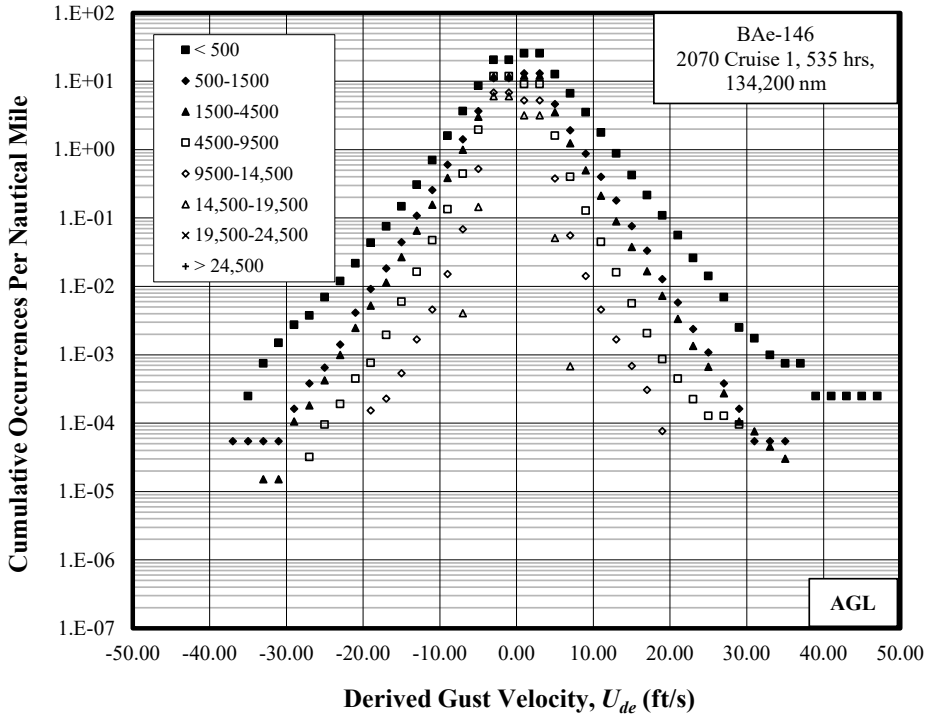

(a) By AGL Altitude

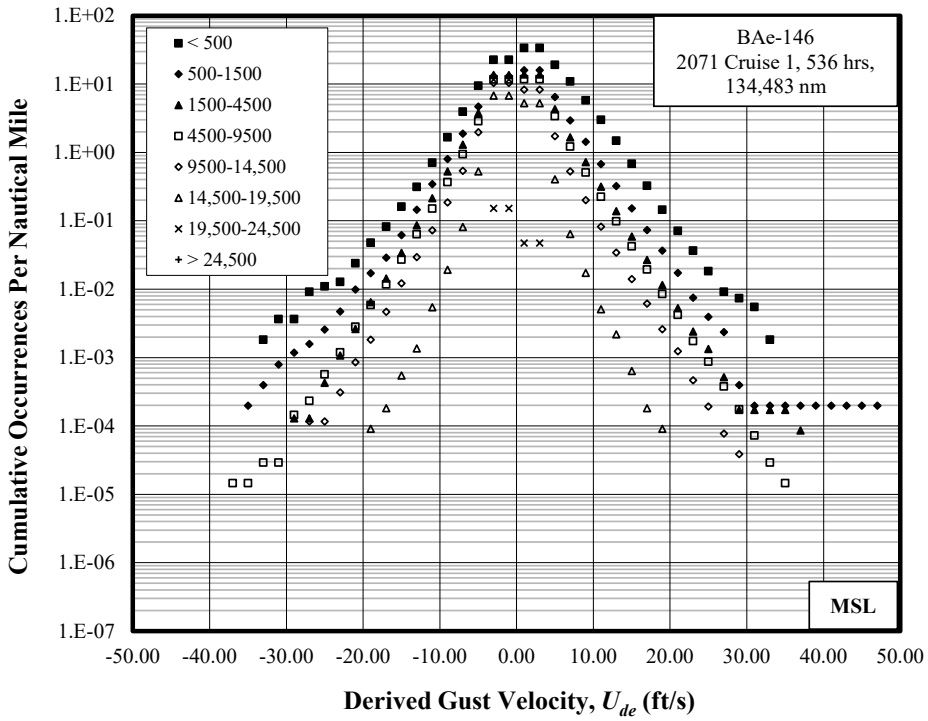

(b) By MSL Altitude

Figure E-1. Cumulative occurrences of derived gust velocity – cruise 1

Table E-5. Summary of durations and distances – cruise 2

	Altitude Band Ceiling (ft)	Duration (hr)	Distance (nm)
By AGL Altitude	500	0.4	66.0
	1500	47.5	8569.1
	4500	146.3	37,276.5
	9500	74.3	23,872.1
	14,500	13.3	4787.3
	19,500	1.5	563.9
	24,500	0	0
	35,000	0	0
	Total	283.3	75,134.8
	Altitude Band Ceiling (ft)	Duration (hr)	Distance (nm)
By MSL Altitude	500	0.1	10.4
	1500	8.2	1336.8
	4500	72.5	16,195.6
	9500	135.6	34,896.5
	14,500	59.9	20,067.5
	19,500	7.3	2721.7
	24,500	0	0
	35,000	0	0
	Total	283.6	75,228.4

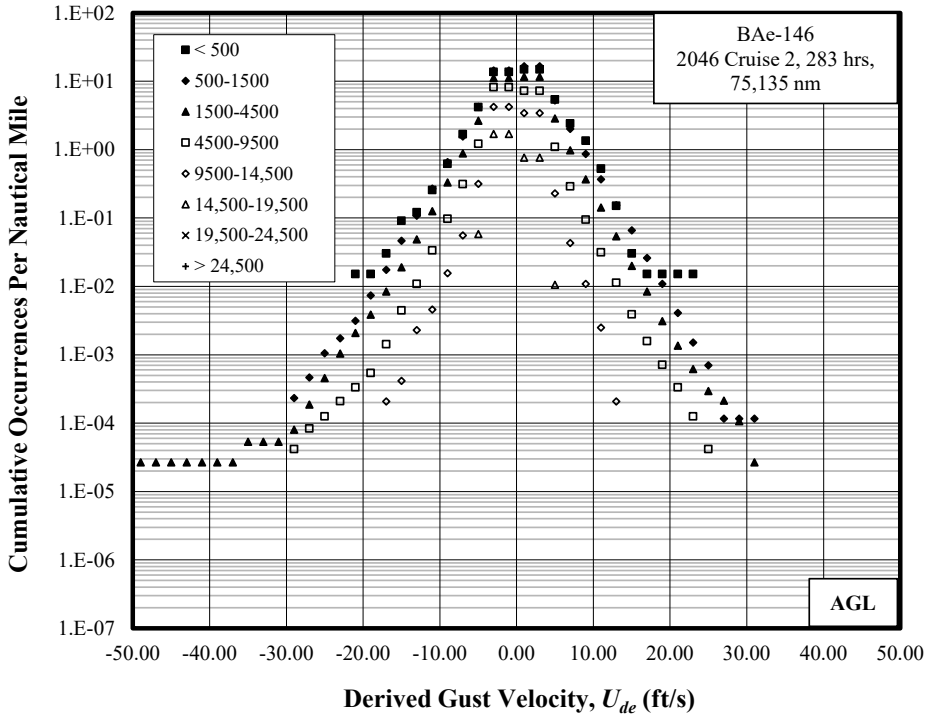

(a) By AGL Altitude

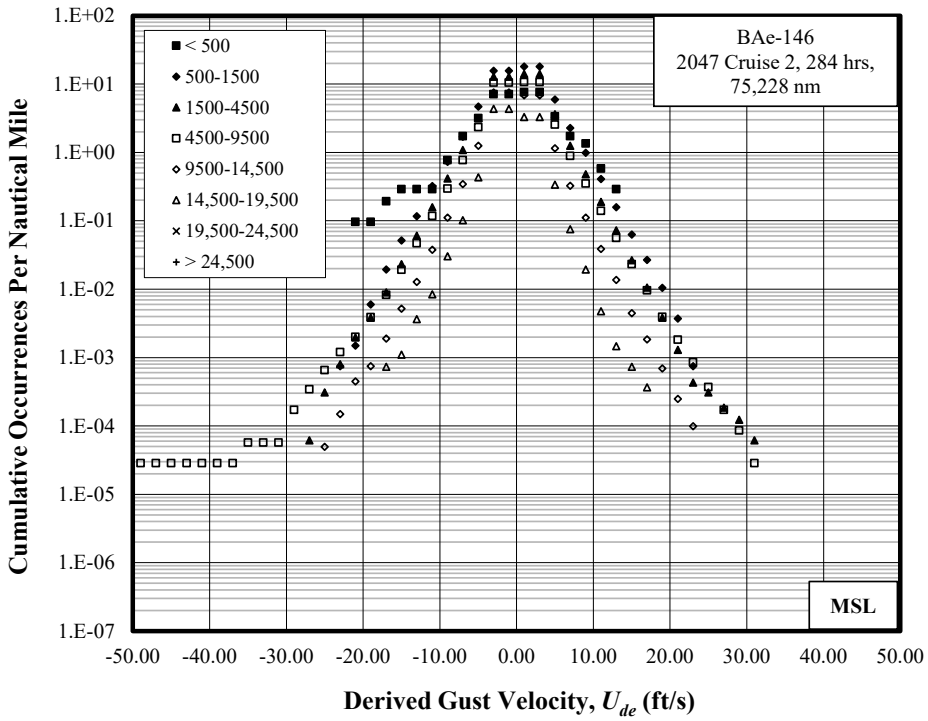

(b) By MSL Altitude

Figure E-2. Cumulative occurrences of derived gust velocity – cruise 2

Table E-6. Summary of durations and distances – entry

	Altitude Band Ceiling (ft)	Duration (hr)	Distance (nm)
By AGL Altitude	500	9.03	1357.0
	1500	29.35	4530.5
	4500	16.04	2622.4
	9500	0.16	29.0
	14,500	0	0
	19,500	0	0
	24,500	0	0
	35,000	0	0
	Total	54.58	8538.9
	Altitude Band Ceiling (ft)	Duration (hr)	Distance (nm)
By MSL Altitude	500	1.13	157.1
	1500	6.85	992.1
	4500	13.42	2020.2
	9500	31.27	5039.5
	14,500	1.93	333.4
	19,500	0	0
	24,500	0	0
	35,000	0	0
	Total	54.60	8542.4

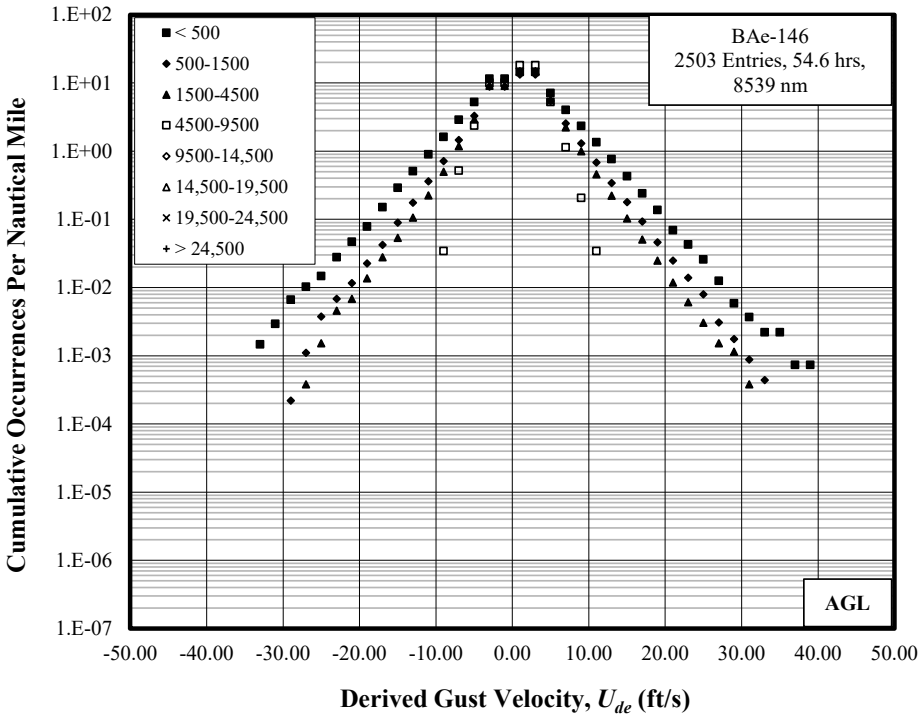

(a) By AGL Altitude

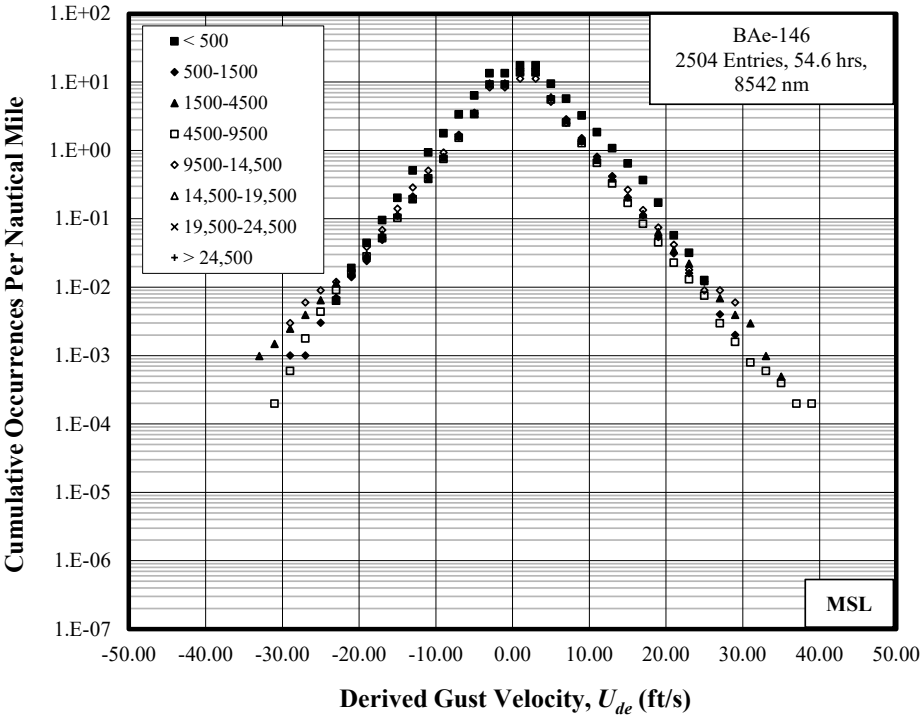

(b) By MSL Altitude

Figure E-3. Cumulative Occurrences of Derived Gust Velocity – entry

Table E-7. Summary of durations and distances – drop

	Altitude Band Ceiling (ft)	Duration (hr)	Distance (nm)
By AGL Altitude	500	3.96	597.6
	1500	0.23	38.9
	4500	0.13	28.1
	9500	0	0
	14,500	0	0
	19,500	0	0
	24,500	0	0
	35,000	0	0
	Total	4.32	664.5
	Altitude Band Ceiling (ft)	Duration (hr)	Distance (nm)
By MSL Altitude	500	0.59	79.6
	1500	0.19	27.8
	4500	1.45	227.2
	9500	2.02	317.6
	14,500	0.07	12.5
	19,500	0	0
	24,500	0	0
	35,000	0	0
	Total	4.32	664.8

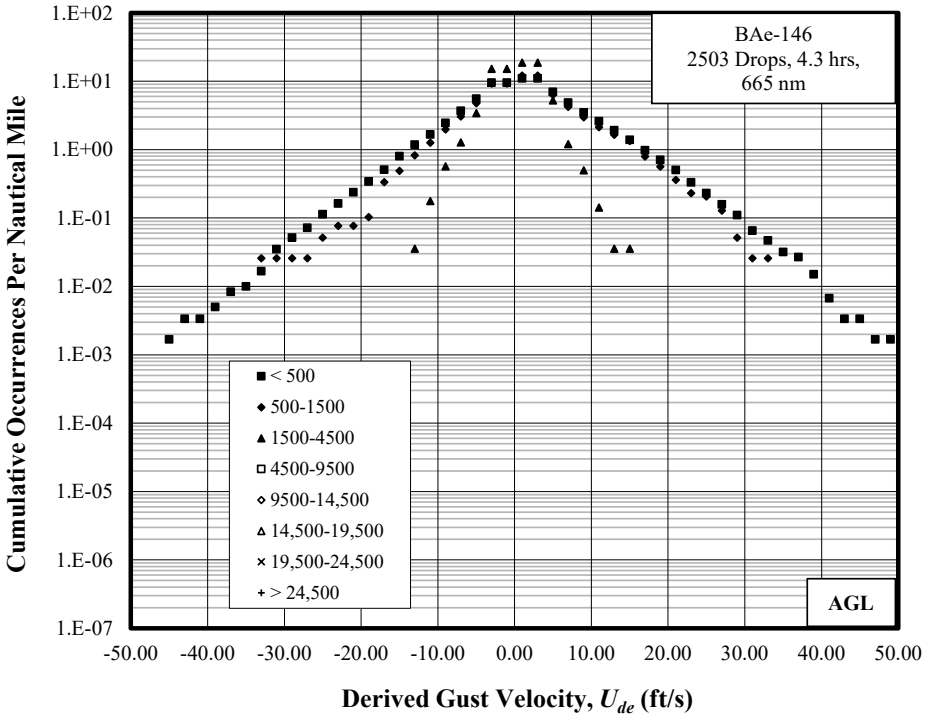

(a) By AGL Altitude

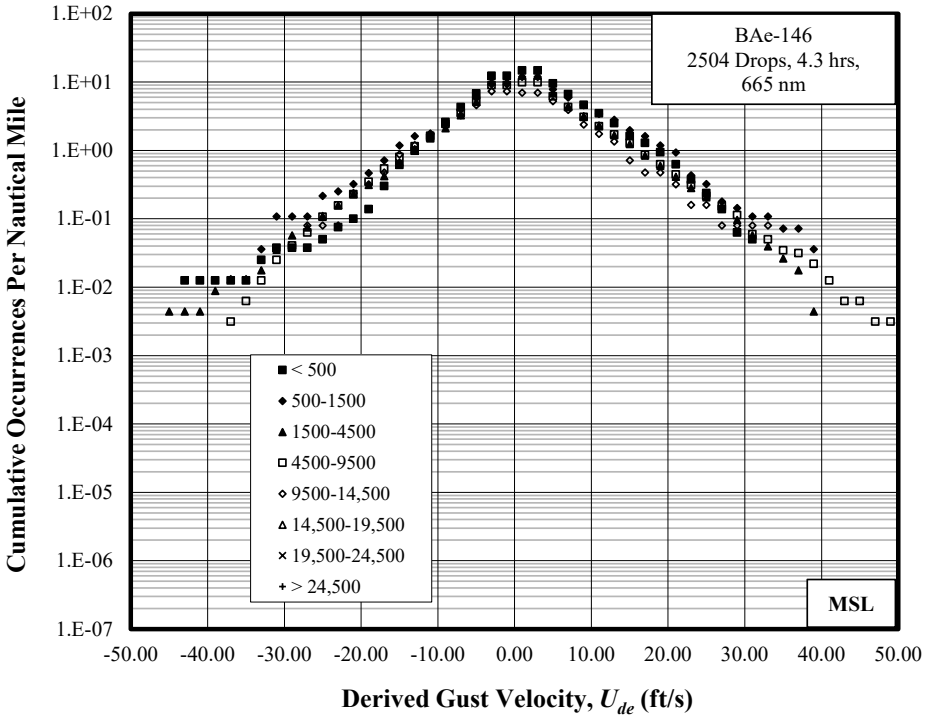

(b) By MSL Altitude

Figure E-4. Cumulative occurrences of derived gust velocity – drop

Table E-8. Summary of durations and distances – exit

	Altitude Band Ceiling (ft)	Duration (hr)	Distance (nm)
By AGL Altitude	500	9.02	1395.3
	1500	15.51	2572.4
	4500	4.92	853.6
	9500	0.02	4.8
	14,500	0	0
	19,500	0	0
	24,500	0	0
	35,000	0	0
	Total	29.47	4826.1
	Altitude Band Ceiling (ft)	Duration (hr)	Distance (nm)
By MSL Altitude	500	1.39	194.3
	1500	4.20	650.7
	4500	9.07	1469.7
	9500	14.06	2372.9
	14,500	0.77	140.8
	19,500	0	0
	24,500	0	0
	35,000	0	0
	Total	29.49	4828.5

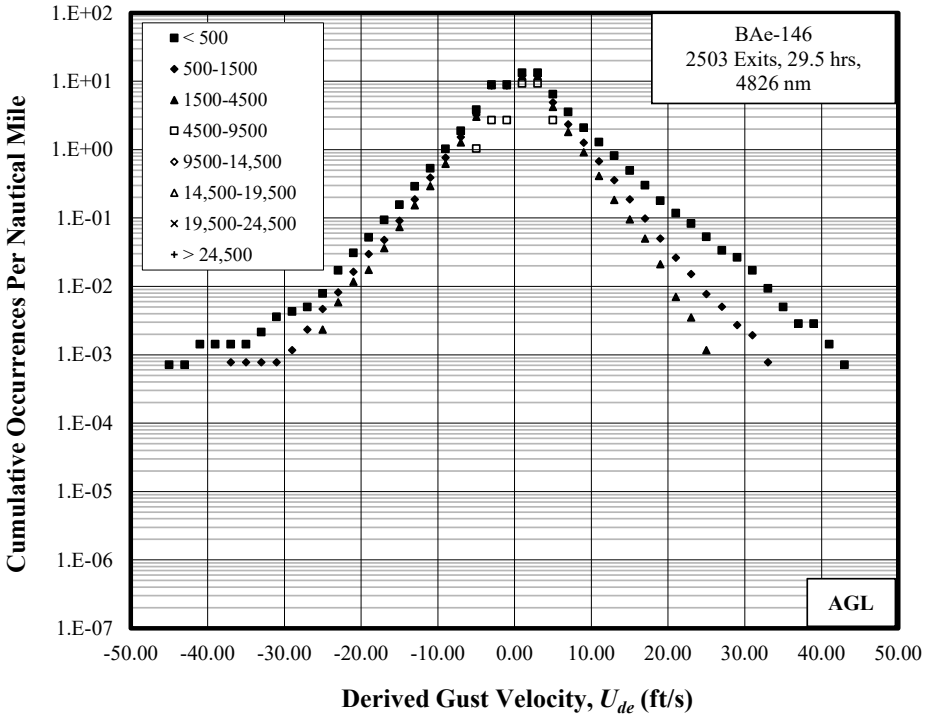

(a) By AGL Altitude

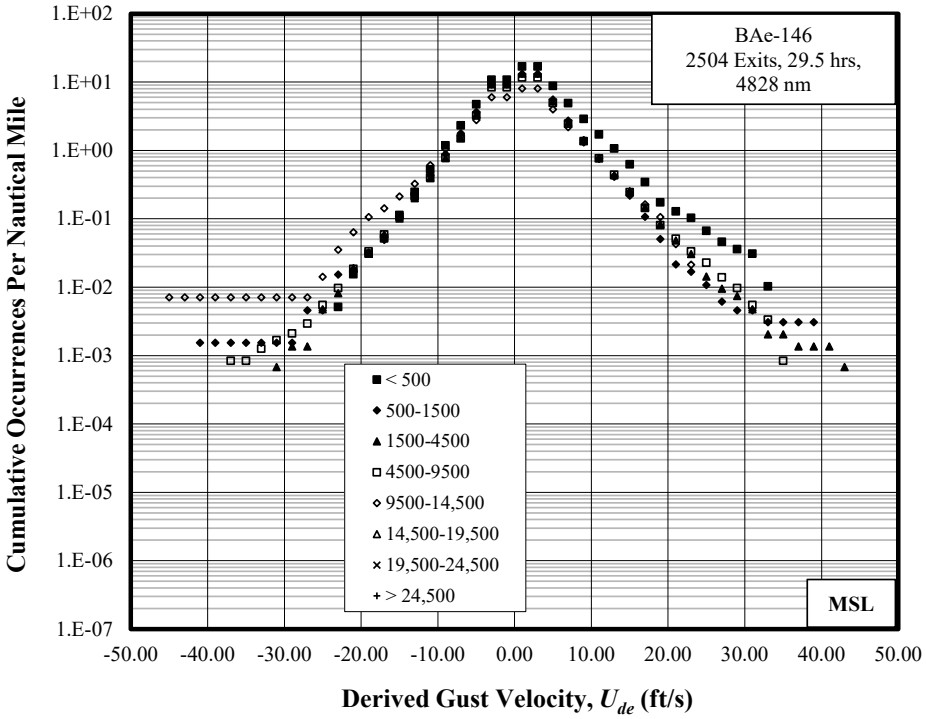

(b) By MSL Altitude

Figure E-5. Cumulative occurrences of derived gust velocity – exit

Table E-9. Summary of durations and distances for overall firefighting flights

	Altitude Band Ceiling (ft)	Duration (hr)	Distance (nm)
By AGL Altitude	500	46.98	7415.8
	1500	180.73	34,089.0
	4500	448.50	106,774.6
	9500	175.99	55,180.2
	14,500	49.22	17,869.6
	19,500	5.32	2035.1
	24,500	0	0
	35,000	0	0
	Total	906.74	223,364.2
	Altitude Band Ceiling (ft)	Duration (hr)	Distance (nm)
By MSL Altitude	500	6.7	985.7
	1500	45.1	8066.5
	4500	203.2	43,169.8
	9500	471.3	111,370.2
	14,500	144.9	46,363.1
	19,500	36.7	13,687.0
	24,500	0.3	105.2
	35,000	0	0
	Total	908.1	223,747.4

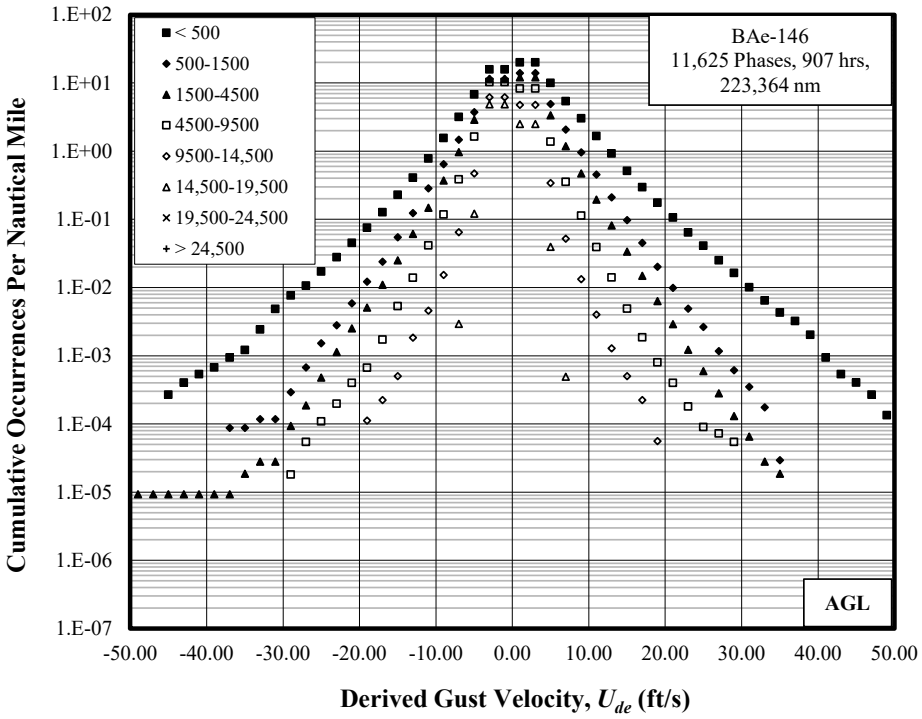

(a) By AGL Altitude

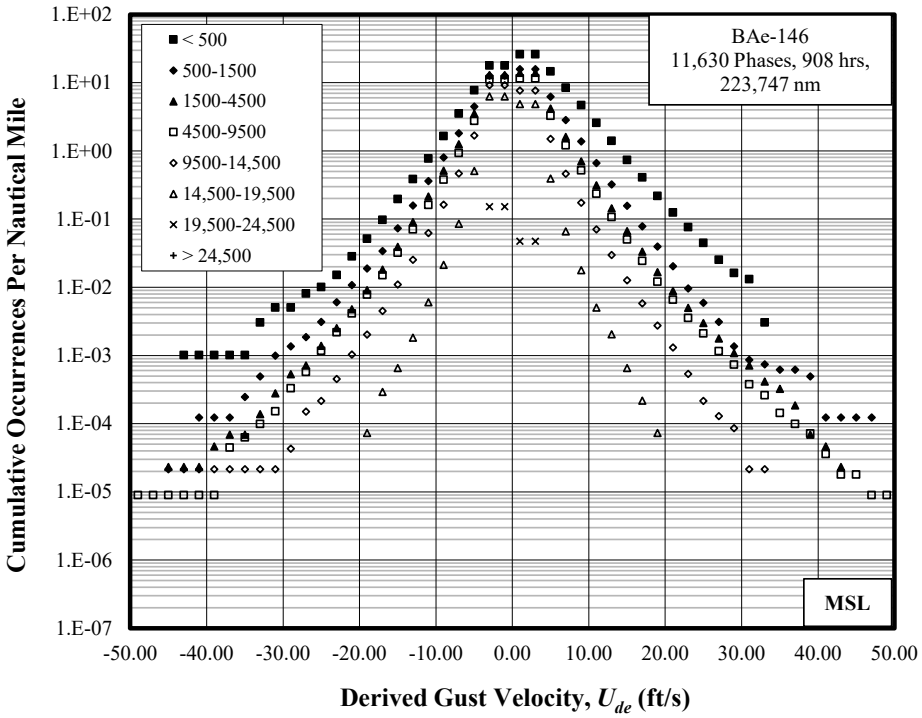

(b) By MSL Altitude

Figure E-6. Cumulative occurrences of derived gust velocity, overall firefighting flight with all phases

Table E-10. Summary of durations and distances for overall ferry flights

	Altitude Band Ceiling (ft)	Duration (hr)	Distance (nm)
By AGL Altitude	500	0.005	0.6
	1500	1.62	293.1
	4500	6.67	1573.5
	9500	8.11	2598.6
	14,500	9.58	3458.6
	19,500	7.44	3021.7
	24,500	4.84	2018.5
	35,000	4.85	2093.1
	Total	43.12	15,057.6
	Altitude Band Ceiling (ft)	Duration (hr)	Distance (nm)
By MSL Altitude	500	0	0
	1500	0.27	40.0
	4500	3.95	850.0
	9500	6.07	1543.3
	14,500	7.75	2581.6
	19,500	10.09	3741.8
	24,500	6.75	2761.0
	35,000	8.24	3540.0
	Total	43.12	15,057.8

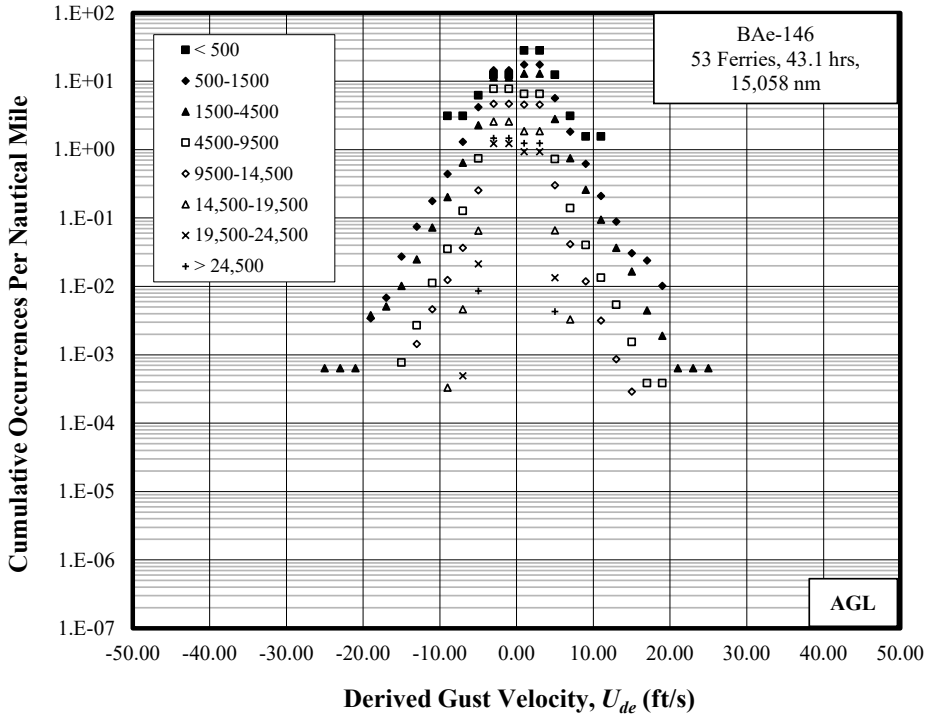

(a) By AGL Altitude

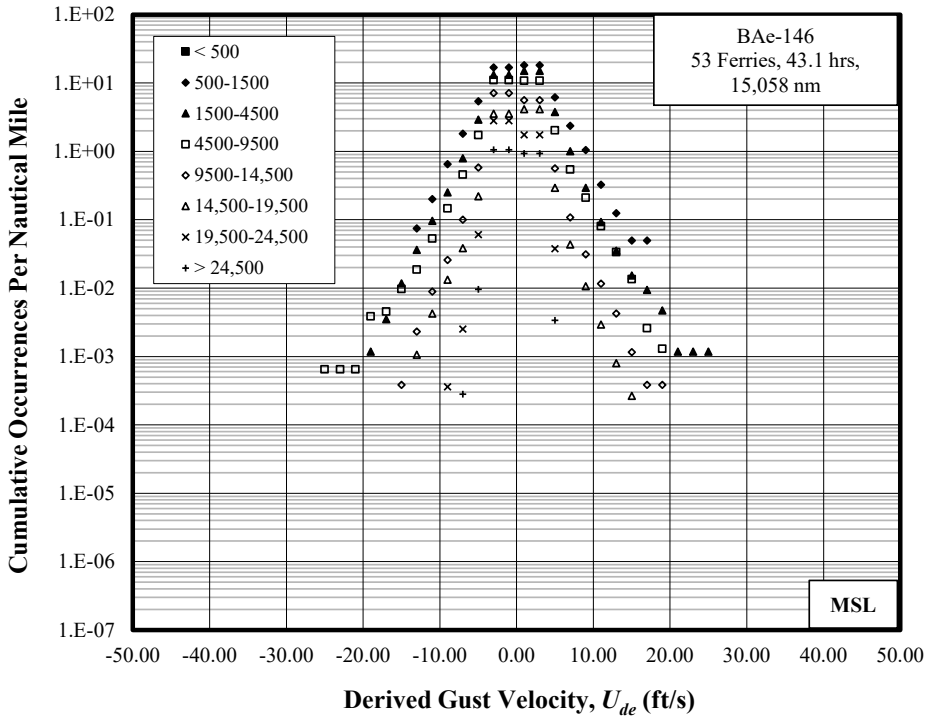

(b) By MSL Altitude

Figure E-7. Cumulative occurrences of derived gust velocity, ferry flights

Table E-11. Summary of durations and distances for overall maintenance/training flights

	Altitude Band Ceiling (ft)	Duration (hr)	Distance (nm)
By AGL Altitude	500	0.33	46.1
	1500	6.30	1111.0
	4500	19.46	4248.1
	9500	6.79	1720.6
	14,500	0.41	100.4
	19,500	0	0
	24,500	0	0
	35,000	0	0
	Total	33.29	7226.1
	Altitude Band Ceiling (ft)	Duration (hr)	Distance (nm)
By MSL Altitude	500	0.03	3.8
	1500	0.56	81.4
	4500	12.94	2561.3
	9500	15.36	3423.2
	14,500	4.30	1121.4
	19,500	0.11	35.0
	24,500	0	0
	35,000	0	0
	Total	33.29	7226.1

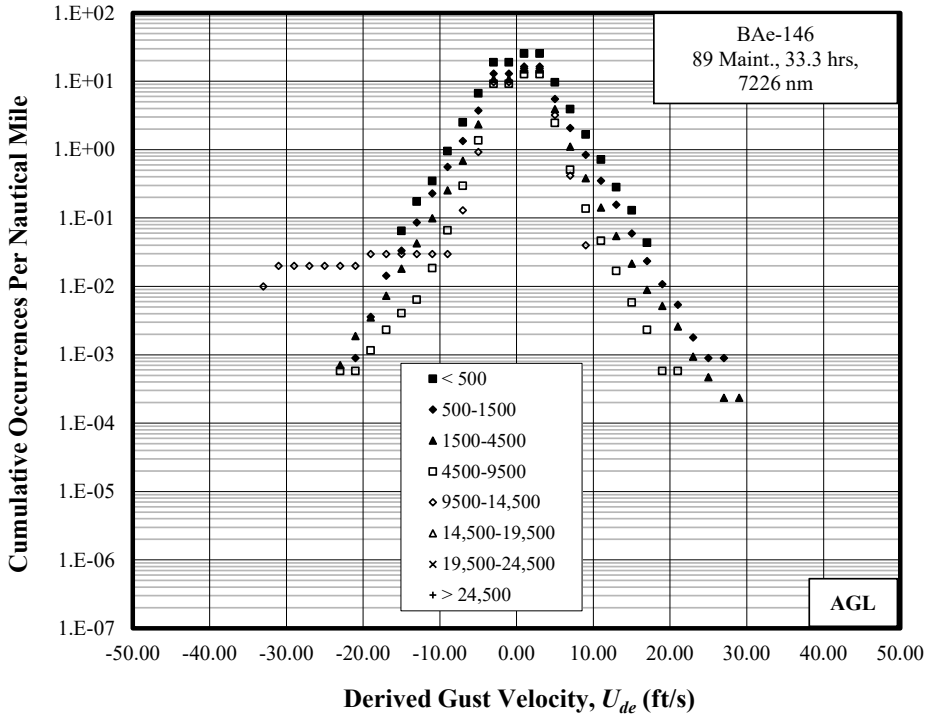

(a) By AGL Altitude

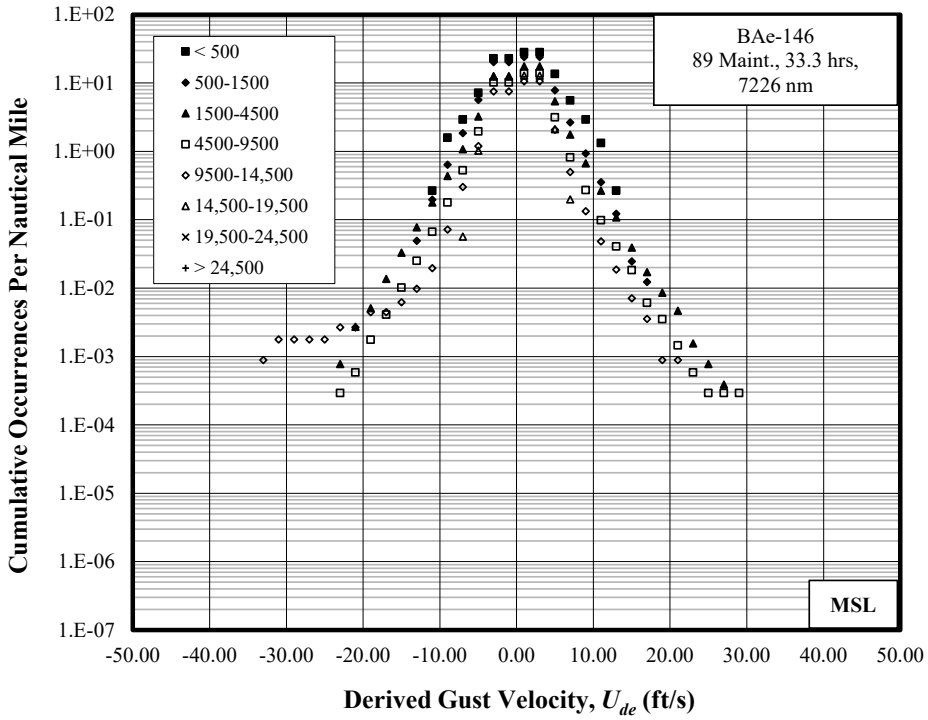

(b) By MSL Altitude

Figure E-8. Cumulative occurrences of derived gust velocity, maintenance flights

APPENDIX F—COMPARISONS WTH OTHER SOURCES

Table F-1. Statistical formats – comparisons with other sources

Comparisons	Figure
Cumulative Occurrences of Incremental Vertical Gust Load Factor, Comparison of all Firefighting Phases	Figure F-1
Cumulative Occurrences of Incremental Vertical Maneuver Load Factor, Comparison of all Firefighting Phases	Figure F-2
Cumulative Occurrences of Incremental Vertical Load Factor for Different Missions Compared with Boeing 737-400, Airbus A-320, and Civil Aircraft Airworthiness Data Recording Program (CAADRP) 2	Figure F-3
Cumulative Occurrences of Incremental Vertical Gust Load Factor for Different Missions Compared with Boeing 737-400 and Airbus A-320	Figure F-4
Cumulative Occurrences of Incremental Vertical Gust Load Factor for Different Missions Compared with USFS Lead Airplane	Figure F-5
Cumulative Occurrences of Incremental Vertical Maneuver Load Factor for Different Missions Compared with Boeing 737-400, Airbus A-320, and CAADRP 1	Figure F-6
Cumulative Occurrences of Incremental Vertical Maneuver Load Factor for Different Missions Compared with USFS P2V and P3A	Figure F-7
Cumulative Occurrences of Derived Gust Velocity for Different Missions Compared with Commercial Operations	Figure F-8

USFS = United States Forest Service

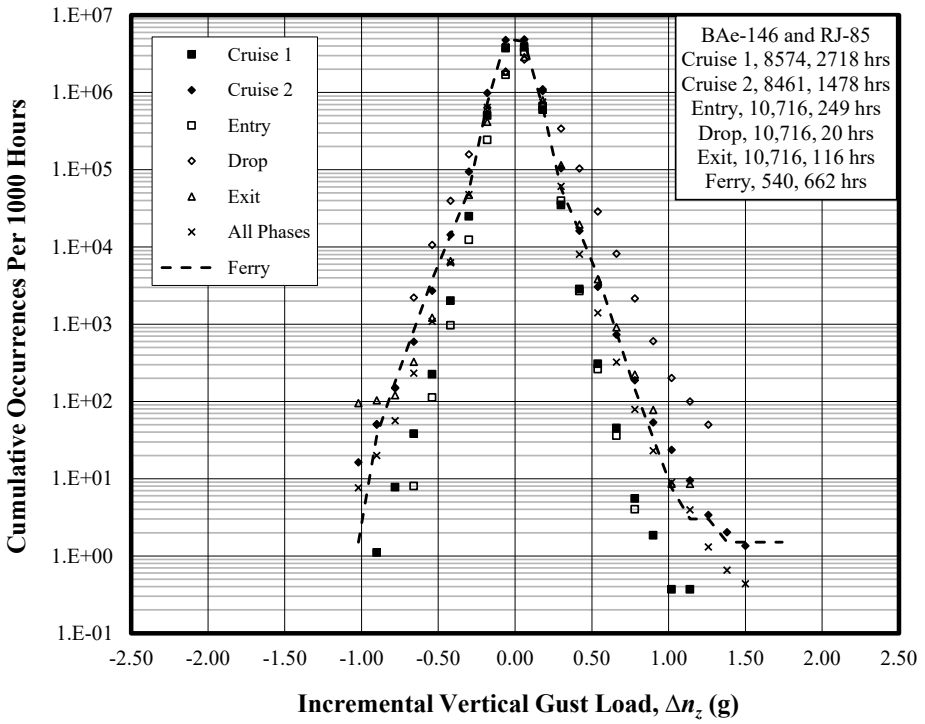

Figure F-1. Cumulative occurrences of incremental vertical gust load factor, comparison of all firefighting phases

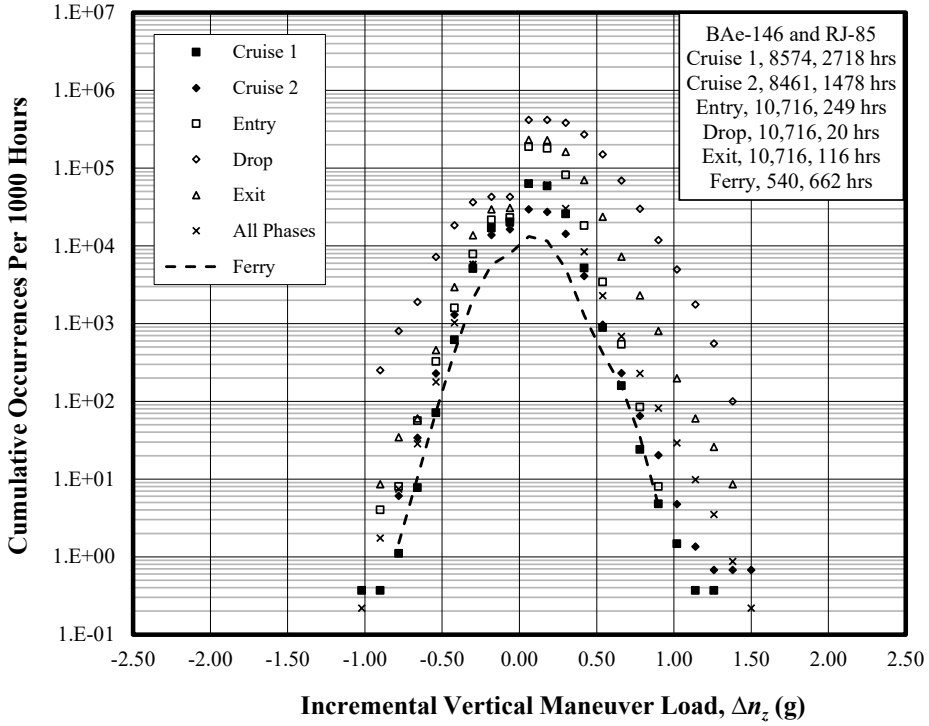

Figure F-2. Cumulative occurrences of incremental vertical maneuver load factor, comparison of all firefighting phases

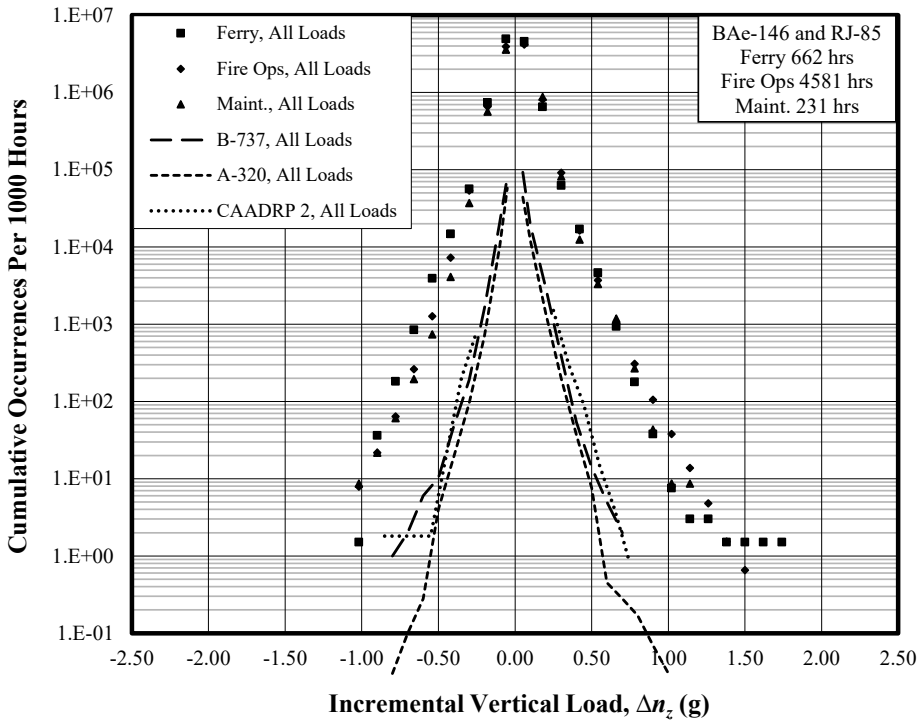

Figure F-3. Cumulative occurrences of incremental vertical load factor for different missions compared with Boeing 737-400, Airbus A-320, and CAADRP 2

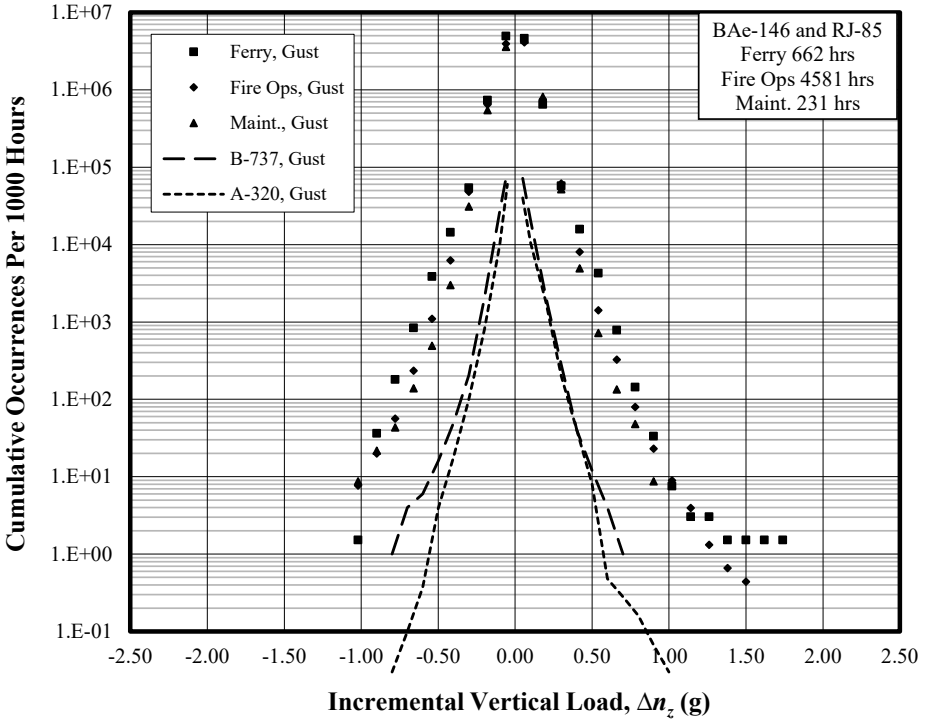

Figure F-4. Cumulative occurrences of incremental vertical gust load factor for different missions compared with Boeing 737-400 and Airbus A-320

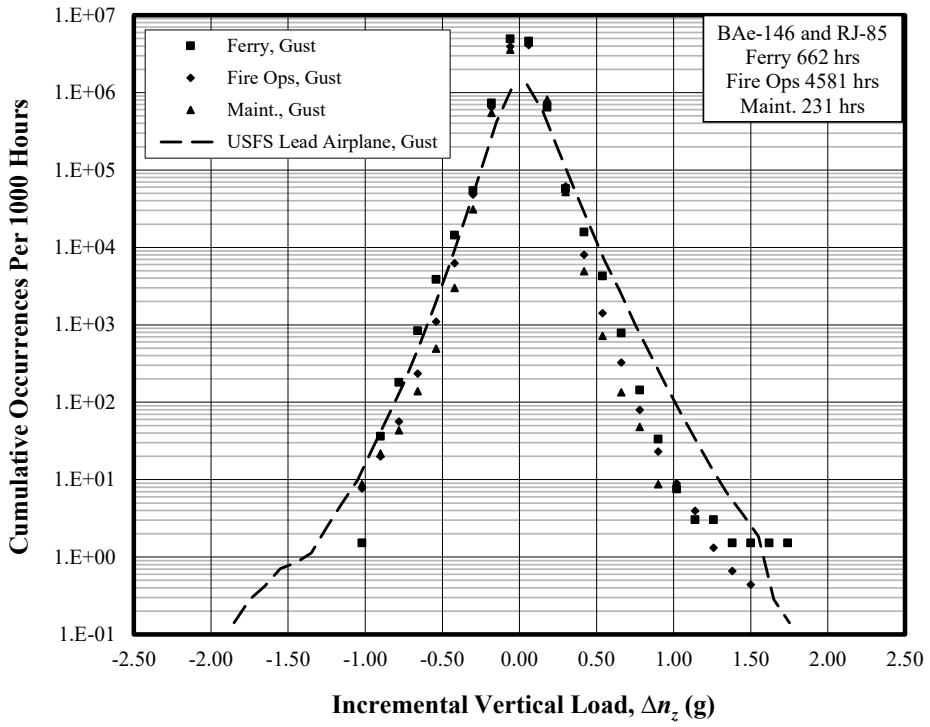

Figure F-5. Cumulative occurrences of incremental vertical gust load factor for different missions compared with USFS lead airplane

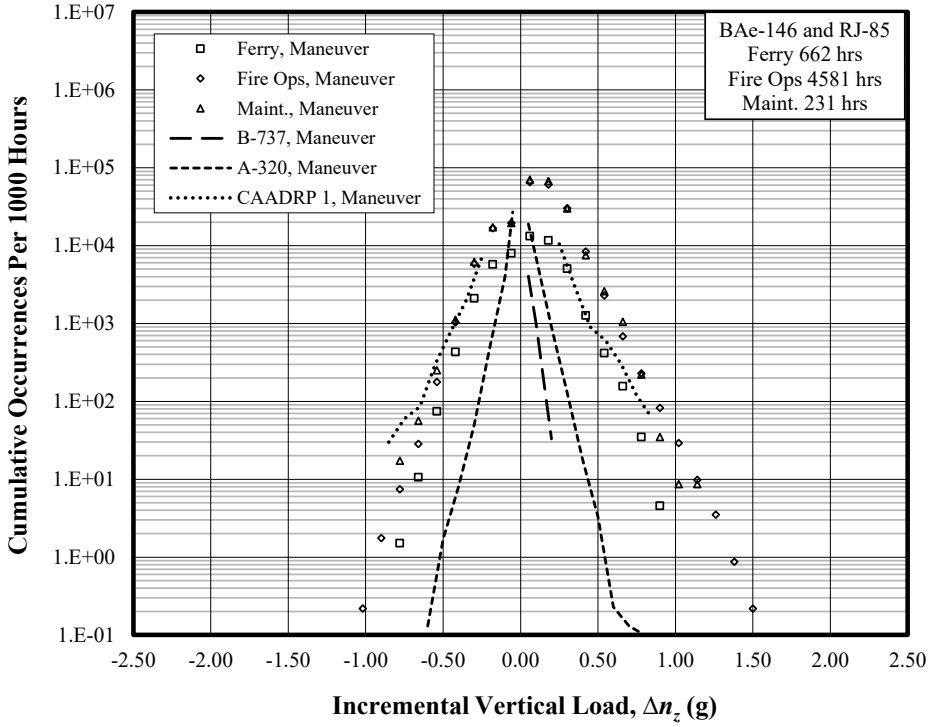

Figure F-6. Cumulative occurrences of incremental vertical maneuver load factor for different missions compared with Boeing 737-400, Airbus A-320, and CAADRP 1

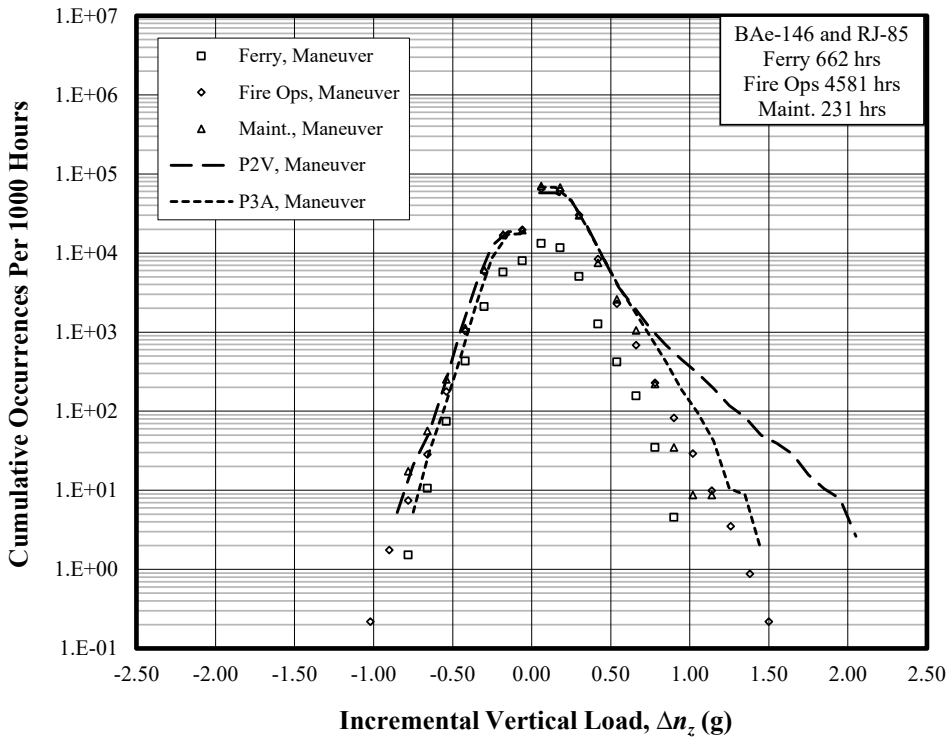

Figure F-7. Cumulative occurrences of incremental vertical maneuver load factor for different missions compared with USFS P2V and P3A

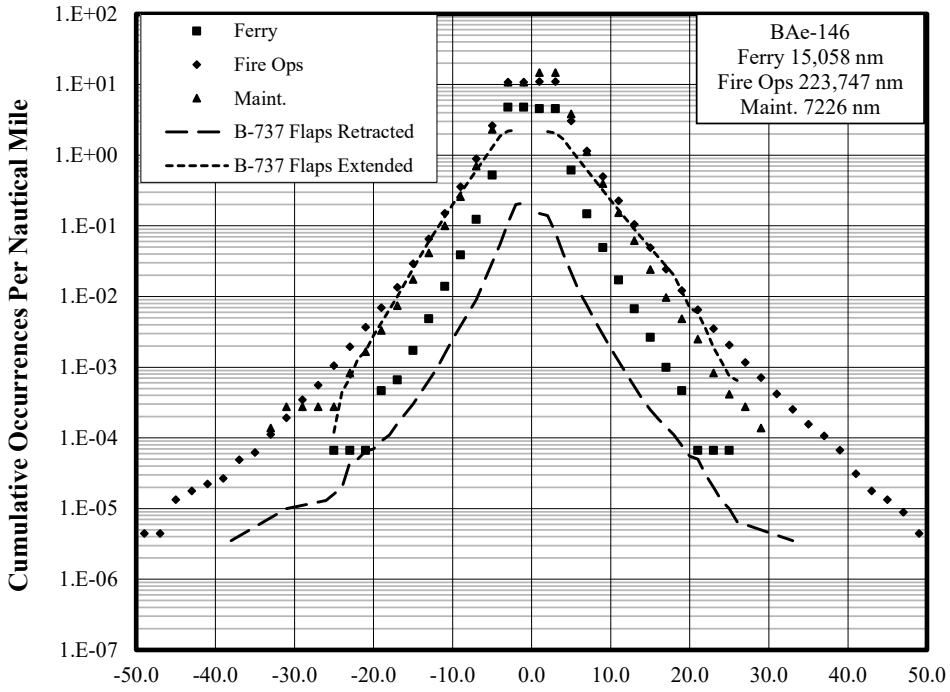

(a) Compared with Boeing 737-400

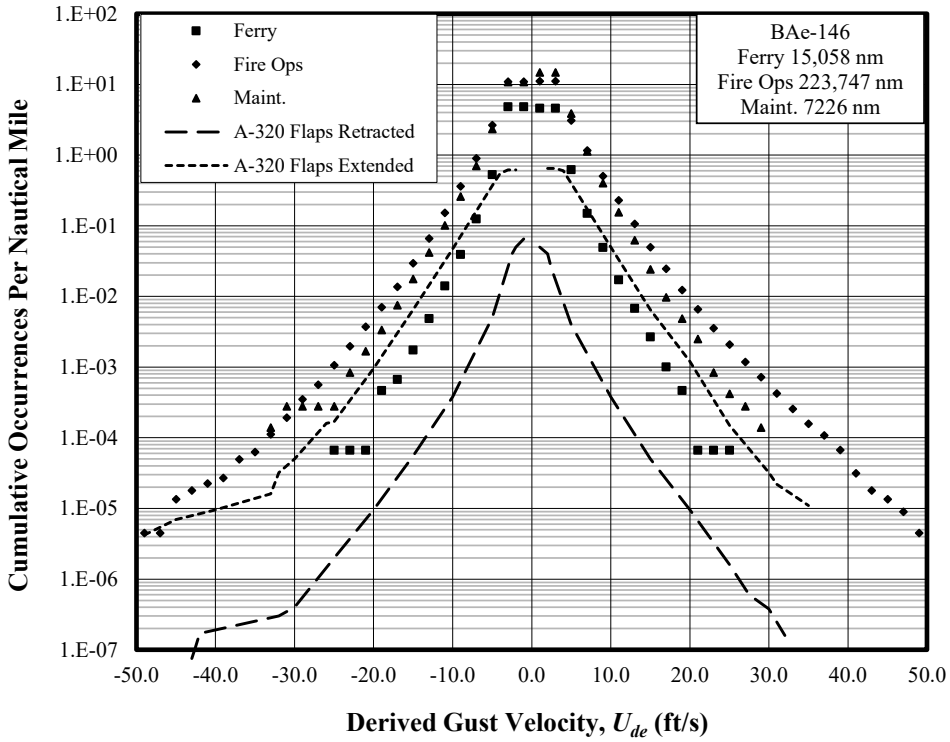

(b) Compared with Airbus A-320

Figure F-8. Cumulative occurrences of derived gust velocity for different missions compared with commercial operations